TECHNISCHE UNIVERSITÄT MÜNCHEN

Lehrstuhl für Genetik

Characterization of the Small Molecule Kinase Inhibitor SU11248 (Sunitinib/ SUTENT *in vitro* and *in vivo*

- Towards Response Prediction in Cancer Therapy with Kinase Inhibitors

Michaela Bairlein

Vollständiger Abdruck der von der Fakultät Wissenschaftszentrum Weihenstephan für Ernährung, Landnutzung und Umwelt der Technischen Universität München zur Erlangung des akademischen Grades eines

Doktors der Naturwissenschaften

genehmigten Dissertation.

Vorsitzender:	Univ.-Prof. Dr. K. Schneitz
Prüfer der Dissertation:	1. Univ.-Prof. Dr. A. Gierl
	2. Hon.-Prof. Dr. h.c. A. Ullrich
	(Eberhard-Karls-Universität Tübingen)
	3. Univ.-Prof. A. Schnieke, Ph.D.

Die Dissertation wurde am 07.01.2010 bei der Technischen Universität München eingereicht und durch die Fakultät Wissenschaftszentrum Weihenstephan für Ernährung, Landnutzung und Umwelt am 19.04.2010 angenommen.

FOR MY PARENTS

1 Contents

2 Summary

SU11248 is a multi-targeted kinase inhibitor approved by the FDA for the treatment of metastatic renal cell carcinoma (mRCC) and gastrointestinal stromal tumors (GIST). For an optimal clinical impact of the drug and its precise response prediction *in patients* including adverse side-effects, drug target interaction profiles and molecular sites of action are of major importance. Using an efficient affinity chromatography based chemical proteomics approach the target spectrum of SU11248 was profiled in 30 cancer cell lines from 9 different tissue origins and primary mRCC tumors. 313 putative kinase targets belonging to almost all prominent kinase families were identified. Gene Ontology annotation of the biological target function revealed a diverse implication of SU11248 in cellular signalling processes regulating cell proliferation, -survival, -migration, -invasion as well as energy metabolism and protein-biosynthesis. To rank and prioritize target relevance, qualitative binding data were supported by target affinities and quantitative K_d-values directly from cancer cells. In addition, new non-kinase targets, including metabolic enzymes, were also found in the proteome-wide cell-based interaction screen of the small molecule kinase inhibitor.

Moreover, a SU11248 activity and sensitivity screen in 63 cancer cell lines from different tumor types including brain, breast, colon, kidney, liver, lung, ovary, pancreas, prostate and skin, concerning cancer cell proliferation, survival, migration and invasion, revealed potential new tumor indications suitable for SU11248 treatment in the future.

The data constitute a comprehensive study of SU11248 activity and selectivity under cell physiological conditions and provides cancer-type specific target interaction profiles.

Functional target analyses using RNAi showed that newly identified kinase targets including ROS1, NME4, BMP2K, NEK9, TBK1 and FAK have anti-proliferative and programmed cell death effects. Knock-down of these targets significantly reduced SU11248 activity indicating important sites of molecular drug action. A strong correlation was shown between target inhibition by SU11248, the biological consequence of the drug treatment and the functional relevance of the target. Hence, a direct correlation between target expression and SU11248 anti-tumor activity was shown in cellular cancer model systems. Those high affinity targets may function as biomarkers for the prediction of SU11248 efficacy *in vivo* considering the genetic background of a tumor in the context of individualized targeted cancer therapies.

A quantitative mass spectrometry-based phosphoproteomic analysis revealed a strong impact of SU11248 on signalling networks within cancer cells. Inhibition of protein phosphorylation after SU11248 treatment was observed on proteins exerting diverse biological functions including cell proliferation, survival, adhesion, motility as well as endo-/exocytosis.

Protein expression profiling showed that sensitive cell lines are mesenchymal-like with high levels of Vimentin, compared to insensitive cell lines which are more epithelial-like, expressing high levels of E-cadherin. The expression of these two proteins in tumors could therefore be used to screen for sensitivity to SU11248 in patients.

3 Zusammenfassung

SU11248 gehört zur Klasse der niedermolekularen Kinase Inhibitoren, die in der Krebsmedizin für die gerichtete Krebstherapie eingesetzt werden. Unter gerichteter Krebstherapie versteht man das gezielte Inaktivieren krebsrelevanter Moleküle, genauer Proteine, wie zum Beispiel Kinasen, mittels chemischer Substanzen, in der Krebszelle. SU11248 war das erste Krebsmedikament seiner Klasse, welches im Jahre 2006 gleichzeitig für zwei Indikationen, nämlich metastasierendes Nierenzellkarzinom und imatinib-resistente Tumore des Magen-Darm Traktes, von der `Food And Drug Administration` (FDA) in den Vereinigten Staaten zugelassen wurde. 2007 erhielt es eine Zulassung in Europa. Für eine optimale therapeutische Wirkung eines Krebsmedikamentes ist es von großer Bedeutung, das genaue molekulare Wirkspektrum zu kennen. Wirkmechanismen und Angriffspunkte des Inhibitors innerhalb der Zelle geben Aufschluss über seine Wirkeffizienz in bestimmten Tumorindikationen sowie Hinweise auf mögliche Nebenwirkungen während einer Therapie.

Die Kombination von Affinitätschromatographie mit immobilisierter Inhibitor-Matrix und anschließender massenspektrometrischer Identifizierung potentieller Bindungspartner, auch `chemical proteomics` genannt, ermöglicht die Identifizierung zellweiter Interaktionspartner niedermolekularer Inhibitoren. In dieser Arbeit wurde das Profil von SU11248 in 30 Krebszelllinien verschiedener Tumorindikationen, sowie primären Nierenzellkarzinomen analysiert. Insgesamt wurden 313 potentielle Kinasetargets verteilt auf alle Kinaseklassen identifiziert. Die funktionelle Charakterisierung gefundener Interaktoren mittels Gene Ontology ergab ein breites biologisches SU11248 Wirkspektrum, welches mit Prozessen zur Regelung von Zellproliferation, Zellmigration und -Invasion, Zelltod, sowie Energiemetabolismus und Proteinbiosynthese interferiert. Zur Abschätzung der Targetrelevanz während einer Therapie, sind Bindungsaffinitäten zwischen Zielprotein und Inhibitor von großer Bedeutung. Ziel war es deshalb, die endogenen Bindungsaffinitäten der SU11248 Targets quantitativ zu bestimmen.

Ein SU11248 Aktivitätsscreen in 63 Krebszelllinien unterschiedlichster Indikationen, wie Tumore des Gehirns, der Brust, des Darms, der Lunge, der Niere, der Bauchspeicheldrüse, der Haut und der Prostata, zeigte eine starke antitumorigene Wirkung. Die starken anti-proliferativen und zelltod-induzierenden Effekte lassen auf weitere mögliche Anwendungsgebiete von SU11248 in der Krebstherapie schließen.

Durch die funktionelle Charakterisierung hoch-affiner SU11248 Kinasetargets, konnte gezeigt werden, dass Zielproteine, wie ROS1, NME4, BMP2K, NEK9, TBK1 und FAK, eine essentielle Rolle bei der Wirkung von SU11248 in Krebszelllinien haben. Ihre Expression und zelluläre biologische Relevanz korreliert mit der Aktivität des Inhibitors. Sie könnten als `Marker of Responsiveness` in der Klinik zur Diagnose der Wirkeffizienz von SU11248 in Tumoren eines bestimmten genetischen Hintergrundes verwendet werden.

Ein Vergleich der zellweiten Proteinexpression in SU11248 sensitiven und weniger reaktiven Krebszellen, ergab, dass Zelllinien, welche hochempfindlich auf SU11248 reagieren, einen mesenchymalen Zellcharakter haben, mit hoher Vimentin Expression, wohingegen, weniger reaktive Zellen, einen epithelialen Zelltyp aufweisen, gekennzeichnet durch ein starke E-Cadherin Expression. Die Expression dieser beiden Proteine

könnte in der Zukunft als schneller Bioindikator für die Charakterisierung der SU11248 Reaktivität von Tumoren und somit zur Vorhersage der Wirksamkeit einer SU11248 Therapie im Patienten genutzt werden.

Zusammenfassend zeigt die in dieser Arbeit durchgeführte umfassende Charakterisierung des niedermolekularen Inhibitors SU11248, seine krebstypübergreifende starke anti-tumorigene Wirkung, basierend auf einem breiten zellulären Targetspektrum, welches in die Regelung verschiedenster krebsrelevanter zellulärer Prozesse, wie Proliferation, Migration, Invasion und Überleben sowie Homöostase im Allgemeinen, involviert ist. Durch die gezeigte Relevanz bestimmter hoch-affiner Kinasetargets und die Zelltypcharakterisierung basierend auf den Proteinen Vimentin und E-Cadherin, konnten Biomarker zur Charakterisierung der SU11248 Wirksamkeit gefunden werden.

4 Introduction

4.1 Cancer

Cancer is the second frequent cause of human death in the world with 11 million new incidences every year. It is responsible for one in eight deaths worldwide. There are more than 100 distinct types of cancer originating from most of the cell types and organs throughout the human body. Cancer is characterized by relatively unrestrained proliferation of cells escaping from apoptosis that can invade beyond normal tissue boundaries and metastasize to distant organs. Cancer types can be grouped into broader categories. The main categories of cancer include carcinoma (cancer that originates in the skin or in tissues that line or cover internal organs), sarcoma (cancer that originates in bone, cartilage, fat, muscle, blood vessels, or other connective or supportive tissue), leukemia (cancer that starts in blood-forming tissue such as the bone marrow and causes large numbers of abnormal blood cells to be produced and enter the blood), lymphoma and myeloma (cancers that originates in the cells of the immune system) and cancers of the central nervous system (cancers that originate in the tissues of the brain and spinal cord). Not all tumors are cancerous. They can be classified in benign or malignant tumors with the following definition: Benign tumors aren't cancerous. They can often be removed, and, in most cases, they do not come back. Cells in benign tumors do not spread to other parts of the body whereas malignant tumors are cancerous. Cells in these tumors can invade nearby tissues and spread to other parts of the body and form metastases.

4.1.1 The hallmarks of cancer

After a quarter century of rapid advances in cancer research, cancer is revealed to be a disease involving spontaneous changes of the genome. Mutations have been discovered that produce oncogenes with dominant gain of function and tumor suppressor genes with recessive loss of function. Both classes of cancer genes have been identified through their alteration in human and animal cancer cells. Tumorigenesis in humans is a multi-step process with genetic alterations that drive the progressive transformation of normal human cells into highly malignant derivates. Many types of cancer are diagnosed in the human population with an age-dependent incidence implicating four to seven rate-limiting, stochastic mutagenic events (Renan, 1993). Pathological analyses of a number of organ sites in 1954, revealed already lesions that appear to represent the intermediate steps in a process through which cells evolve progressively from normalcy via a series of premalignant states into invasive cancers (Foulds, 1951; Foulds, 1954). These observations have been affirmed and rendered more concrete by a large body of work. The genomes of tumor cells are invariably altered at multiple sites, e.g. point mutations or changes in the chromosome complement (Kinzler and Vogelstein, 1996). The alterations can be divided into four major categories and are shown in Figure 1. Subtle sequence changes which involve base substitutions or deletions or insertions of a few nucleotides, alterations in chromosome numbers, chromosome translocations and gene amplifications (Lengauer et al., 1998). Taken together, observations of human cancers and animal models argue that tumor development proceeds via a process formally analogous to Darwinian evolution, in which a succession of genetic changes,

each confirming one or another type of selective advantage, leads to the progressive conversion of normal human cells into cancer cells (Cahill et al., 1999).

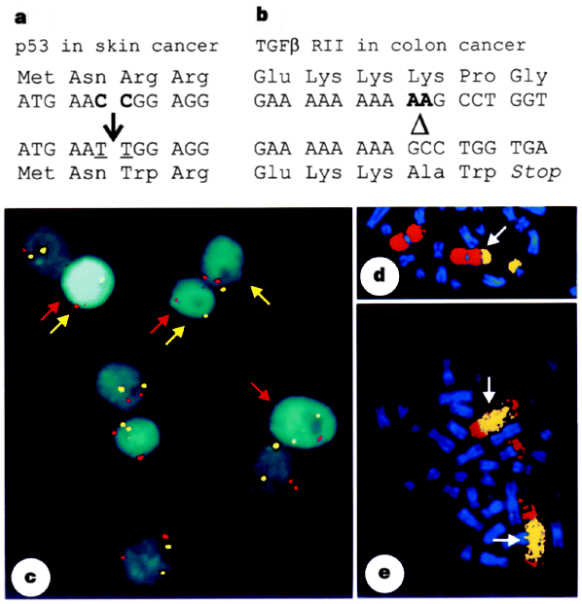

Figure 1 a, **b)** Subtle sequence alterations: **a**) mutation at a dipyrimidine site (bold letters) of the *p53* gene (codons 247–248) found in a xeroderma pigmentosum patient with a defect in nucleotide-excision repair (NER) (Williams et al., 1998); **b**) a two-base deletion located within a sequence of ten repeating adenines of the transforming growth factor- β receptor II (TGF β RII) gene (codons 125–128) in a colorectal cancer cell line with mismatch-repair (MMR) deficiency (Markowitz et al., 1995). **c)** Gross chromosomal change. Loss of chromosomes 3 (red arrows) and 12 (yellow arrows) in colorectal cancer (CRC) cells. A clone of the CRC cell line SW837 was expanded through 25 generations before fluorescence *in situ* hybridization (FISH). Interphase nuclei were hybridized with labelled centromeric DNA probes specific for chromosome 3 (red spots) and chromosome 12 (yellow spots). The number of signals detected in SW837 cells was diverse, indicating CIN; normal cells, as well as cancer cells exhibiting microsatellite instability (MIN), had two red and two yellow signals in nearly every nucleus (Lengauer et al., 1997). **d)** Chromosome translocation. A metaphase plate of the neuroblastoma cell line GIMEN was hybridized by FISH with labelled whole-chromosome-painting probes specific for chromosome 1 (red) and chromosome 17 (yellow), revealing a t(1;17) translocation (arrow). **e)** Gene amplification. FISH with a N-*myc* probe (yellow) and a whole-chromosome-painting probe specific for chromosome 1 (red) revealed an area of N-*myc* amplification (arrow) within the derivative chromosomes 1 of the neuroblastoma cell line Kelly.

There are more than 100 distinct types of cancer, and subtypes of tumors can be found within specific organs. Weinberg and Hanahan suggested that the vast catalogue of cancer cell genotypes is a manifestation of essential alterations in cell physiology that collectively dictate malignant growth (Hanahan and Weinberg, 2000). The major characteristics are self-sufficiency in growth signals, insensitivity to growth-inhibitory (antigrowth) signals, evasion of programmed cell death (apoptosis), limitless replicative potential, sustained angiogenesis, and tissue invasion and metastasis (Figure 2). The most important characteristic of cancer cells however, that is not considered by Weinberg and Hanahan, is the instability of the cancer genome that allows cancer progression.

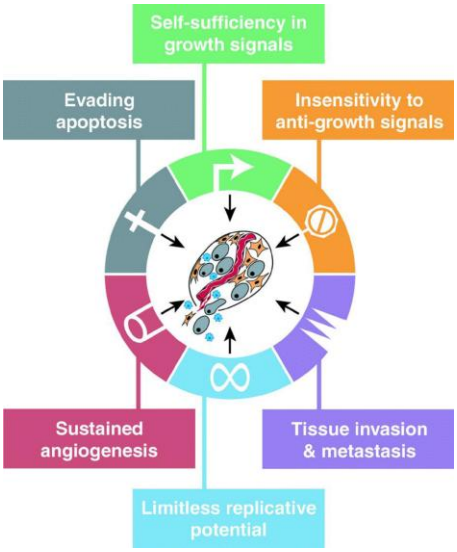

Figure 2 Acquired capabilities of cancer (image from (Hanahan and Weinberg, 2000)).

These capabilities are shared in common by most perhaps all types of human tumors. Nevertheless, the paths that cells take on their way to become malignant are highly variable. Parallel Pathways of tumorigenesis are shown in Figure 3. Within a given cancer type, mutations of particular target genes such as ras or p53 may be found in only a subset of otherwise histologically identical tumors. Further, mutations in certain oncogenes and tumor suppressor genes can occur early or late in tumor progression pathways. As a consequence, the acquisition of biological capabilities such as resistance to apoptosis, sustained angiogenesis, and unlimited replicative potential can appear at different times during these various progressions. Accordingly, the particular sequence in which capabilities are acquired can vary widely, both among tumors of the same type and certainly between tumors of different types. Nonetheless, independent of how the steps in these genetic pathways are arranged, the biological endpoints that are ultimately reached, namely malignant progression stages, are shared by all types of tumors.

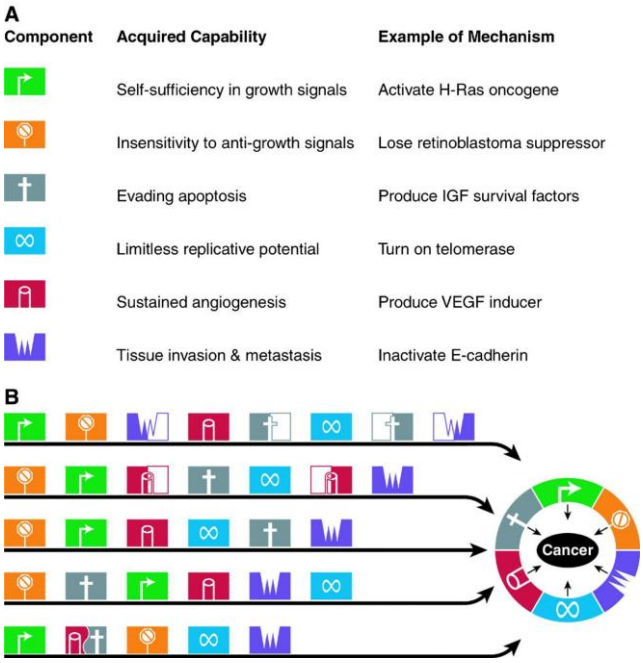

Figure 3 Parallel pathways of tumorigenesis. All cancers must acquire the same six hallmark capabilities (**A**), their means of doing so will vary significantly, both mechanistically and chronologically (**B**). Thus, the order in which these capabilities are acquired seems likely be quite variable across the spectrum of cancer types and subtypes. Moreover, in some tumors, a particular genetic lesion may confer several capabilities simultaneously, decreasing the number of distinct mutational steps required to complete tumorigenesis. Thus, loss of function of the p53 tumor suppressor can facilitate both angiogenesis and resistance to apoptosis (e.g., in the five-step pathway shown), as well as enabling the characteristic of genomic instability. In other tumors, a capability may only be acquired through the collaboration of two or more distinct genetic changes, thereby increasing the total number necessary for completion of tumor progression. Thus, in the eight-step pathway shown, invasion/metastasis and resistance to apoptosis are each acquired in two steps (image from (Hanahan and Weinberg, 2000)).

4.2 Protein kinases and cancer

Protein kinases are a family of enzymes that catalyze the transfer of the gamma phosphate groups from ATP to serine, threonine or tyrosine hydroxyl group in target protein substrates (Edelman et al., 1987; Fantl et al., 1993; Yarden and Ullrich, 1988). This process, which is reversed by specific phosphatases, serves as an activation step in many signaling cascades and in turn induces a whole series of subsequent cellular responses. In the human kinome, there are over 500 genes encoding protein kinases (Manning et al., 2002) with at least 30% of the human proteome being phosphorylated by protein kinases (Cohen, 2001). The reversible phosphorylation of proteins regulates almost all aspects of cell life, while abnormal phosphorylation is a cause or consequence of many diseases. Mutations in particular protein kinases and phosphatases give rise to a number of disorders and many naturally occurring toxins and pathogens exert their effects by altering the phosphorylation states of intracellular proteins. A number of diseases that result from mutations in particular protein kinases and phosphatases are listed in Table 1(Cohen, 2001).

Table 1 Diseases caused by mutations in particular protein kinases and phosphatises (Cohen, 2001)

Disease	Kinase/phosphatase
Myotonic muscular dystrophy	Myotonin protein kinase
X-Linked agammaglobulinaemia	Bruton tyrosine kinase
Hirschsprungís disease	Ret2 kinase
Autosomal recessive SCID	Zap70 kinase
X-Linked SCID	Jak3 kinase
Chraniosynostosis	FGF receptor kinase
Papillary renal cancer	Met receptor kinase
Chronic myelomonocytic leukaemia	Tel-PDGF receptor kinase
Chronic myelogenous leukaemia	Abelson tyrosine kinase
Non-Hodgkins lymphona	Alk kinase
Peutz–Jeghers syndrome	Lkb1 kinase
Coffin–Lowry syndrome	MAPKAP-K1b (RSK-2)
Ataxia-telangiectasia	Atm kinase
Li–Fraumeni syndrome	Chk2 kinase
Williams syndrome	Lim kinase-1
Leprechaunism, diabetes	Insulin receptor kinase
Wolff–Parkinson–White syndrome	AMP activated kinase
Wolcott–Rallison syndrome	eIF2A-kinase 3
X-Linked myotubular myopathy	MTM1 Tyr phosphatase

Already in 1980, Hunter and co-workers defined the relative amounts of protein-derived phosphoamino acids and found a distribution of 0.05%, 10% and 90% for phosphotyrosine (pY), phosphothreonine (pT) and phosphoserine (pS) under physiological cell conditions, respectively (Hunter and Sefton, 1980). Recently these observations could be verified in a global phosphoproteomic analysis by Olsen *et al.*, who identified more than 2000 phosphorylated proteins in HeLa cells containing 103 pY (1.8%), 670 pT (11.8%) and 4901 pS (86.4%) sites (Olsen et al., 2006). Even though tyrosine phosphorylation accounts only for a small part of total protein phosphorylation, it has been shown to be a key regulatory mechanism of many different cellular processes such as proliferation, differentiation, survival, control of cell shape and migration in virtually all major organs (Hunter, 1998). In general protein phosphorylation controls many cellular processes, especially those involved in intercellular communication and coordination of complex functions.

These data indicate that kinases exert pervasive effects on human physiology and pathophysiology. Kinases serve central roles in mediating the biological action of many extracellular stimuli such as hormones and growth factors being important for cell communication and to ensure the homeostasis of organs and tissues.

Most kinases consist of at least two domains- a catalytic domain which serves to bind and phosphorylate target proteins, and a regulatory region that interacts directly with ancillary proteins that allosterically modulate activity of the catalytic domain (Hubbard, 2002; Superti-Furga and Courtneidge, 1995). Because of their substrate recognition sites, kinases are divided into two major classes- tyrosine kinases (TKs) and serine/threonine kinases (STKs) (Edelman et al., 1987; Ullrich and Schlessinger, 1990; Yarden and Ullrich, 1988). In humans, over 100 genes encode protein TKs, many of which are soluble, intracellular proteins, although others act as cell surface receptors such as epidermal growth factor receptor (EGFR) and platelet-derived growth factor receptor (PDGFR). 58 encode transmembrane receptor protein tyrosine kinases (RPTKs) distributed into 20 subfamilies, and 32 encode cytoplasmic, non-receptor protein tyrosine kinases in 10 subfamilies (Manning et al., 2002; Robinson et al., 2000). Human receptor and non-receptor protein tyrosine kinases are shown in Figure 4 A and B, respectively.

A

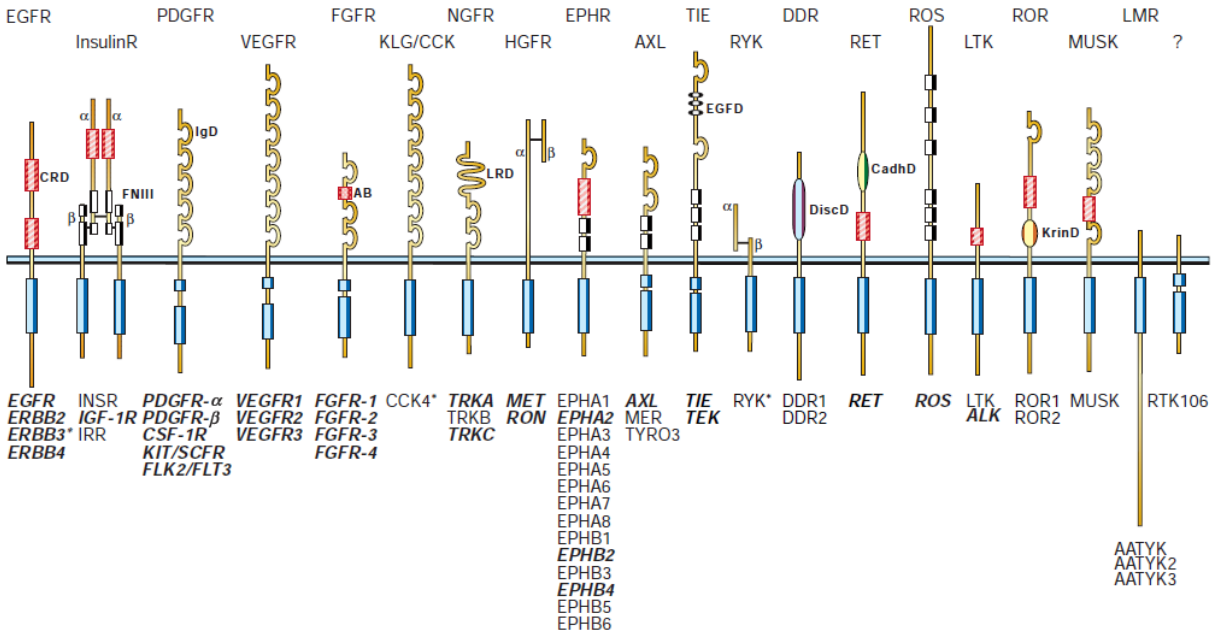

B

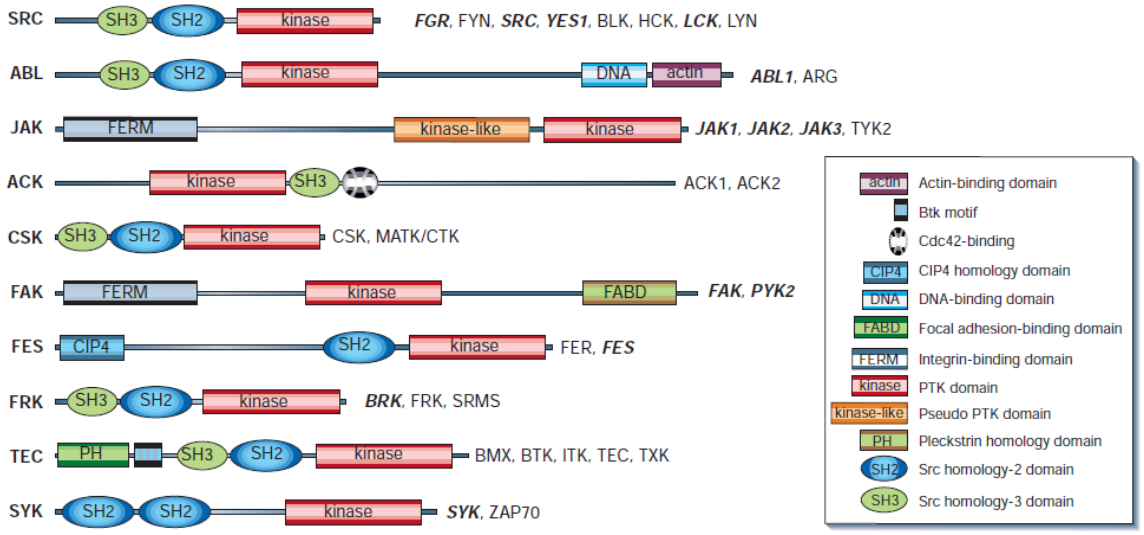

Figure 4 (A) The prototypic receptor for each family is indicated above the receptor, and the known members are listed below. Abbreviations of the prototypic receptors: EGFR, epidermal growth factor receptor; InsR, insulin receptor; PDGFR, platelet-derived growth factor receptor; VEGFR; vascular endothelial growth factor receptor; FGFR, fibroblast growth factor receptor; KLG/CCK, colon carcinoma kinase; NGFR, nerve growth factor receptor; HGFR, hepatocyte growth factor receptor, EphR, ephrin receptor; Axl, a Tyro3 PTK; TIE, tyrosine kinase receptor in endothelial cells; RYK, receptor related to tyrosine kinases; DDR, discoidin domain receptor; Ret, rearranged during transfection; ROS, RPTK expressed in some epithelial cell types; LTK, leukocyte tyrosine kinase; ROR, receptor orphan; MuSK, muscle-specific kinase; LMR, Lemur. Other abbreviations: AB, acidic box; CadhD, cadherin-like domain; CRD, cysteine-rich domain; DiscD, discoidin-like domain; EGFD, epidermal growth factor-like domain; FNIII, fibronectin type III-like domain; IgD, immunoglobulin-like domain; KrinD, kringle-like domain; LRD, leucine-rich domain. The symbols α and β denote distinct RPTK subunits. RPTK members in bold and italic type are implicated in human malignancies (see Table 2). An asterisk indicates that the member is devoid of intrinsic kinase activity. **(B)** The family members are indicated to the right and the family name to the left of each PTK. The PTK members in bold and italic type are implicated in human malignancies (image from (Blume-Jensen and Hunter, 2001).

Activation of receptor TKs (RTKs) catalyzes phosphorylation of a range of cellular pathways controlling cell proliferation, differentiation and survival. Moreover, when RTKs bind their activating ligand they also catalyze autophosphorylation of their receptor domains, resulting in sustained receptor activation. The protein kinase activation mechanism after ligand binding is illustrated in Figure 5.

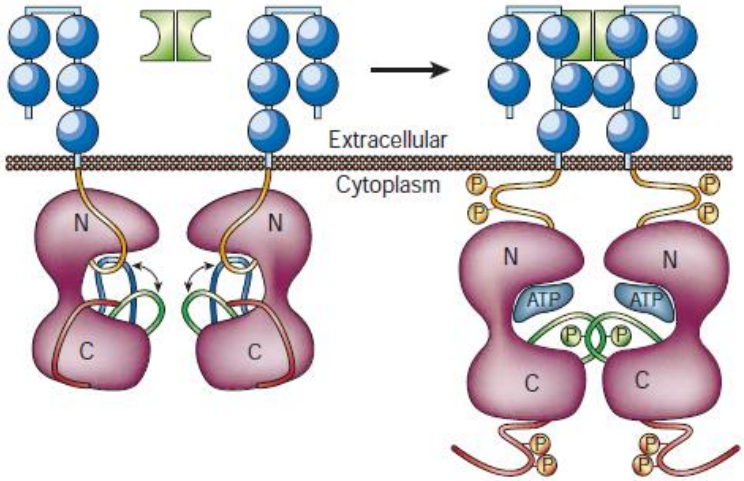

Figure 5 Receptor protein tyrosine kinase (RPTK) activation. Left: RPTK kinase activity is tightly repressed in the unstimulated state. The activation and catalytic loops exist in an equilibrium between a substrate-precluding (blue) and substrate-accessible (green) conformation. In addition, the juxtamembrane region (orange) and C-terminal region (red) might interfere with the conformation of the N-terminal kinase lobe ('N') and/or substrate access. Right: ligand-induced receptor dimerization and tyrosine autophosphorylation result in relief of the inhibitory constraints exerted by the activation loop, and the juxtamembrane and C-terminal regions (image from (Blume-Jensen and Hunter, 2001).

Such constitutive activity is particularly important in the regulation of cellular homeostasis, e.g. cell proliferation, with the corollary being that its dysregulation is implicated in many cancer etiologies. Abnormalities in kinase activity, due to either changes in expression level or mutations in the protein sequence have been responsible in many disease pathologies and in the human genome, over 250 protein kinase genes map to disease loci (Knuutila et al., 1998). Many cancers are caused by kinase mutations, including chronic myelogenous leukemia (Abelson TK), chronic myelomonocytic leukemia (Tel-platelet-derived growth factor receptor kinase), papillary renal cancer (Met receptor kinase) and non-Hodgkin`s lymphoma (Alk kinase) (Noble et al., 2004). So far, >100 dominant oncogenes are known of which protein kinases, in particular protein tyrosine kinases, comprise the largest group. Examples of dominant protein tyrosine kinase oncogenes are listed in Table 2.

Table 2 Examples of dominant protein tyrosine kinase oncogenes (Blume-Jensen and Hunter, 2001)

PTK (proto-oncogene)	Viral oncogene* (viral oncoprotein)	Oncogenic alteration	Tumour/cancer types (only the most frequent, mainly human types are described)
EGFR/ErbB1 (c-*erb*B)	v-*erb*B from AEV ($p68/74^{erbB}$)	v-*erb*B: Truncated EGFR PTK c-*erb*B: Overexpression (amplification) Extracellular domain deletions	v-ErbB: fibrosarcomas c-ErbB: mammary carcinoma, glioblastoma multiforme, ovarian, non-small-cell lung and other cancers
ErbB2/HER2/Neu		Overexpression (amplification) No recurrent human mutations (Val664Glu in rodents)	Mammary, ovarian, gastric, non-small-cell lung and colon cancer
ErbB3/HER3		Overexpression; constitutive tyrosine phosphorylation (heterodimer with ErbB2)	Mammary carcinoma
ErbB4/HER4		Overexpression	Mammary carcinoma, granulosa cell tumours
IGF-1R		Overexpression (expression required for *in vitro* transformation by many oncogenes and DNA viruses)	Cervical and other carcinomas, sarcomas
PDGFR-α		Overexpression (amplification)	Glioma, glioblastoma, ovarian carcinoma
PDGFR-β		Tel-PDGR-β (t(5; 12) translocation fusing Ets-like Tel with PDGFR-β PTK domain) Overexpression	Tel-PDGFR-β: chronic myelomonocytic leukaemia PDGFR-β: glioma
CSF-1R (c-*fms*)	v-*fms* from FeSV ($p170^{gag\text{-}fms}$)	v-*fms*: Truncated CSF-1R PTK with mutant C-terminal tail Constitutively active c-*fms*: GOF point mutations Overexpression	v-*fms*: feline sarcomas c-*fms*: acute and chronic myelomonocytic leukaemias, monocytic tumours, malignant histiocytosis, endometrial cancer, glioma
Kit/SCFR (c-*kit*)	v-*kit* from FeSV ($p80^{gag\text{-}kit}$)	v-*kit*: Truncated Kit/SCFR PTK with mutant C-terminal tail Constitutively active c-*kit*: GOF point mutations and small deletions Overexpression	v-*kit*: feline fibrosarcomas c-*kit*: malignant gastrointestinal stromal tumours, acute myeloid leukaemias, myelodysplastic syndromes, mast-cell leukaemia/systemic mastocytosis, seminomas/dysgerminomas, small-cell lung cancer and other carcinomas
Flk2/Flt3		Overexpression Internal tandem gene duplications in JM region	Haematopoietic malignancies
Flt1/VEGFR1		Expression	Tumour angiogenesis
Flk1/VEGFR2		Expression	Tumour angiogenesis
Flt4/VEGFR3		Overexpression	Tumour angiogenesis; vascular tumours (Kaposi's sarcoma, haemangiosarcoma, lymphangiosarcomas)
FGFR1		ZNF198-FGFR1 (t(8; 13) translocation fusing a novel Zn finger protein with the FGFR1 PTK domain) Overexpression Point mutations	ZNF198-FGFR1: acute myelogenous leukaemia (8p11 myeloproliferative syndrome), lymphomas Overexpression: various tumours Point mutations: autosomal skeletal disorders/dysplasias
FGFR2/K-SAM		Overexpression (amplification) and C-terminal truncation	Gastric carcinoma (mammary, prostate carcinomas)
FGFR3		IgH locus/MMSET translocation (t(4; 14) translocation placing FGFR3 PTK downstream of IgH/MMSET). Additional activating FGFR3 point mutations in skeletal dysplasias	Multiple myelomas (achondroplasia, thanatophoric dysplasia and hypochondroplasia)
FGFR4		Overexpression (amplification)	Mammary, ovarian carcinomas
TrkA		Tropomyosin(Tpm)-TrkA (t(1; 1) with N-terminal Tpm sequence fused to TrkA PTK) Tpr-TrkA (t(1; 1) with N-terminal Tpr sequence fused to TrkA PTK) Tfg-TrkA (t(1; 3) with N-terminal Tfg sequence fused to TrkA PTK domain)	Papillary thyroid carcinomas, neuroblastomas
TrkC		Tel-TrkC (t(12; 15) with H-L-H domain of Tel fused to TrkC PTK domain)	Congenital fibrosarcoma, acute myeloid leukaemias
HGFR (c-*met*)		Tpr-Met (t(1; 7) with N-terminal of Tpr fused to Met PTK domain) Overexpression GOF point mutations	Tpr-Met: Papillary thyroid carcinomas Overexpression: rhabdomyosarcoma, hepatocellular carcinoma GOF point mutations: renal carcinoma
RON		Overexpression/increased kinase activity of splice variants	Colon cancer, hepatocellular cancer
EphA2		Overexpression	Metastasizing malignant melanomas
EphB2		Overexpression	Gastric, oesophageal and colon carcinomas
EphB4		Overexpression	Infiltrating ductal mammary carcinomas
Axl		Overexpression	Acute myeloid leukaemias
TIE/TIE1		Overexpression	Capillary haemangioblastomas, haemangiopericytomas, gastric adenocarcinoma
Tek/TIE2		Expression	Tumour angiogenesis (endothelium)
Ret		Fusions: H4-Ret (PTC1), inversion; Rlα-Ret (PTC2), t(10; 17); ELE1-Ret (PTC3 & PTC4), inversion; RFG5-Ret (PTC5), inversion; HTIF1-Ret (PTC6), t(7; 10); RFG7-Ret (PTC7), t(1; 10); KTN1-Ret (PTC8), t(10; 14); ELKS-Ret, t(10; 12) GOF point mutations: primarily in MEN2A, MEN2B and FMTC (familial), but also in a few sporadic cases	PTCs and ELKS-RET: papillary thyroid carcinomas (5–30% of spontaneous carcinomas, 60–70% of radiation-induced carcinomas (Chernobyl accident) MEN2A: medullary thyroid carcinoma, parathyroid hyperplasia, pheochromocytoma MEN2B: medullary thyroid carcinoma, pheochromocytoma and enteric mucosal ganglioneuromas. FMTC: medullary thyroid carcinoma

PTK (proto-oncogene)	Viral oncogene* (viral oncoprotein)	Oncogenic alteration	Tumour/cancer types (only the most frequent, mainly human types are described)
ROS (c-*ros*)	v-*ros* from avian UR2 SV ($p68^{gag\text{-}ros}$)	v-*ros*: Truncated Ros PTK domain. Constitutively active c-*ros*: Overexpression Rare truncations/point mutations?	v-*ros*: avian fibrosarcomas c-*ros*: glioblastomas, astrocytomas
Alk		NPM-Alk (t(2; 5) nucleophosmin fused to Alk PTK domain) Igλ-Alk (t(2; 22) Igλ fused to Alk PTK domain) Other sporadic fusions with tropomyosin, etc.	Non-Hodgkin lymphomas, $CD30^+$ and $CD30^-$ anaplastic large-cell lymphoma
Src (c-*src*)	v-*src* from RSV ($pp60^{v\text{-}src}$)	v-*src*: C-terminal truncation and point mutations (increased kinase activity) c-*src*: C-terminal truncation (increased kinase activity) Overexpression and/or increased kinase activity	$pp60^{v\text{-}src}$: avian sarcomas c-Src truncation: colon cancer c-Src overexpression: mammary and pancreatic cancers, neuroblastomas, others
Fgr (c-*fgr*)	v-*fgr* from FeSV ($p70^{gag\text{-}fgr}$)	v-*fgr*: C-terminal truncated c-*fgr* and point mutations (increased kinase activity)	$p70^{gag\text{-}fgr}$: feline fibrosarcomas c-Fgr: acute myeloblastic leukaemias, chronic lymphocytic leukaemias, EBV-infected lymphomas; differentiation marker?
Yes (c-*yes*)	v-*yes* from ASV ($p90^{gag\text{-}yes}$)	v-*yes*: C-terminal truncated c-*yes* and point mutations (increased kinase activity) Over expression and/or increased kinase activity	$p90^{gag\text{-}yes}$: avian sarcomas c-Yes: colon carcinomas, malignant melanomas, other cancers
Lck		TCRβ-Lck (t(1; 7) T-cell receptor-β upstream of Lck causes overexpression) Overexpression GOF point mutations	TCRβ-Lck: T-cell acute lymphocytic leukaemias Lck: chronic lymphocytic leukaemias?
Abl (c-*abl*)	v-*abl* from Abelson MLV ($p160^{gag\text{-}abl}$) or from PI-FeSV	v-*abl*: N-terminal (ΔSH3) truncation of Abl Fusions: $p190^{Bcr\text{-}Abl}$, (t(9; 22) m-*bcr*); $p210^{Bcr\text{-}Abl}$, (t(9; 22) M-*bcr*); $p230^{Bcr\text{-}Abl}$, (t(9; 22) μ-*bcr*. M-, m- and μ-*bcr*: 3 breakpoint cluster regions in *BCR*. The chimaeric mRNA usually starts with exon a2 of *ABL*, it never includes exon 1a or 1b. Tel-Abl (t(12; 22) N-terminal (H-L-H region) of Tel fused with Abl exon 2a	$p160^{gag\text{-}abl}$: murine acute leukaemias $p190^{Bcr\text{-}Abl}$: ~50% of Ph^+ acute lymphocytic leukaemias, rarely chronic myelomonocytic leukaemias $p210^{Bcr\text{-}Abl}$: chronic myeloid leukaemias, ~30% of Ph^+ acute lymphocytic leukaemias $p230^{Bcr\text{-}Abl}$: some Ph^+ chronic neutrophilic leukaemias Tel-Abl: rare cases of acute lymphocytic leukaemias
Arg		Tel-Arg (t(1; 12))	Acute myeloid leukaemias (rare in M3 and M4Eo subtypes)
Jak1		Overexpression	Various leukaemias
Jak2		Tel-Jak2 (t(9; 12) H-L-H region (N-terminal) of Tel fused with kinase region (C-terminal) of Jak2)	T-cell childhood acute lymphocytic leukaemias, acute myeloid leukaemias, acute lymphocytic leukaemias, atypical chronic myeloid leukaemias
Jak3		Overexpression (increased kinase activity)	Various leukaemias and B-cell malignancies
Fak		Overexpression and/or altered tyrosine kinase activity	Modulation of adhesion, invasion and metastasis of diverse malignancies
Pyk2		Overexpression and/or altered tyrosine kinase activity	Modulation of adhesion, invasion and metastasis of diverse malignancies
Fes (c-*fes*)	v-*fps* from ASV; v-*fes* from FeSV ($p130$ and $p140^{gag\text{-}fps}$; $p135$ and $p140^{gag\text{-}fes}$)	The viral *gag* sequence essential for transforming activity. Viral *gag* fused to slightly truncated and/or point mutated *fps* or *fes*	$p130$ and $p140^{gag\text{-}fps}$: diverse avian sarcomas and myeloid leukaemias $p135$ and $p140^{gag\text{-}fes}$: feline sarcomas c-Fes: no implication in cancers
Brk		Overexpression (increased kinase activity)	Mammary carcinomas
Syk		Downregulation (recessive?)	Potential mammary carcinoma tumour suppressor; PTK-dependent?

Since kinases regulate cell growth, differentiation and proliferation, abnormal functioning leads to uncontrolled growth, neoplasias or metastasis, and ultimately cancer. Many of the processes involved in tumor growth, progression and metastasis are mediated by signaling molecules acting downstream of activated RTKs. An overview of signaling pathways involved in key processes such as cancer cell survival are given in Figure 6 (Klein et al., 2005). In particular, several members of the split kinase domain superfamily of RTKs are expressed on solid tumor cells and participate in autocrine loops implicated in cancer growth and survival (e.g. VEGF receptors in melanoma, PDGF receptors in gliomas, KIT in small cell lung cancer and FLT3 in acute myelogenous leukemia).

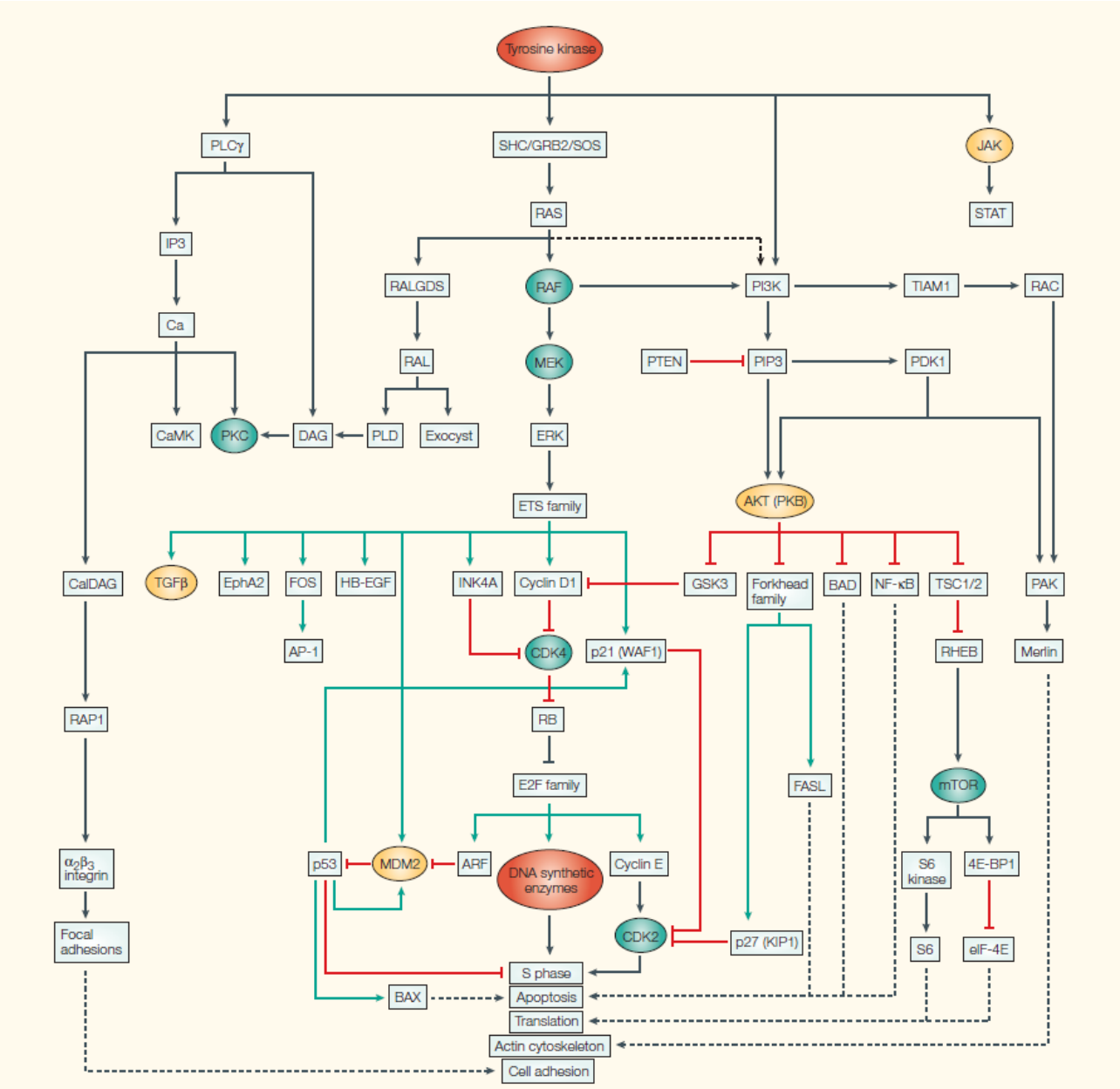

Figure 6 Activation of cell signaling by a selected repertoire of protein tyrosine and serine/threonine kinases is the hallmark of many cancers. Green arrows denote direct transcriptional targets. Red lines show direct inhibitory pathways. Black arrows show direct activation events, and dashed arrows show events that are either indirect or questionable. 4E-BP1, eukaryotic translation initiation factor 4E (eIF4E)-binding protein 1; Ca, calcium; CalDAG, calcium- and diacylglycerol-regulated guanine nucleotide exchange factor; CaMK, calcium/calmodulin-dependent protein kinase; CDK, cyclin-dependent kinase; DAG, diacylglycerol; EphA2, ephrin receptor A2; ERK, extracellular signal-regulated kinase; FASL, FAS ligand; GRB2, growth-factor-receptor-bound protein 2; GSK3, glycogen synthase kinase 3; HB-EGF, heparin-binding epidermal growth factor; IP3, inositol 3,4,5 triphosphate; JAK, Janus kinase; MEK, mitogen-activated protein kinase/ERK kinase; mTOR, mammalian target of rapamycin; NF-κB, nuclear factor-κB; PAK, p21-activated kinase; PDK1, 3-phosphoinositide-dependent protein kinase 1; PI3K, phosphatidylinositol 3-kinase; PIP3, phosphatidylinositol 3,4,5-triphosphate; PKB, protein kinase B; PKC, protein kinase C; PLC γ, phospholipase C γ; PLD, phospholipase D; RAL, RAS-related protein; RALGDS, RAL guanine nucleotide dissociation stimulator; RB, retinoblastoma; RHEB, RAS homolog enriched in brain; STAT, signal transducer and activator of transcription; TGF β, transforming growth factor-β; TIAM1, T-cell lymphoma invasion and metastasis 1; TSC, tuberous sclerosis complex (image from (Klein et al., 2005).

The role of tyrosine kinases in cancer etiology was initially suggested by the observation that viral oncogenes express constitutively active protein kinases. In 1978, Ray Erikson found that the transforming factor of the Rous sarcoma virus (v-Src) was a protein kinase (Collett and Erikson, 1978). Already two years earlier, the Nobel laureates Michael Bishop and Harold Varmus described the first link of protein tyrosine phosphorylation with cancer. They found that the Rous sarcoma virus oncogene product is of cellular origin

and speculated that deregulation of this oncogene could lead to cancer (Stehelin, 1976). This was confirmed in 1980 by the finding that v-Src is a protein tyrosine kinase (Hunter, 1980; Hunter and Sefton, 1980). The breakthrough discovery of Bishop and Varmus that cancer-inducing genes of animal retroviruses such as v-Src and v-Ras represent mutated host genes that were recombined into the viral genome raised the question of whether the oncogenes concept was also relevant to human cancer (Varmus and Bishop, 1986). The first cloning and sequence analysis of a cDNA encoding a cell surface protein, the human EGF receptor by Axel Ullrich in 1984, provided a partial answer to this question by revealing a close relationship with the v-erbB oncogenes (Downward et al., 1984; Ullrich et al., 1984). This first connection between a human gene product that regulates normal cell proliferation and a viral oncogene strongly suggested that human cancer development may also involve abnormalities in the expression and structure of endogenous genes that have regulatory roles in cell proliferation. A search for such genetic aberrations in tumor tissues using cDNA probes of EGFR and an EGFR-related gene, termed HER2 (human EGFR-related gene), resulted in the discovery that the gene encoding the HER2/neu receptor-like tyrosine kinase is amplified up to 100-fold in tumors of about 30% of patients with invasive breast cancer. A significant clinical correlation was shown between HER2/neu gene amplification and overexpression and parameters of malignancy, including reduced survival and reduced time to relapse, relative to patients with normal receptor levels (Chazin et al., 1992; Slamon et al., 1987). Later it could be shown that EGFR expression is linked to activation of ErbB-2 in human breast cancers (DiGiovanna et al., 2005). Abnormalities in kinase activity have also been elucidated for many other protein tyrosine kinases such as BCR-ABL in chronic myeloid leukaemia (Van Etten, 2004), Ret/GDNFR in multiple endocrine neoplasia, Kit/SCFR in gastrointestinal stromal tumors and acute myeloid leukaemia, Met/HGFR in papillary thyroid carcinomas and Src in colon cancer (Blume-Jensen and Hunter, 2001).

4.3 Protein kinase inhibitors in targeted cancer therapy

Protein kinases mediate most of the signal transduction in eukaryotic cells; by modification of substrate activity, protein kinases also control many other cellular processes, including metabolism, transcription, cell cycle progression, cytoskeletal rearrangement and cell movement, apoptosis, and differentiation. Protein phosphorylation also plays a critical role in intercellular communication during development, in physiological responses and in homeostasis, and in the functioning of the nervous and immune systems. Protein kinases are among the largest families of genes in eukaryotes (Hunter, 1987; Lander et al., 2001). Mutations and dysregulation of protein kinases play causal roles in human diseases (Blume-Jensen and Hunter, 2001; Hunter, 2000).

As such, protein kinases are important targets in drug discovery aimed at treating many devastating diseases, including autoimmune disorders, diabetes, neurological disorders and cancer.

The idea that one could actually target protein kinases came up in the late 1980s with the discovery that rapamycin inhibits the protein kinase mTOR (mammalian target of rapamycin), a member of the phosphatidylinositide 3-kinase superfamily, which is required for interleukin-2-dependent T cell

proliferation. In the field of cancer, Herceptin, an anti-HER2 monoclonal antibody (trastuzumab), was the first genomic research-based, targeted anti-kinase therapeutic approved for cancer therapy (Fendly et al., 1990; Hudziak et al., 1989).

In general, protein kinase inhibitors can be divided into two functional groups, namely therapeutic antibodies (biologics) and small-molecule kinase inhibitors, respectively, both in clinical use for cancer-specific targeted therapies of a broad range of different tumor indications. A shortened list of clinically approved kinase-targeted oncology agents is provided in Table 3. Protein kinase inhibitors are a class of chemotherapy drugs. Drugs in this classification include: Axitinib, Bosutinib, Cediranib, Dasatinib, Erlotinib, Gefitinib, Imatinib, Lapatinib, Lestaurtinib, Nilotinib, Semaxanib, Sorefenib and Sunitinib. These drugs are prescribed by themselves or often in a treatment package (combination therapy) which includes protein kinase inhibitors along with other methods of treating cancer.

These inhibitors are commonly used in the treatment of cancers including: non-small-cell lung cancer (NSCLC), head and neck, colorectal, renal, prostate, breast, and primary brain cancer. This drug type has only been around since the 1980s, so some drugs are currently still in clinical trials while others are in current use.

Small-molecule inhibitors of tyrosine kinases compete with the ATP binding site of the catalytic domain of several oncogenic kinases with the kinase activation loop in the active (type 1 inhibitor) or inactive (type 2 inhibitor) conformation. They are orally active, have a favourable safety profile and can be easily combined with other forms of chemotherapy or radiation therapy. To date, approximately 80 inhibitors have been advanced to some stage of clinical evaluation.

Table 3 Clinically approved kinase-targeted oncology agents

Drug	Number	Known targets
Small molecules		
Imatinib (Gleevec)	STI-571	Abl, PDGFR, c-Kit
Gefitinib (Iressa)	ZD-1839	EGFR
Erlotinib (Tarceva)	OSI-774/CP358774	EGFR
Sorafenib (Nexavar)	BAY 43-9006	VEGFR, PDGFR, FLT3, c-Kit, B-raf, Raf-1
Sunitinib (Sutent)	SU11248	VEGFR, PDGFR, FLT3, c-Kit
Biologics		
Trastuzumab (Herceptin)	-	ErbB2 (HER-2/neu)
Cetuximab (Erbitux)	-	EGFR
Bevacizumab (Avastin)	-	VEGF

Agents included in the table are approved by the Food and Drug Administration for use in the United States. Abl, Abelson leukaemia virus; EGFR, epidermal growth factor receptor; PDGFR, platelet-derived growth factor receptor; VEGFR, vascular endothelial growth factor receptor.

In 1986 Umezawa and colleagues discovered the first inhibitor of the epidermal growth factor receptor tyrosine kinase (Umezawa et al., 1986). EGFR and additional PTK inhibitors were subsequently tested for

their ability to interfere with enzymatic PTK activity and to block cell proliferation and oncogenesis (Levitzki and Gazit, 1995).

A major success in the area of small-molecule protein kinase inhibitors was the tyrosine kinase inhibitor imatinib (Gleevec), a potent inhibitor of the constitutively active BCR-ABL fusion protein. This drug is approved for the treatment of leukemia and gastrointestinal stromal tumors (Druker, 2002; Druker et al., 2001; Druker et al., 1996; Noble et al., 2004). This was followed by other small-molecule drugs, such as the EGFR inhibitors erlotinib (Tarceva) and gefitinib (Iressa), both receiving approval for the treatment of non-small cell lung carcinoma (Barker et al., 2001; Bulgaru et al., 2003; Cohen et al., 2005; Comis, 2005; Perez-Soler, 2004). The critical role of angiogenesis in cancer was first proposed more than 30 years ago by Folkman (Folkman, 1971) and led to the development of the small-molecule kinase inhibitor sunitinib (SUTENT), inhibiting vascular endothelial growth factor and platelet-derived growth factor receptors. Angiogenesis is essential for tumors to grow beyond 1-2 mm^3 (Folkman, 1990), and switch from local vascular supply to novel microcapillary formation. It also allows tumor cells to enter the circulation, enabling the spread of cancer cells to multiple organs (metastasis). Angiogenesis correlates with tumor progression and disease severity, and is controlled by pro-angiogenic factors such as vascular endothelial growth factors (VEGFs) and platelet-derived growth factors (PDGFs). Sorafenib (Nexavar), a Raf kinase and VEGFR inhibitor, is a further prominent example of a small-molecule protein kinase inhibitor, approved for the treatment of renal cell carcinoma (RCC). Structures of some representative small molecule tyrosine kinase inhibitors used in cancer therapy are shown in Figure 7.

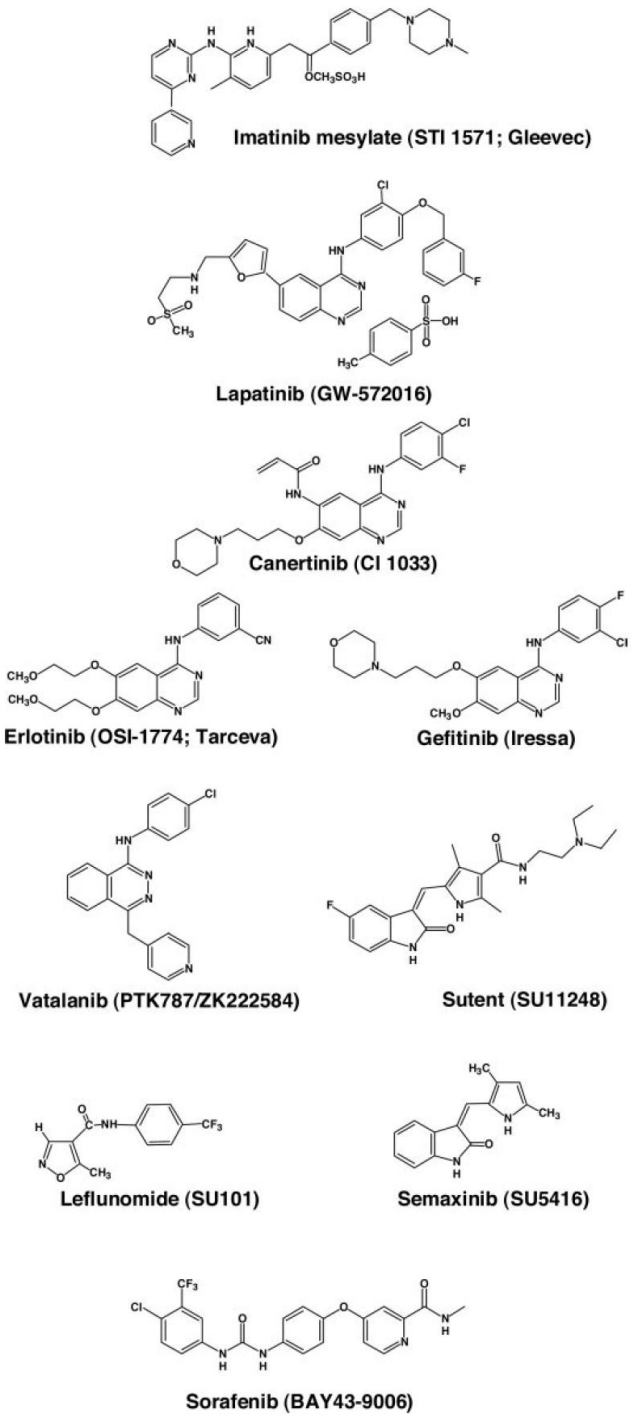

Figure 7 Structures of some representative small molecule tyrosine kinase inhibitors used in cancer therapy (image from (Arora and Scholar, 2005).

Kinase inhibitors are generally multi-targeted agents, such as erlotinib, gefitinib and imatinib, sorafenib, sunitinib, respectively. These drugs block several kinases to achieve a broader spectrum of activity thereby circumventing fast developing tumor resistances and addressing the complexity of solid tumors.

Taken together, kinase inhibitors represent a new paradigm in anti-cancer therapy (Faivre et al., 2006b).

4.3.1 Classes of small-molecule protein tyrosine kinase inhibitors

In the last few years, there has been significant progress in the development of small-molecule inhibitors for protein tyrosine kinases. They belong to different chemical groups and a summary of structural inhibitor classes is shown in Figure 8.

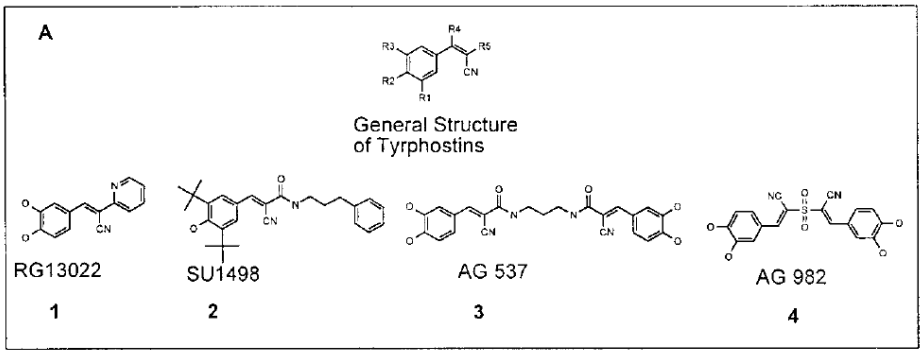

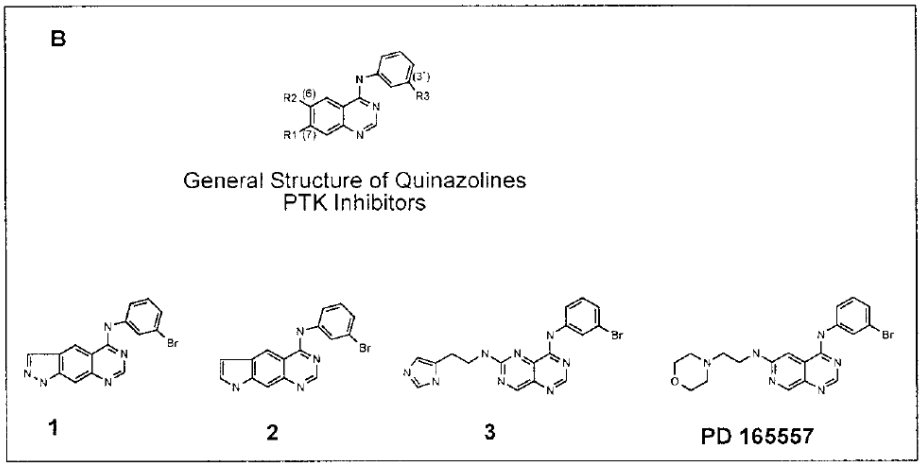

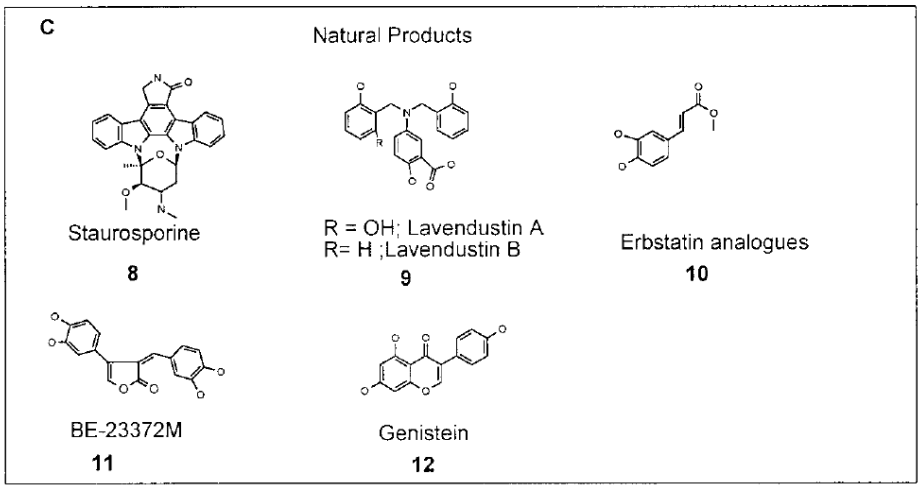

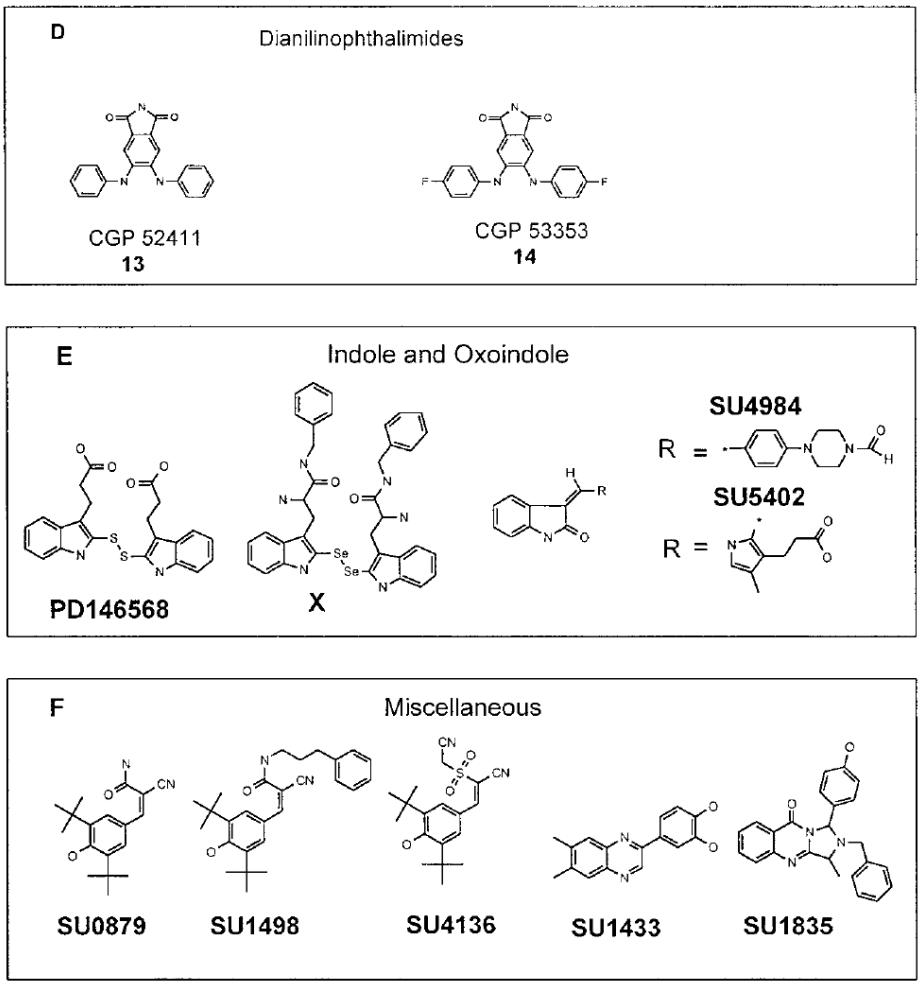

Figure 8 Chemical structures of representative small molecule tyrosine kinase inhibitors(image from (al-Obeidi et al., 1998).

The first step in the development of PTK inhibitors began soon after the recognition in the early 1980s that natural compounds, such as quercetin, erbstatin, genistein, and lavendustin A, inhibit the activities of PTKs such as Src and EGFR. Although these natural compounds have rather poor selectivity or mediocre potency, they served as lead compounds for the design and development of synthetic, more potent, and selective PTK inhibitors (**tyrphostins**) (Levitzki and Mishani, 2006). Tyrphostins (Figure 8 a) belong to the class of benzylidene malononitriles. Tyrphostins have been shown to be competitive inhibitor for PTKs at either or both ATP and substrate binding sites.

Quinazolines and **Pyridopyrimidines** (Figure 8 b). 4-anilinoquinazolinones are potent inhibitors of EGFR by competing at the ATP binding site. Expanding the bicyclic quinazoline inhibitors into tricyclic derivates resulted in the discovery of imidazolo-, pyrazolo-, and pyrroloquinazolines derivatives. However, the poor aqueous solubility of these tricyclic compounds led to the development of **pyrimidopyrimidines** with good water solubility.

Another class are **pyrrolopyrimidines**, a series of 4-(phenylamino)pyrolopyrimidines, which were reported to specifically inhibit the EGFR tyrosine kinase without activity against other kinases such as Src or PKA. **Dianilinophthalimides** are a unique class of PTK inhibitors. They were rationally designed and based on a natural product staurosporin aglycon.

Indoles and **Oxindoles** are tyrosine PTK inhibitors containing an indole moiety in their structure. Their antitumor activity was very low and as a consequence they were chemically modified resulting in PTK inhibitors containing an **oxindole** scaffold. This new class of inhibitors showed very low activity against the tyrosine kinase EGFR, but FGFR1 and other kinases.

4.3.2 Multi-targeted small-molecule protein kinase inhibitors

The multi-targeted approach has emerged as a new paradigm for novel kinase inhibitors. Such agents can simultaneously target the tumor and surrounding or supportive cells, as well as several single or intersecting pathways in a cancer cell, and thereby interact with the complex multi-molecular lesions that drive tumor growth and survival; more specific single-targeted agents are unlikely to have significant effects on cancer complexity, especially in solid tumors, were many different disease-driving proteins have been identified to regulate cancer cell transformation, proliferation and survival. Another advantage of the multi-targeted approach is that resistance- due to mutations, overexpression of key components of signaling pathways, drug-efflux systems and/or signaling bypass- is likely to arise with multi-targeted inhibitors. Although combinations of multiple kinase inhibitors have been investigated, the use of single multi-targeted agents offers the benefit of reducing the number of drugs a patient is required to take, decreasing the risk of drug-drug interactions and toxicity, and increasing the likelihood of compliance (Faivre et al., 2007).

4.4 Sunitinib malate

Sunitinib malate (SUTENT, SU11248 (named after **S**chlessinger and **U**llrich who created SUGEN, a biotech company later acquired by Pharmacia and subsequently Pfizer)) is an orally bio-available, oxindol, multi-targeted small molecule tyrosine kinase inhibitor with antitumor and antiangiogenic activities. Originally it was developed as an anti-angiogenesis inhibitor on the basis of the discovery by Millauer *et al.* (1994) that inhibition of Flk-1/VEGFR2 function in a mouse glioblastoma model prevented tumor growth. Subsequently it was developed into a multi-targeted kinase inhibitor with anti-angiogenic and anti-tumor activity. It has received approval from the US Food and Drug Administration (FDA) in two indications simultaneously in 2006: advanced metastatic renal cell carcinoma (mRCC) and gastrointestinal stromal tumors (GIST), in patients who are resistant or intolerant to the treatment with imatinib (Demetri et al., 2006; Motzer et al., 2007a; Motzer et al., 2007b; Motzer et al., 2006c). In 2007, Sunitinib was also approved by the European Union for these indications.

Sunitinib has been identified as a potent inhibitor of vascular endothelial growth factor receptors (VEGFR) (types 1-3), fetal liver tyrosine kinase receptor 3 (FLT3), KIT (stem cell factor [SCF] receptor), platelet-derived growth factor receptor (PDGFR) (types α and β), as well as colony-stimulating factors type 1 (CSF-1R) and glial cell-line derived neurotrophic factor receptor (RET) in both biochemical and cellular assays (Abrams et al., 2003a; Mendel et al., 2003; O'Farrell et al., 2003a; O'Farrell et al., 2003b).

A summary of the biological effects of Sunitinib against target receptors is given in Table 4.

Table 4 Summary of the biological effects of Sunitinib against target receptors (Faivre et al., 2007)

Receptor	Biochemical K_i (μM)	Cellular IC_{50} (μM)	
		Receptor phosphorylation	Proliferation
VEGFR1*	0.002	Not determined	Not determined
VEGFR2‡	0.009	0.01	0.004
VEGFR3§	0.017	Not determined	Not determined
PDGFRβ	0.008	0.01	0.039
PDGFRα	Not determined	Not determined	0.069
KIT	0.004	0.001–0.01	0.002
FLT3 (wild-type)	Not determined	0.25	0.01–0.05
RET	Not determined	0.05	0.05
CSF1R	Not determined	0.05–0.1	Not determined

*Also known as FLT1. ‡Also known as FLK1 or KDR. §Also known as FLT4. CSF1R, colony stimulating factor 1 receptor; FLT3, fms-related tyrosine kinase 3; KIT, stem-cell growth factor receptor; PDGFR, platelet-derived growth factor receptor; VEGFR, vascular endothelial growth factor receptor.

Based on the anti-angiogenic oxindol inhibitors SU5416 and SU6668, Sunitinib was identified in a drug discovery program designed to identify a more potent inhibitor of VEGFRs and PDGFRs, since SU5416 and SU6668 had inadequate pharmacokinetic properties for clinical development and failed in clinical trials. In biochemical and cell-based assays, sunitinib was found to be 10-30 times more potent against VEGFR2 and PDGFRα than other candidate drugs (Mendel et al., 2003; Sun et al., 2003) (Figure 9). Sunitinib inhibited the VEGF-dependent mitogenic response of human umbilical vein endothelial cells, prevented migration of these cells and attenuated capillary-like tubule formation (Osusky et al., 2004). *In vivo*, Sunitinib decreased tumor microvessel density, prevented neovascularization in a tumor vascular-window model and attenuated the formation of lung metastasis in a Lewis lung carcinoma model (Osusky et al., 2004). Sunitinib is likely to have an important role in cancer cell proliferation, microcapillary angiogenesis and lymphangiogenesis, as well as macrophage-induced tumor cell intravasation (Figure 10).

The inhibition of other tyrosine kinases by Sunitinib was predicted to be beneficial for specific types of cancer. For example, KIT is activated and/or mutated in GIST (Duensing et al., 2004), FLT3 may be mutated in acute myeloid leukaemia (Naoe and Kiyoi, 2004), RET is often dysregulated in neuroendocrine tumors (NETs) (Ichihara et al., 2004) and CSF1R is implicated in metastatic breast cancer (Sapi, 2004).

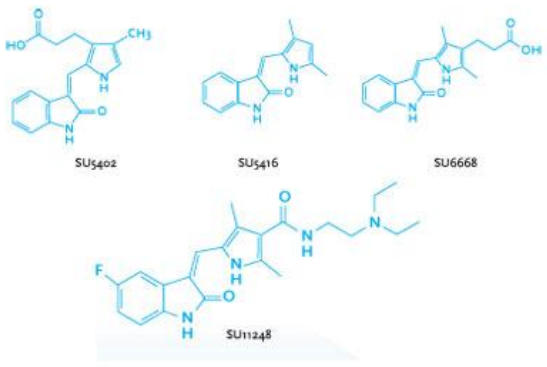

Figure 9 COMPOUND EVOLUTION**:** Evolution in the development of oxindole compounds, which led to the development of SU11248 (5- [5-fluoro-2-oxo-1,2- dihydroindol-(3*Z*)-ylidenemethyl]-2, 4-dimethyl-1*H*-pyrrole-3-carboxylic acid [2-diethylaminoethyl]amide) (image from Schlessinger et al., 2005).

In vitro, SU11248 inhibits growth of cell lines driven by VEGF, SCF, and PDGF and induced apoptosis of human umbilical vein endothelial cells (Mendel et al., 2003). *In vivo*, SU11248 caused bone marrow depletion and effects in the pancreas in rats and monkeys, as well as adrenal toxicity in rat (microhemorrhage). SU11248 exhibited dose- and time-dependent antitumor activity in mice, potently repressing the growth of a broad variety of human tumor xenografts including renal, breast, lung, melanoma, liver and epidermoid carcinoma (Abrams et al., 2003b; Huynh et al., 2009; Mendel et al., 2003; Morimoto et al., 2004; Murray et al., 2003; Yee et al., 2004). Furthermore, antitumor activity was observed in numerous tumor types such as RCC, GIST, NETs, non-small-cell lung cancer (NSCLC), sarcoma other than GIST, thyroid cancer, melanoma, hepatocellular carcinoma and head and neck squamous cell carcinoma in clinical studies (Choong et al., 2009; Faivre et al., 2006a; Motzer et al., 2006a; Zhu et al., 2009a).

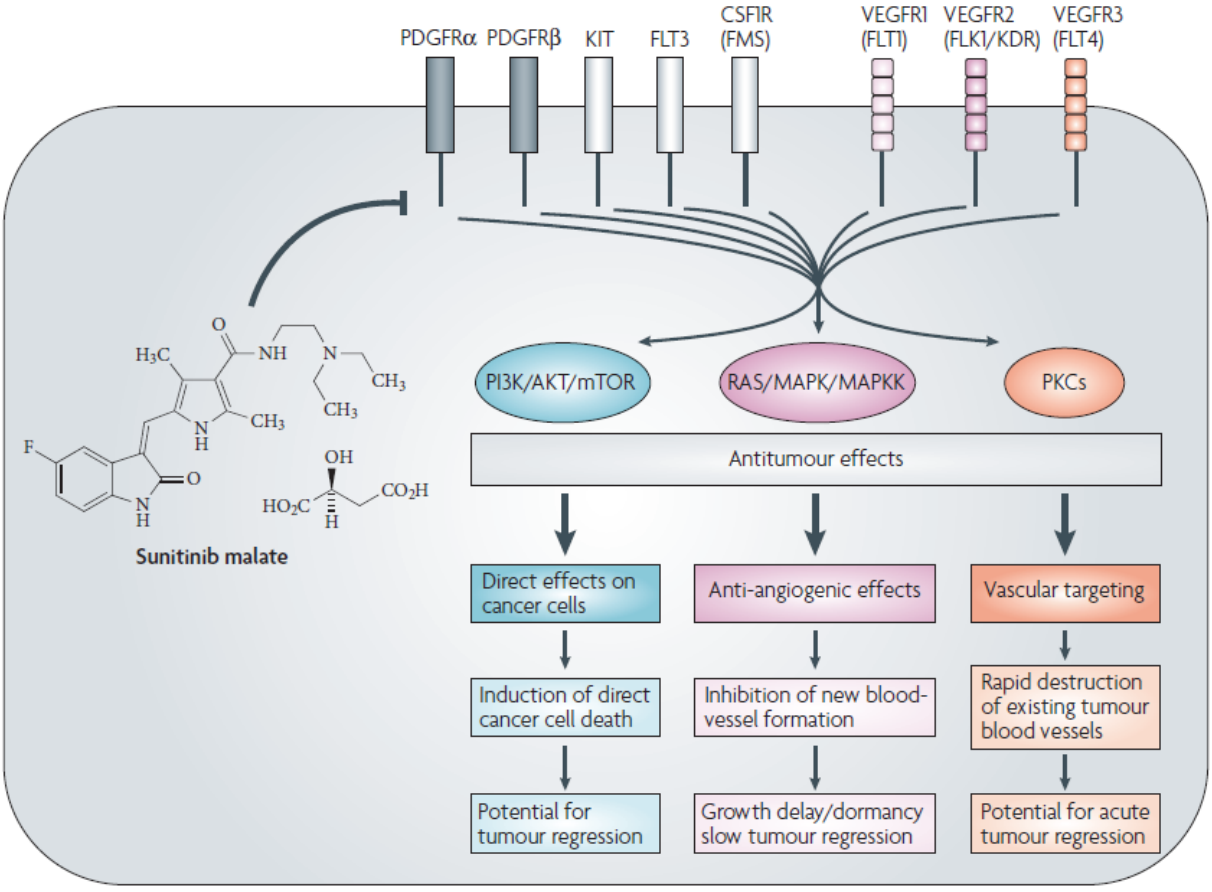

Figure 10 Sunitinib malate is an oxindol molecule designed to interact selectively with the intracellular ATP-binding sites of tyrosine kinase vascular endothelial growth factor receptors 1–3 (VEGFR1–3), platelet-derived growth factor receptors (PDGFRs), stem-cell growth factor receptor (KIT), fms-related tyrosine kinase 3 (FLT3) and colony-stimulating factor 1 receptor (CSF1R). Receptor inhibition has multiple effects on cellular processes including tumour cell survival, endothelial cell growth and migration, vascular permeability, pericyte recruitment and lymphangiogenesis. The final antitumour effects may be classified as follows: direct cytotoxic effects on tumour cells by induction of cell death; anti-angiogenic effects leading to growth delay and/or tumour regression by cytostatic inhibition of new blood-vessel formation; vascular disruption by inhibition of existing VEGF/VEGFR-dependant tumour blood vessels leading to central tumour cell necrosis, and cavitation that may be associated or not with tumour regression. MAPK, mitogen-activated protein kinase; MAPKK, MAPK kinase; mTOR, mammalian target of rapamycin; PI3K, phosphatidylinositol 3-kinase; PKC, protein kinase C (image from (Faivre et al., 2007).

In vitro metabolism studies demonstrated that SU11248 is primarily metabolized by cytochrome CYP3A4, resulting in formation of a major pharmacologically active N-desethyl metabolite, SU12662. This metabolite was shown to be equipotent to the parent compound in biochemical tyrosine kinase and cellular proliferation assays, acting toward VEGFR, PDGFR, and KIT (Baratte et al., 2004). In patients, at the dose of 50 mg/d (4 weeks on, 2 weeks off), SU11248 displays manageable toxicity, but strong reduction of intratumoral vascularization and central tumor necrosis (Faivre et al., 2006a). Most of the adverse events reported in patients receiving Sunitinib in clinical studies were mild to moderate in severity and generally consistent across indications (Demetri et al., 2006; Kulke et al., 2008; Motzer et al., 2007a; Motzer et al., 2006b; Motzer et al., 2006c). The most commonly reported treatment-related, non-haematological adverse effects include fatigue, gastrointestinal toxicities (diarrhea, nausea, vomiting, stomatitis and dyspepsia), anorexia, hypertension, skin discoloration and hand-foot syndrome.

4.5 A closer look at targeted cancer therapy and small-molecule kinase inhibitors

4.5.1 The advantages and drawbacks of targeted cancer therapy with kinase inhibitors

Conventional chemotherapy has been one of the major medical advances in the last few decades. However, although directed toward certain macromolecules or enzymes, cancer chemotherapy typically does not discriminate effectively between rapidly dividing normal cells (e.g., bone marrow and gastrointestinal tract) and tumor cells, thus leading to a variety of toxic side effects. Tumor responses from cytotoxic chemotherapy are usually partial, brief, and unpredictable. In contrast, targeted therapies interfere with molecular targets that have a role in tumor growth or progression. These targets are usually located in tumor cells, although some like the antiangiogenic agents may target other cells such as endothelial cells. Thus, targeted therapies have a high specificity toward tumor cells, providing a broader therapeutic window with less toxicity (Arora and Scholar, 2005). They are often useful in combination with cytotoxic chemotherapy or radiation to produce additive or synergistic anticancer activity because their toxicity profiles often do not overlap with traditional cytotoxic chemotherapy. Thus, targeted therapies represent a new and promising approach to cancer therapy with good clinical benefit.

Targeted therapies take advantage of the fact that in healthy cells, a myriad of interacting signaling pathways provide redundancy, whereas cancer cells accumulate assorted mutations in oncogenes and tumor-suppressor genes, rendering a few signaling pathways overactive, which are susceptible to targeted kinase inhibitor treatment. Other mutations lead to the elimination of redundant signaling pathways. Cancer cells are particularly sensitive to inhibition of the remaining hyperactive pathways (Benhar et al., 2002).

Cancer therapy directed at specific, frequently occurring molecular alterations in signaling pathways of cancer cells has been validated through the clinical development and regulatory approval of agents such as Herceptin for the treatment of advanced breast cancer, imatinib (Gleevec) for chronic myelogenous leukemia and gastrointestinal stromal tumors and Sunitinib (Sutent) for metastatic renal cell carcinoma and gastrointestinal stromal tumors.

Nonetheless, the use of targeted therapies is not without limitations such as the development of resistance and the lack of tumor response in the general population. An improved patient selection will help to overcome these problems in the future.

4.5.2 Challenges for multi-targeted kinase inhibitors

Most compounds that have been called multi-targeted kinase inhibitors were developed as inhibitors of a primary target, and activity against secondary targets was either tolerated or initially not recognized, and was discovered and exploited opportunistically later, as was done for imatinib (Gleevec) and dasatinib (Sprycel) (Joensuu et al., 2001; Shah et al., 2004). For some compounds, it is not completely understood whether clinical activity is due to inhibition of one or of multiple targets. For example, the clinical efficacy of sorafenib (Nexavar) is probably not primarily due to inhibition of RAF, the initial primary target for which the compound was developed (Flaherty, 2007). Similar observations were made for Sunitinib (SUTENT), originally designed to inhibit split-kinase domain receptor tyrosine kinases such as PDGFR family members, VEGFR2 and KIT (Faivre et al., 2006a; Mendel et al., 2003). Target profiling studies of Sunitinib elucidated a broad drug target spectrum and gave first hints of its multi-targeted function *in vivo* (Fabian et al., 2005; Karaman et al., 2008). Based on these findings, it is of great importance to reveal a multi-targeted kinase inhibitor`s true selectivity and consider more than the already known drug targets to precisely understand and predict its pharmacodynamic efficacy in patients. Moreover, a comprehensive understanding of a multi-targeted kinase inhibitor´s function leads to further applications in new tumor indications in the clinic in the future.

4.5.3 Drug resistance –single versus multi-targeted small-molecule protein kinase inhibitors

As many kinase inhibitors exert their cytotoxic effects primarily by inhibiting a specific kinase (single-target small molecule drugs), there is a strong selective pressure for cells to acquire resistance through mutations in the kinase gene that abrogate drug binding. Additional non-mutation kinase inhibitor resistance mechanisms have been documented, including target amplification in the case of BCR-ABL in chronic myeloid leukemia (CML) patients (le Coutre et al., 2000) and upregulation of alternative kinase pathways such as hepatocyte growth factor receptor in the acquisition of resistance to EGFR kinase inhibitors that has been observed in lung cancer (Engelman et al., 2007). Owing to the rapid proliferation of cancer cells, the acquisition of mutations conferring drug resistance has become a recurring theme in the clinic. Indeed, resistance as a result of kinase mutations has been documented for inhibitors of BCR-ABL, EGFR, FLT3, KIT and PDGFR (Carter et al., 2005; Cools et al., 2004; Fletcher and Rubin, 2007; Kobayashi et al., 2005; Roumiantsev et al., 2002). To date the most extensive clinical and laboratory characterization of resistance-causing mutations has been performed for BCR-ABL in the context of imatinib and second-generation inhibitors. Additionally, it has been shown in several haematological tumors that quiescent stem cells are refractory to tyrosine kinase inhibitors, and these cell populations are probably also involved in resistance mechanisms (Copland et al., 2006; Graham et al., 2002).

Several strategies are being investigated to overcome kinase inhibitor resistance mutants. A first approach is to develop inhibitors that can tolerate diverse amino acids at the gatekeeper position. Inhibitor resistance conferred by mutation at the gatekeeper residue- so called because the size of the amino acid side chain at this position determines the relative accessibility of a hydrophobic pocket located adjacent to the ATP binding site- appears to be common theme for a variety of kinases. Access to this pocket is important to many kinase inhibitors because hydrophobic interactions in this site are crucial for the binding affinity of the inhibitor. A second approach is to target the kinase with inhibitors that bind at alternative binding sites. A third approach involves targeting other pathways that are required for cancer cell transformation, cancer cell proliferation and survival in a certain tumor type. However, a general drawback of target-specific monotherapy, namely the fact that a single genetic alteration conferring target resistance to an individual tumor cell can eventually lead to a relapse, still exists even with second-generation single-target drugs. All targeted kinases have the ability to mutate in response to the selective pressure created by the drug treatment. Therefore, a strong rationale for hitting more than one essential target at the same time in the tumor cells came into the focus of interest (Druker, 2003; La Rosee et al., 2004). Alternatively, simultaneous targeted inhibition of both an essential protein component in the cancer cells and of endothelial cell-dependent tumor neovascularization aims not only at increased therapeutic potency, but also a reduction in the risk of molecular resistance formation by reducing the tumor cell population as a result of anti-angiogenic therapy (Hampton, 2004). Multi-targeted therapy can be achieved with either a combination of medicines or single `promiscuous´ drugs that act on a set of disease-relevant proteins (Morphy et al., 2004). Protein kinases, which share a relatively conserved ATP-binding site, are amenable to the latter concept of targeted poly-pharmacology. The emerging shift towards multi-targeted kinase inhibitors can also be illustrated by a series of indolinone inhibitors developed for antitumor therapy in recent years. The first of these compounds, SU5416, was originally developed as a monospecific inhibitor of vascular endothelial growth factor receptor (VEGFR) tyrosine kinase, which is involved in tumor angiogenesis (Fong et al., 1999). The follow-up drug SU6668 had improved pharmacological properties and an increased potency as an anti-angiogenic agent, because it simultaneously inhibited three receptor tyrosine kinases (RTKs) known to have a role in neovascularization: VEGFR2, PDGFRβ and FGFR1 (Laird et al., 2000). Both SU5416 and SU6668 have not performed very well in clinical trials. This led to the development of the most recent drug out of this compound development line, SU11248 (sunitinib), showing comparable potency against several RTKs, including PDGFRα, PDGFRβ, VEGFR2, KIT and FLT3 (Abrams et al., 2003a; Mendel et al., 2003; O'Farrell et al., 2003a). In contrast to SU5416 and SU6668, sunitinib had a strong anti-angiogenic and antitumor activity *in vitro* and *in vivo* and as a consequence it was the first multi-targeted small-molecule kinase inhibitor approved for clinical treatment of mRCC and GIST in 2006.

Even though, multi-targeted small-molecule inhibitors, such as sunitinib and sorafenib, being very potent in the clinic, there is, however, a drawback to this approach. The simultaneous inhibition of multiple targets with either `promiscuous´ small-molecule kinase inhibitors or cocktails of these drugs, runs the risk of becoming too unselective; this might interfere with normal cellular function and result in dose-limiting toxicity. To keep potential adverse side-effects to a minimum, compounds must ideally posses a multi-target

selectivity that is restricted to cancer-relevant protein kinases and must be ineffective against proteins not linked to the actual disease. To address this challenge, a thorough analysis of the kinase selectivity of drug candidates must be undertaken. This can be done in high throughput by screening large collections of recombinant kinases against drug candidates in parallel (Bain et al., 2003; Davies et al., 2000) or by using proteomic techniques, which make use of immobilized kinase inhibitors for the affinity purification or cellular drug targets followed by sensitive mass spectrometry for subsequent protein identification (Daub, 2005; Daub et al., 2004a; Daub et al., 2004b; Godl et al., 2003).

Taken together, there are several lines of evidence indicating that both new combination therapies, as well as multi-targeted protein kinase inhibitors, will become more and more important elements in future cancer therapy and will have essential roles in preventing or overriding drug resistance in human malignancies.

4.6 Drug discovery of selective kinase inhibitors

The success of small molecule kinase inhibitors, such as imatinib as the first small-molecule kinase inhibitor to be approved for use in humans, and sunitinib, the first multi-targeted kinase inhibitor applied for the treatment of cancer, has demonstrated hat targeting kinases can be a very effective therapeutic approach. Small molecule kinase inhibitors therefore are a new class of drugs that will grow significantly as the large number of compounds currently in preclinical and clinical development progress towards marketing approval (Baselga, 2006; Collins and Workman, 2006; Sebolt-Leopold and English, 2006; Verweij and de Jonge, 2007). The central role of kinases in cellular processes that are important in disease, and the discovery of dysregulation of kinase activity in an expanding list of disorders, suggest that the number of kinases with the potential as drug targets is significant, perhaps eclipsing G-protein-coupled receptors as a target class. To fully explore and exploit this opportunity, potent and selective inhibitors will be required for a multitude of kinases, both as tool compounds for target validation and as leads for drug development.

Kinase-inhibitor discovery can be performed either in a largely linear process that addresses one kinase at a time, which has been traditionally used, or in a high-throughput setting, where compound libraries are profiled against a large panel of kinases in parallel in a single screen. Compound potency and selectivity are determined simultaneously leading to high-quality candidates for multiple targets (Goldstein et al., 2008) (Figure 11).

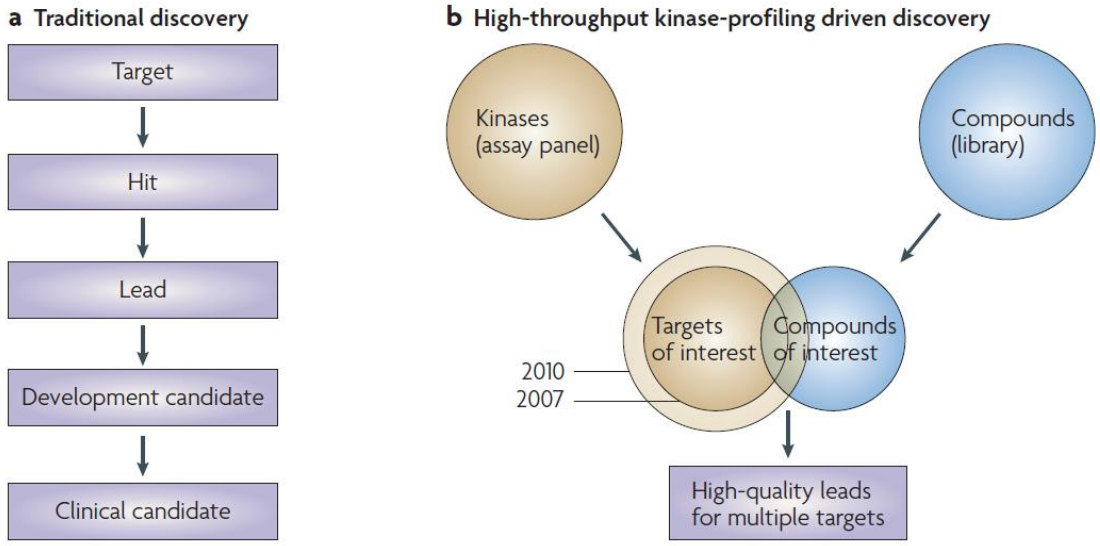

Figure 11 The ability to efficiently screen compound libraries against many kinases in parallel enables a more systematic approach to drug discovery. **A**) Discovery of new inhibitors traditionally has been a linear, target-centric process, proceeding from target validation, hit identification and lead generation to designation of a candidate molecule for preclinical and clinical development. In this paradigm, decisions about which targets to pursue are based on target biology alone. **B)** A novel, parallel, compound-centric approach to discovery. Profiling of compound libraries against a large panel of kinases allows the efficient identification of the overlap between targets of interest, defined by target biology, and compounds of interest, defined by compound properties and the potency and selectivity results obtained from the screen. Interrogating many targets in parallel reveals those targets for which high-quality leads are available, and focuses medicinal chemistry efforts on projects that are most likely to yield development candidates. Decisions are based on biological and chemical considerations (image from (Goldstein et al., 2008)).

In the linear process, a library of compounds is screened against a carefully selected individual kinase to identify hits- compounds capable of inhibiting enzymatic activity of the target. First hits are often weak or modestly potent and are optimized in a second step to generate lead compounds. Lead compounds are then further modified to improve pharmaceutical properties until a candidate for clinical development is identified (Morwick et al., 2006; Pevarello et al., 2004). Decisions about which targets to pursue are based on biology. In comparison to the target-centric approach, the compound-centric screening technique using high-throughput kinase profiling, identifies the overlap between targets of interest, defined by target biology, and compounds of interest, defined by compound properties and the potency and selectivity results obtained from the screen. Interrogating many targets in parallel reveals those targets for which high-quality leads are available. Decisions are based on biological and chemical considerations.

Profiling of compound libraries against large panels of kinases might enable a new strategy to find true multi-targeted yet non-promiscuous inhibitors that could be leads for further optimization, and tool compounds to investigate the utility of specific target combinations in cellular and animal models. Targeting multiple kinases with distinct mechanisms of action and involvement in different pathways, e.g., angiogenesis, cell cycle or signal transduction, at a time, may improve cancer therapy in the future. Moreover, concurrent inhibition of multiple targets may also make it more difficult for genetically unstable tumors to develop resistance, and would allow the same compound to be used for more than one indication with different relevant targets.

5 Aims of this PhD thesis

Cancer is the second frequent killing disease in the world. Every year 11 million new incidences are registered with 8 million people dying of cancer. Current treatment opportunities are chemotherapy, radiation therapy, surgery and other cancer treatment methods such as hormone therapy, biological therapy and targeted therapy including therapeutic antibodies and small-molecule inhibitors or a combination of different methods used for first- and second-line treatment. Nevertheless, due to their aggressiveness, for many cancer types such as melanoma, breast, liver and pancreatic cancer, the survival rate is very low with a high risk of recurrence. Often these secondary tumors are highly metastatic and resistant to standard-of-care therapies including chemotherapy and radiation. Therefore, there is an urgent need for new and better forms of cancer therapies. One possibility to improve the treatment of cancer, which was developed over the last two decades, is the use of targeted therapies such as antibodies and small-molecule inhibitors directed against tumor-specific driving factors. This targeted therapy based on underlying mechanisms of tumor development and progression of a particular cancer type, is of clinical benefit compared to standard-of-care treatments. It allows for an efficient tumor-type specific and individualized therapy. This is of great importance due to the fact that every cancer type even same cancer types from different individuals differ from each other. Nevertheless, also these new forms of cancer therapy such as low-molecular weight kinase inhibitors, show limitations in the clinic. Therefore, to obtain maximal clinical benefits, the understanding of the precise molecular function of a particular targeted therapy such as an inhibitor` s selectivity and cellular sites of action is of important relevance. Moreover it is a prerequisite for choosing suitable tumor indications. Taken together, a profound comprehension of a drug aids in the optimal patient selection with highly responsive tumors and may help to predict and circumvent possible mechanisms of resistance as well as toxic side-effects.

In this context, the aim of this study was to comprehensively characterize the multi-targeted small-molecule kinase inhibitor SU11248, which is approved for the treatment of metastatic renal cell carcinoma (mRCC) and imatinib-resistant gastro-intestinal stromal tumors (GIST), to get a better understanding of the inhibitor` s biological function and underlying molecular mechanisms of action. This might lead to an improved pharmacodynamic prediction including toxic side-effects of the drug *in vivo* and a better clinical application in the future. An inhibitor` s true target selectivity is a crucial step in revealing molecular sites of action and understanding its biological function. Therefore, an efficient chemical proteomic approach should be used to profile the target protein interaction pattern of SU11248 directly from cancer cell lines and primary mRCC tumors. The goal was to reveal proteome-wide interaction patterns of SU11248 with endogenously expressed proteins under physiological conditions in different tumor types to obtain a complete picture of drug activity within a cell. Furthermore, to reveal the efficacy spectrum of SU11248 and to find new tumor indications suitable for SU11248 treatment, a biological screen of SU11248 activity should be performed in cancer cell lines of different tissue origins. For this purpose, the effect of SU11248 on cancer cell viability, cancer cell growth, proliferation, survival, cancer cell migration and invasiveness was supposed to be analysed. All these biological processes are hallmarks of cancer and impaired in tumorigenesis and tumor progression. In

addition, to fully understand a drug` s function not only its target selectivity but also its cell-wide inhibition spectrum of cellular signalling networks and pathways is of interest. Cellular signalling events regulating key processes of a cell such as proliferation and survival are carried out by phosphorylation and dephosphorylation of signalling molecules including kinases organized in signalling cascades. Therefore, the aim was to investigate cellular signalling networks being inhibited or impaired after treatment with SU11248. For this purpose, a mass-spectrometry based phospho-proteomic study was performed.

In summary, the overall intention of this study was to find cellular markers for SU11248 sensitivity which can be used as markers of responsiveness in the clinic and aid in the optimal patient selection to increase the clinical anti-tumor efficacy of SU11248.

6 Materials and Methods

6.1 Materials

6.1.1 Laboratory chemicals, biochemicals and inhibitors

Acrylamide	Serva, Heidelberg
Aprotinin	Sigma, Taufkirchen
APS (Ammonium peroxodisulfate)	Bio-Rad, München
Bisacrylamide	Roth, Karlsruhe
Bisindolylmaleimide I	Calbiochem, Darmstadt
Bromphenol blue	Sigma, Taufkirchen
BSA (Bovine serum albumin)	Sigma, Taufkirchen
Coomassie G250	Serva, Heidelberg
Crystal Violet	Sigma, Taufkirchen
HEPES (N-(2-Hydroxyethyl)piperazine-N'-(2-ethanesulfonic acid))	Serva, Heidelberg
IAA (Iodoacetic acid)	Sigma, Steinheim
L-Glutamine (GibCo)	Invitrogen, Eggenstein
Lysozyme	Sigma, Taufkirchen
Matrigel	BD Biosciences, Heidelberg
MTT	Sigma, Taufkirchen
PKA Inhibitor (14-22 Amide)	Calbiochem, Darmstadt
PMSF (Phenylmethanesulfonyl fluoride)	Sigma, Taufkirchen
Ponceau S	Sigma, Taufkirchen
Propidium iodide	Roche, Mannheim
SDS (Sodium dodecyl sulfate)	Roth, Karlsruhe
Sodium azide	Serva, Heidelberg
Sodium fluoride	Sigma, Taufkirchen
Sodium orthovanadate	Sigma, Taufkirchen
Sulforhodamine B	Sigma, Taufkirchen
SU11248 (SUTENT, sunitinib)	ACC Corporation, USA
TEMED (N,N,N',N'-Tetramethylethylenediamine)	Serva, Heidelberg
Triton X-100	Serva, Heidelberg

All other chemicals were purchased in analytical grade from Merck (Darmstadt).

6.1.2 Chemicals for SILAC and MS-analysis

Acetonitrile for HPLC	Sigma, Taufkirchen
Ammoniumbicarbonate	Sigma, Taufkirchen
Ammonium hydroxide	Merck, Darmstadt
Antioxidance	Invitrogen, Eggenstein
2,5-Dihydroxybenzoic acid	Fluka, Taufkirchen
DTT	Sigma, Taufkirchen
Fetal bovine serum, dialyzed	Gibco, USA
Iodoacetamide	Sigma, Taufkirchen
L-Arginine	Gibco, USA
L-Arginine: HCl, U-13C614N4	Cambridge Isotope Laboratories, USA
L-Arginine: HCl, U-13C615N4	Cambridge Isotope Laboratories, USA
L-Glutamine	Gibco, USA
L-Lysine	Gibco, USA
L-Lysine: 2 HCl, 2H4	Cambridge Isotope Laboratories, USA
L-Lysine: 2 HCl, U-13C615N2	Cambridge Isotope Laboratories, USA
Lys-C	WAKO, Neuss
n-octosylglucoside	Roche, Mannheim
Penicillin/Streptomycin, 100x	PAA, Germany
SILAC DMEM	Gibco, USA
SILAC RPMI	Gibco, USA
Thio urea	Invitrogen, Eggenstein
Trypsin (seq. grade modified)	Promega, USA
Urea	Merck, Darmstadt

6.1.3 Enzymes

DNAse I, RNAse free	Roche, Mannheim
LA Taq-DNA Polymerase	Takara, Japan
Trypsin (GibCo)	Invitrogen, Eggenstein
Reverse Transcriptase (AMV)	Roche, Mannheim

6.1.4 "Kits" and other materials

BrdU Incorporation Assay (colorimetric)	Roche, Mannheim
Cell culture materials	Greiner, Solingen
Cellulose nitrate 0.45 µm	Schleicher & Schüll, Dassel
Caspase 3/7 Glo Assay	Promega, USA
ECL Kit	PerkinElmer/NEN, Köln
	Falcon, UK
Hyperfilm MP	Amersham Pharmacia, Freiburg
Micro BCA Protein Assay Kit	Pierce, Sankt Augustin
	Nunclon, Dänemark
Parafilm	Dynatech, Denkendorf
Protein A-Sepharose	Amersham Pharmacia, Freiburg
Protein G-Sepharose	Amersham Pharmacia, Freiburg
QIAGEN Plasmid Maxi Kit	Qiagen, Hilden
QIAGEN Plasmid Mini Kit	Qiagen, Hilden
QIAGEN RNeasy Mini Kit	Qiagen, Hilden
QIAquick PCR Purification Kit (50)	Qiagen, Hilden
Sterile filter 0.22 µm, cellulose acetate	Nalge Company, USA
Sterile filter 0.45 µm, cellulose acetate	Nalge Company, USA
Transwells, 0.8 µM pore-size	BD Biosciences, Heidelberg
Whatman 3MM	Whatman, Rotenburg/Fulda

6.1.5 Growth factors and ligands

EGF (human)	Peprotech, USA
PDGF-BB (human)	Peprotech, USA
PDGF-AA (human)	Peprotech, USA
SCF (human)	Peprotech, USA
MSP (human)	Peprotech, USA
GAS6 (human)	Peprotech, USA

6.2 Media

6.2.1 Bacterial media

LB or 2xYT media were used for cultivation of all *Escherichia coli* strains. If and as required 100 µg/ml Ampicillin or 70 µg/ml Kanamycin were added to media after autoclavation. For the preparation of LB-plates 1.5% Agar was also added.

LB-Medium
1.0 % Tryptone
0.5 % Yeast Extract
1.0 % NaCl
pH 7.2

6.2.2 Cell culture media

GibcoTM media and additives were obtained from Invitrogen (Eggenstein). Media were supplemented to the requirements of each cell line. Freeze medium contained 95% heat-inactivated FCS and 5% DMSO.

6.3 Stock solutions and commonly used buffers

BBS (2x)	50 mM	BES
	280 mM	NaCl
	1.5 mM	Na2HPO4
	pH 6.96	
Collecting gel	0,5 M	Tris/HCl pH6.8
buffer (4x)	0,4 %	SDS
HBS (2x)	46 mM	HEPES, pH 7.5
	274 mM	NaCl
	1.5 mM	Na2HPO4
	pH 7.0	
HNTG	20.0 mM	HEPES, pH 7.5
	150 mM	NaCl
	0.1 %	TritonX-100
	10 .0 %	Glycerol
	10.0 mM	Na4P2O7
DNA loading buffer (6x)	0.05 %	Bromphenol blue
	0.05 %	Xylencyanol
	30.0 %	Glycerol
	100.0 mM	EDTA pH 8.0
Laemmli buffer (3x)	100 mM	Tris/HCl pH 6.8
	3.0 %	SDS
	45.0 %	Glycerol
	0.01 %	Bromphenol blue
	7.5 %	ß-Mercaptoethanol
NET	50.0 mM	Tris/HCl pH 7.4
	5.0 mM	EDTA
	0.05 %	Triton X-100
	150.0 mM	NaCl
PBS	137.0 mM	NaCl
	27.0 mM	KCl
	80.9 mM	Na2HPO4
	1.5 mM	KH2PO4
	pH 7.4	
SD-Transblot	50.0 mM	Tris/HCl pH 7.5
	40.0 mM	Glycine
	20.0 %	Methanol
	0.004 %	SDS
Separating gel buffer (4x)	0,5 M	Tris/HCl pH 8.8
	0,4 %	SDS
"Strip" buffer	62.5 mM	Tris/HCl pH 6.8
	2.0 %	SDS
	100.0 mM	β-Mercaptoethanol
	TAE 40.0 mM	Tris/Acetate pH 8.0
	1.0 mM	EDTA
TE10/0.1	10.0 mM	Tris/HCl pH 8.0
	0.1 mM	EDTA pH 8.0
Tris-Glycine-SDS	25.0 mM	Tris/HCl pH 7.5
	200.0 mM	Glycine
	0.1 %	SDS

6.4 Cells

6.4.1 Eukaryotic cell lines

Cell Line Description	Origin/Reference
786-0	Human primary renal cell carcinoma ATCC, USA
A498	Human renal metastatic cell carcinoma ATCC, USA
A549	NSCLC ATCC, USA
A590	Human pancreas adenocarcinoma ATCC, USA

A704	Human renal metastatic cell carcinoma ATCC, USA
ACHN	Human primary renal cell carcinoma ATCC, USA
AsPc1	Human pancreas adenocarcinoma ATCC, USA
BH1604	prostate ATCC, USA
C8161	Human melanoma ATCC, USA
Caki-1	Human renal metastatic cell carcinoma ATCC, USA
Caki-2	Human renal metastatic cell carcinoma ATCC, USA
Calu1	NSCLC ATCC, USA
Colo357	Human pancreas adenocarcinoma ATCC, USA
DLD1	Human colon carcinoma ATCC, USA
DU145	Human prostate carcinoma ATCC, USA
HCT 116	Human colon carcinoma ATCC, USA
HCT 15	Human colon carcinoma ATCC, USA
Hs578T	mammary ATCC, USA
HT29	Human colon carcinoma ATCC, USA
K562	Chronic myelogenous leukemia cell line, ATCC, USA
Malme3M	Human melanoma ATCC, USA
MDA-MB-231	mammary ATCC, USA
MDA-MB-435s	mammary ATCC, USA
MDA-MB-453	mammary ATCC, USA
NCI-H-1568	NSCLC ATCC, USA
NCI-H-1650	NSCLC ATCC, USA
NCI-H-1666	NSCLC ATCC, USA
NCI-H-1755	Human liver adenocarcinoma ATCC, USA
NCI-H-1781	NSCLC ATCC, USA
NCI-H-1838	NSCLC ATCC, USA
NCI-H-1975	NSCLC ATCC, USA
NCI-H-2122	NSCLC ATCC, USA
NCI-H-2347	NSCLC ATCC, USA
NCI-H-292	NSCLC ATCC, USA
NCI-H-441	NSCLC ATCC, USA
NCI-H-460	NSCLC ATCC, USA
NCI-H-522	NSCLC ATCC, USA
NCI-H-596	NSCLC ATCC, USA
NCI-HCC15	NSCLC ATCC, USA
NCI-HCC366	NSCLC ATCC, USA
NCI-HCC44	NSCLC ATCC, USA
NIC-H-661	NSCLC ATCC, USA
OVCAR3	Human ovary adenocarcinoma ATCC, USA
OVCAR4	Human ovary adenocarcinoma ATCC, USA
OVCAR5	Human ovary adenocarcinoma ATCC, USA
OVCAR8	Human ovary adenocarcinoma ATCC, USA
PaTu	Human pancreas adenocarcinoma ATCC, USA
PC3	prostate ATCC, USA
PC9	NSCLC ATCC, USA
PPC1	prostate ATCC, USA
SF126	Human glioblastoma ATCC, USA
SF763	Human glioblastoma ATCC, USA
SF767	Human glioblastoma ATCC, USA
SkMes1	NSCLC ATCC, USA
SkOv3	Human ovary adenocarcinoma ATCC, USA
SW1116	Human colon carcinoma ATCC, USA
SW13	Human renal metastatic cell carcinoma ATCC, USA
SW850	Human pancreas adenocarcinoma ATCC, USA
U118	Human glioblastoma ATCC, USA
U1242	Human glioblastoma ATCC, USA
U138	Human glioblastoma ATCC, USA
U373	Human glioblastoma ATCC, USA
WM115	Human melanoma ATCC, USA
WM266-4	Human melanoma ATCC, USA

All mRCC tumor samples were provided by the Department of Pathology, Prof. Höfler, Klinikum Rechts der Isar, München

ATCC, American Type Culture Collection, Manassas, USA
DKFZ, Deutsches Krebsforschungszentrum, Heidelberg

6.5 Antibodies and recombinant proteins

Names of people given as reference without further designation were members of this group.

6.5.1 Primary antibodies

The following antibodies were used for immunoprecipitation or as primary antibodies in immunoblot or immunofluorescence analysis.

Antibody	Description/ Immunogen	Origin/Reference
pTyr (4G10)	mouse, monoclonal, recognizes phospho-tyrosine residues	UBI, USA
α-Tubulin	mouse, monoclonal, ascites	Sigma, Taufkirchen
ROS1	rabbit	Abcam, USA
ROS1	rabbit	Santa-Cruz, USA
NEK9	goat	Santa-Cruz, USA
SKY	rabbit	Santa-Cruz, USA
E-cadherin	mouse	Cell Signaling Tech., USA
Vimentin	mouse	Cell Signaling Tech., USA
Actin	rabbit	Cell Signaling Tech., USA
FAK	mouse	Cell Signaling Tech., USA
AXL	goat	Santa-Cruz, USA
MER	rabbit	Santa-Cruz, USA
pERK	rabbit	Cell Signaling Tech., USA
ERK	rabbit	Cell Signaling Tech., USA
PDGFRa	rabbit	Cell Signaling Tech., USA
PDGFRb	rabbit	Cell Signaling Tech., USA

6.5.2 Secondary antibodies

For immunoblot analysis corresponding secondary antibodies conjugated with horseradish peroxidase (HRP) were utilized.

Antibody	Dilution	Origin/Reference
Goat anti-mouse-HRP	1 : 10.000	Sigma, Taufkirchen
Goat anti-rabbit-HRP	1 : 50.000	BioRad, München
Rabbit anti-goat-HRP	1 : 50.000	BioRad, München

6.6 Oligonucleotides

6.6.1 siRNA oligonucleotides

siRNA	Description/Sequence	Reference
gl2	directed against firefly luciferase CGUACGCGGAAUACUUCGAdTdT	Stefan Hart
ROS1	ID1: 353; ID2: 110795; ID3: 110797	Ambion
NEK9	ID1: 1114; ID2: 1115	Ambion
BMP2K	ID1: 1583; ID2: 1489; ID3: 111088	Ambion
NME4	sequence 1: AGAUUGGACCAAUCCUUUUtt	Ambion
	sequence 2: AGCACAAGAUUGGACCAAUtt	Ambion
TBK1	validated	Ambion
FAK	validated	Ambion
AURKA	validated	Ambion
AURKB	validated	Ambion
RPS6KA1	validated	Ambion
RPS6KA3	validated	Ambion
NEK2	validated	Ambion
RON	validated	Ambion

6.7 Methods

6.7.1 Cellular Assays

6.7.1.1 MTT Assay

In a 96-well flat-bottomed plate, 1000- 2000 cells/100 µl cell suspension was seeded. After 24h, cells were exposed to different concentrations of compound. Each treatment was tested in triplicate wells. At the end of exposure (24h, 48h and 72h), 20 µl of MTT (5 mg/ml in PBS) [3-(4,5-dimethylthiazol-2-y1)-2,5-diphenyltetrazolium bromide; thiazolyl blue, SIGMA, St. Louis, MO] was added to each well, and the plates were incubated at 37 ºC for 4h. Then 50 µl triplex solution (10% SDS, 5% isobutanol, 0.012 M HCl) was added and the plates were incubated at 37ºC overnight in a cell incubator. The optical density (OD) was measured using a multiwell spectrophotometer at a wavelength of 570 nm. The inhibitory rate of cell proliferation was calculated by the following formula: Inhibition Rate (%) = [1-(ODtreated- ODtreated (day0)/ODcontrol- ODcontrol (day0))]×100%. The IC_{50}-value (i.e. the drug concentration that reduced the absorbance observed in untreated cells by 50%) was calculated by using Hill threeparameter log fit or the sigmoidal dose-response curve fitting algorithm in SIGMA Plot 10 on log-transformed data.

6.7.1.2 SRB Assay

The assay was performed as described in Vichai *et al*. ((Vichai and Kirtikara, 2006)). In a 96-well flat-bottomed plate, 1000- 2000 cells/100 µl cell suspension was seeded. After 24h, cells were exposed to different concentrations of compound. Each treatment was tested in triplicate wells. At the end of exposure (24h, 48h and 72h), cells were fixed with ice-cold 10% TCA for 1h at 4°C, washed with dH_2O and incubated with sulforhodamine B (0.057% in 1% AcCOOH) for 30 min at room temperature. Incorporated dye was dissolved in 10 mM Tris- buffer (pH= 10.5) and the optical density (OD) measured in an ELISA reader at 510 nm. The inhibitory rate of cell proliferation was calculated by the following formula: Inhibition Rate (%) = [1-(ODtreated- ODtreated (day0)/ODcontrol- ODcontrol (day0))]×100%. The IC_{50}-value (i.e. the drug concentration that reduced the absorbance observed in untreated cells by 50%) was calculated by using Hill threeparameter log fit or the sigmoidal dose-response curve fitting algorithm in SIGMA Plot 10.0 on log-transformed data.

6.7.1.3 BrdU Assay

The assay was performed as described in the manufacturer`s protocol (Roche). Briefly, in a 96-well flat-bottomed plate, 1000- 2000 cells/100 µl cell suspension was seeded. After 24h, cells were exposed to different concentrations of compound. Each treatment was tested in triplicate wells. At the end of exposure (24h, 48h and 72h) cells were incubated with BrdU for 6- 18h at 37°C. The labeled cells were fixed with ethanol and prior to incubation with a monoclonal antibody to BrdU, the DNA was partially digested with nucleases to allow the antibody to access BrdU. Next, the anti-BrdU antibody [labeled with peroxidase (POD)] was added for 30 min at 37°C and finally incubated with the POD substrate ABTS for 10- 30 min until coloring of the solution was visible. POD catalyzes the cleavage of ABTS, producing a colored reaction product. The absorbance of the samples was determined with a standard microplate (ELISA) reader at a wavelength of 405 nm.

6.7.1.4 Flow Cytometry

Transfected or compound- treated cells were trypsinized after 72h of siRNA transfection or drug application and collected by centrifugation. For fixation, cells were washed once with PBS, resuspended in 1ml cold 70% ethanol and stored overnight at 4°C. Cells were then collected by centrifugation, washed once with PBS and incubated with 0.01% Triton, 0.1% sodium citrate, 0.02mM propidium iodide (Sigma) in the dark for 2h at 4°C. Cells were analyzed by flow cytometry (FACS Calibur, BD Bioscience). Using the CellQuestPro software, each of the three peaks (representing cells in G_1, S, and G_2/M phases, respectively) obtained in the flow cytometry profile of fluorescence plotted against cell number was gated and quantified.

6.7.1.5 Caspase 3/7- Assay

Caspase 3/7 activity of siRNA transfected or compound- treated cells was measured using the Caspase 3/7 Glo- Assay from Promega according to manufacturer`s instruction.

6.7.1.6 Wound Assay

Cancer cells were seeded in 6-well cell culture plates and grown to confluence under serum conditions (10 % FCS (w/v)) for two to three days. Confluent monolayers were scratched with a pipette tip and maintained under standard conditions. Plates were washed once with fresh medium to remove non-adherent cells. Migrating cells were monitored by photomicroscopy.

6.7.1.7 Transwell Migration Assay

The lower chamber of a transwell plate (8- µm pore size polycarbonate membrane; Corning Costar Corp., Cambridge, MA) was filled with 600 µl normal cell culture media (10% (w/v) FCS) and 15 x 10^3 to 30 x 10^3 cells were resuspended in 200 µl starvation media (0% (w/v) FCS) and seeded in the upper chamber containing either increasing compound concentrations or DMSO as vehicle control. After 16h the cells were methanol- fixed and stained with crystal violet. After taking images stained cells were dissolved in 5% AcCOOH and the optical density (OD) was measured at 590 nm in an ELISA Reader. The transwell migration was expressed as a percentile "migration index" (number of migrating cells treated with compound divided by the number of migrating cells from the control multiplied by one hundred). The SEM was calculated from the migration indices of independent performed experiments. The statistical significance of the data was analyzed using the Student` s *t* test unpaired.

6.7.1.8 Matrigel outgrowth assay

Determination of the morphology of cells grown on matrigel was carried out in a matrigel-outgrowth assay. Briefly, in a 96-well flat-bottomed plate, 5000- 10000 cells/100µl cell suspension was seeded on the surface of pre-coated matrigel. Colony outgrowth was visualized with a Zeiss Axiovert S100 microscope (Carl Zeiss UK, Welwyn Garden City, UK).

6.7.2 Affinity chromatography and mass spectrometry

6.7.2.1 Compound Synthesis and Immobilization

Sunitinib maleate (SU11248) was purchased from ACC Corporation (San Diego, USA).
For immobilization, SU11248 was chemically modified and kindly provided by VICHEM CHEMIE Ltd., Budapest, Hungary. Drained epoxy-activated Sepharose 6B was resuspended in 2 vol of 0.1, 0.3, 1 or 3 mM Sunitinib dissolved in 50% DMSO/50% 0.05M Na_2CO_3 (pH11). After adding of 10 mM NaOH, coupling was performed overnight at 30°C in the dark. After three washes with 50% DMSO/50% 0.05M Na_2CO_3 (pH11), remaining reactive groups were blocked with 1 M ethanolamine. Subsequent washing steps were performed according to the manufacturer's instructions. To generate the control matrix, epoxy-activated Sepharose 6B was incubated with 1 M ethanol-amine and equally treated as described above. The beads were stored at 4°C in the dark as a suspension in 20% ethanol.

6.7.2.2 Affinity Chromatography

Cells (80 mg protein) were lysed in 30 ml of buffer containing 20 mM Hepes (pH 7.5), 150 mM NaCl, 0.25% Triton X-100, 1 mM EDTA, 1 mM EGTA, 1 mM DTT plus additives (10 mM sodium fluoride/1 mM orthovanadate/10 µg/ml aprotinin/10 µg/ml leupeptin/1 mM phenylmethylsulfonylfluoride/10% glycerol), cleared by centrifugation, and adjusted to 1 M NaCl. The filtrated lysate was loaded with a flow rate of 100 µl/min on an HR 5/2 chromatography column (Amersham Biosciences) containing 600 µl of SU11248 matrix equilibrated to lysis buffer without additives containing 1 M NaCl. The column was washed with 15 column volumes and equilibrated to lysis buffer without additives containing 150 mM NaCl, and bound proteins were eluted in the same buffer containing 1 mM SU11248, 10 mM ATP, and 20 mM $MgCl_2$ with a flow rate of 50 µl/min. The volume of protein-containing elution fractions was reduced to 1/10 in a Centrivap concentrator (Labonco, Kansas City, MO) before precipitation according to Wessel and Fluegge ((Wessel and Flugge, 1984)). Protein pellets were desolved in 1.5x SDS- sample buffer, pooled and subjected to 1D-SDS- Gel electrophoresis.

6.7.2.3 Cell Lysis, *in vitro*-Association Experiments and Target-K_d-Calculation

SILAC-labeled or non-labeled cells were lysed in buffer containing 50 mM Hepes (pH 7.5), 150 mM NaCl, 0.5% Triton X-100, 10% glycerol, 1 mM EDTA, 10 mM sodium pyrophosphate plus additives (10 mM

sodium fluoride/1 mM orthovanadate/10 µg/ml aprotinin/10 µg/ml leupeptin/1 mM phenylmethylsulfonyl fluoride/0.2 mM DTT). Lysates were precleared by centrifugation and equilibrated to 1 M NaCl for *in vitro* association (IVA) experiments ((Godl et al., 2003)). Twenty microliters of drained SU11248 matrix (0.3 or 3 mM) or control resin was incubated with 1 ml of high-salt lysate for 2.5 h at 4°C. In case of the two-step-target enrichment the supernatant of the first round of binding was transferred to a second round of *in vitro* association. After washing with 500 µl of 2× lysis buffer without additives containing 1 M NaCl (high salt) and with 500 µl of 1× lysis buffer without additives containing 150 mM NaCl (low salt), the beads were eluted with 1.5× SDS sample buffer. Eluted proteins were pooled, separated on a 1D-SDS-PAGE, subjected to LC/MS analysis and quantified using MaxQuant.
The target K_d-value was calculated with the formula: $K_d = [I_{effective}] * (r/(1-r))$ with r being the ratio of relative amount of target retained in the second *versus* the first round of binding. $I_{effective}$ is the amount of inhibitor available for protein binding.

6.7.2.4 Cell Lysis and Anti-Tyr(P) Immunoprecipitation

Cell labeling and anti-Tyr(P) Immunoprecipitation was performed as described previously ((Mertins et al., 2008)). Briefly, cancer cells labeled with L-arginine and L-lysine, L-arginine-U-13C615N4 and L-Lysine-U-13C6-15N2, or L-arginine-U-13C6 and L-lysine-2H4 were cultured for 6 passages in the SILAC medium on 15-cm dishes and lysed for 20 min in ice-cold lysis buffer (50 mM Tris-HCl, pH 7.5, 150 mM NaCl, 1% Nonidet P-40, 0.1% sodium deoxycholate, 1 mM EDTA, 1 mM sodium orthovanadate, 1 mM PMSF, 0.1 µg/ml aprotinin, 10 mM NaF). Lysates were precleared by centrifugation at 16,500 x g for 15 min. Protein amount determination was performed using the BCA assay (Pierce). In SILAC experiments, cell lysates were mixed 1:1 (double labeling) or 1:1:1 (triple labeling) after determination of protein amounts. For immunoprecipitation, 200 µg of anti-Tyr(P) 4G10 antibody were added together with 40 µl of protein A-Sepharose (GE Healthcare) to mixed cell lysates containing up to 20 mg of total protein of each label and incubated for 4 h at 4 °C. Precipitates were washed four times with lysis buffer, and precipitated proteins were eluted twice with urea buffer (7 M urea, 2 M thiourea, 50 mM HEPES, pH 7.5, 1% n-octyl glucoside) for 10 min at 37 °C. For further phosphopeptide enrichment eluted proteins were subjected to in-solution digestion and Titansphere enrichment.

6.7.2.5 1D-SDS-PAGE and in-gel digestion

Protein pellets after Wessel-Fluegge precipitation were boiled in 1.5 x LDS-sample buffer with 0.5 mM DTT for 10 min at 70°C and subsequently separated by one-dimensional SDS-PAGE using NuPage Novex Bis-Tris gels and NuPage MOPS SDS running buffer (Invitrogen) according to the manufacturer`s instruction. The gel was stained with Coomassie Blue using the colloidal blue staining kit (Invitrogen).
Gel bands were cut into 1 mm^3 cubes and washed with 50 mM ammonium bicarbonate, 50 % ethanol. For protein reduction, gel pieces were incubated with 10 mM DTT in 50 mM ammonium bicarbonate for 1h at 56°C. Alkylation of cysteines was performed by incubating the samples with 55 mM iodoacetamide in 50 mM ammonium bicarbonate for 45 min at 25°C in the dark. Gel pieces were washed two times with 50 mM ammonium bicarbonate and incubated with 12.5 ng/µl Trypsin in 50 mM ammonium bicarbonate for 16h at 37°C for protein digestion. Supernatants were transferred to fresh tubes and remaining peptides were extracted by incubating the gel pieces two times in 30% acetonitrile in 3% TFA followed by dehydration with 100% acetonitrile.
The extracts were combined and used for direct peptide identification by mass spectrometry after desalting the samples using RP-C18 stage tip columns.

6.7.2.6 In-solution digestion

Protein pellets after Wessel-Fluegge precipitation were resolubilized in 20 mM Hepes buffer (pH 7.5) containing 7 M urea, 2 M thiourea, 1% n-octylglucoside. For protein reduction, 1 mM DTT in 20 mM ammonium bicarbonate was added and incubated for 45 min at room temperature. Alkylation of cysteines was performed by incubating the sample with 5.5 mM iodoacetamide in 20 mM ammonium bicarbonate for 30 min at 25°C in the dark. Protein digestion was done by adding Lys-C for 4h and a subsequent tryptic digestion over night at room temperature. The sample was quenched by adding 30% TFA to 0.5 % final concentration.

6.7.2.7 Phosphopeptide enrichment by Titansphere

For enrichment of phosphopeptides from in solution digestion- fractions TiO2-beads were used. After washing the beads twice with 50% ACN + 0.1% trifluoroacetic acid and preloading them with 30 g/l 2,5

dihydrobenzoic acid (DHB) in 80% acetonitrile the beads were incubated with the peptide mixture for 30 min at room temperature. After washing bound peptides were eluted by using a two-step incubation with 20% ACN (pH > 10.5) and analyzed by mass spectrometry.

6.7.2.8 Mass Spectrometric Analysis

All digested peptides were separated by on-line nanoLC and analyzed by tandem mass spectrometry as described before (Olsen et al., 2005). The experiments were performed on an Agilent 1100 nanoflow system connected to an LTQ-Orbitrap mass spectrometer (Thermo Electron, Bremen, Germany) equipped with a nanoelectrospray ion source (Proxeon Biosystems, Odense, Denmark). The instrument was operated with the "lock mass" option. Binding and separation of the peptides was done in a 15-cm fused silica emitter (75-µm inner diameter from Proxeon Biosystems, Odense, Denmark) in-house packed with reversed-phase ReproSil-Pur C18-AQ 3µm resin (Dr. Maisch GmbH, Ammerbuch-Entringen, Germany).
The peptide mixture was injected onto the column with a flow of 0.5 µl/min and subsequently eluted with a 5-40 % acetonitrile gradient in 0.5 % acetic acid with a flow of 0.25 µl/min. The gradient was 140 min.
Mass spectra were acquired in the positive ion mode applying a data-dependent automatic switch between survey scan and tandem mass spectra (MS/MS) acquisition.
The hybrid linear ion trap/orbitrap instrument was used with the lock mass option in both MS and MS/MS mode. The polydimethylcyclosiloxane (PCM) ions generated in the electrospray process from ambient air were used for internal mass recalibration in real time.
Survey full scan MS spectra (from m/z 300-1800) were acquired in the orbitrap with a resolution r= 60.000 at m/z= 400 after accumulation to a target value of 1.000.000 charges in the linear ion trap. Up to the five most intense ions were sequentially isolated for fragmentation using collisionally induced dissociation at a target value of 30.000 charges. The resulting fragment ions were recorded in the linear ion trap with resolution r=15.000 at m/z=400.
During fragmentation the neutral loss species at 97.97, 48.99 or 32.66 m/z below the precursor ion were activated in turn for 30 ms (pseudo-MS3; (Schroeder et al., 2004)).

6.7.2.9 Data Analysis

Mass spectrometric data were analyzed with the in-house developed software MaxQuant (version 1.0.12.0 for the proteome and version 1.0.11.5 for the phosphoproteome analysis) (Cox and Mann, 2007; Cox and Mann, 2008). MS/MS spectra were searched by Mascot (version 2.2.2, Matrix Science) against the Human IPIBase (version 3.37) combined with common contaminants and concatenated with the reversed versions of all sequences. The following parameters were set for the Mascot searches. Trypsin allowing for cleavage N-terminal to proline and cleavage between aspartic acid and proline was chosen as enzyme specificity. Cysteine carbamidomethylation eas selected as a fixed modification, while protein N-terminal acetylation, methionine oxidation and serine, threonine and tyrosine phosphorylation were selected as variable modifications. Maximally three missed cleavages and up to three labeled amino acids according to SILAC or non- SILAC study were allowed. Initial mass deviation of precursor ion and fragment ions were up to 5 ppm and 0.5 Da, respectively. MaxQuant automatically identified and quantified SILAC peptides and proteins. SILAC protein ratios were calculated as the median of all peptide ratios assigned to the protein. A false discovery rate (FDR) of 0.01 was required for proteins and peptides with a minimum length of 6 amino acids. Furthermore, a posterior error probability (PEP) for each MS/MS spectrum below or equal to 0.01 was required. In case the identified peptides of two proteins were the same or the identified peptides of one protein included all peptides of another protein, these proteins (e.g. isoforms and homologs) were combined by MaxQuant and reported as one protein group.
Phosphorylation sites were made non-redundant with regards to their surrounding peptide sequence. In addition, all alternative proteins that match a particular phosphor site were reported as one group. The PTM score was used for assignment of the phosphorylation site as previously described (Olsen et al., 2006). Only Class I phosphorylation sites were considered. Class I phosphorylation sites are defined by a localization probability of 0.75 and probability localization score difference higher or equal to 5 (Olsen et al., 2006).

6.7.3 Molecular methods

6.7.3.1 RNA interference

Cancer cells were cultured in DMEM, MEM or RPMI medium supplemented with 10 % fetal bovine serum (FBS). 24 h prior to RNAi transfection 15.000 cells/ml were seeded into 6-well cell culture plates. At 30% confluency cells were transfected with 30 pmol of validated or pre-designed siRNA from Ambion using

RNAiMax (Invitrogen) according to the manufacturer`s instruction. Gl2 siRNA was taken as control. 5 d after transfection cells were used for cell cycle analysis by flow cytometry, MTT-, SRB-, BrdU-, assay and western blotting. The knock-down efficiency was monitored by RT-PCR and Western Blotting.

6.7.3.2 RNA extraction, cDNA synthesis, PCR

Total RNA extraction was performed using the RNeasy Protect Mini-Kit (Qiagen) according to the manufacturer's instruction. The resulting pellet was dissolved in nuclease-free water. RNA concentrations were measured using a spectrophotometer (260 nm/280 nm). After heating at 65°C for 5 min to denature RNA and to inactivate RNases, 3 µg total RNA was subjected to reverse transcription using 25 U AMV Reverse Transcriptase, 125 pmol Oligo(dT)n- primer, 200 µm dNTPs (each) and 5x RT buffer containing 7.5 mM Mg^{2+} in a total volume of 20 µl at 42°C for 2 h. The reaction was terminated by heating at 65°C for 10 min.

For each PCR, 5 µl cDNA (diluted 1:10 in nuclease-free water), 5 µl RedTaq PCR Master Mix, 125 pmol forward and reverse primer and nuclease-free water were added to a final volume of 20 µl. Amplification was performed with an Eppendorf Cycler. The thermal cycle used was 3 min at 94°C, 25 cycles of 1min denaturation at 94°C, 1 min annealing at 60°C, 1 min elongation at 72°C and a final elongation step for 10 min at 72°C.

Detection of the PCR-products was done on a 1% agarose-gel. Analysis and quantification was performed with the AIDA Image Reader.

6.7.3.3 cDNA Array Hybridization

cDNA Array Hybridization was performed as earlier described ((Abraham et al., 2005)). Briefly, radioactive labeling of the cDNA was achieved using the Megaprime-DNA labeling kit (Amersham Biosciences) and 50 µCi of [α-^{33}P]ATP per reaction. The labeled cDNA was purified via the Nucleotide Removal Kit from Qiagen and incubated with 0.5 mg/ml COT-DNA (Invitrogen) in hybridization buffer (5x SSC, 0.1% SDS) for 5 min at 95 °C and 30 min at 68 °C to block repetitive sequences in the cDNA. The cDNA was added to pre-warmed (68 °C) hybridization buffer containing 100 µg/ml tRNA (baker's yeast, Roche Applied Science). The cDNA arrays were incubated in pre-hybridization buffer (5x Denhardt's, 5x SSC, 100 mM $NaPO_4$, 2 mM $Na_4P_2O_7$, 100 µg/ml tRNA) for 4 h and subsequently with the labeled cDNA in hybridization buffer for 16 h. The cDNA was removed, and the cDNA arrays were washed with increasing stringency, dried, and exposed on phosphorimaging plates (Fuji). The plates were read on a FujiBas2500 phospho-imaging device, and the raw spot values (volume) were determined using ArrayVision (RayTest, Canada).

6.7.3.4 Western Blotting

Cells were lysed in RIPA- buffer and equal amounts of protein were resolved by SDS-PAGE. Proteins were transferred to PVDF (Perkin Elmer Polyscreen) membranes, blocked for 1h in TBS containing 0.1% Tween-20 (TBST) + 4% nonfat dry milk and incubated overnight at 4°C with primary antibody in TBST + 3% BSA. Primary antibodies used included mouse antibodies recognizing pTyrosine (4G10) (1:1000; homemade), E-cadherin (1:1000; Cell Signaling), Vimentin (1:1000; Cell Signaling), AuroraA (1:1000; Cell Signaling), Tubulin (1:1000; Cell Signaling)), rabbit antibodies detecting ROS1 (1:500; Abcam), TYRO3 (1:1000; Santa Cruz), RON (1:1000; Santa Cruz), PDGFRa (1:1000; Santa Cruz), PDGFRb (1:1000; Santa Cruz) and goat antibodies for NEK9 (1:1000; Santa Cruz), AXL (1:1000; homemade), all of which were obtained from Cell Signaling Technologies. Membranes were washed three times with TBST and incubated with horseradish peroxidase-conjugated antimouse, antirabbit or antigoat secondary antibody in TBST + 4% nonfat dry milk for 1h at room temperature. Membranes were washed three times with TBST and visualized by ECL (Western Lightning, Perkin Elmer) on X-ray films.

6.7.3.5 Cellular Kinase Assay

Cancer cells were seeded at a density of 150.000 cells/well in 6-well flat-bottom cell culture dishes. 24h prior to SU11248 treatment, cells were starved for 24h in medium containing 0% FCS. Drug incubation was performed for 2h, followed by pervanadate stimulation for 5min at 37°C. Cells were lysed and subjected to immunoprecipitation over night.

7 Results

7.1 Profiling of SU11248 activity in cancer cells

SU11248 is so far known to inhibit PDGF receptors, VEGFR2, KIT, FLT3, CSF1R and RET (Kim et al., 2006; Mendel et al., 2003; O'Farrell et al., 2003a) and is highly efficacious *in vitro* as well as in preclinical cancer mouse models (Abrams et al., 2003a; Murray et al., 2003). Currently there are clinical studies ongoing in different types of cancer such as breast cancer, liver cancer, small cell lung cancer (SCLC) and acute myeloid leukemia (AML) (Fiedler et al., 2005; O'Farrell et al., 2003b; Polyzos, 2008; Zhu et al., 2009b).

Due to its broad inhibitory activity it is of great interest to better understand the exact underlying cellular mechanisms of action and its pattern of biological efficacy concerning physiological processes such as cell growth and survival inhibition. Therefore the effect of SU11248 on cancer cell proliferation, apoptosis induction, migration, invasiveness and morphological changes after drug treatment was screened in a broad panel of cancer cell lines from different tumor indications ranging from brain, breast, colorectal, kidney, lung, ovary, pancreatic, prostate to skin cancer. All tested processes are hallmarks of cancer (Hanahan and Weinberg, 2000), e.g. uncontrolled proliferation due to self-sufficiency in growth signals and insensitivity to anti-growth signals or evasion of apoptosis by overexpression of survival genes like survivin and Bcl-XL, which solid tumors acquire in the process of transformation. The inhibition of these phenotypes by small-molecule kinase inhibitors such as SU11248 is of great importance in the attempts of curing cancer. Caused by aberrant gene activation or overexpression such cellular events are susceptible to low molecular weight drugs targeting single or multiple proteins in a specific cellular signal transmission pathway (Zhang et al., 2009a).

7.1.1 Effect of SU11248 on cancer cell proliferation

One very important and crucial aspect for tumor initiation, development and progression is aberrant cell growth caused by oncogenes being constitutively active due to mutations or increased gene expression driving cellular transformation. The goal of a successful cancer therapy is to repress the uncontrolled cell proliferation of a transformed tumor cell at a very early stage. In comparison to classical chemotherapeutic treatments targeting all proliferating cells of either normal or cancerous tissue the advantage of small-molecule inhibitors such as SU11248 is the more specific interaction with tumor cells thereby showing an augmented efficiency in inhibition and lesser toxic side-effects compared to `standard-of-care` therapies. Therefore it is of great importance to reveal the sensitivity spectrum of SU11248 in order to find new indications beyond mRCC (metastatic renal cell carcinoma) and GIST (gastro-intestinal-stromal tumor) were chemotherapy can be accompanied or even replaced by a target-specific small-molecule application.

In a SU11248 efficacy screening of drug induced cancer cell growth inhibition in a panel of 63 cancer cell lines of 10 different tissue origins it could be shown that SU11248 has a strong anti-proliferative anti-tumor effect. It inhibits cancer cell growth in a time- and dose-dependent manner which is shown in Figure 12 for the prostate cancer cell line DU145 over 3 days of drug treatment. An overview of SU11248 inhibition rates at a concentration of 2.5 µM in the tested cell line panel is given in Figure 13. Inhibition curves at 72h are illustrated in Figure 14 and averaged IC_{50}-values of all tested cell lines are summarized in Figure 15 and listed in Table 5.

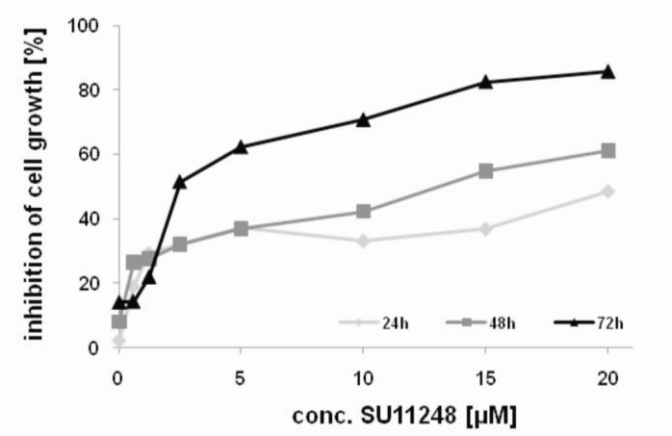

Figure 12 Cancer cell growth inhibition by SU11248 in a time-and dose-dependent manner.
Data are shown for the prostate cancer cell line DU145 in percent inhibition relative to DMSO vehicle control for three different time-points (24, 48, 72h). Cells were grown in 96-well flat-bottom plates under serum conditions (10 % FCS (w/v)) and treated with the indicated SU11248 concentrations for 72h. Cell numbers were determined by using a colorimetric MTT assay.

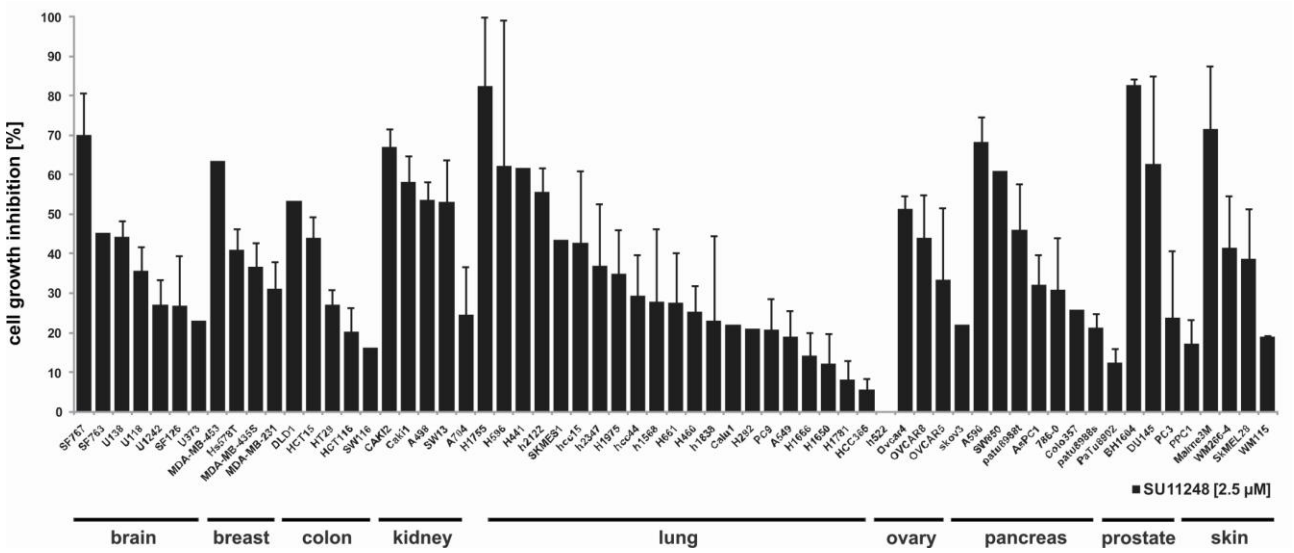

Figure 13 Cancer cell growth inhibition by SU11248 at a concentration of 2.5 µM.
Averaged inhibition rates of cancer cell growth of the small-molecule kinase inhibitor SU11248 at a concentration of 2.5 µM are shown for all treated cell lines ranging from brain, breast, colon, kidney, lung, ovary, pancreas, prostate and skin cancer. Cancer cell lines are sorted by tissue origin and SU11248 reactivity. The inhibition rates are averaged over three to five independent experiments and shown as mean values including s.e.m. as standard error.

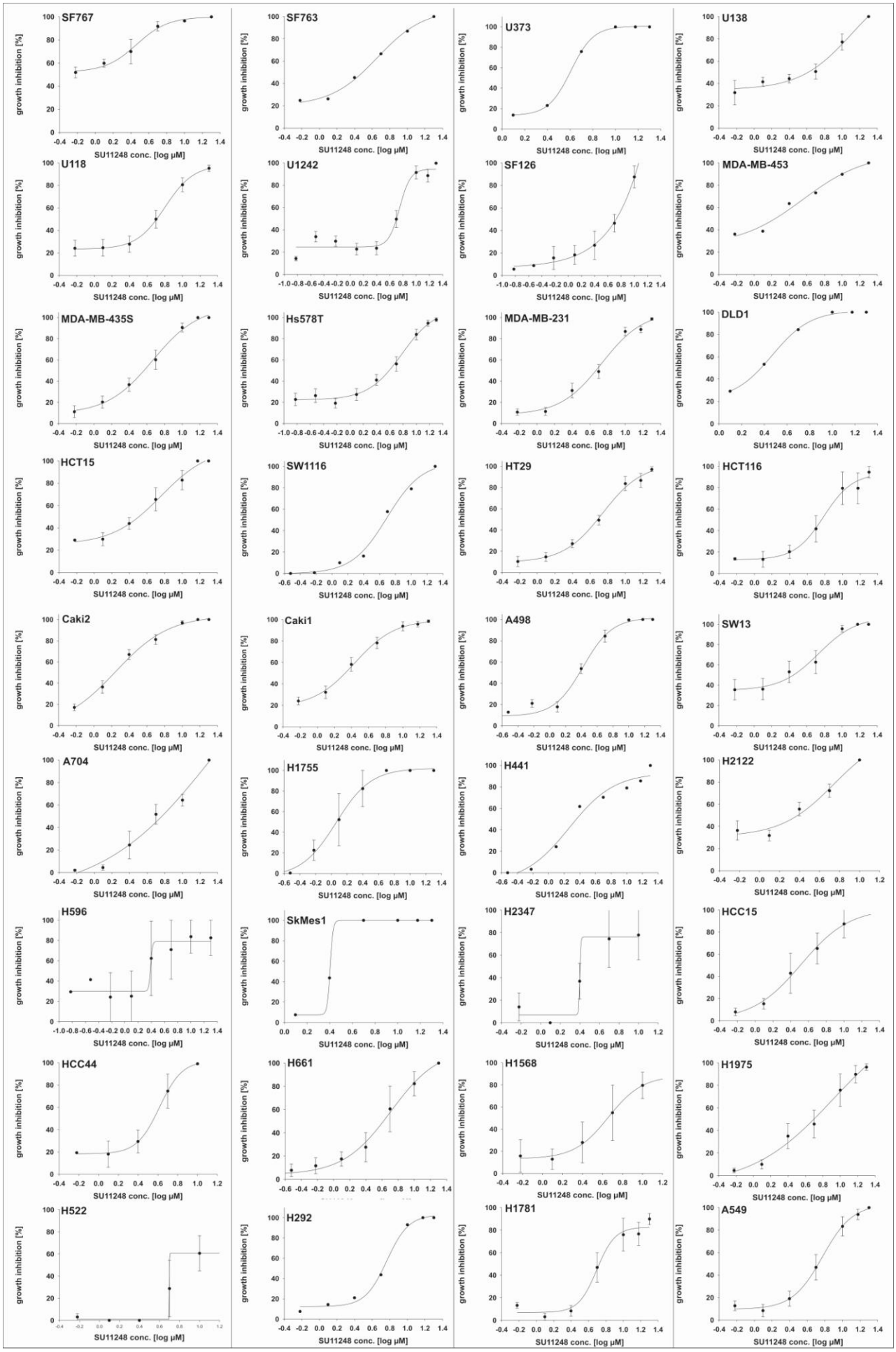
SF767
SF763
U373
U138
U118
U1242
SF126
MDA-MB-453
MDA-MB-435S
Hs578T
MDA-MB-231
DLD1
HCT15
SW1116
HT29
HCT116
Caki2
Caki1
A498
SW13
A704
H1755
H441
H2122
H596
SkMes1
H2347
HCC15
HCC44
H661
H1568
H1975
H522
H292
H1781
A549
growth inhibition [%]
SU11248 conc. [log µM]

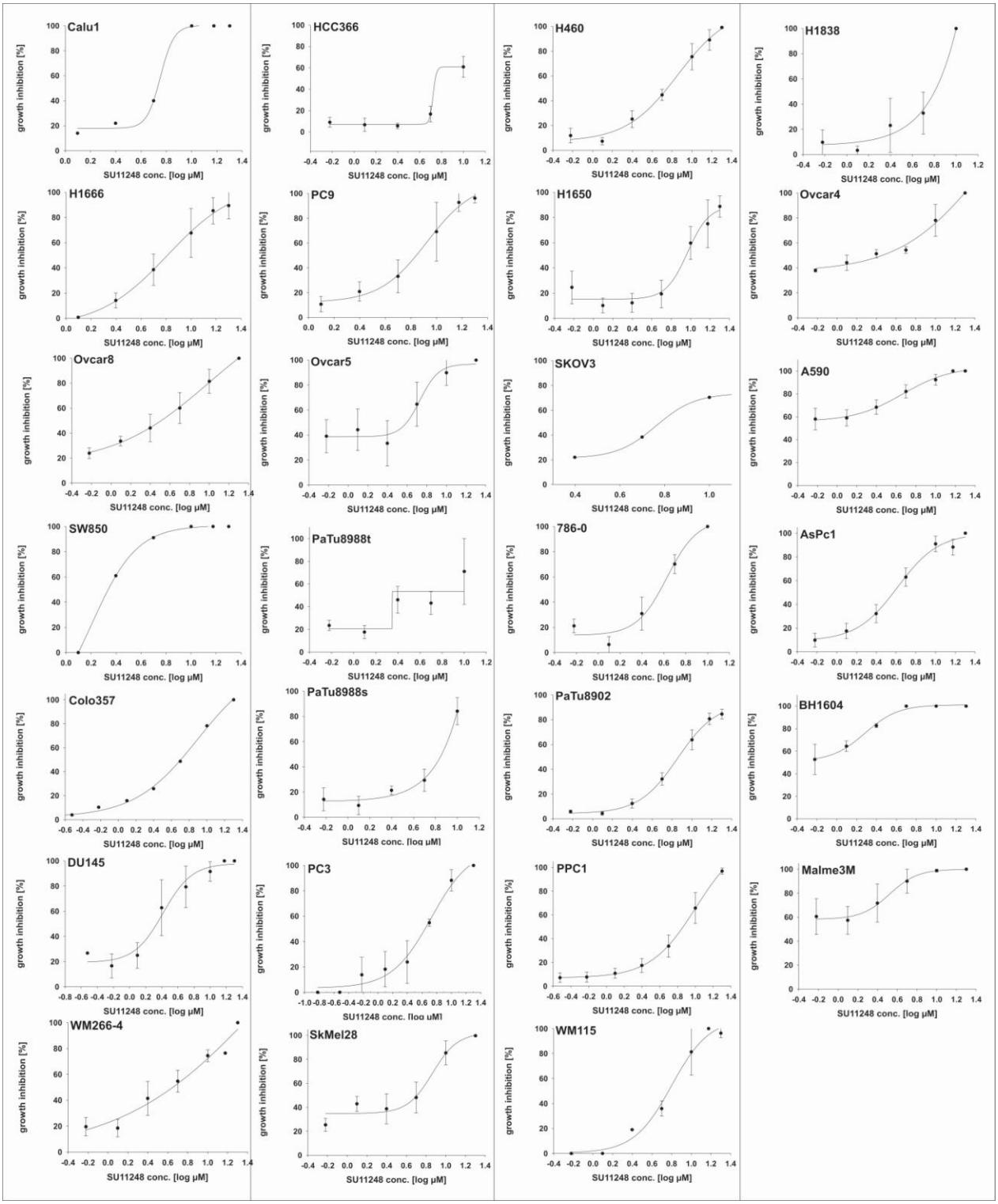

Figure 14 Dose-inhibition curves of cancer cell growth after SU11248 treatment for 72h monitored by MTT.

Cells were grown in 96-well flat bottom plates under serum conditions (10 % FCS (w/v)) and treated with the indicated SU11248 concentrations for 72h. Metabolic active cells were measured using the MTT colorimetric method and data analysis was performed in Sigma-Plot 10.0 using a sigmoidal-dose-response curve fitting algorithm on log-transformed data points for simple ligand binding. Cell lines are sorted by tumor tissue and drug-sensitivity.

Among all tested tissues SU11248 sensitive cancer cell lines were found with IC_{50}-values ranging from <1 to 10 µM. Cell lines like A590 (pancreas), Caki1 (kidney), Caki2 (kidney), H1755 (liver), SF767 (glioblastoma), Malme3M (melanoma), BH1604 (prostate) and others with an IC_{50}-value lower than 3 μM were considered as sensitive to SU11248 whereas cell lines like AsPc1, HT29, PaTu and others with IC_{50}-values of 4 µM and higher were taken as not very responsive to the drug treatment. Similar results were apparent in a Sulforhodamine B (SRB) assay which measures cell densities containing viable and apoptotic cells based on a dye-based protein content staining within a cell (Vichai and Kirtikara, 2006). Results are shown in Figure 16. Mean IC_{50}-values are listed in Table 6.

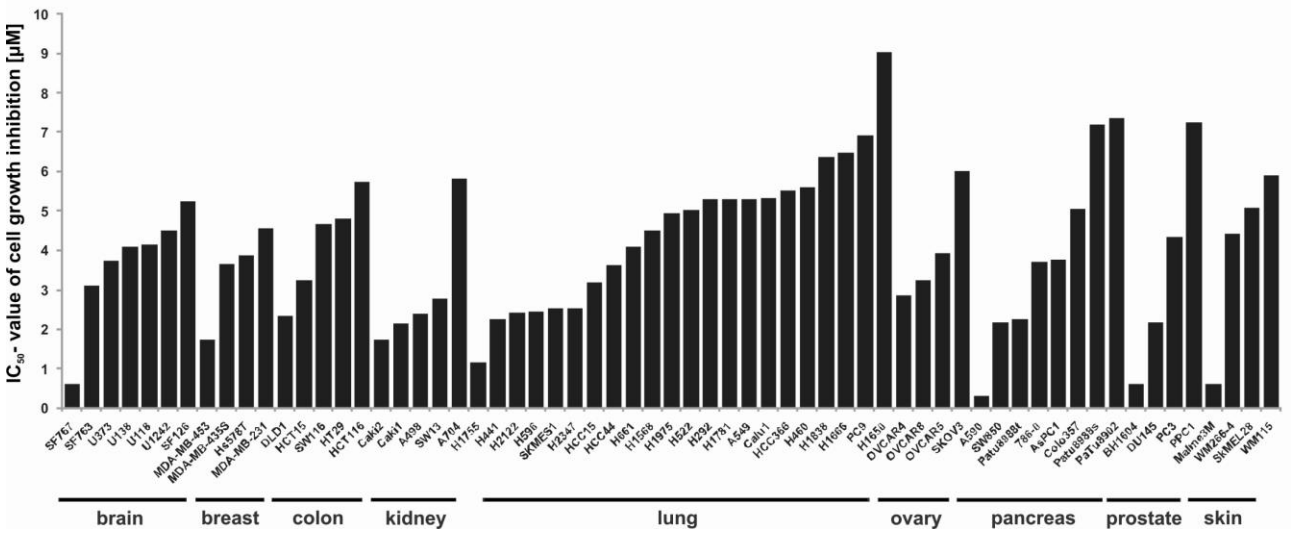

Figure 15 IC_{50}-values of cell growth inhibition of cancer cells by SU11248 after 72h sorted by tissue origin and sensitivity.
IC_{50}-values represent the average of independent experiments and were calculated with Sigma Plot 10.0 using a sigmoidal-dose-response curve fitting algorithm.

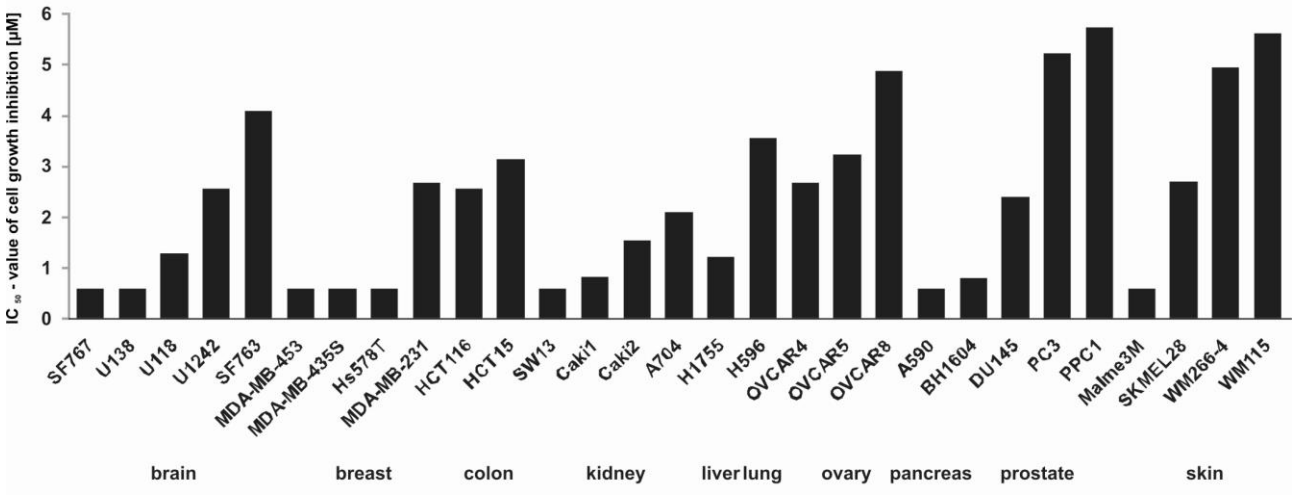

Figure 16 IC_{50}-values of cell growth inhibition of cancer cells by SU11248 after 72h sorted by tissue origin and sensitivity.
IC_{50}-values represent the average of independent experiments and were calculated with Sigma Plot 10.0 using a sigmoidal-dose-response curve fitting algorithm. Drug dependent cell growth inhibition was measured using the Sulforhodamine B (SRB) colorimetric assay.

Table 5 IC_{50}-value overview of cancer cell growth inhibition by SU11248 sorted by tissue origin and sensitivity.
Data are shown for the cell growth assay MTT.

tissue	cell line	IC_{50} [µM]	tissue	cell line	IC_{50} [µM]
brain	SF767	**0.60**	lung	H522	**5.01**
brain	SF763	**3.10**	lung	H292	**5.30**
brain	U373	**3.73**	lung	H1781	**5.30**
brain	U138	**4.08**	lung	A549	**5.30**
brain	U118	**4.14**	lung	Calu1	**5.34**
brain	U1242	**4.50**	lung	HCC366	**5.52**
brain	SF126	**5.25**	lung	H460	**5.59**
breast	MDA-MB-453	**1.72**	lung	H1838	**6.37**
breast	MDA-MB-435S	**3.66**	lung	H1666	**6.48**
breast	Hs578T	**3.87**	lung	PC9	**6.92**
breast	MDA-MB-231	**4.57**	lung	H1650	**9.04**
colon	DLD1	**2.34**	ovary	OVCAR4	**2.86**
colon	HCT15	**3.23**	ovary	OVCAR8	**3.23**
colon	SW116	**4.68**	ovary	OVCAR5	**3.92**
colon	HT29	**4.81**	ovary	SKOV3	**6.01**
colon	HCT116	**5.75**	pancreas	A590	**0.30**
kidney	Caki2	**1.72**	pancreas	SW850	**2.17**
kidney	Caki1	**2.15**	pancreas	Patu8988t	**2.24**
kidney	A498	**2.40**	pancreas	786-0	**3.72**
kidney	SW13	**2.78**	pancreas	AsPC1	**3.76**
kidney	A704	**5.83**	pancreas	Colo357	**5.05**
liver	H1755	**1.16**	pancreas	Patu8988s	**7.19**
lung	H441	**2.26**	pancreas	PaTu8902	**7.36**
lung	H2122	**2.43**	prostate	BH1604	**0.60**
lung	H596	**2.44**	prostate	DU145	**2.18**
lung	SKMES1	**2.53**	prostate	PC3	**4.34**
lung	H2347	**2.53**	prostate	PPC1	**7.26**
lung	HCC15	**3.19**	skin	Malme3M	**0.60**
lung	HCC44	**3.64**	skin	WM266-4	**4.43**
lung	H661	**4.09**	skin	SkMEL28	**5.08**
lung	H1568	**4.49**	skin	WM115	**5.91**
lung	H1975	**4.95**			

Table 6 IC_{50}-value overview of cancer cell growth inhibition by SU11248 sorted by tissue origin and sensitivity.
Data are shown for the cell growth assay SRB.

tissue	cell line	IC_{50} [µM]
brain	SF767	<0.6
brain	U138	<0.6
brain	U118	1.29
brain	U1242	2.56
brain	SF763	4.08
breast	MDA-MB-453	0.60
breast	MDA-MB-435S	0.60
breast	Hs578T	<0.6
breast	MDA-MB-231	2.67
colon	HCT116	2.56
colon	HCT15	3.15
kidney	SW13	<0.6
kidney	Caki1	0.82
kidney	Caki2	1.54
kidney	A704	2.09
liver	H1755	1.22
lung	H596	3.56
ovary	OVCAR4	2.67
ovary	OVCAR5	3.23
ovary	OVCAR8	4.88
pancreas	A590	<0.6
prostate	BH1604	0.79
prostate	DU145	2.39
prostate	PC3	5.23
prostate	PPC1	5.75
skin	Malme3M	<0.6
skin	SKMEL28	2.71
skin	WM266-4	4.95
skin	WM115	5.62

The strong anti-proliferative effect of SU11248 on cancer cells could also be shown in a BrdU- incorporation assay with again A590 and Caki1 being the most sensitive cell lines with an IC_{50}-value of smaller 1.25 µM and 2.24 µM, respectively (Figure 17). BrdU-labelling directly measures cells undergoing DNA-replication in the S-phase of the cell cycle. In contrast to the MTT-assay that measures viable cells in general, the BrdU-assay directly indicates the amount of proliferating cells.

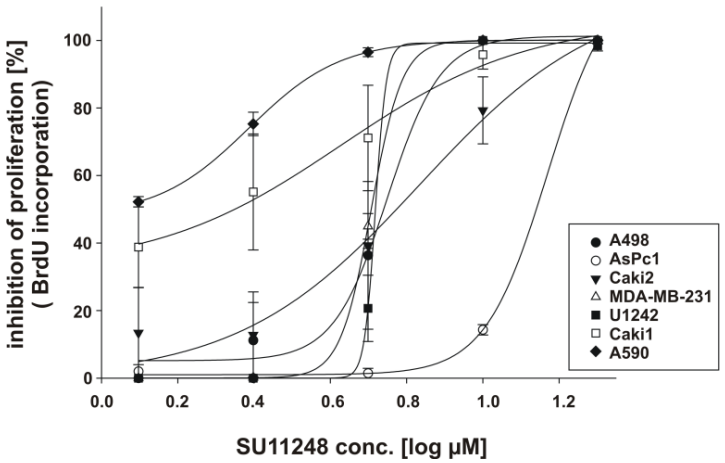

	IC50	SEM
A590	< 1.25	0.18
Caki1	2.24	1.27
MDA-MB-231	5.01	0.01
U1242	5.24	0.07
A498	5.50	0.42
Caki2	5.95	0.83
AsPc1	13.80	1.38

Figure 17 Inhibition of cancer cell proliferation after SU11248 treatment for 72h monitored by BrdU-incorporation.
Cells were grown in 96-well flat-bottom plates under serum conditions (10 % FCS (w/v)) and treated with the indicated SU11248 concentrations for 72h. Replicating cells were detected using the DNA-intercalation agent BrdU for incorporation. Data analysis was performed in Sigma- Plot 10.0 using a sigmoidal-dose-response curve fitting algorithm on log-transformed data points for simple ligand binding. Mean IC_{50}-values of tested cell lines are shown in the right table and are sorted by SU11248 sensitivity.

In general, IC_{50}-values in the BrdU-assay are higher than those in the MTT-assay due to the combinative effect of cell proliferation inhibition and induction of apoptosis measured by the MTT-assay. In summary, it could be shown that many cell lines are reactive to SU11248 exposure and by comparing the mean sensitivity of cell lines from one tissue origin with cell lines from other tumor types which is shown in Figure 18 and listed in Table 7 new tumor indications beyond mRCC such as prostate, ovary, breast and brain could be found to be highly responsive to SU11248 treatment being possible new indications for future SU11248 applications in the clinic.

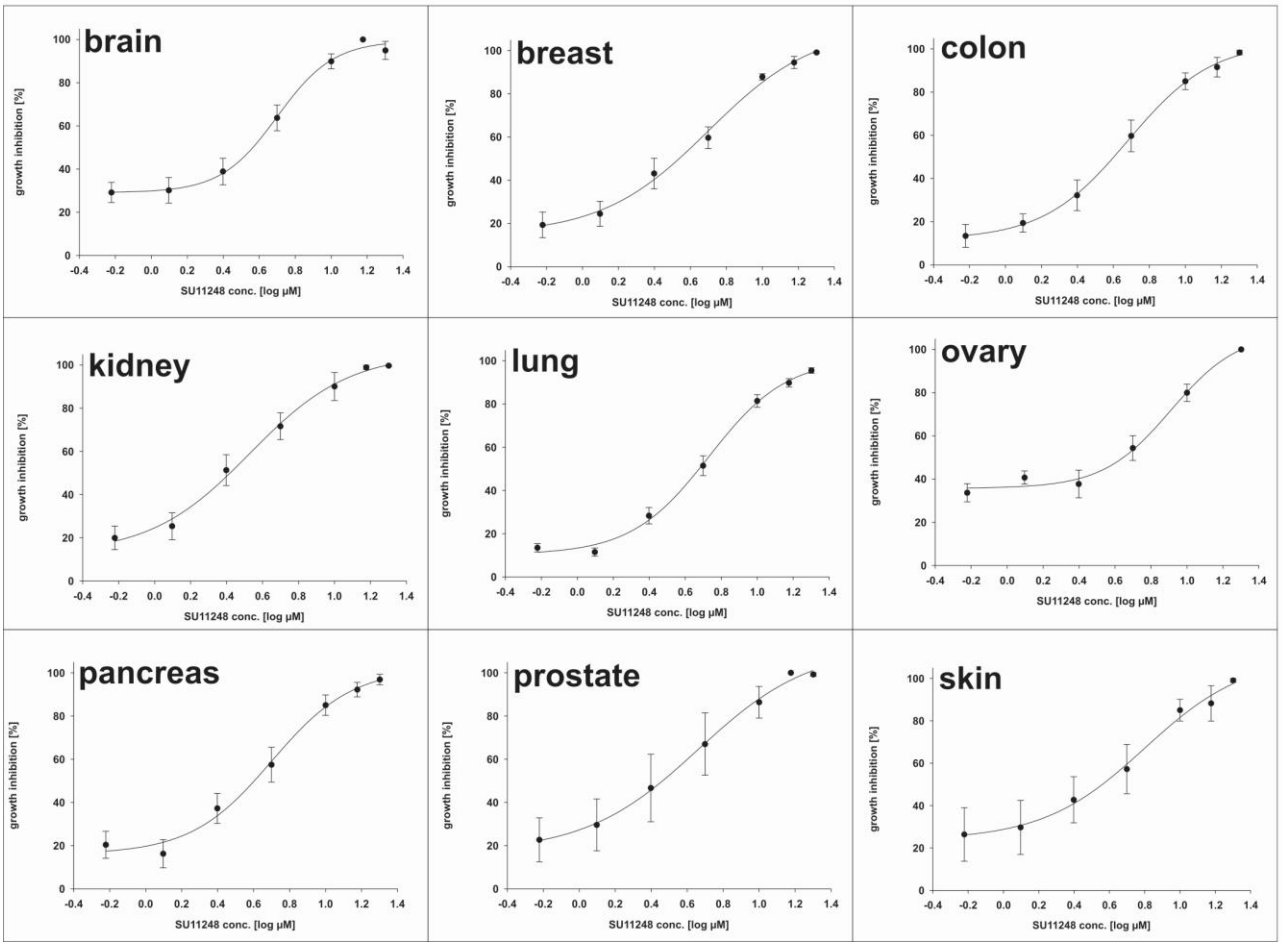

Figure 18 Averaged dose-inhibition curves of tissue specific cancer cell growth after SU11248 treatment for 72h monitored by MTT.
Cells were grown in 96-well flat bottom plates under serum conditions (10 % FCS (w/v)) and treated with the indicated SU11248 concentrations for 72h. Metabolic active cells were measured using the MTT method and data analysis was performed in Sigma-Plot 10.0 using a sigmoidal-dose-response curve fitting algorithm on log-transformed data points for simple ligand binding. The inhibition curves of cell lines belonging to the same tumor indication were averaged and are shown as cancer type specific growth inhibition curves.

Table 7 Mean IC_{50}-values of cancer type specific cell growth inhibition by SU11248 after 72h.
Data are shown for the cell growth assay MTT.

tissue	mean IC_{50} [µM]
kidney	2.63
prostate	2.90
breast	3.46
brain	3.66
skin	3.66
colon	4.03
pancreas	4.03
ovary	4.43
lung	4.75

7.1.2 Effect of SU11248 on cancer cell apoptosis and cell cycle distribution

Beside unlimited cell proliferation the evasion of apoptosis is a second criterion of transformed tumorigenic cells.

In a subset of cell lines the ability of SU11248 to induce apoptosis was assessed using the FACS-PI staining method (Riccardi and Nicoletti, 2006). Apoptosis rates after drug treatment were quantified from the subG$_1$-peak seen in the FACS images (Figure 19) and are shown in percent relative to DMSO vehicle control for three different SU11248 concentrations (5, 10, 20 µM) at 72h in Figure 20. SU11248 induced apoptosis in a dose- and time-dependent manner with up to 90 % of dead cells after treatment with 20 µM SU11248. The cell lines are tissue-sorted.

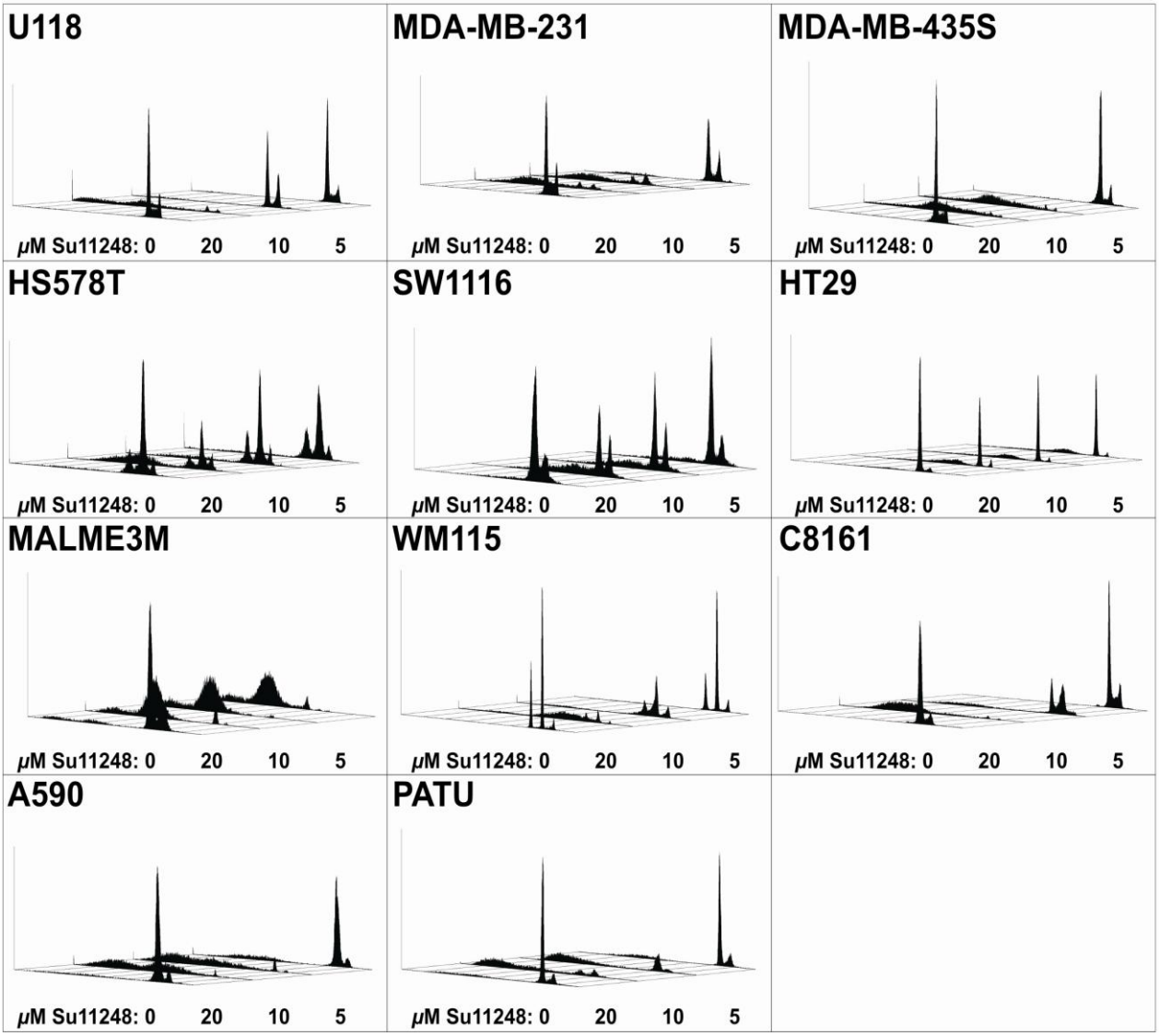

Figure 19 FACS-images of cancer cell lines from different tissue origins treated with the indicated SU11248 concentrations for 72h.

Histograms showing the distribution of cells in subG$_1$-, G$_1$-, S- and G$_2$/M- phase. For measuring the rate of apoptosis induction 30.000 cells/well were seeded in 24-well flat-bottom plates 24h prior to SU11248 treatment and incubated with the indicated inhibitor concentrations for 72h under serum conditions (10 % FCS (w/v)). The subG$_1$-peak is a direct measure for apoptotic cells and increased with higher SU11248 concentrations.

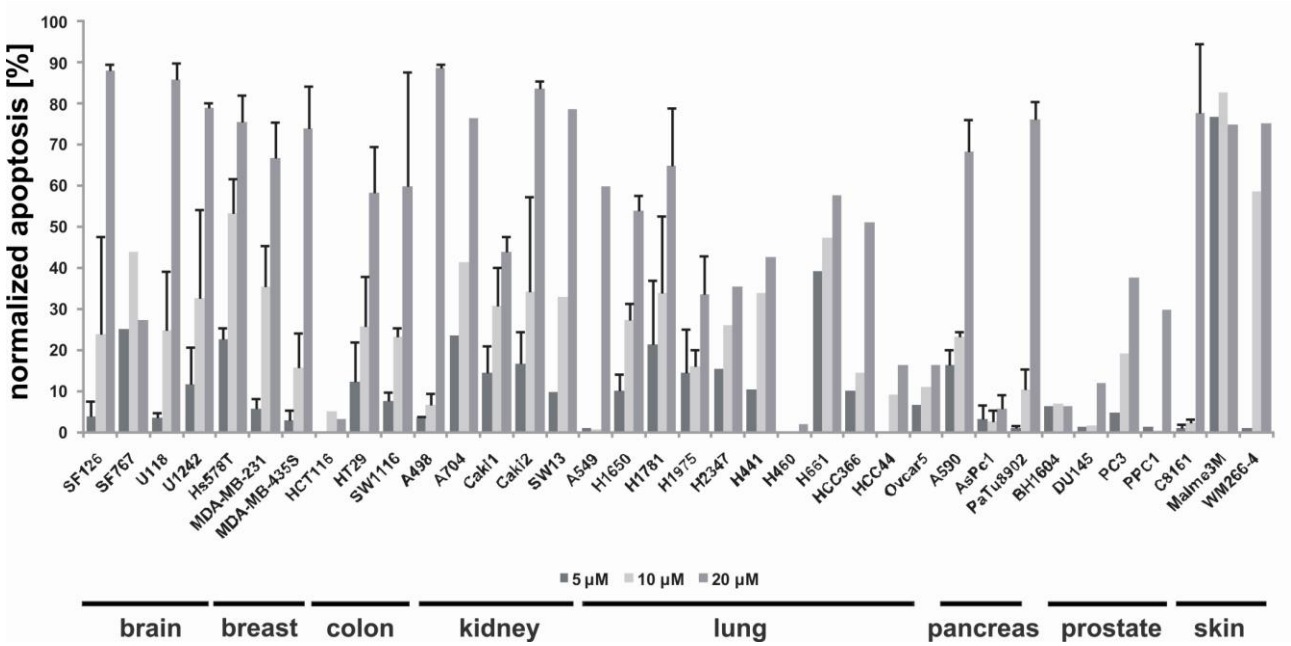

Figure 20 Quantification of apoptosis rates in a variety of cancer cells from different tissue origins after SU11248 treatment for 72h.
SU11248 strongly induces apoptosis in cancer cells. For measuring apoptosis induction, cells were treated with the indicated concentrations of SU11248 for 72h in the presence of 10 % FCS and the number of dead cells was measured by FACS using the PI-staining method. Data are expressed as the percentage of apoptotic cells relative to DMSO vehicle control quantified from subG_1-peaks using the analyzing software Cell Quest Pro.

LD_{50}-values which could be determined in the applied concentration range of 1 to 20 µM SU11248 are summarized in Table 8.

Table 8 LD_{50}-values of apoptosis-induction in cancer cell lines by SU11248 sorted by tissue origin and sensitivity.

cancer cell line	tissue	LD_{50} [µM]
U118	brain	8.78
U1242	brain	16.60
MDA-MB-231	breast	6.56
Hs578T	breast	6.65
MDA-MB-435S	breast	8.42
Ovcar4	ovary	15.50
A590	pancreas	6.14
Capan1	pancreas	12.00
C8161	skin	11.59
WM115	skin	12.90

Interestingly, not all cell lines being highly responsive in the MTT assay showed an apoptotic effect to a similar extent. For example, Caki1, very sensitive in the cell growth assay, showed a relative low apoptosis rate after drug treatment for 72h whereas A590 and Caki2 are reactive in both biological assays. As a result, these data illustrate that there is a clear-cut difference between the anti-proliferative and apoptosis-inducing effect of SU11248, presumably due to different cellular targets hit by SU11248, reflecting different gene expression states of the used cell lines. In this context and the fact that SU11248 is a multi-targeted inhibitor

the shown physiological effects and differences between cancer cell lines even of the same tissue origin are quite reasonable. Each tumor type and even cancer cell lines of the same tissue origin depend on different driving genes relevant for the functional integrity of a cell (Greenman et al., 2007; Stratton et al., 2009).

The apoptosis inducing effect of SU11248 was also seen using a caspase-3/7-activity assay (Figure 21). Caspases are key regulators of induced cell death and can be used as discrimination markers for cytotoxic versus mechanism-based anti-survival effects of a small-molecule drug (Thornberry, 1998; Thornberry and Lazebnik, 1998). Both apoptosis-assays showed a clear-cut difference between SU11248 sensitive and insensitive cell lines. The pancreas cancer cell line A590, the kidney cancer cell lines Caki1, Caki2, A498, the brain cancer cell line U1242, the lung cancer cell line H1975 and the breast cancer cell lines MDA-MB-231, MDA-MB-435S and Hs578T were highly responsive whereas the colon cancer cell line HT29 and the pancreas cancer cell line AsPc1 did not show any or very weak caspase-3/7-activity nor apoptotic staining in the FACS analysis. In addition, a very high induction of apoptosis after drug treatment was also seen in the cell lines U1242, SF126, U118 (glioblastoma), Malme3M, WM266-4 (melanoma) and H1781 (lung). Differences between the FACS- and the caspase-3/7-assay are due to the different markers taken as a measurement of apoptosis. The two apoptosis-read-outs are DNA-fragmentation and caspase-activity. Caspases are early markers of apoptosis with a maximum activation after 24 to 48h of death-stimulus, whereas nuclear destruction followed by DNA-fragmentation measured by propidiumiodide-staining is a very late event in the process of cell death. This occurs between 3-6 days after the apoptotic stimulus and varies from cell line to cell line. For example, the kidney cancer cell line A498 showed a relative high caspase-activity after 48h but almost no DNA-fragmentation at the taken time-point of 72h after drug treatment. The apoptotic rate in the FACS-analysis was only visible after 5 days of treatment (data not shown). Nevertheless, with both assays similar results were obtained.

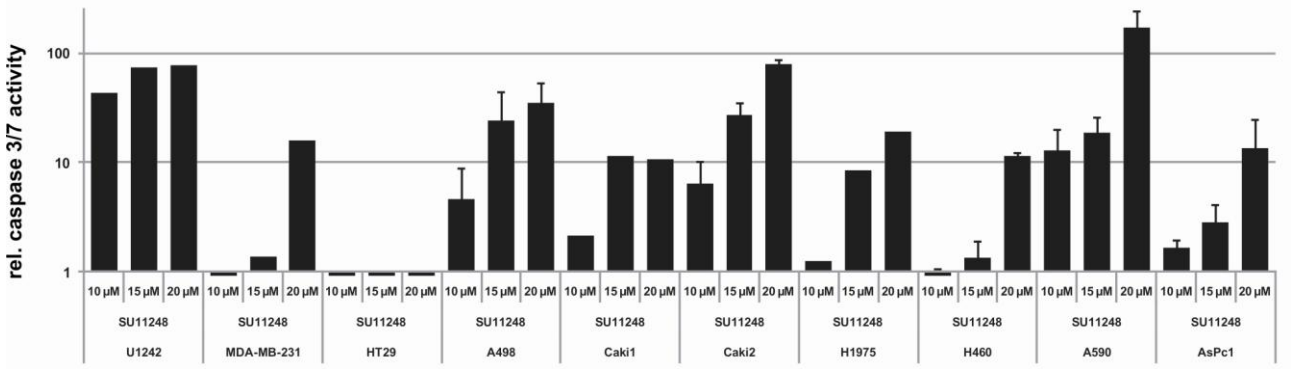

Figure 21 Caspase 3/7-activity after SU11248 treatment of the pancreatic cancer cell lines A590, AsPc1, the mRCC cell lines Caki1, Caki2, A498, the breast cancer cell line MDA-MB-231, the colon cancer cell line HT29, the brain cancer cell line U1242 and the lung cancer cell lines H1975, H460 for 48h.

Cells were grown under high serum conditions (10 % FCS (w/v)) and treated with increasing SU11248 concentrations or DMSO vehicle control for 48h. The caspase-3/7-activity was measured using a luminescence based assay from Promega (*Caspase 3/7-Glo-Assay*).

Taken together, these data underline a mechanism-based anti-survival effect of SU11248 in a variety of different cancer cell lines of different tissue origins. The fold-induction of caspase-3/7-activity is a direct

measure and proportional to induced cell death caused by SU11248 treatment and shows the same cell line-sensitivity-hierarchy as seen in the PI-staining method after SU11248 exposure.

With having a closer look at the cell cycle distribution after SU11248 treatment one could see that SU11248 induces a strong G_2/M-cell cycle arrest at high concentrations of 20 and 10 µM and leads to a G_1-cell cycle arrest at lower doses (5 and 2.5 µM, respectively). Figure 22 shows the FACS-images after 24h of drug treatment with 20 µM SU11248 and the quantification is plotted in Figure 23. The dose-dependent cell-cycle distribution of two representative breast cancer cell lines MDA-MB-231 and MDA-MB-435S are displayed in Figure 24. This prominent cell-cycle arrest is in line with the observed anti-proliferative phenotype of SU11248 as described above.

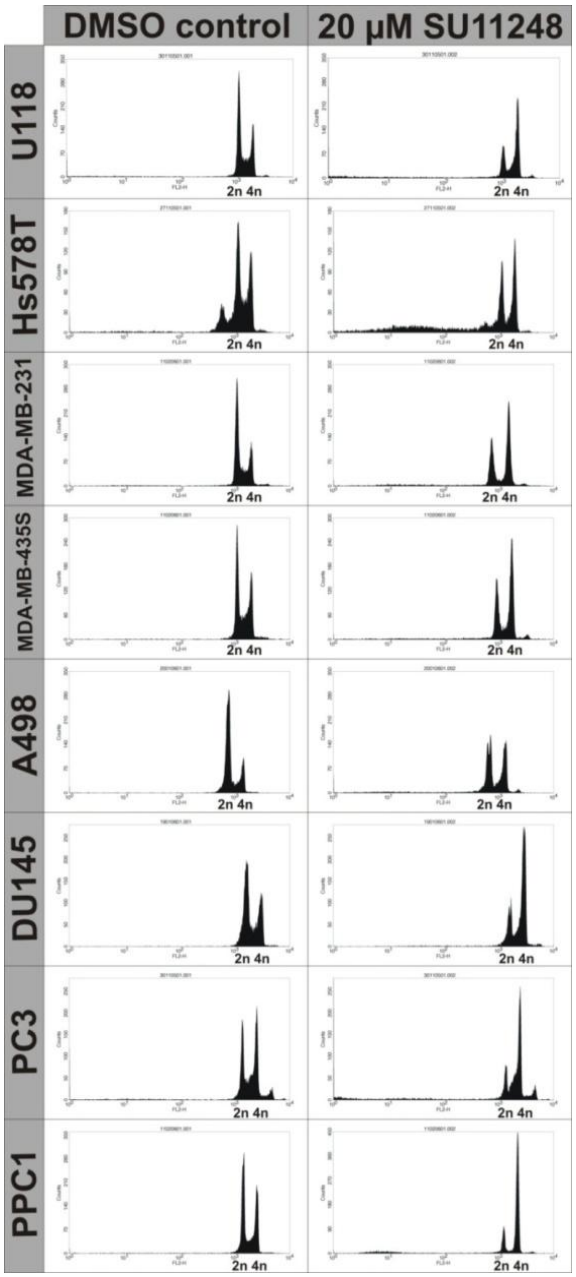

Figure 22 FACS-analysis of cell cycle distribution of SU11248 treated cancer cell lines.
FACS- images showing a G_2/M- cell cycle arrest after SU11248 treatment for 24h. Cells were grown under serum conditions (10 % FCS (w/v)) and treated with either DMSO vehicle control or 20 µM SU11248 for 24h. The DNA-content was labeled with propidiumiodide (PI) and analyzed by flow-cytometry.

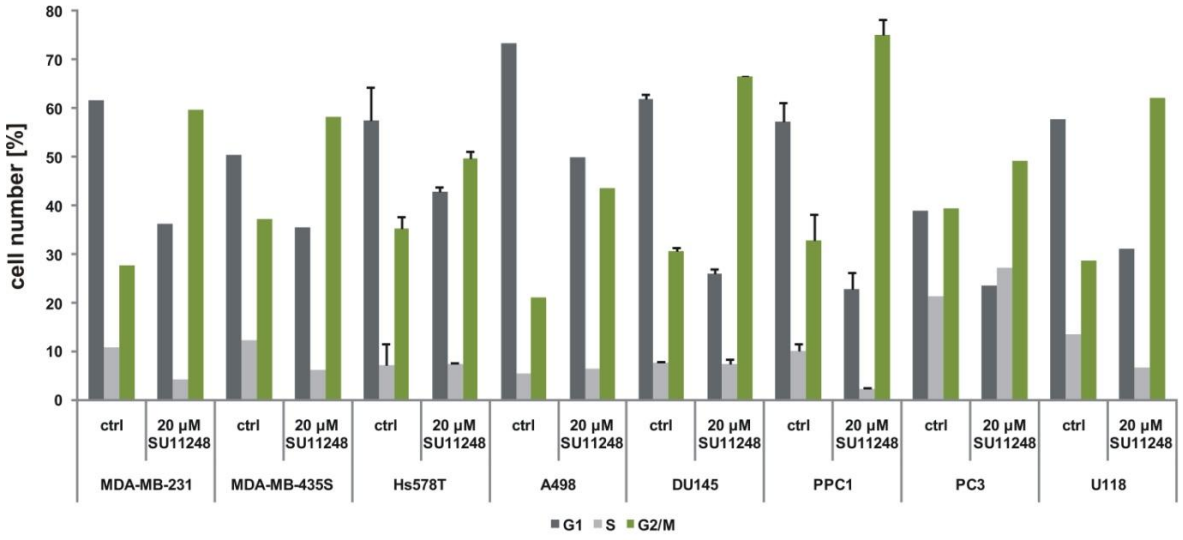

Figure 23 Quantification of cell cycle analysis after 24h of SU11248 treatment using the PI-staining method for flow cytometry.
Data are shown as the cell number in percent distributed in G_1-, S- and G_2/M- cell cycle phases quantified from FACS-images using the software CellQuestPro.

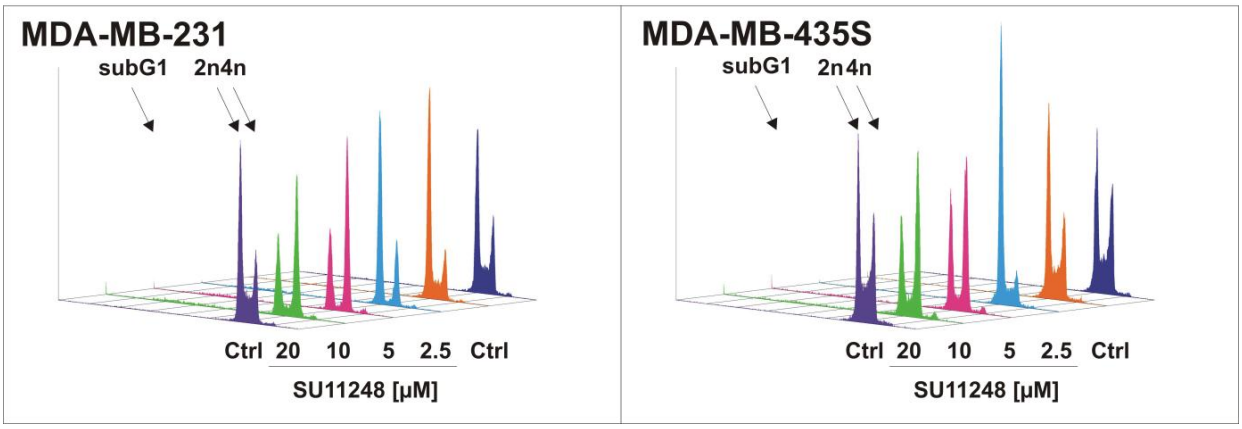

Figure 24 Cell-cycle-distribution after 24h of SU11248 treatment with increasing drug concentrations under serum conditions (10 % FCS).
Cells were grown under serum conditions (10 % FCS) and treated with increasing SU11248 concentrations for 24h. PI-staining was used for DNA-content measurement reflecting the cell-cycle-distribution of a single cell. FACS-images were analyzed using the CellQuestPro software.

7.1.3 Effect of SU11248 on cancer cell migration and invasion

In the process of cancerous diseases, especially tumor progression, one very critical and devastating step is the occurrence of metastasis. This usually takes place if primary cancer cells are getting more aggressive and invade other tissues via the blood system. Due to an inherent genetic instability of tumor cells, by the time, they gain the ability of moving from the primary tumor site to other tissues in the body, e.g. lymph nodes, bone and lung. Usually this is in accordance with the expression of certain proteins like matrix-metalloproteinases and other key-regulators of invasion and metastasis (Chiang and Massague, 2008; Olson, 2007). Another crucial step in the development of tumor metastasis is the transition of a cancer cell from an

epithelial-like non-migrating cell shape to a more aggressive and migrating mesenchymal-like state, so called EMT. This EMT (epithelial-to-mesenchymal-transition) is a prerequisite for cancer cell migration from the first tumor location to new spots within the organism (Thompson et al., 2005; Voulgari and Pintzas, 2009; Wu and Zhou, 2008; Yang and Weinberg, 2008).

In general, primary tumors can be often surgically removed or are susceptible to standard-of-care therapies like chemotherapeutics and radiotherapy. At this stage many tumors are still curable with conventional methods. Nevertheless, a major problem of standard-of-care therapies is the fact that usually not all cancer cells are removed by surgery or killed by chemotherapeutics and radio-therapy even if there is no visible tumor left. Those remaining cells, often quiescent cancer stem cells resistant to apoptosis induction (Bao et al., 2006; Dalerba et al., 2007; Diehn and Clarke, 2006; Huff et al., 2006; Wicha et al., 2006), are the reason for a relapse, often seen with many aggressive tumors like for example liver cancer, pancreatic cancer or highly aggressive breast cancer types. Those secondary tumors are vastly more aggressive than their primary counterparts and usually tend to spread very fast throughout the body. This phenomenon correlates with a poor prognosis and a shortened overall survival rate compared to non-spreading tumors. Furthermore, metastasizing cells and secondary tumors are in general less reactive to standard-of-care therapeutics due to gained resistances like target mutations or activated side-pathways relevant for cell survival and proliferation of the respective cancer cell compensating the inhibited cellular process. Based on these developed resistances the need of second-line-treatments or alternative first-line-medications came into the focus of interest and are fundamental steps in curing cancer. One huge branch of second-line-treatment or substitutes for chemotherapeutics with an augmented reduction of side-effects are for example therapeutic antibodies and the even larger group of low-molecular-weight drugs/inhibitors targeting specific molecular sites like protein kinases or enzymatic enzymes within a cancer cell. For a successful second-line-treatment it is of great importance to inhibit cancer cell migration and followed tissue invasion. With SU11248 being used as a second-line inhibitor it is of general interest to test its anti-migratory and anti-invasive effects *in vitro* and *in vivo* to better understand its pharmacodynamic potential.

Therefore migration- and invasion-assays were performed in a subset of migrating and invading cancer cells of different tissue origins like breast, brain, kidney and colon and the SU11248 inhibitory efficacy in those cellular systems was tested. The very aggressive breast cancer cell lines MDA-MB-231, MDA-MB-435S, Hs578T, the mRCC cell lines Caki1 and Caki2, the liver cancer cell line H1755, the glioblastoma cell lines U1242, U118 and SF126 as well as the prostate cancer cell lines PC3, PPC1 and the pancreas cancer cell line Colo357 were selected for further experiments. All cells were employed in wound-closure experiments and transwell-migration assays. SU11248 inhibited wound closure in a dose-dependent manner in most cell lines to varying extents and two representative experiments for MDA-MB-231 and Hs578T are shown in Figure 25.

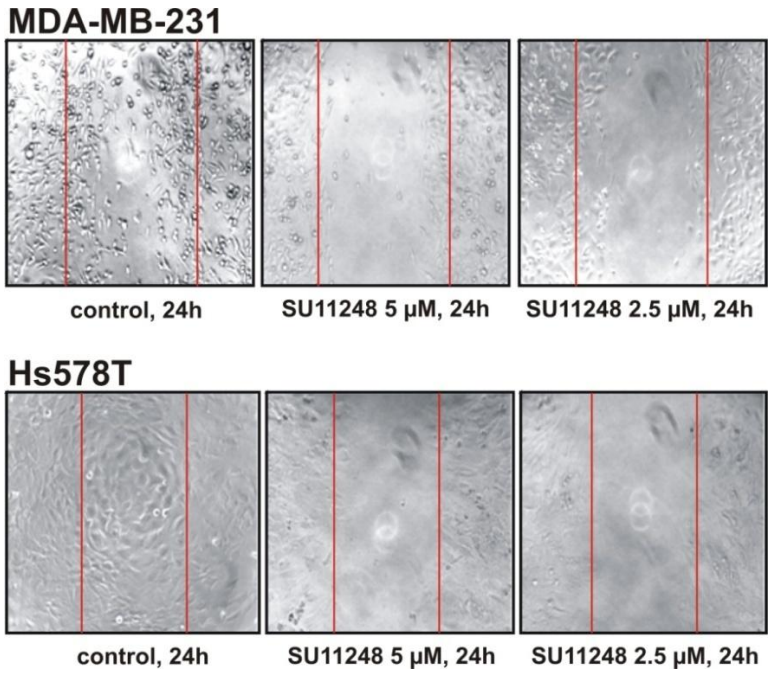

Figure 25 Wounding assay of the aggressive breast cancer cell line MDA-MB-231 and Hs578T.
Cells were seeded in 24-well flat-bottom plates and grown to confluency under normal serum conditions (10 % FCS (w/v)). A scratch was done with a pipette tip followed by medium change and the wound closure was visualized after 24h by phase- contrast microscopy (x10). The red line indicates the scratch edges at the starting time point (0h).

5 µM of SU11248 completely blocked cell migration in both cases and the IC_{50}-values are below 1 µM. To obtain quantitative data of migration-inhibition the same cell lines were tested in a transwell-migration assay and treated with increasing SU11248 concentrations for 16h. Data are presented in Figure 26 and Figure 27. Figure 26 shows photomicrographs of migrated cells taken after 16h of SU11248 treatment. For visualization and followed quantification, migrated cells were stained with crystal violet, documented and dissolved in acetic acid to extract the dye from the cells. Relative optical densities were measured in an ELISA-well-plate reader at 595 nm.

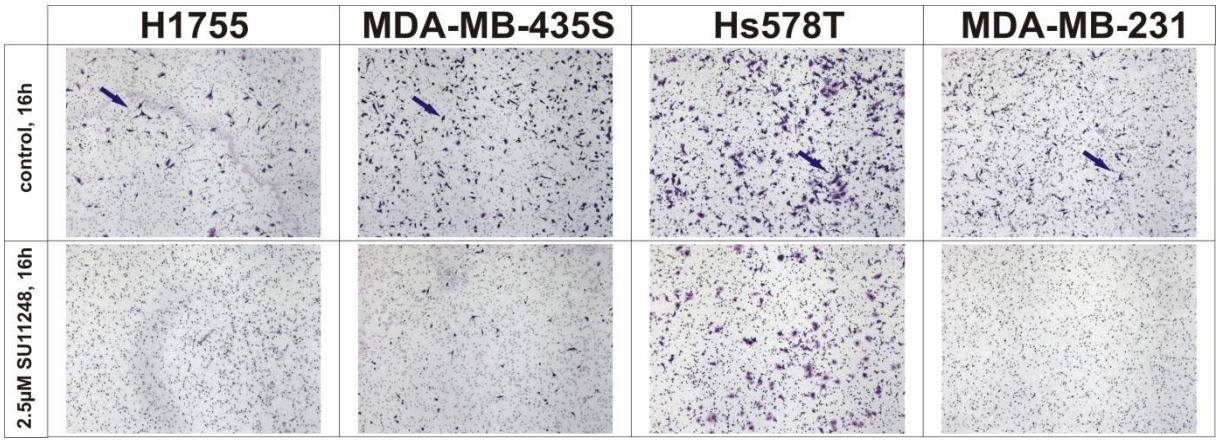

Figure 26 Transwell Migration Assay performed in Boyden chambers.
Cells cultured in medium containing 0 % FCS were seeded in the upper chamber and incubated with 2.5 µM SU11248 for 16h. As a migratory stimulus 10 % FCS was used. Migrated cells were stained with crystal violet and phase-contrast photomicrographs (x4) were taken from each well.

Similar results and an even higher SU11248 efficacy than in the wound closure assay was observed in the transwell-Boyden-chamber assay. Quantification of the data at 5 µM SU11248 is shown in Figure 27.

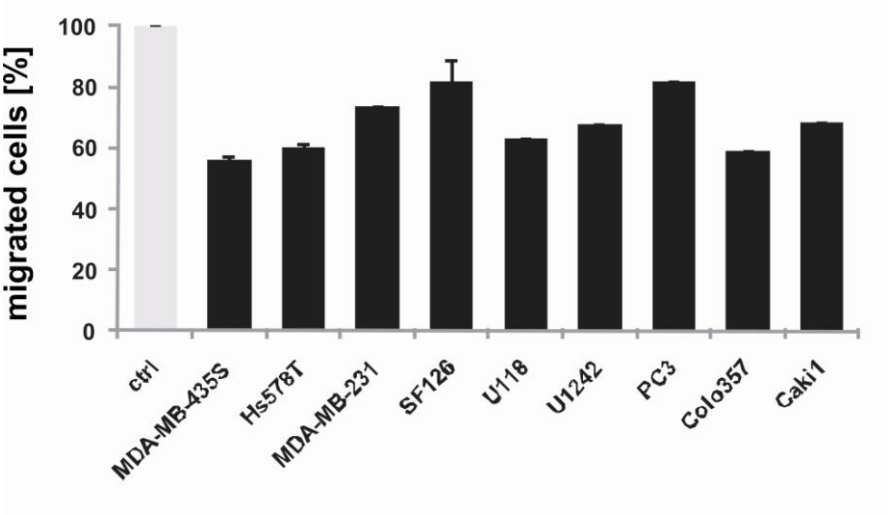

Figure 27 Quantification of transwell migration assays.
The anti-migratory effect of SU11248 on cancer cells was also quantitatively determined using Transwell Migration Assays. Cells cultured in medium containing 0 % FBS were seeded in the upper chamber and incubated with 5 µM SU11248 for 16h. Migrated cells were stained with crystal violet, dissolved in 5 % AcCOOH and the number of cells was determined in an ELISA reader at 595 nm. Data are shown as the percentage of migrated cells relative to DMSO vehicle control.

Migrated cells were measured after 16h of drug treatment with 5 µM SU11248 using crystal violet staining. Data are shown as percentage of migrated cells relative to DMSO control. These data show that SU11248 inhibits cancer cell migration *in vitro* by up to 50 % at a concentration of 5 µM SU11248 and even very aggressive breast cancer cell lines like Hs578T, MDA-MB-231 and MDA-MB-435S could be inhibited at concentrations of 5 µM and below.

In addition, to test for the anti-invasive potential of SU11248 a matrigel-outgrowth assay was performed. Cells were seeded on an ECM (extracellular matrix) –like matrix, so called matrigel, treated with increasing SU11248 concentrations for 3 days and branching/outgrowth of invaded cells was visualized by photomicrographs. One hallmark of invading cells is their ability of crossing the extracellular matrix and disrupting the basement membrane in order to reach the blood vessels. The ECM consists of collagen, laminin, fibronectin, elastin and other fibrous proteins as well as glycosaminoglycan (GAGs) (Bosman and Stamenkovic, 2003). Matrigel serves as a model for the ECM. Invasive cancer cell lines can form branches in this structure which is a direct measure of their metastasizing ability. It could be shown that SU11248 completely blocks matrigel-outgrowth at concentrations equal and lower than 1 µM. The results for two aggressive breast cancer cell lines MDA-MB-435S and Hs578T are illustrated in Figure 28. These data suggest a strong anti-invasive potential of SU11248 which is of great importance for clinical applications.

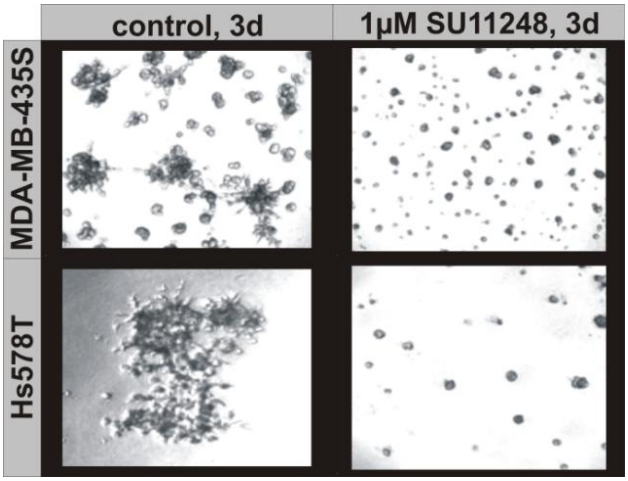

Figure 28 SU11248 completely blocks cancer cell invasion in a matrigel-outgrowth assay.
Cells were seeded under serum conditions (10 % FCS) in 96-well flat-bottom plates covered with 50 µl matrigel and treated with increasing SU11248 concentrations from 0.1 to 1 µM. Three days after drug treatment photomicrographs were taken (x4) to visualize cell branching.

In summary, it was shown that SU11248 interferes with cancer cell migration and has an inhibitory effect on cancer cell invasion which in combination results in a good clinical benefit for the treatment of highly aggressive tumors such as breast and pancreatic cancer where the occurrence of metastasis is the mostly lethal event in tumor progression and a frequent cause of tumor relapse.

7.1.4 Morphological changes of cancer cells after SU11248 treatment

The morphology of a cell gives information about the vitality and the cellular state such as a dividing, senescent or differentiated stage. Therefore the morphological changes of cancer cell lines of different tissue origins were analysed after SU11248 treatment and it was shown that cells exposed to SU11248 undergo a mesenchymal-to-epithelial transition (MET). Before treatment the tested cell lines grow randomly distributed on the plate. After drug application for 24h cells tend to grow in clusters and patches which is shown for three representative cancer cell lines in Figure 29.

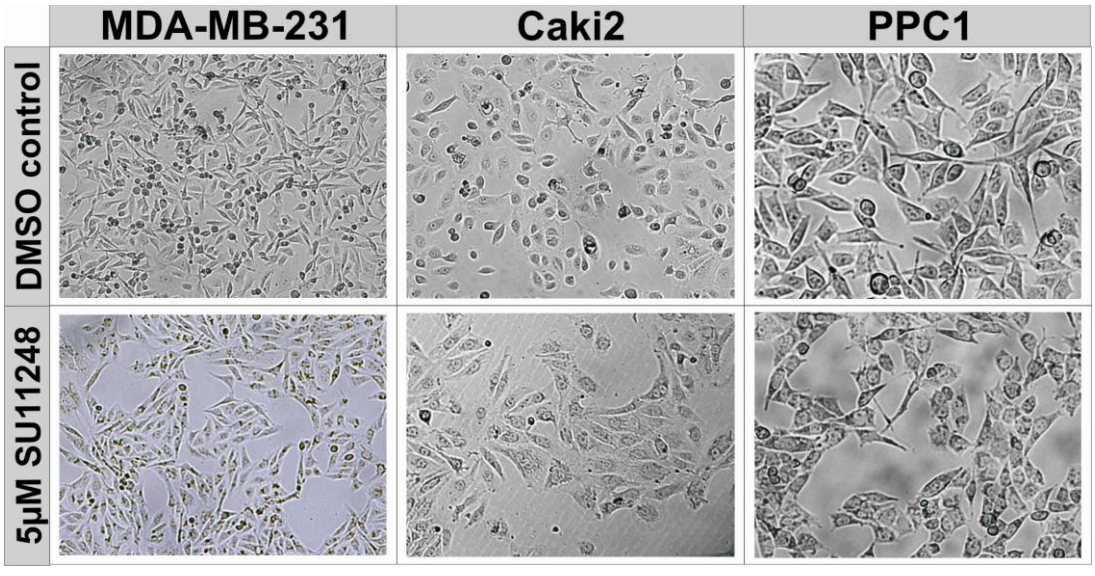

Figure 29 Morphological changes of cancer cells after SU11248 treatment for 24h.

SU11248 induces cell clustering in random distributed growing cancer cell lines. Three representative cancer cell lines (MDA-MB-231: breast cancer; Caki2: kidney cancer; PPC1: prostate cancer) were treated with 5 µM SU11248 and photomicrographs (x4) were taken after 24h of drug exposure. Cells grow randomly distributed over the plate when treated with DMSO vehicle control and form patches and cell clusters under SU11248 treatment.

In this context, the mesenchymal marker Vimentin and the epithelial marker E-cadherin were analyzed and it could be shown that Vimentin-expression levels are decreased while E-cadherin is increasing after SU11248 application. There was a clear cut between these two cell states before and after drug application which is documented in Figure 30. The expression changes were monitored by macro-gene-arrays of SU11248-treated against DMSO-vehicle-control treated cells and are shown as the average of three independent experiments. In addition, N-cadherin levels were also decreased after compound exposure.

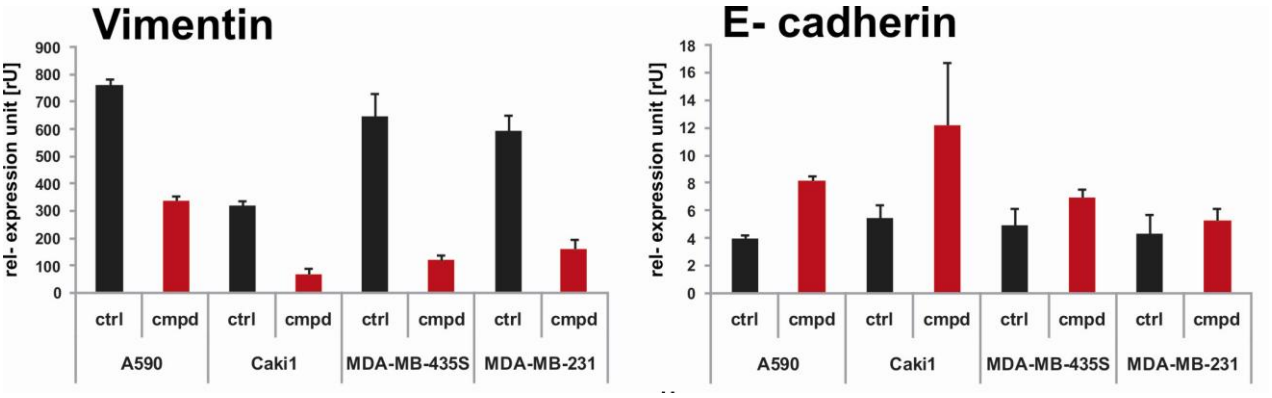

Figure 30 Expression changes of the mesenchymal-marker Vimentin and the epithelial marker E-cadherin after 24h of 5 µM SU11248 treatment.
Cells were treated with either 5 µM SU11248 or DMSO as a vehicle-control under serum conditions for 24h, lysed and the mRNA isolated. Radioactive labeled cDNA was used for macro-arrays. Expression levels for control cells are shown in black and for compound-treated cells in red. Expression levels are expressed in expression units calculated with the analyzing software ArrayVision Version 8.0 from GE Healthcare Life Sciences.

Taken together, these data show that SU11248 can invert the epithelial-to mesenchymal transition (EMT) of cancer cells. EMT is directly connected to aggressive cancer progression, metastasis and poor prognosis of a tumor (Bates and Mercurio, 2005; Gavert and Ben-Ze'ev, 2008; Guarino et al., 2007; Kokkinos et al., 2007; Prudkin et al., 2009; Thompson et al., 2005; Voulgari and Pintzas, 2009; Wu and Zhou, 2008). This induction of MET by SU11248 is in line and a possible explanation for the anti-migratory and anti-invasive effect of SU11248 shown in this work.

In summary, the functional biological screen of SU11248 in a variety of cancer cell lines from different cancer tissues revealed a broad activity spectrum of SU11248. Its anti-tumor activity ranges from cell proliferation inhibition over induction of programmed cell death, inhibition of motility and invasiveness to inducing differentiation of cancer cells from an aggressive mesenchymal-like cell state to a less invasive epithelial-like cell type. Taken together, the observed phenotypes of SU11248 on cancer cells and its universal strong anti-tumor impact on cellular processes give evidence of a diverse target-panel. SU11248

seems to inhibit and act on several key signalling pathways within cancer cells which are not only involved in a single phenotype but regulating almost all hallmarks of cancer. The responsible molecular sites of drug action have to be analyzed in a next step by profiling the target interaction panel of SU11248 in cancer cells. Drug target profiling of SU11248 was performed in a global cell-wide manner using mass spectrometry.

7.2 Target-selectivity profiling of SU11248 in cancer cell lines and metastatic renal cell carcinoma (mRCC) tumors

SU11248, based on the specific indolinone precursor compounds SU5402 and SU6668, was developed as the first multi-targeted small-molecule inhibitor (Atkins et al., 2006) addressing class III and class V RTKs, including PDGF receptors, VEGF receptors, KIT, and FLT3 (Abrams et al., 2003a; Faivre et al., 2006a; Mendel et al., 2003; Motzer et al., 2006b; Murray et al., 2003; O'Farrell et al., 2003a). *In vitro*, it inhibits these RTKs in biochemical, ligand-dependent phosphorylation with IC_{50}-values in the low micromolar range. SU11248 acts as an ATP-competitor and binds to the ATP-binding site of particular kinases. *In vivo*, SU11248 was described to be highly efficacious (frequently cytoreductive) in all tumour xenograft models investigated (Zhang et al., 2009b) and its full anti-tumour efficacy against solid tumours was so far associated with the inhibition of receptor tyrosine kinases like PDGFR and VEGFR (Mendel et al., 2003; Schueneman et al., 2003). Clinical studies with SU11248 showed a strong efficacy in advanced renal cell carcinoma (RCC) (Motzer et al., 2006b; Polyzos, 2008; Reddy, 2006) and in gastrointestinal stromal tumours (GIST) that are refractory or intolerant to imatinib (Prenen et al., 2006)' (Demetri et al., 2006; Norden-Zfoni et al., 2007). Furthermore, ongoing therapeutic investigations in several other tumour indications such as acute myeloid leukemia (AML) or metastatic breast cancer provide hints of a broad anti-tumour activity spectrum of SU11248 (Abrams et al., 2003a; Abrams et al., 2003b; Fiedler et al., 2005; Kim et al., 2006; Motzer et al., 2006a; Murray et al., 2003; O'Farrell et al., 2003b). Due to its strong anti-tumor and anti-angiogenic activity *in vitro* and *in vivo* SU11248 was approved for the treatment of metastatic renal cell carcinoma (mRCC) and gastrointestinal stromal tumors (GIST) by the FDA in 2006.

The clinically observed wide spectrum of anti-tumor action of SU11248 and its broad biological efficacy seen in the performed cellular screen, gives evidence of a broad inhibitor target-panel far beyond described targets such as PDGFR and VEGFR receptors. In addition, for future applications of SU11248 or small-molecules in general and an improved pharmacodynamic prediction of the inhibitor` s efficacy which will eventually help in a better patient selection and prediction of therapeutic responses including toxic side-effects, it is of great importance to reveal the underlying mechanisms of action and cellular sites of interference of the small-molecule inhibitor. In summary, to know an inhibitor` s true selectivity, reflected by its molecular targets within the cell, is a prerequisite for an optimal therapeutic benefit of the drug.

Therefore the cellular target protein interaction panels of SU11248 in 30 cancer cell lines and primary mRCC tumor samples being responsive to SU11248 was profiled. To get a comprehensive picture of interaction sites, an efficient chemical proteomics approach was employed. This allowed to study the drug` s proteome-wide target interaction profile directly from the cell with endogenously expressed proteins under

native conformations and physiological conditions such as ATP concentration, post-translational modifications and cofactor binding.

Based on their high SU11248 sensitivity the glioblastoma cell lines U118, U1242, SF767, U138, the melanoma cell lines WM266-4, WM115, C8161, Skmel28, Malme3M, the pancreatic cancer cell lines A590, AsPc1, PaTu, Colo357, the kidney cancer cell lines SW13, A704, Caki1, Caki2, A498, the liver cancer cell line H1755, the prostate cancer cell lines BH1604, DU145, the colon cancer cell lines SW1116, HT29, the ovary cancer cell line Ovcar5 and the breast cancer cell lines Hs578T, MDA-MB-231, MDA-MB-453, MCF7, T47D and MDA-MB-435S were used. All cell lines showed strong sensitivity to SU11248 treatment in either proliferation-, apoptosis induction- or migration- and invasion-assays.

For the affinity purification of cellular drug targets and subsequent mass-spectrometry based protein identification, the primary amino moiety of the chemically modified SU11248 was linked to the free carboxy-group of ECH-Sepharose in a carbodiimide-mediated coupling reaction. The chemical structures of SU11248 and the SU11248 affinity matrix are shown in Figure 31 and 32.

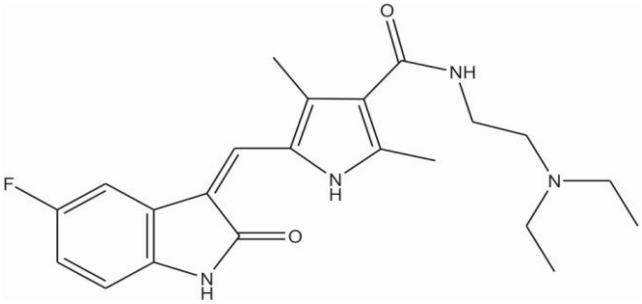

Figure 31 Chemical structure of the small-molecule receptor- tyrosine kinase inhibitor SU11248.
SU11248 is a multi-targeted kinase inhibitor belonging to the class of indolinone kinase inhibitors so far described to inhibit split-kinase receptor tyrosine kinases of class III and IV.

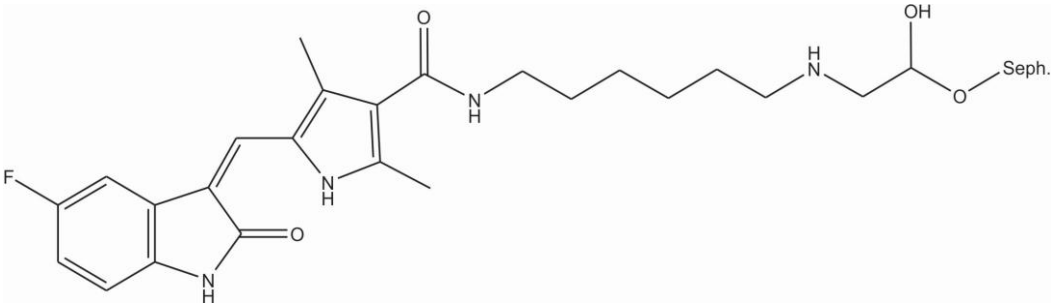

Figure 32 SU11248 affinity matrix for affinity chromatography and *in vitro*-association (IVA) experiments.
Chemically modified SU11248 was covalently linked with the primary amino moiety to the free carboxy-group of ECH-Sepharose in a carbodiimide-mediated coupling reaction.

7.2.1 Workflow of drug target profiling by affinity chromatography and mass spectrometry

To characterize SU11248 targets within a cellular proteome, total cell lysates from cancer cell lines and mRCC tumor samples were subjected to affinity chromatography on a SU11248 matrix employing a

purification protocol recently described (Daub, 2005; Daub et al., 2004a; Godl and Daub, 2004; Godl et al., 2003). The target enrichment was either performed on a FPLC or in an *in vitro*-association experiment (IVA). Specifically retained proteins were eluted using a combination of 10 mM ATP and 1 µM free SU11248. The highly enriched fractions of potential SU11248 targets were Wessel-Fluegge (Wessel and Flugge, 1984) precipitated and resolved by 2D-SDS-PAGE gel electrophoresis. Gel slices covering different molecular weight regions were excised and subjected to in-gel tryptic digestion. Subsequent LC/MS analysis of all peptide fractions was performed on a LTQ-Orbitrap as described before (Olsen et al., 2006). The workflow is described in Figure 33.

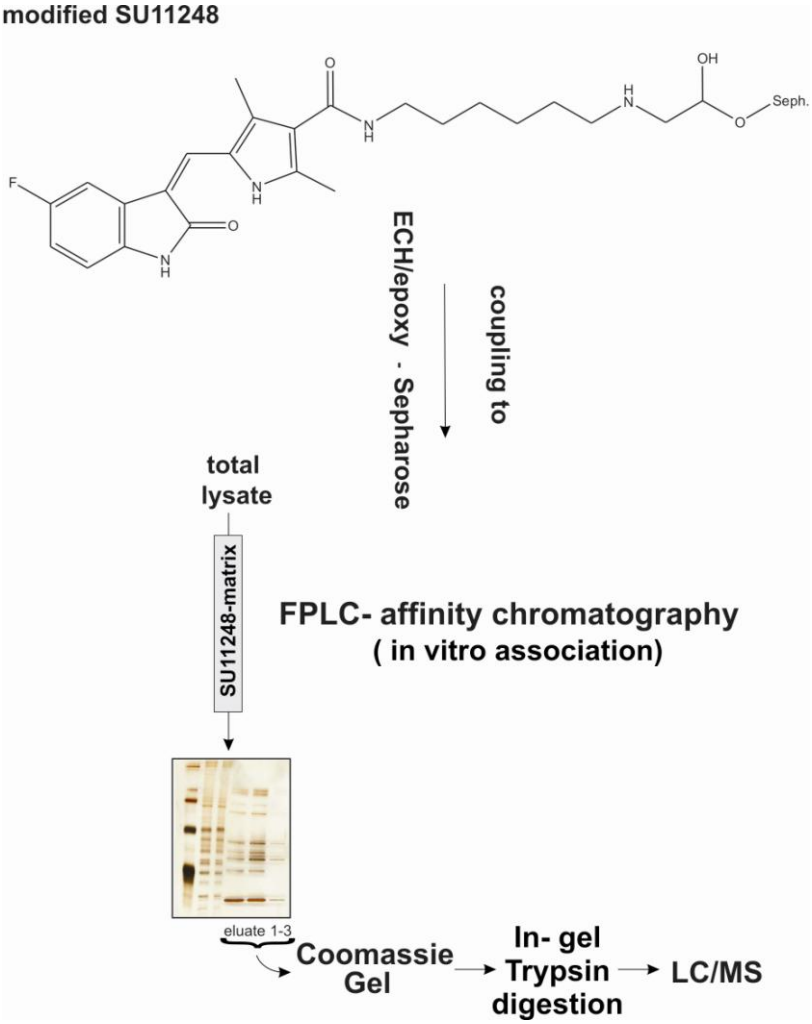

Figure 33 Workflow of cellular drug target profiling of SU11248 by affinity chromatography and mass spectrometry.
For affinity purification of cellular drug targets the primary amino moiety of the chemically modified SU11248 was covalently linked to the free carboxy group of ECH Sepharose in a carbodiimide-mediated coupling reaction. Total cell lysates were subjected to affinity chromatography on a SU11248 matrix and target enrichment was either performed on a FPLC or in an *in vitro*-association experiment. Specifically retained proteins were eluted using a combination of 10 mM ATP and 1 µM free SU11248. The highly enriched fractions of potential SU11248 targets were Wessel-Fluegge precipitated and resolved by 2D-SDS-PAGE gel electrophoresis. Gel slices covering different molecular weight regions were excised and subjected to in-gel tryptic digestion. Subsequent LC/MS analysis of all peptide fractions was performed on a LTQ-Orbitrap™.

7.2.2 Target identification and functional classification of SU11248 protein interaction partners

Cellular target screenings of SU11248 in 30 different cancer cell lines and mRCC tumor samples revealed a broad interaction panel with 25 to 146 different kinase targets in each cell line which is shown in Figure 34.

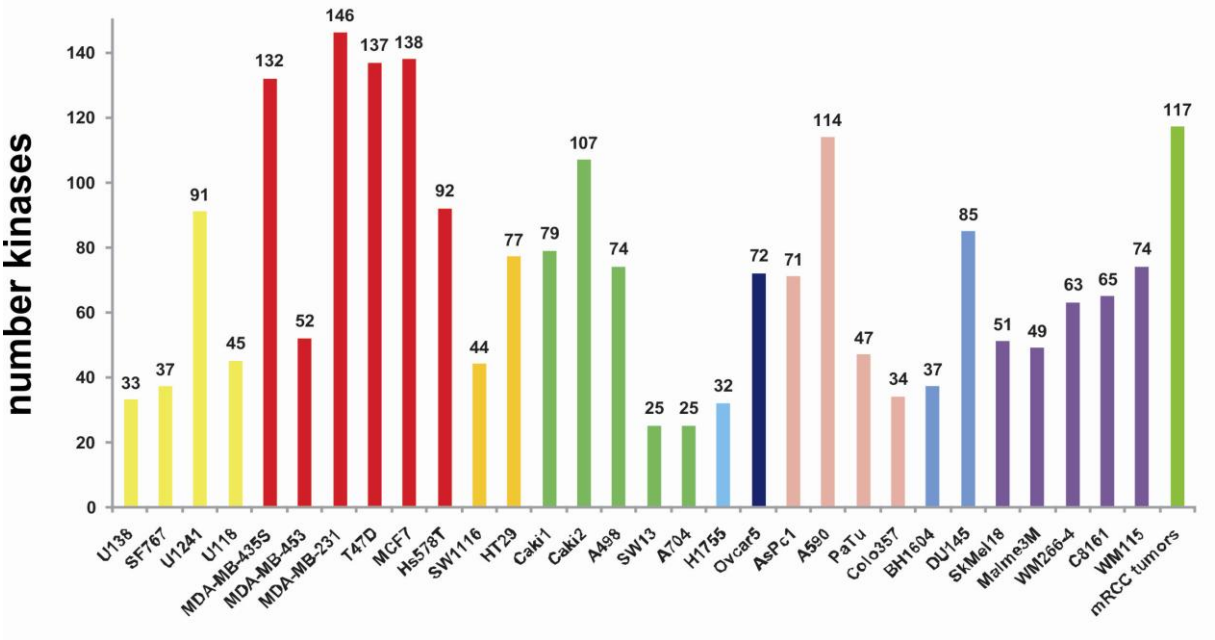

Figure 34 Number of targets with kinase activity bound to SU11248 matrix in cancer cell lines and mRCC tumors identified by mass spectrometry.
Total cell lysates from either cancer cell lines or mRCC tumors were subjected to SU11248 matrix based affinity chromatography and specifically retained proteins were identified by LC/MS. Shown is the number of kinase targets with at least one unique peptide, including different isoforms, per cell line binding to SU11248.

Beside these kinase targets also non-kinase targets such as Acetyl-CoA acetyltransferases, Acyl-coenzyme A thioesterases, Ribosyldihydronicotinamide dehydrogenases and more in general other ATP- or purine-binding proteins like chaperones, helicases, ATPases, motor proteins and metabolic enzymes were frequently identified as potential SU11248 interaction partners and possible molecular sites of cellular drug action.

Cellular kinase targets of SU11248 identified with at least one unique peptide per protein in the different cell lines are shown in Figure 34. Only peptides with a significance of pep< 0.01 were considered for protein identification. Kinase hits in cell lines of the same tissue were summarized and the percent detection rate per tissue calculated. Based on the detection frequency of each kinase per tissue (shown in percent) a two-dimensional hierarchical cluster analysis was performed to identify targets being identified with a high occurrence within cell lines of the same tissue origin as well as a high detection rate in different tissues. Three clusters of frequently detected SU11248 kinase targets within the tested cancer cell line panel could be identified which are magnified in Figure 35.

SU11248, originally designed to inhibit split-kinases such as PDGF receptors, VEGF receptors and KIT, also targets other receptor tyrosine kinases (RTKs) including RET, MET, ROS1, DDR1, DDR2, FGFR- and Ephrin receptor- family members. A complete list of all identified RTKs and their respective frequency of detection in each tissue-sorted cell line group, sorted alphabetically, is listed in Table 9. In addition,

interesting cytosolic kinases including FAK, FER and YES1 were found to be inhibited by SU11248. For details see Table 10.

Table 9 Receptor Tyrosine Kinases (RTKs) targeted by SU11248.
RTKs are alphabetically sorted and their detection frequency (binding to SU11248 matrix) in cancer cell lines of the same tissue origin is shown in percent.

		cancer cell lines									tumor samples
RTK	Protein Name	brain	breast	colon	kidney	liver	ovary	pancreas	prostate	skin	mRCC
ALK	ALK tyrosine kinase receptor		13					11		20	
CSF1R	Macrophage colony-stimulating factor 1 receptor	25	20								67
DDR1	discoidin domain receptor family, member 1 c		20					11			
DDR2	Discoidin domain-containing receptor 2	50	13								
EGFR	Epidermal growth factor receptor		20		9		67				33
EPHA1	Ephrin type-A receptor 1		7								
EPHA2	Ephrin type-A receptor 2		13								
EPHA3	Ephrin type-A receptor 3				9						
EPHA4	Ephrin type-A receptor 4	25	7	25	18			22			
EPHA7	Ephrin type-A receptor 7		7								
EPHB1	Ephrin type-B receptor 1		13								
EPHB2	Ephrin type-B receptor 2		13						50	20	
EPHB3	Ephrin type-B receptor 3		13								
EPHB4	Ephrin type-B receptor 4		7								
ERBB2	Receptor tyrosine-protein kinase erbB-2		7								
ERBB4	Receptor tyrosine-protein kinase erbB-4		7					11			
FGFR1	Basic fibroblast growth factor receptor 1		13					22	50		
FGFR2	Fibroblast growth factor receptor 2	25	13								
FGFR3	Fibroblast growth factor receptor 3	25	7								
FGFR4	Fibroblast growth factor receptor 4 variant	50	20								
FLT1	Vascular endothelial growth factor receptor 1			25	9					40	67
FLT3	Tyrosine-protein kinase receptor	25	7		9					20	
FLT4	fms-related tyrosine kinase 4 1	25	20						50	20	67
INSR	Insulin receptor										100
KDR	Vascular endothelial growth factor receptor 2		27	25	9					20	
KIT	Mast/stem cell growth factor receptor	50	13		9			22	50	40	67
MET	Hepatocyte growth factor receptor		20		27					20	
MST1R	Macrophage-stimulating protein receptor (RON)										33
MUSK	Muscle, skeletal, receptor tyrosine kinase	25	13							40	
NTRK1	High affinity nerve growth factor receptor (TrkA-II)		7	25	9	100					
PDGFRA	Alpha-type platelet-derived growth factor receptor	100	80	25	64		67	89	100	80	33
PDGFRB	Beta-type platelet-derived growth factor receptor	100	87	50	73		100	89	100	100	100
PTK7	Tyrosine-protein kinase-like 7		7		18						
RET	Tyrosine-protein kinase RET		20							20	
ROS1	Tyrosine-protein kinase ROS	25	20	25	27			33	50	60	67
TFG/ALK fusion	Tyrosine-protein kinase receptor		27	50	55		67	44			33

Table 10 Cytosolic Tyrosine Kinases targeted by SU11248.
TKs are alphabetically sorted and their detection frequency (binding to SU11248 matrix) in cancer cell lines of the same tissue origin is shown in percent.

		cancer cell lines									tumor samples
TK	Protein Name	brain	breast	colon	kidney	liver	ovary	pancreas	prostate	skin	mRCC
ABL1	Proto-oncogene tyrosine-protein kinase ABL1	50	33								
ABL2	Tyrosine-protein kinase ABL2		7		9			11	50		
BLK	Tyrosine-protein kinase BLK	25									
FAK	Focal adhesion kinase 1	25	53	25	18		67	33	50	80	67
FER	Proto-oncogene tyrosine-protein kinase FER	100	93	25	55		100	78	100	100	
FES	Proto-oncogene tyrosine-protein kinase Fes/Fps		20						50		
FGR	Proto-oncogene tyrosine-protein kinase FGR		7								100
FYN	Proto-oncogene tyrosine-protein kinase Fyn		7							20	67
HCK	Tyrosine-protein kinase HCK		7							20	33
JAK1	Tyrosine-protein kinase JAK1	100	100	100	100	100	100	78	100	100	
JAK2	Tyrosine-protein kinase JAK2				9			22		20	
JAK3	Tyrosine-protein kinase JAK3		20					11		20	
LCK	Proto-oncogene tyrosine-protein kinase LCK		7								67
LYN	Tyrosine-protein kinase Lyn		13							40	100
PTK2B	Protein tyrosine kinase 2 beta	25	40	25	27		33	56	50		
SGK269	Tyrosine-protein kinase SgK269							22		20	
SRC	Proto-oncogene tyrosine-protein kinase Src		47		36						100
SRMS	Tyrosine-protein kinase Srms									20	
TNK1	Non-receptor tyrosine-protein kinase TNK1		27								
TYK2	Non-receptor tyrosine-protein kinase TYK2		33		9		33	11		20	
YES1	Proto-oncogene tyrosine-protein kinase Yes	100	93	25	36		67	67	100	80	100

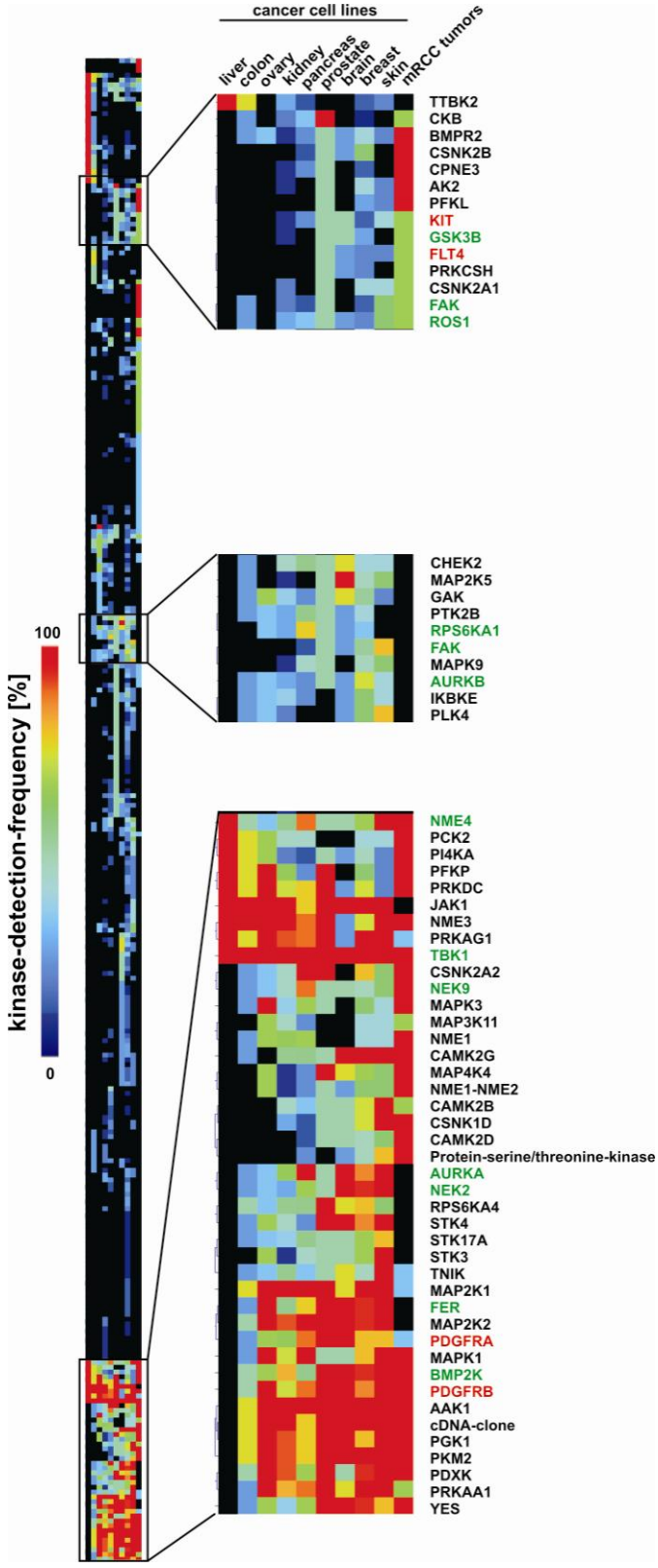

Figure 35 Target interaction map of the small-molecule kinase inhibitor SU11248 in cancer cell lines and mRCC tumors.

Selectivity profiles of SU11248 are tissue sorted and shown in percentile kinase detection per tissue and analyzed by a two-dimensional hierarchical cluster algorithm Euclidean distance-based. Three clusters of frequently detected kinase targets based on identification coverage per tissue or occurrence among different cancer types are magnified. Already described SU11248 targets are marked in red, interesting new hits are highlighted in green.

Beside known targets such as PDGFRa, PDGFRb, KIT, and FLT4 which are highlighted in red interesting new interaction partners including ROS1, FER, YES1, FAK, NME3, NME4, RPS6KA1, RPS6KA3, BMP2K, NEK9, TBK1, AAK1, CAMKinases, Casein Kinases, AURKA and AURKB were frequently detected to bind to SU11248 (marked in green in Figure 35).

In total, 313 different kinases were identified of which 236 were protein kinases distributed among all kinase families with tyrosine kinases being the largest group and 77 non-protein kinases. The annotation is shown in Figure 36.

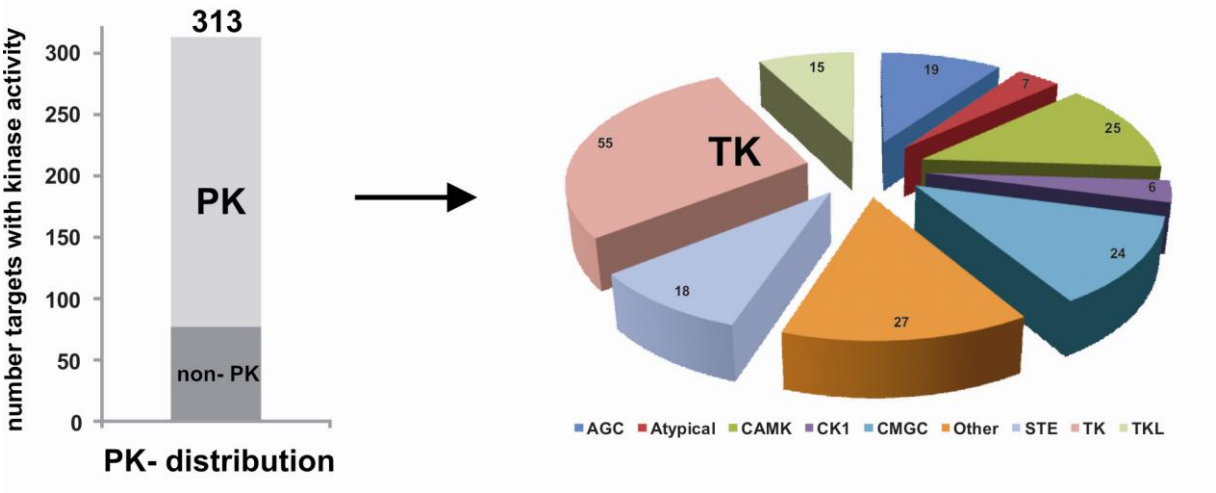

Figure 36 Kinase family annotation of identified cellular SU11248 protein kinase targets.
In total, 236 different protein kinases were detected and SUGEN-annotated based on Manning *et al*., Science 2003. Tyrosine kinases are the largest group of identified kinase interaction partners binding to SU11248.

In order to understand an inhibitor`s biological function and its anti-tumor activity molecular interaction maps of the drug are important. The knowledge of a target`s function and the fact that its inhibition negatively regulates the cellular process controlled by the respective protein leads to molecular explanations for the anti-tumor efficacy of SU11248. Therefore, all kinase- and non-kinase targets were analyzed by their biological function to reveal cellular processes and signaling networks being impaired by the small-molecule kinase inhibitor SU11248 after its application to cancer cells. The functional annotation was Gene Ontology based and executed with the gene annotation software Cytoscape Version 2.6.1 using the BINGO 2.0 plug-in.

Gene Ontology annotation of identified kinase targets shows a strong enrichment of kinases being involved in biological processes such as cell proliferation, motility, migration, cell cycle regulation and apoptosis which is shown in Figure 37 and is in accordance with the biological effect of SU11248 on cancer cells.

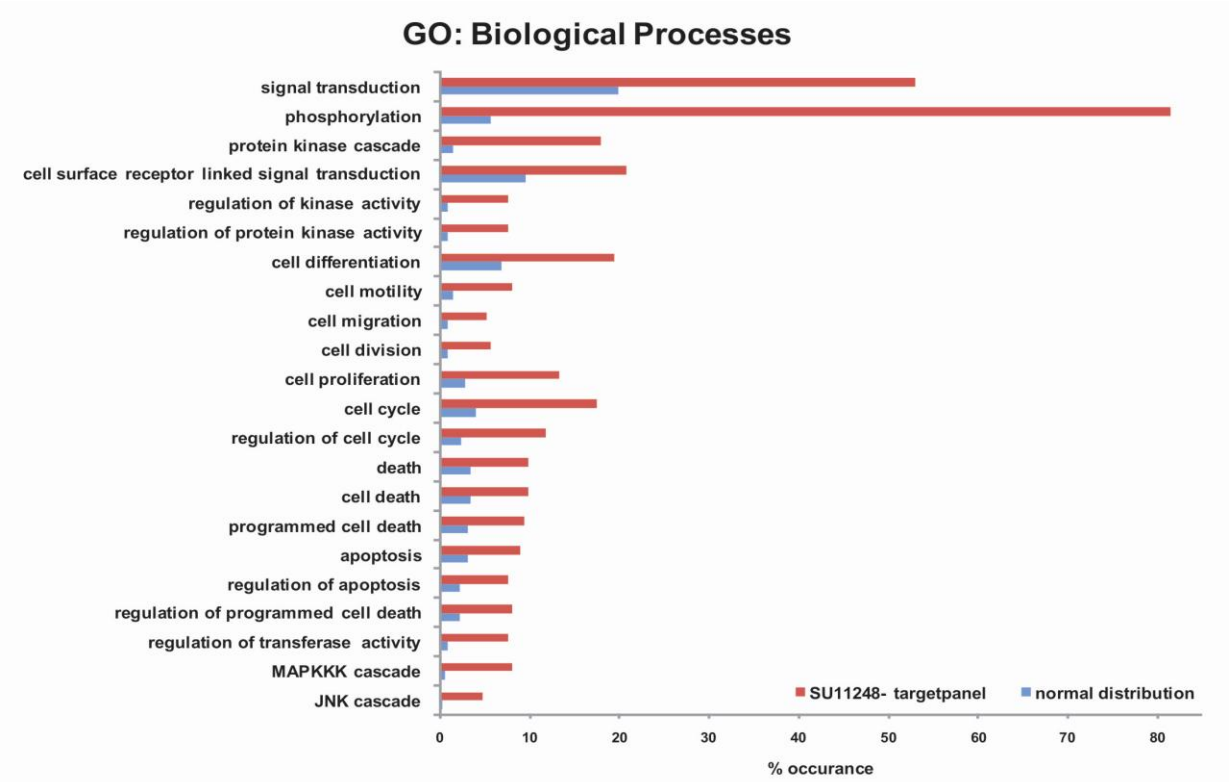

Figure 37 Gene Ontology annotation for biological processes of SU11248 targets with kinase activity.
All targets were annotated using Cytoscape 2.6.1 with a BINGO plug-in. Shown are categories with an enrichment factor of at least two-fold within the SU11248 target-panel against the normal protein distribution.

A molecular function analysis revealed the broad spectrum of identified kinases ranging from lipid kinase activity such as AMPKs (e.g. PRKAA1, PRKAG1) over receptor signalling, MAP kinase activity including MAP2K1, MAP2K2, MAP3K11, MAP3K4 and MAP4K4, calmodulin-dependent kinase activity (CAMK2D, CAMK2G) to inositol or phosphatidylinositol kinase activity like PI4KA and PIP5K1A (Figure 38).

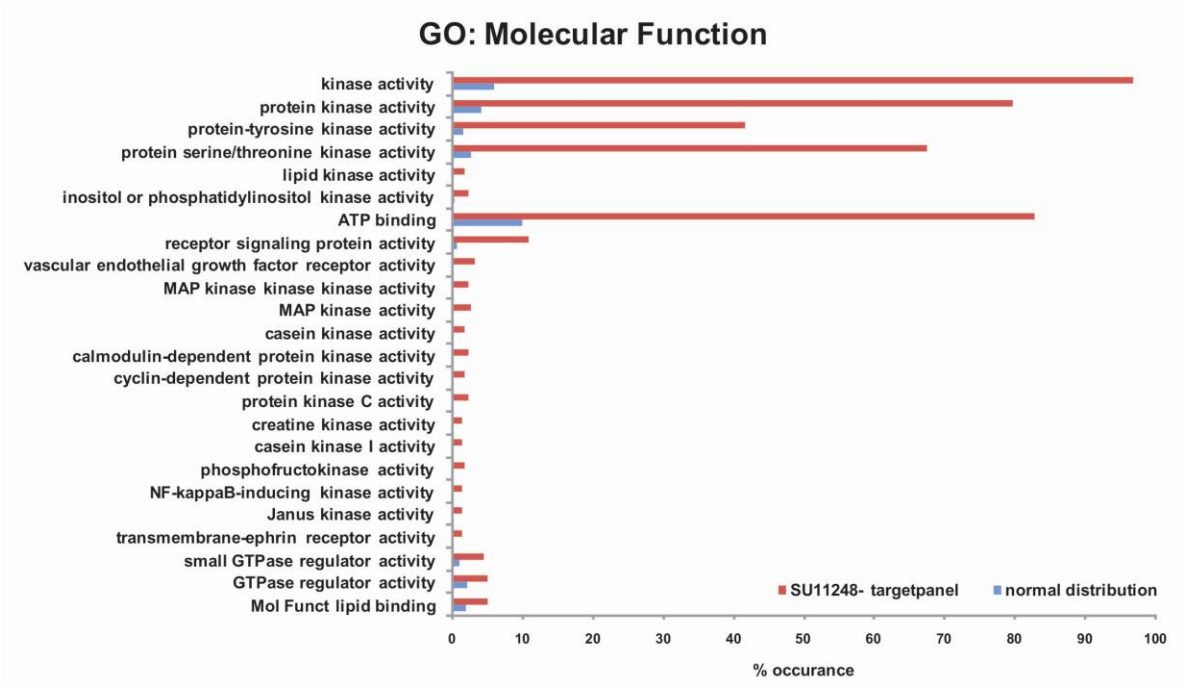

Figure 38 Gene Ontology annotation for molecular function of SU11248 targets with kinase activity.
All targets were annotated using Cytoscape 2.6.1 with a BINGO plug-in. Shown are categories with an enrichment factor of at least two-fold within the SU11248 target-panel against the normal protein distribution.

The cellular distribution of identified SU11248 kinase targets is shown in Figure 39. Kinases are assigned to structures involved in cell cycle regulation including the centrosome, the spindle complex and spindle pole as well as subcellular formations regulating cell adhesion and motility such as focal adhesion complexes and the cytoskeleton.

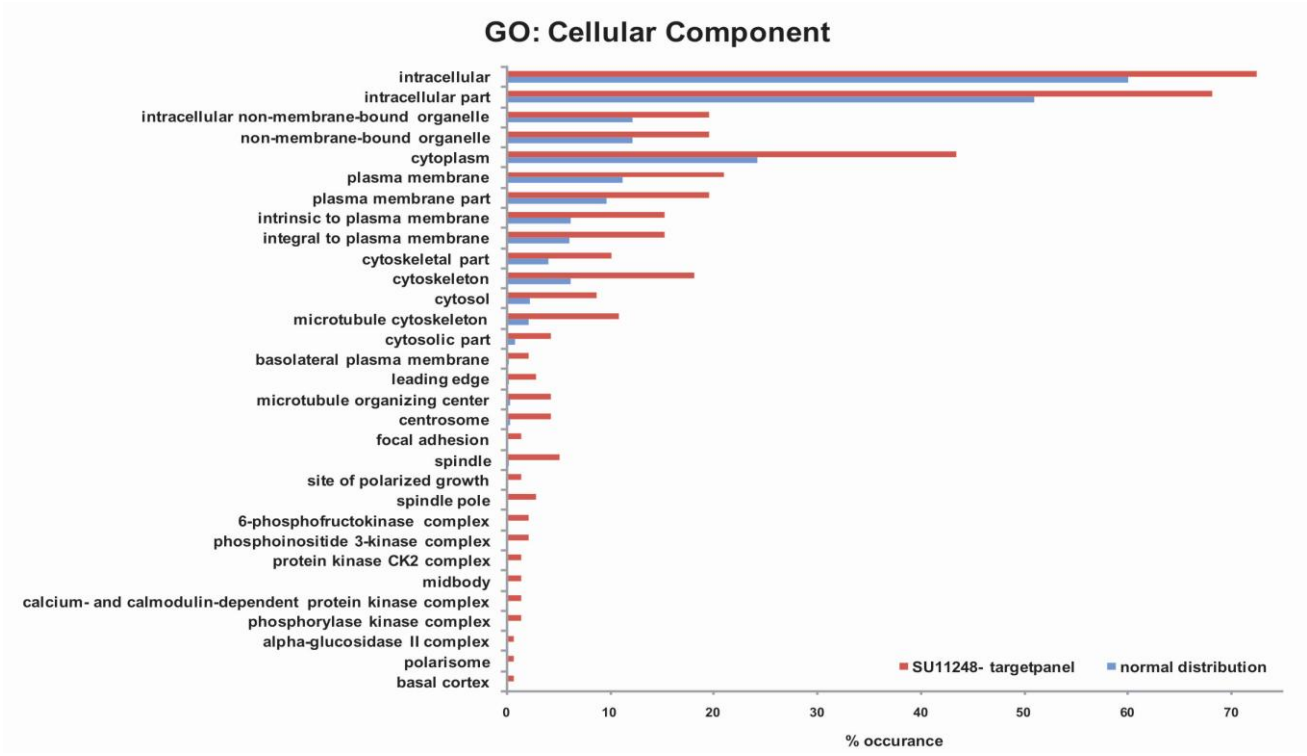

Figure 39 Gene Ontology annotation for cellular component distribution of SU11248 targets with kinase activity.
All targets were annotated using Cytoscape 2.6.1 with a BINGO plug-in. Shown are categories with an enrichment factor of at least two-fold within the SU11248 target-panel against the normal protein distribution.

Functional annotation of non-kinase SU11248 binding partners showed a strong impact on metabolic processes such as glycolysis, citrate cycle, fatty acid and amino acid metabolism, purine/pyrimidine metabolism as well as on protein synthesis, translation and mRNA processing (Figure 40). Gene Ontology annotation of non-kinase targets for molecular function and cellular component analysis revealed a broad spectrum of metabolic enzymes including ligases, transferases and dehydrogenases binding to SU11248 (Figure 41, Figure 42).

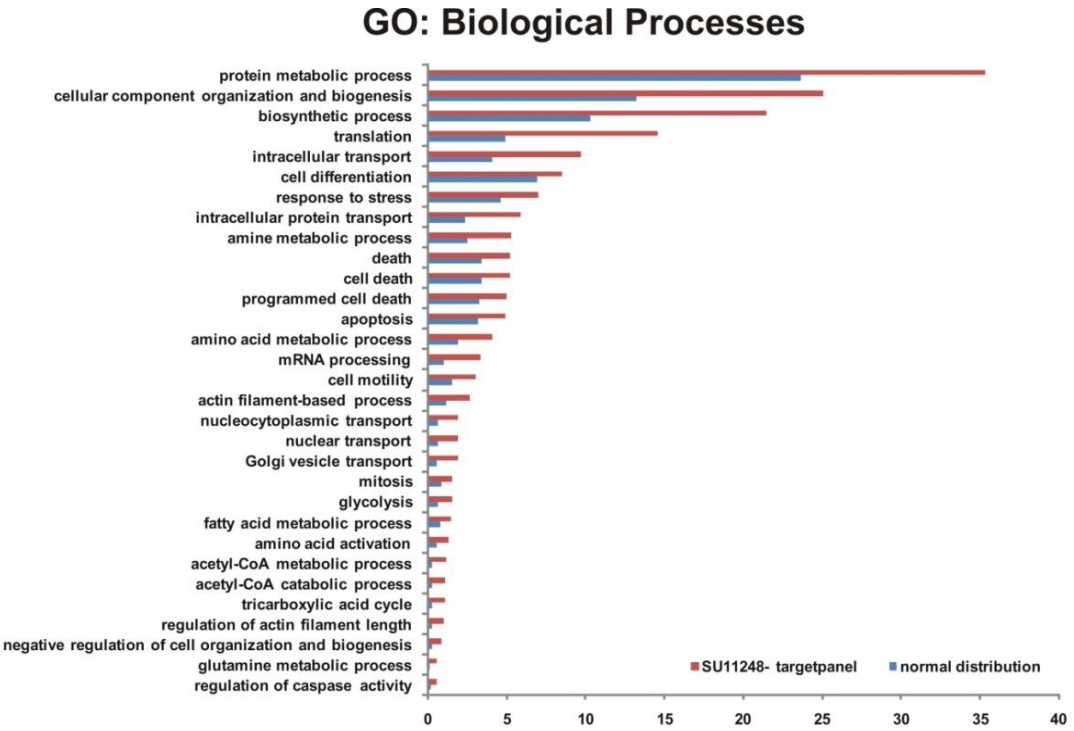

Figure 40 Gene Ontology annotation for biological processes of non-kinase SU11248 targets.
All targets were annotated using Cytoscape 2.6.1 with a BINGO plug-in. Shown are categories with an enrichment factor of at least two-fold within the SU11248 target-panel against the normal protein distribution.

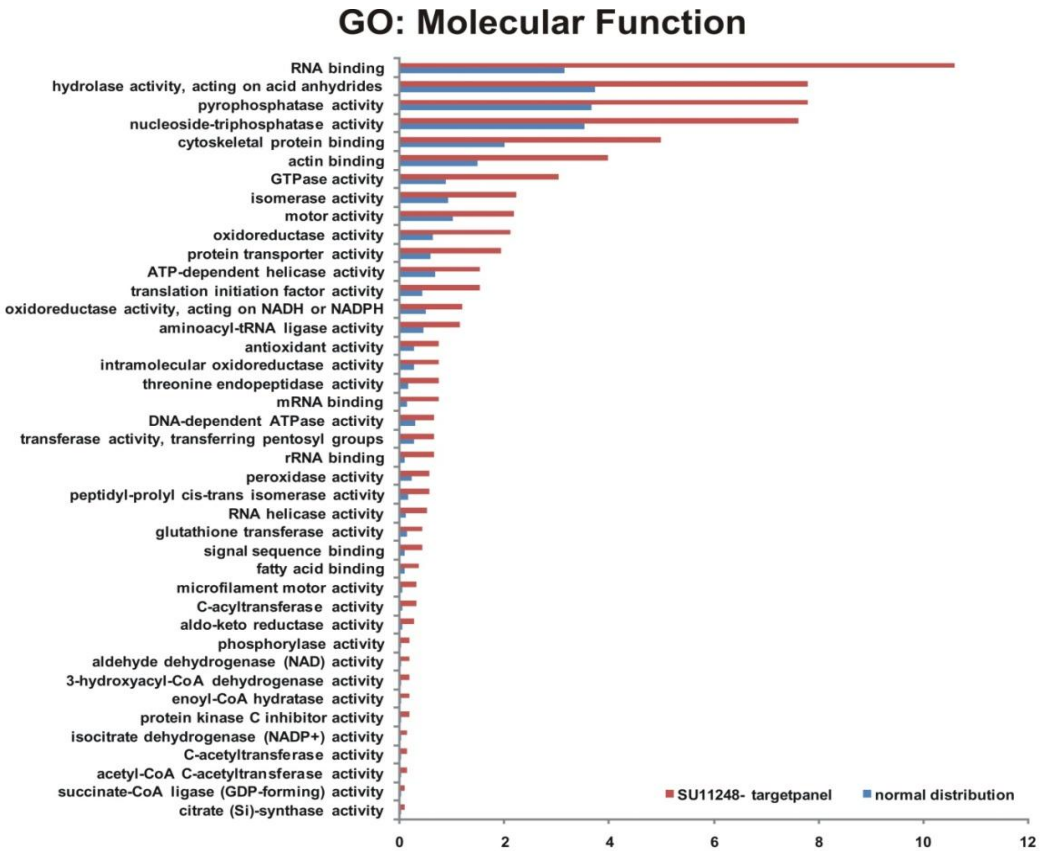

Figure 41 Gene Ontology annotation for molecular function of non-kinase SU11248 targets.
All targets were annotated using Cytoscape 2.6.1 with a BINGO plug-in. Shown are categories with an enrichment factor of at least two-fold within the SU11248 target-panel against the normal protein distribution.

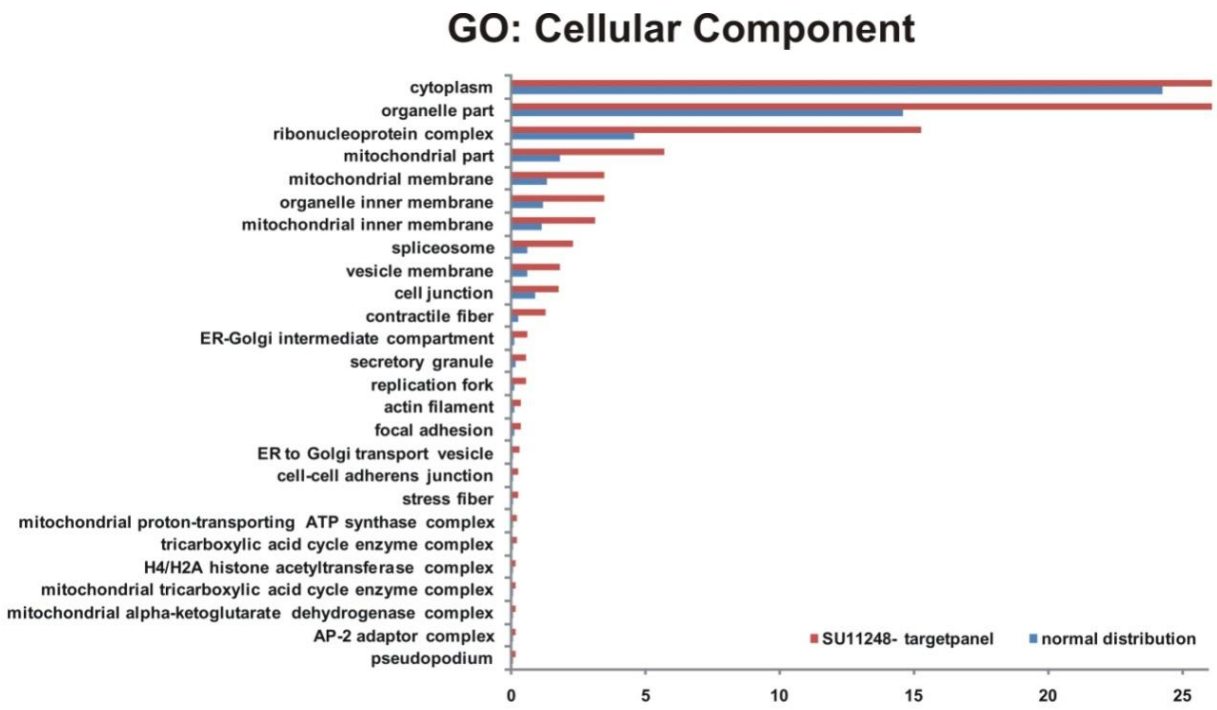

Figure 42 Gene Ontology annotation for cellular component analysis of non-kinase SU11248 targets.
All targets were annotated using Cytoscape 2.6.1 with a BINGO plug-in. Shown are categories with an enrichment factor of at least two-fold within the SU11248 target-panel against the normal protein distribution.

In summary, target-profiling of the small-molecule kinase inhibitor SU11248 revealed a broad cellular interaction panel including kinase- as well as non-kinase targets with diverse functions controlling key processes such as cell proliferation, survival, motility and energy metabolism as well as protein synthesis. The identified cellular sites of action strongly correlate with the effect of SU11248 on cancer cells and might be the molecular basis and explanation for the observed broad anti-tumor efficacy of the multi-targeted small-molecule inhibitor not only seen in the cell-based functional screen performed in this study but also in ongoing clinical trials in a variety of different tumor indications.

7.3 Binding-affinity-analysis of SU11248 towards qualitatively identified cellular targets

Mass spectrometry (MS)-based qualitative target protein capture strategies with immobilized inhibitors as described in the previous chapter can be performed in a large panel of different cellular model systems such as cancer cell lines and tumor samples of almost all indications. This gives comprehensive insights into an inhibitor` s selectivity and provides tissue specific interaction maps of the drug. Nevertheless, to rank and prioritize molecular interactions, binding-affinity information of the drug against its target panel is important in order to identify the strongest molecular associations that are likely the most relevant in physiological conditions. Cellular targets are blocked at different concentrations which are of clinical importance and relevance where certain concentrations may or may not be reached *in vivo* during patient treatment.

To screen for binding affinities of SU11248 towards cellular protein targets in a broad range of cancer cell lines and tumor samples a semi-quantitative mass spectrometry based chemical proteomics approach was established to measure target-binding amounts directly from cells under physiological conditions. Native

conditions of a target-protein are of great importance while studying interaction-affinities because binding of SU11248 towards cellular proteins is influenced by the native conformation of a particular target, its activation status and posttranslational modifications, its association with cofactors and other interacting molecules as well as the ATP-concentration within the cell. To distinguish between high, moderate and low affinity binding partners to further characterize their functional relevance two SU11248 matrices of different ligand densities (0.3 and 3mM immobilized SU11248) were used in sequence. With this strategy one differentially enriches for high, moderate and low affinity binding partners on the respective SU11248 matrix. High affinity targets are preferably retained in the low-ligand-density fraction whereas low-affinity interaction partners are only captured with higher ligand concentrations. Moderate affinity binding partners are equally distributed in both matrices with even a slight shift to higher concentrations. This helps to define relative affinities of kinases bound to SU11248.

To get a global picture of SU11248 target-affinities among diverse tumor indications cancer cell lines of different tissue origins were used. Total cell lysates from glioblastoma cell lines U118, U1242, from breast cancer cell lines Hs578T, MDA-MB-435S, MDA-MB-231, from melanoma cell lines WM266-4, WM115, C8161, from the pancreatic cancer cell line A590 and the prostate cancer cell line DU145 were applied consecutively to the two different SU11248 matrices and eluted separately for protein identification by mass spectrometry. Targets binding to the low ligand density matrix are binding tighter (higher affinity) than targets binding only to higher ligand concentrations. The workflow is shown in Figure 43.

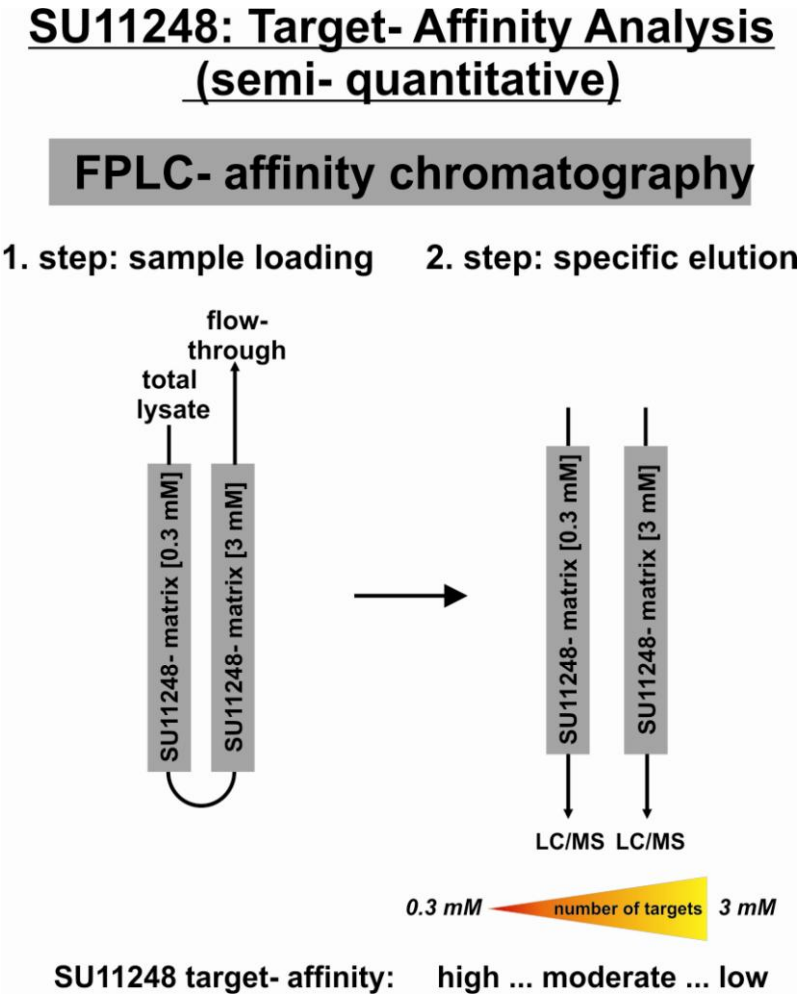

Figure 43 Workflow of target-affinity estimation for SU11248 interaction partners based on a semi-quantitative affinity chromatography procedure followed by LC/MS analysis.
Total cell lysates were subjected to a two-step affinity purification strategy with two SU11248 matrices of different ligand densities, bound proteins specifically eluted and both fractions analyzed separately by mass spectrometry for binding partner identification.

As a measure of binding of interaction partners to SU11248 the number of spectrum-to-sequence matches for each protein were used as a semi-quantitative indicator of the amount of protein captured on the SU11248 matrix (Rappsilber et al., 2002). The more protein was retained the more spectra for each protein can be detected via LC/MS due to wider elution peaks in the HPLC chromatography. To compare the protein binding to both matrices the number of spectrum-to-sequence matches per protein of each elution fraction were normalized to the ligand density and used to calculate a fold-enrichment of kinase-amount bound to 0.3 mM as a direct measure for target affinity (Figure 44).

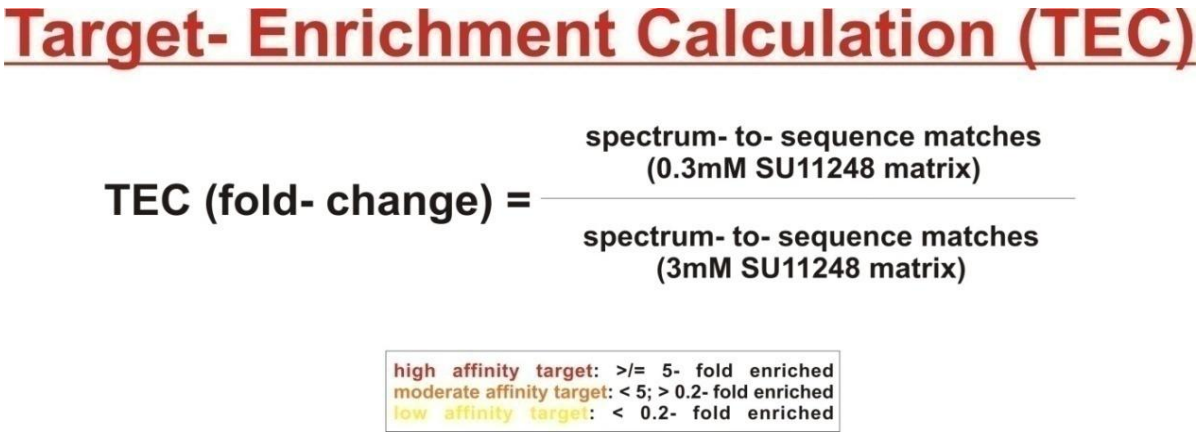

Figure 44 Formula for Target Enrichment Calculation (TEC) in the lower ligand density fraction. Spectrum-to-sequence matches per protein were taken as a semi-quantitative amount of protein binding, normalized to ligand density and fold-enrichment-factors calculated. Proteins were grouped in three categories ranging from high to moderate to low affinity targets depending on their fold-enrichment on the 0.3 mM SU11248 matrix.

Enrichment > 5-fold was considered as high affinity interaction, kinases binding equally to both resins were grouped as moderate and proteins captured more efficiently on the higher ligand density matrix were classified as low affinity binding partners of SU11248. Coomassie-staining of differentially enriched proteins on the two SU11248 matrices is shown in Figure 45.

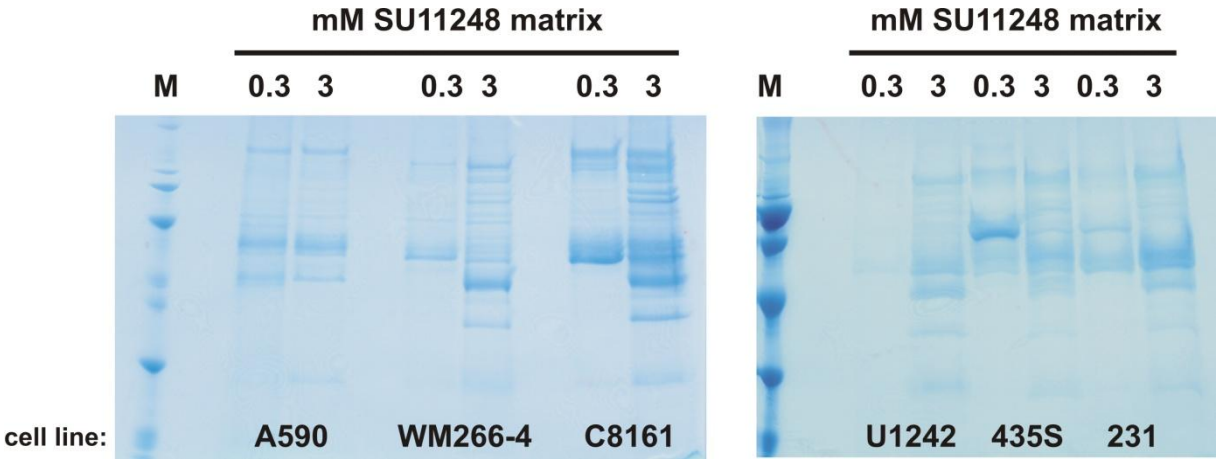

Figure 45 Coomassie-staining of protein fractions after SU11248-matrix based target affinity chromatoghraphy and specific elution with free inhibitor.
Total cell lysates were loaded on two consecutive SU11248 matrices with different ligand densities and bound proteins eluted specifically fractions-wise with 1 mM free inhibitor, `Wessel- Fluegge`- precipitated and separated on a 1D-SDS-page-gel-electrophoresis.

The Coomassie-staining shows that more proteins are retained in the higher ligand-density fraction but for some proteins enrichment in the first fraction (0.3 mM SU11248 matrix) is visible. This is in accordance with the data obtained from the LC/MS analysis and reflects the differential target-binding behaviour of cellular SU11248 interaction partners.

The tissue-specific target-affinities of SU11248 towards all identified kinases in cancer cell lines and tumor samples are listed in Table 11.

Table 11 SU11248 binding affinities against endogenously expressed kinases in cancer cell lines and mRCC primary tumors.

Target-affinities are averaged in cell lines of the same tissue origin and in all tested tumor samples and divided into three categories of high affinity binding partners (3; red), moderate affinity targets (2; orange) and low-affinity interaction partners (1; yellow) based on the fold-enrichment on the 0.3 mM SU11248 matrix as described in Figure 44.

Kinase	Kinase-Family	Protein ID	PEP	SU11248-Affinity					
				cancer cell lines					tumor samples
				brain	breast	pancreas	prostate	skin	mRCC
AAK1	Other	IPI00479760	0.00	3	3	3	3	3	3
ABL1	TK	IPI00221171	0.00	3	3	nd	1	nd	nd
ABL2	TK	IPI00329488	0.00	1	3	3	3	3	nd
ADPGK		IPI00556385	0.00	1	3	nd	3	3	nd
AK1		IPI00640817	0.00	1	nd	nd	3	3	1
AK2		IPI00215901	0.00	nd	3	1	3	3	2
AK3		IPI00465256	0.00	1	3	nd	nd	3	2
AKAP13		IPI00065931	0.01	1	3	3	nd	3	nd
ALDH18A1		IPI00008982	0.00	3	1	3	3	3	1
ALK	TK	IPI00395632	0.00	1	3	3	nd	nd	nd
ATM	Atypical	IPI00298306	0.00	3	3	nd	nd	3	nd
ATR	Atypical	IPI00412298	0.01	3	3	3	1	3	nd
AURKA	Other	IPI00298940	0.00	3	3	2	1	3	nd
AURKB	Other	IPI00176642	0.00	3	3	nd	nd	3	nd
AURKC	Other	IPI00099756	0.00	nd	3	nd	nd	nd	nd
AXL	TK	IPI00296992	0.00	nd	3	nd	nd	nd	nd
BCR	Atypical	IPI00004497	0.00	3	3	nd	nd	nd	2
BLK	TK	IPI00554756	0.00	3	1	nd	nd	1	nd
BMP2K	Other	IPI00337426	0.00	3	3	3	3	3	3
BMPR2	TKL	IPI00783156	0.00	1	1	3	1	1	3
CALM1		IPI00794543	0.00	3	3	1	3	3	3
CAMK2A	CAMK	IPI00550056	0.00	nd	nd	nd	nd	1	nd
CAMK2B	CAMK	IPI00221305	0.00	3	3	3	3	3	3
CAMK2D	CAMK	IPI00876923	0.00	3	3	3	3	3	2
CAMK2G	CAMK	IPI00296678	0.00	3	3	3	3	3	3
CASK	CAMK	IPI00514301	0.00	3	3	3	3	nd	nd
CDC2	CMGC	IPI00026689	0.00	1	3	nd	3	3	nd
CDC2L5	CMGC	IPI00456970	0.00	3	3	1	3	3	nd
CDC42BPB		IPI00477763	0.00	1	3	3	nd	3	nd
CDK2	CMGC	IPI00031681	0.00	3	1	nd	3	1	nd
CDK3	CMGC	IPI00023503	0.00	nd	1	nd	nd	nd	nd
CDK4	CMGC	IPI00007811	0.00	3	1	nd	nd	nd	nd
CDK5	CMGC	IPI00023530	0.00	1	1	nd	3	1	nd
CDK6	CMGC	IPI00023529	0.00	nd	1	nd	3	nd	nd
CDK9	CMGC	IPI00552413	0.00	3	3	nd	nd	nd	nd
CHEK2	CAMK	IPI00423156	0.00	3	1	nd	nd	1	nd
CHKA		IPI00409761	0.00	nd	3	1	nd	nd	nd
CHKB		IPI00031758	0.00	nd	nd	1	nd	nd	nd
CIT		IPI00719285	0.01	3	1	1	1	1	nd
CKB		IPI00022977	0.00	nd	1	nd	3	nd	1
CKMT1A		IPI00658109	0.00	3	3	nd	nd	nd	nd
CLK2	CMGC	IPI00028071	0.00	1	3	nd	nd	nd	nd
CMPK		IPI00219953	0.00	nd	3	nd	3	3	1
CPNE3		IPI00024403	0.00	nd	1	nd	3	nd	1
CRKL		IPI00004839	0.01	nd	nd	nd	3	1	1
CRKRS	CMGC	IPI00021175	0.00	3	3	3	1	nd	nd
CSF1R	TK	IPI00011218	0.00	3	3	nd	nd	nd	3
CSNK1A1	CK1	IPI00183400	0.00	nd	1	nd	3	1	nd
CSNK1A1L	CK1	IPI00167096	0.00	nd	3	nd	nd	3	nd
CSNK1D	CK1	IPI00011102	0.00	2	3	3	2	3	2
CSNK1E	CK1	IPI00027729	0.00	1	2	nd	3	3	nd
CSNK2A	CMGC	IPI00741317	0.00	3	3	1	3	3	nd
CSNK2A1	Other	IPI00016613	0.00	nd	3	nd	nd	nd	2
CSNK2A2	Other	IPI00020602	0.00	1	2	3	3	3	2
CSNK2B		IPI00640088	0.00	3	3	1	3	1	2
DCK		IPI00020454	0.00	1	1	2	1	1	nd
DCLK2	CAMK	IPI00552471	0.01	3	3	1	3	3	nd
DDR2	TK	IPI00004409	0.00	3	1	1	nd	nd	nd
DLG1		IPI00218729	0.01	3	1	3	3	3	1
DTYMK		IPI00013862	0.00	1	nd	nd	3	3	nd
DYRK2	CMGC	IPI00304942	0.01	1	3	nd	nd	3	nd
EPHA1	TK	IPI00294250	0.00	nd	3	nd	nd	nd	nd
EPHA10	TK	IPI00166339	0.00	3	1	nd	nd	3	nd
EPHA2	TK	IPI00021267	0.00	1	1	nd	nd	nd	nd
EPHB2	TK	IPI00644408	0.00	1	3	1	3	3	nd
ERBB4	TK	IPI00016371	0.00	nd	1	3	nd	nd	nd
ERN1	Other	IPI00015974	0.01	3	3	nd	nd	nd	nd
FAK	TK	IPI00413961	0.00	2	2	3	2	3	3
FER	TK	IPI00029263	0.00	2	3	3	2	2	nd
FES	TK	IPI00294344	0.00	nd	3	nd	nd	1	nd
FGFR1	TK	IPI00216859	0.00	nd	3	1	3	nd	3
FGFR2	TK	IPI00218424	0.01	nd	1	nd	nd	3	1
FGFR3	TK	IPI00220254	0.01	3	3	nd	nd	nd	1
FGFR4	TK	IPI00556393	0.00	nd	3	nd	nd	nd	1
FGR	TK	IPI00016871	0.00	nd	3	nd	nd	nd	3
FLJ00120		IPI00414455	0.00	1	1	3	3	3	nd
FLT1	TK	IPI00018335	0.00	1	1	1	nd	3	2
FLT3	TK	IPI00005722	0.00	3	nd	nd	nd	3	1
FLT4	TK	IPI00293565	0.00	3	3	nd	3	nd	3
FN3KRP		IPI00099986	0.00	nd	1	nd	nd	1	1
FYN	TK	IPI00219012	0.00	nd	1	nd	1	3	2
GAK	Other	IPI00298949	0.00	2	2	nd	2	1	nd

Kinase	Kinase-Family	Protein ID	PEP	SU11248-Affinity cancer cell lines brain	breast	pancreas	prostate	skin	tumor samples mRCC
Galactokinase		IPI00442827	0.00	1	1	nd	3	nd	nd
GALK1		IPI00019383	0.00	nd	3	nd	nd	3	1
GSK3A	CMGC	IPI00292228	0.00	1	3	1	nd	3	nd
GSK3B	CMGC	IPI00216190	0.00	3	3	nd	3	1	2
HCK	TK	IPI00646510	0.00	1	3	nd	nd	3	3
HISPPD2A		IPI00398511	0.00	3	3	3	nd	nd	nd
HK2		IPI00102864	0.01	nd	1	nd	nd	3	2
ICK	CMGC	IPI00414132	0.00	nd	3	nd	3	nd	1
IGF1R	TK	IPI00027232	0.00	3	1	nd	nd	nd	nd
IKBKB	Other	IPI00024709	0.01	1	3	nd	nd	3	nd
IKBKE	Other	IPI00029045	0.00	2	2	3	1	2	nd
INSR	TK	IPI00783573	0.00	nd	3	1	1	3	2
INSRR	TK	IPI00027212	0.00	nd	3	nd	nd	nd	nd
IRAK3	TKL	IPI00026984	0.00	nd	1	3	2	1	nd
IRAK4	TKL	IPI00007641	0.00	1	1	2	nd	1	2
JAK1	TK	IPI00784013	0.00	3	3	3	3	3	nd
JAK2	TK	IPI00031016	0.00	nd	nd	nd	nd	3	nd
KALRN		IPI00877065	0.00	1	3	1	3	1	nd
KDR	TK	IPI00021396	0.00	nd	3	nd	nd	3	1
KIT	TK	IPI00022296	0.00	3	3	3	3	nd	3
LATS1	AGC	IPI00005858	0.00	1	nd	nd	nd	nd	nd
LCK	TK	IPI00515097	0.00	1	1	nd	nd	1	3
LIMK1	TKL	IPI00291702	0.00	1	3	nd	nd	nd	nd
LOC346521		IPI00039639	0.00	nd	1	nd	nd	nd	nd
LOC407835		IPI00419792	0.00	1	1	3	1	3	3
LRRK2	TKL	IPI00175649	0.00	3	3	3	nd	3	nd
LYN	TK	IPI00872474	0.00	3	1	nd	1	1	3
MAGI-3		IPI00170865	0.00	nd	3	3	nd	3	nd
MAK	CMGC	IPI00025489	0.00	3	3	nd	nd	1	1
MAP2K1	STE	IPI00219604	0.00	2	2	3	1	3	1
MAP2K2	STE	IPI00003783	0.00	2	3	3	2	3	1
MAP2K5	STE	IPI00158248	0.00	2	2	1	1	3	nd
MAP3K1	STE	IPI00855985	0.01	3	3	1	nd	nd	nd
MAP3K10	TKL	IPI00295401	0.00	3	3	3	nd	nd	nd
MAP3K11	TKL	IPI00000977	0.00	1	1	nd	1	2	3
MAP3K2	STE	IPI00513803	0.00	1	1	nd	1	1	nd
MAP3K3	STE	IPI00181703	0.00	3	2	1	nd	1	nd
MAP3K4	STE	IPI00872899	0.01	3	3	3	nd	nd	nd
MAP3K7	STE	IPI00295738	0.00	3	3	nd	nd	3	nd
MAP3K7IP1		IPI00019459	0.00	nd	1	nd	nd	nd	nd
MAP3K9	TKL	IPI00179189	0.00	nd	1	nd	nd	nd	nd
MAP4K2	STE	IPI00658102	0.00	1	3	nd	nd	1	nd
MAP4K3		IPI00219510	0.00	1	1	1	2	2	nd
MAP4K4	STE	IPI00006752	0.00	2	2	2	2	3	2
MAP4K5		IPI00294842	0.00	1	3	1	1	1	nd
MAPK1	CMGC	IPI00003479	0.00	3	2	3	3	3	2
MAPK14	CMGC	IPI00002857	0.00	nd	1	nd	3	1	nd
MAPK3	CMGC	IPI00018195	0.00	1	3	1	3	1	1
MAPK4	CMGC	IPI00873645	0.00	nd	1	1	nd	nd	3
MAPK6	CMGC	IPI00003431	0.00	nd	3	1	nd	nd	1
MAPK9	CMGC	IPI00024673	0.00	1	2	2	2	1	nd
MAPKBP1		IPI00783044	0.00	nd	1	3	3	3	nd
MARK2	CAMK	IPI00555838	0.00	1	3	nd	nd	3	nd
MARK3	CAMK	IPI00827718	0.00	3	3	nd	nd	3	nd
MAST4	AGC	IPI00788168	0.01	nd	3	nd	nd	nd	nd
MERTK	TK	IPI00029756	0.00	nd	1	3	3	3	nd
MET	TK	IPI00294528	0.00	nd	3	nd	nd	3	1
MINK1	STE	IPI00166680	0.00	nd	3	3	nd	3	nd
MLTK	TKL	IPI00329638	0.00	1	3	nd	3	3	nd
MST1R	TK	IPI00030273	0.00	nd	1	nd	nd	nd	3
MST4	STE	IPI00760722	0.00	1	3	nd	nd	nd	nd
MUSK	TK	IPI00289243	0.00	3	3	1	nd	3	nd
MYLK2		IPI00221127	0.00	3	1	3	1	3	3
MYLK3	CAMK	IPI00871561	0.00	1	nd	nd	nd	nd	nd
MYO3A	STE	IPI00185036	0.00	1	3	3	1	3	nd
N4BP2		IPI00328825	0.01	3	3	nd	nd	3	nd
NEK2	Other	IPI00021331	0.00	3	3	nd	1	3	nd
NEK6	Other	IPI00396662	0.00	3	1	nd	1	nd	nd
NEK9	Other	IPI00301609	0.00	2	1	3	2	3	2
NLK	CMGC	IPI00793695	0.00	nd	nd	nd	3	1	1
NME1-NME2		IPI00604590	0.00	1	3	1	3	3	2
NME3		IPI00012315	0.00	2	1	1	2	3	2
NME4		IPI00658182	0.00	2	3	3	1	3	3
PAK2	STE	IPI00419979	0.00	nd	1	nd	3	nd	nd
PAK3	STE	IPI00553222	0.00	3	3	nd	nd	3	nd
PAK4	STE	IPI00014068	0.00	1	1	2	1	1	nd
PCK2		IPI00797038	0.00	nd	3	1	nd	nd	3
PCTK1		IPI00549858	0.00	nd	3	nd	nd	nd	nd
PCTK2		IPI00376955	0.00	3	3	nd	nd	nd	3
PCTK3		IPI00394661	0.00	1	3	nd	nd	nd	3
PDGFRA	TK	IPI00027721	0.00	3	3	3	3	3	3
PDGFRB	TK	IPI00015902	0.00	3	3	3	3	3	3

Kinase	Kinase-Family	Protein ID	PEP	SU11248-Affinity cancer cell lines brain	breast	pancreas	prostate	skin	tumor samples mRCC
PDPK1	AGC	IPI00002538	0.00	1	1	nd	nd	3	nd
PDXK		IPI00013004	0.00	2	2	3	3	3	2
PFKL		IPI00332371	0.00	nd	3	nd	3	3	2
PFKM		IPI00465179	0.00	1	nd	1	3	3	2
PFKP		IPI00009790	0.00	1	3	nd	3	3	2
PGK1		IPI00169383	0.00	3	3	3	3	3	2
PGK2		IPI00219568	0.00	1	1	1	nd	nd	2
PHKA1		IPI00004247	0.00	nd	1	3	nd	1	nd
PHKA2		IPI00004237	0.00	3	1	nd	nd	3	2
PHKB		IPI00514327	0.00	3	1	nd	nd	1	1
PHKG2	CAMK	IPI00012891	0.00	3	1	nd	nd	3	nd
PI4KA		IPI00070943	0.00	3	3	1	3	3	2
PIP4K2C		IPI00152303	0.00	nd	1	1	nd	nd	nd
PIP5K1A		IPI00022150	0.01	3	3	nd	nd	3	nd
PKM2		IPI00479186	0.00	3	3	1	3	3	2
PLK4	Other	IPI00410344	0.00	2	3	nd	1	2	nd
PPP4C		IPI00012833	0.00	nd	3	nd	nd	nd	nd
PRKAA1	CAMK	IPI00410287	0.00	2	2	2	2	2	2
PRKAA2	CAMK	IPI00307755	0.00	1	3	nd	nd	3	3
PRKAG1		IPI00413318	0.00	2	2	1	3	2	1
PRKAG3		IPI00644202	0.00	nd	3	nd	1	3	nd
PRKCA	AGC	IPI00385449	0.00	nd	1	nd	3	nd	nd
PRKCG	AGC	IPI00007128	0.00	3	3	nd	nd	3	nd
PRKCSH		IPI00026154	0.00	3	3	nd	3	nd	2
PRKD1	CAMK	IPI00014878	0.00	1	nd	3	3	nd	nd
PRKD2	CAMK	IPI00009334	0.00	3	3	nd	3	3	nd
PRKD3		IPI00015538	0.00	nd	3	nd	nd	nd	nd
PRKDC		IPI00296337	0.00	3	3	1	3	3	1
PRPF4B	CMGC	IPI00013721	0.00	3	3	nd	1	3	2
PRPS1		IPI00219616	0.00	nd	3	nd	3	3	1
PRPS2		IPI00718888	0.00	nd	3	nd	3	nd	2
PTK2B	TK	IPI00029702	0.00	3	1	1	1	nd	nd
RET	TK	IPI00013983	0.00	1	3	1	nd	3	nd
RET/PTC2	TK	IPI00783751	0.00	nd	1	nd	nd	3	1
RIPK2	TKL	IPI00021917	0.00	3	3	nd	nd	nd	nd
ROS1	TK	IPI00288965	0.02	1	3	3	nd	3	3
RPS6KA1	AGC	IPI00477982	0.00	2	1	1	3	1	2
RPS6KA2	AGC	IPI00478653	0.00	3	1	nd	nd	3	nd
RPS6KA3	AGC	IPI00020898	0.00	1	1	1	3	1	3
RPS6KA4	AGC	IPI00022536	0.00	2	3	3	2	3	nd
RPS6KA5	AGC	IPI00335101	0.00	2	1	nd	1	1	nd
RPS6KA6	AGC	IPI00007123	0.00	1	1	nd	nd	nd	nd
RPS6KB1	AGC	IPI00216132	0.00	1	1	nd	nd	1	nd
SGK	AGC	IPI00514242	0.00	3	1	nd	nd	3	nd
SGK269	Other	IPI00737545	0.01	3	3	nd	nd	3	nd
SMF		IPI00465164	0.01	3	3	nd	nd	3	nd
SMG1	Atypical	IPI00639874	0.00	3	3	nd	3	3	nd
SNRK	CAMK	IPI00470811	0.01	3	3	3	nd	1	nd
SPEG	CAMK	IPI00830074	0.00	3	3	3	nd	1	nd
SRC	TK	IPI00328867	0.00	nd	2	nd	1	1	2
SRMS		IPI00024884	0.00	nd	nd	1	nd	3	1
STK		IPI00783100	0.00	3	3	nd	nd	3	3
STK10	STE	IPI00304742	0.00	1	3	3	nd	nd	2
STK16	Other	IPI00872027	0.00	nd	1	nd	nd	nd	nd
STK17A	CAMK	IPI00646659	0.00	1	2	3	1	2	nd
STK17B	CAMK	IPI00014934	0.00	3	3	nd	1	nd	nd
STK24	STE	IPI00872754	0.00	1	1	nd	nd	1	nd
STK25	STE	IPI00012093	0.00	nd	3	nd	3	1	nd
STK3	STE	IPI00411984	0.00	3	2	3	1	3	nd
STK33	CAMK	IPI00747557	0.00	nd	nd	nd	1	nd	nd
STK4	STE	IPI00011488	0.00	2	3	3	1	3	nd
STK4/SLC36AL		IPI00784556	0.00	nd	nd	nd	1	1	nd
TBK1	Other	IPI00293613	0.00	2	3	3	2	2	3
TEK	TK	IPI00412829	0.00	3	3	nd	nd	1	nd
TIE1	TK	IPI00019530	0.01	nd	nd	nd	nd	1	nd
TK1		IPI00299214	0.01	1	3	nd	nd	1	nd
TNIK	STE	IPI00514275	0.00	3	3	3	3	2	1
TNK1	TK	IPI00552691	0.00	nd	1	1	1	1	nd
TP53RK	Other	IPI00290305	0.00	nd	1	nd	nd	nd	nd
TRIO	CAMK	IPI00479523	0.00	3	3	3	nd	3	nd
TRPM6	Atypical	IPI00472524	0.00	3	3	1	nd	3	nd
TTBK2	CK1	IPI00217437	0.00	1	3	3	nd	3	2
TWF1		IPI00183508	0.00	3	3	nd	3	nd	1
TYK2	TK	IPI00022353	0.00	1	1	3	nd	3	nd
Tyrosine kinase		IPI00385887	0.00	1	nd	nd	nd	3	nd
VEGFR3	TK	IPI00555993	0.00	1	nd	nd	nd	nd	nd
WEE1	Other	IPI00025830	0.01	nd	3	3	nd	3	nd
YES1	TK	IPI00013981	0.00	2	3	2	2	2	2

The target affinities in all analyzed cancer cell lines as well as the data from mRCC samples were averaged tissue-specific and are shown as differently coloured dots in the kinase tree (Figure 46, Figure 47). The kinase dendrogram was adapted from *Science* (http://www.sciencemag.org/) and Cell Signaling Technology, Inc. (http://www.cellsignal.com/).

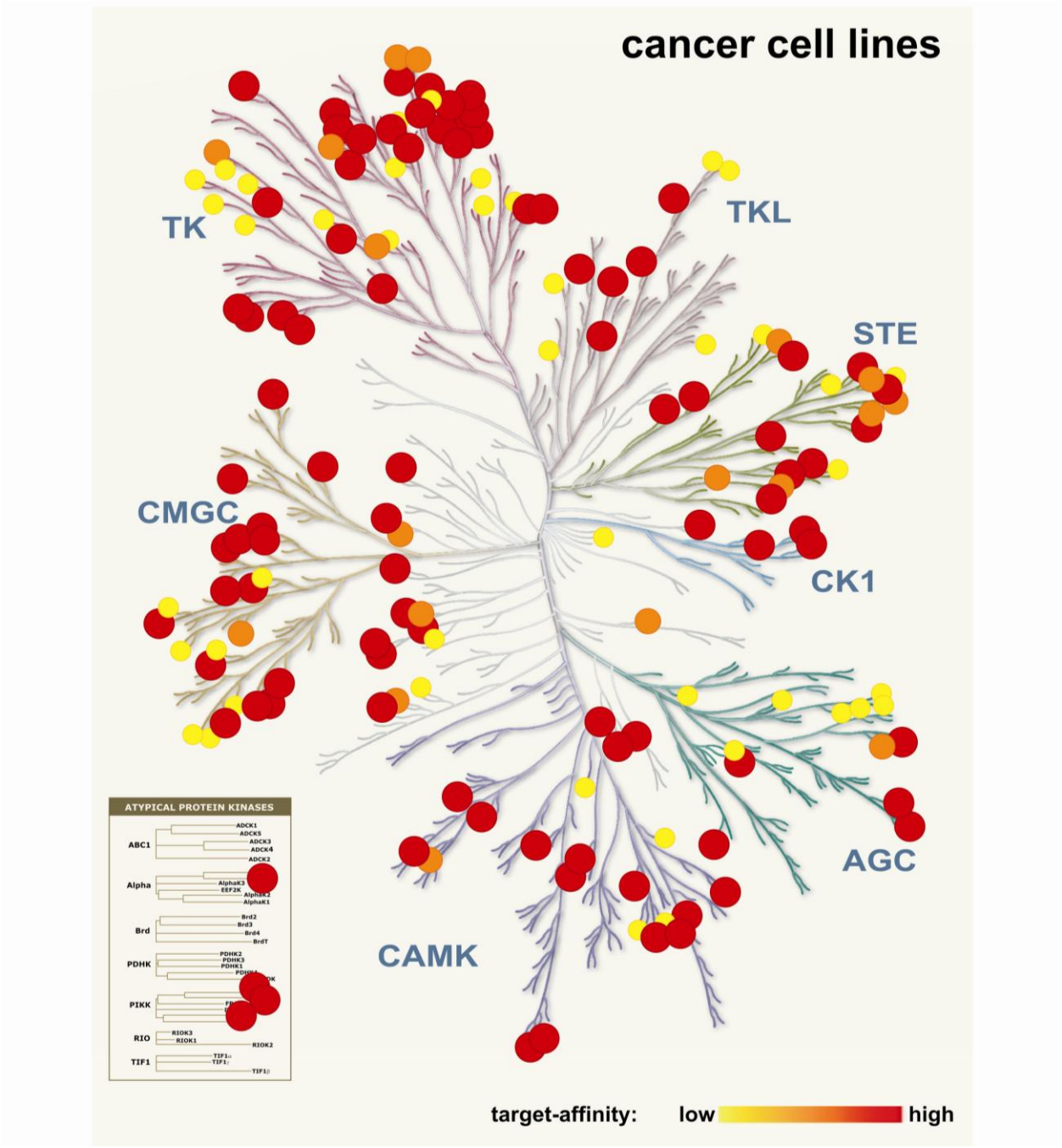

Figure 46 SU11248 binding affinity against endogenously expressed kinases in cancer cell lines. The SU11248 affinity against endogenously expressed kinases was analyzed in the glioblastoma cell lines U118, U1242, the breast cancer cell lines Hs578T, MDA-MB-435S, MDA-MB-231, the melanoma cell lines WM266-4, WM115, C8161, the pancreatic cancer cell line A590 and the prostate cancer cell line DU145 by a two-step affinity chromatography followed by MS-based protein identification. The protein enrichment in the lower-ligand density fraction was calculated based on spectrum-to-sequence matches normalized to the ligand concentration on the respective SU11248 matrix as a measure of protein amount bound to the SU11248 matrix which correlates with the target-affinities. High, moderate and low affinity-binding partners were distinguished and are shown as differentially colored dots in the kinase tree (fold-enrichment: > 5= high affinity (red dot); < 5 > 0.2= moderate affinity (orange dot); < 0.2= low affinity (yellow dot)). The target affinity of a particular protein was averaged over all cancer cell lines. The kinase dendrogram was adapted from *Science* (http://www.sciencemag.org/) and Cell Signaling Technology, Inc. (http://www.cellsignal.com/). TK: tyrosine kinase; TKL: tyrosine kinase-like; STE: Homologs of yeast Sterile 7, Sterile 11, Sterile 20 kinases; CK1: Casein Kinase 1; AGC: Containing PKA, PKG, PKC families; CAMK: Calcium/calmodulin-dependent protein kinase; CMGC: Containing CDK, MAPK, GSK3, CLK families.

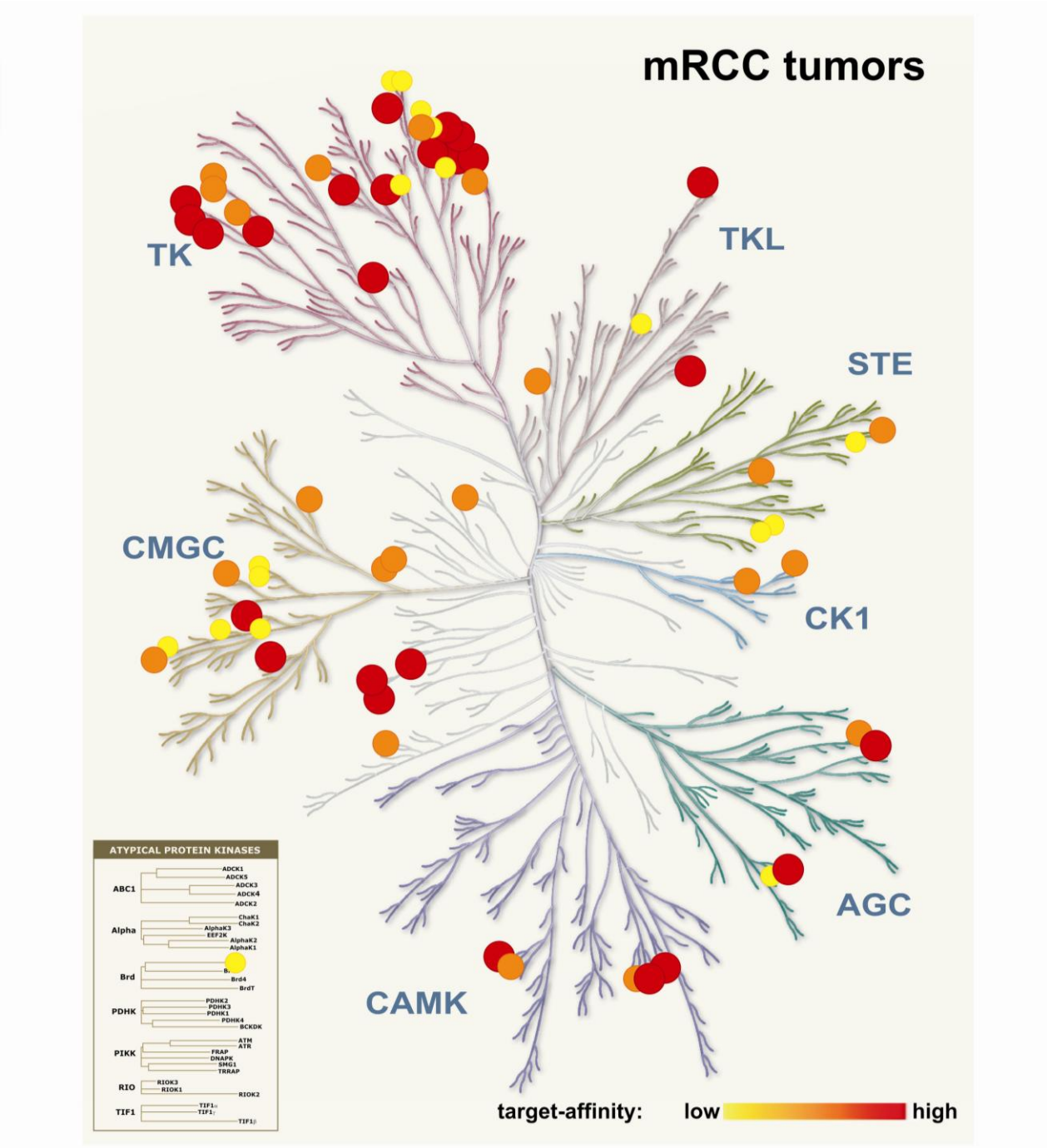

Figure 47 SU11248 binding affinity against endogenously expressed kinases in mRCC tumor samples.

The SU11248 affinity against endogenously expressed kinases was analyzed in metastatic-renal cell carcinoma primary tumor samples by a two-step affinity chromatography followed by MS-based protein identification. The protein enrichment in the lower-ligand density fraction was calculated based on spectrum-to-sequence matches normalized to the ligand concentration on the respective SU11248 matrix as a measure of protein amount bound to the SU11248 matrix which correlates with the target-affinities. High, moderate and low affinity-binding partners were distinguished and are shown as differentially colored dots in the kianse tree (fold-enrichment: > 5= high affinity (red dot); < 5 > 0.2= moderate affinity (orange dot); < 0.2= low affinity (yellow dot)). The target affinity of a particular protein was averaged over all cancer cell lines. The kinase dendrogram was adapted from *Science* (http://www.sciencemag.org/) and Cell Signaling Technology, Inc. (http://www.cellsignal.com/). TK: tyrosine kinase; TKL: tyrosine kinase-like; STE: Homologs of yeast Sterile 7, Sterile 11, Sterile 20 kinases; CK1: Casein Kinase 1; AGC: Containing PKA, PKG, PKC families; CAMK: Calcium/calmodulin-dependent protein kinase; CMGC: Containing CDK, MAPK, GSK3, CLK families.

To get a reliable and better prediction significance of target-relevance *in vivo* SU11248 affinities against kinase targets in cancer cell lines and tumor samples were compared. The results are shown in Figure 48.

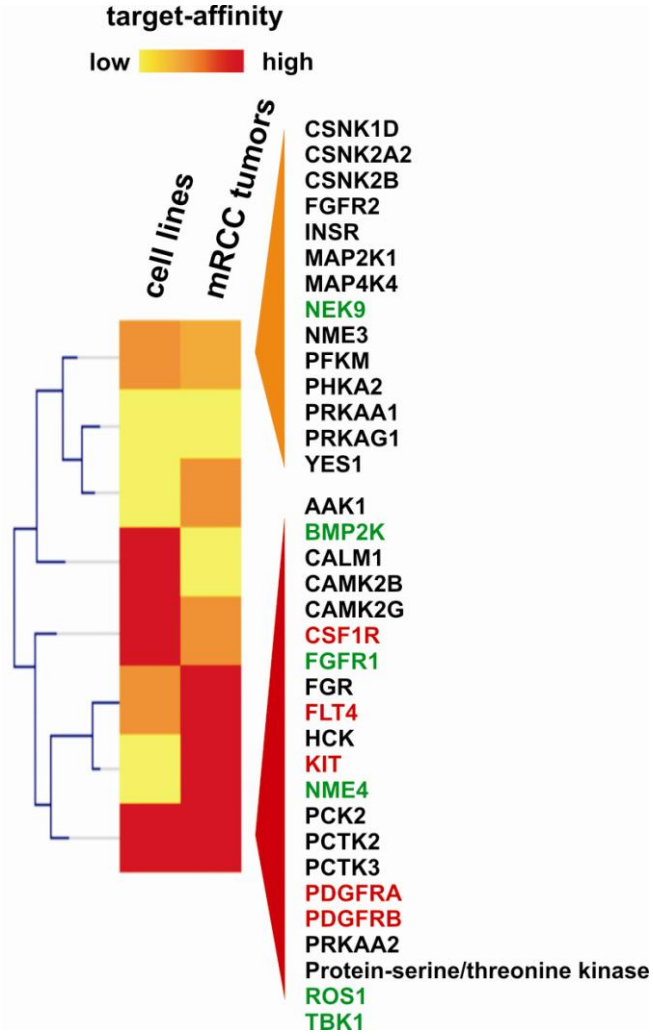

Figure 48 SOTA-cluster of SU11248 target-affinities against endogenously expressed kinases in cancer cell lines and mRCC tumor samples.
Overlapping high and moderate affinity targets in cancer cell lines and mRCC tumor samples are highlighted. Beside known SU11248 targets such as PDGFRa, PDGFRb, CSF1R, FLT4 and KIT (marked in red) which were found to bind tightly to the small-molecule inhibitor, interesting new kinases including ROS1, FGFR1, BMP2K, TBK1, NME4 and NEK9 (marked in green) were identified as high affinity SU11248 targets.

Beside known targets such as the receptor tyrosine kinases PDGFRa, PDGFRb, CSF1R, KIT and FLT4 showing high affinity towards the small-molecule inhibitor SU11248 very interesting new targets including the receptor tyrosine kinases ROS1, INSR, FGFR1 and FGFR2, the cytosolic tyrosine kinase YES1, the serine/threonine- kinases TBK1, BMP2K and NEK9, the nucleoside diphosphate kinase nm23-H4 (NME4) as well as Casein- and CAM- Kinases were identified. All these newly detected interaction partners of SU11248 showed strong binding towards the drug reflected by their enrichment at low inhibitor concentrations. The correlation of high affinity SU11248 targets between cancer cell lines and tumor samples

increases their biological relevance for the drug`s action *in vivo* while patient treatment and they may function as markers of responsiveness towards the small-molecule kinase inhibitor SU11248.

Only overlapping high and few moderate affinity targets were considered for further functional analyses. High affinity targets are more likely relevant for a drug` s biological function and anti-tumor efficacy than low affinity binding partners where effective concentrations of the inhibitor to block these proteins may not be reached under treatment conditions *in vivo*.

For many targets there is a strong correlation between cell line and tumor affinities. Interestingly, SU11248 interaction partners that could be identified in almost all analyzed cancer cell lines and tumor samples in the first qualitative target-profiling (Figure 35) turned out to be enriched or even strongly enriched at low SU11248 concentrations indicating their high affinity.

7.4 Quantification of target-dissociation constants directly from cancer cells

Semi-quantitative target-affinities as obtained for SU11248 in a broad panel of different cancer cell lines and tumor samples help to rank and prioritize molecular interactions in order to identify the strongest molecular target associations that are likely the most relevant under physiological conditions. The established approach is time- and cost-efficient and can be broadly used for the profiling and ranking of drug-target interactions in cancer cell lines and tumor samples of almost all indications.

Nevertheless, quantitative target-dissociation constants reflecting effective inhibitor concentrations needed to efficiently block particular targets are not provided by the semi-quantitative method. Therefore, a quantitative chemical proteomics concept that integrates unbiased, proteome-wide target identification and quality-controlled target affinity measurements was used. This method allows quantification of cellular target protein interactions directly from cells under native protein conformations and physiological ATP-concentrations. Target-specific dissociation constants were determined by combining quantitative mass spectrometry with a defined set of affinity purification experiments as previously described for the small-molecule epidermal growth factor receptor inhibitor gefitinib (Sharma et al., 2009).

7.4.1 Workflow of target affinity measurement based on quantitative mass spectrometry combined with affinity purification experiments

Quantification of cellular target protein interactions directly from cells needs quantitative mass spectrometry. To enable quantitative mass spectrometry based on stable isotope labelling with amino acids in cell culture (SILAC), cancer cells were metabolically labelled with either normal arginine and lysine (Arg^0/Lys^0) or combinations of isotopic variants of the two amino acids (Arg^6/Lys^4, Arg^{10}/Lys^8). The Arg^0/Lys^0-encoded cell lysates was incubated with the inhibitor beads displaying immobilized SU11248, whereas Arg^6/Lys^4-labeled extract was added to control resin devoid of ligand. In case of the Arg^{10}/Lys^8-encoded lysate, supernatant from the first binding to SU11248 resin was subjected to a second incubation with the same amount of inhibitor beads which is schematically described in Figure 49.

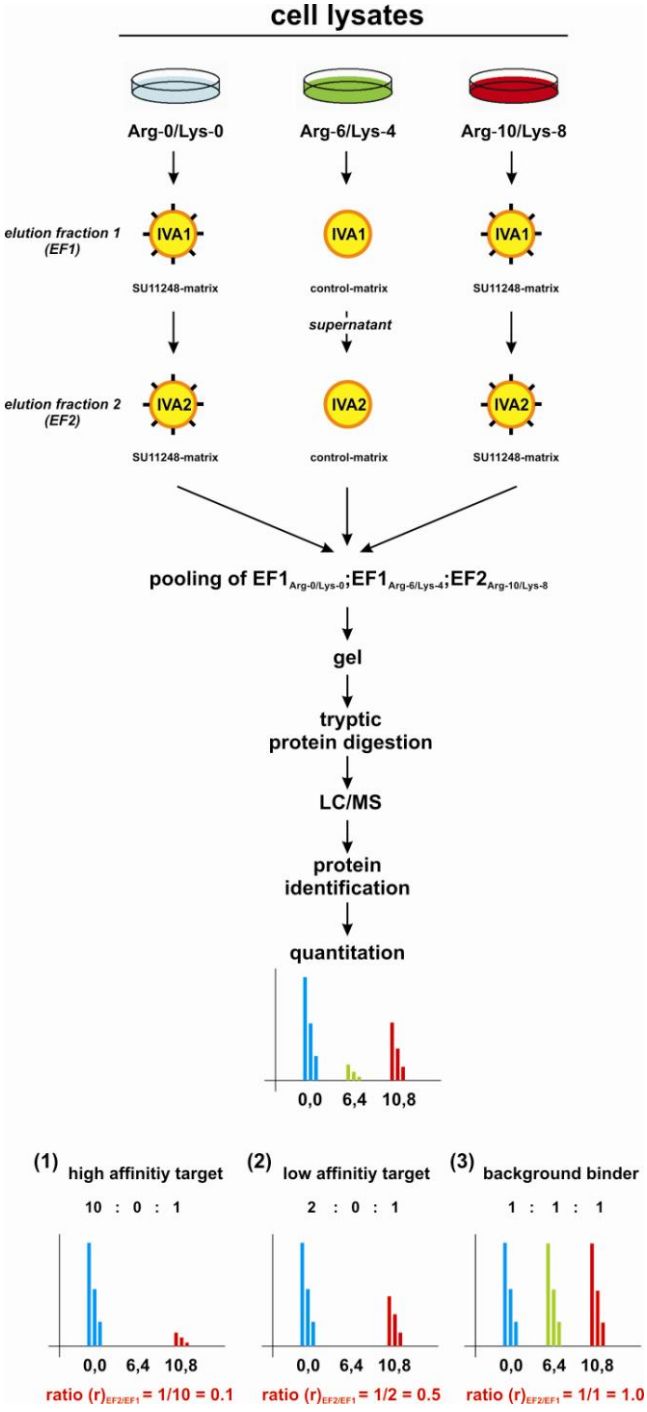

Figure 49 Workflow of drug-target affinity measurement based on quantitative mass spectrometry combined with affinity purification experiments.
Cancer cells were metabolically labelled with either normal arginine and lysine (Arg^0/Lys^0) or combinations of isotopic variants of the two amino acids (Arg^6/Lys^4, Arg^{10}/Lys^8). The Arg^0/Lys^0-encoded cell lysates was incubated with the inhibitor beads displaying immobilized SU11248, whereas Arg^6/Lys^4-labelled extract was added to control resin devoid of ligand. In case of the Arg^{10}/Lys^8-encoded lysate, supernatant from the first binding to SU11248 resin was subjected to a second incubation with the same amount of inhibitor beads. The elution fractions were pooled, proteins separated by 1D-SDS-PAGE, trypsin-digested and analyzed by LC/MS. Protein identification and quantification was done with the MaxQuant software (Cox and Mann, 2008). Binding patterns for three distinct target-affinities are indicated in the lower three panels. High affinity targets are enriched in the first elution fraction, low affinity interaction partners also bind in the second incubation with inhibitor beads and unspecific background binders are equally retained in both fractions as well as the control-resin.

The three resulting elution fractions were combined, resolved by gel electrophoresis and proteolytically digested. Due to the differential SILAC labelling, peptides co-eluted as triplets in online liquid chromatography (LC)-MS. After peptide identification based on the precursor ion masses and the acquired tandem MS spectra, the relative abundance of retained proteins was quantified by determining the ratios of their peptide ion intensities using the MaxQuant software (Cox and Mann, 2008). Proteins showing considerable binding to the control resin (ratio M/L > 0.25) were identified as non-specific interactors and therefore not considered further. For specifically retained proteins according to this criterion, the ratio r for the relative amount of target retained in the second *versus* the first round of binding to SU11248 beads was determined. The ratio r equals the fraction of a target that was not sequestered by the immobilized inhibitor, whereas 1-r indicates the proportion of target that actually bound to the affinity resin. In combination with the known concentration of immobilized SU11248, dissociation constants (K_d-values) could be calculated that provided a quantitative measure of the respective target affinities for the immobilized inhibitor.

$$K_d = [I]_{effective} * (r/(1-r))$$

Quantification of cellular target protein interaction of SU11248 against the cellular proteome was performed in the kidney cancer cell lines Caki1, Caki2, A498 and the breast cancer cell line MDA-MB-435S. All four cell lines were highly responsive to SU11248 treatment seen in biological assays including proliferation, survival, migration as well as invasion, respectively. K_d-values are shown in Table 12 for kinase targets and Table 13 for non-kinase targets. Targets are listed by decreasing affinities and K_d-value cuts were set at < 55 µM for kinase-targets and < 40 µM for non-kinase targets, respectively.

Table 12 Binding results (K_d -values in µM) for SU11248 against endogenous expressed kinases

Kinase	Protein ID	Protein Name	PEP	Caki1 K_d [µM]	Caki1 SEM	Caki2 K_d [µM]	Caki2 SEM	A498 K_d [µM]	MDA-MB-435S K_d [µM]	average K_d [µM]	average SEM
CAMK2B	IPI00221305	Calcium/calmodulin-dependent protein kinase type II beta	0.00	nd	nd	1.41	0.83	0.59	nd	1.00	0.21
CAMK2D	IPI00430291	Calcium/calmodulin-dependent protein kinase type II delta	0.00	3.24	0.70	1.61	0.43	0.62	0.35	1.46	0.57
CAMK2G	IPI00646849	Calcium/calmodulin-dependent protein kinase (CaM kinase) II gamma	0.00	3.88	0.84	1.45	0.31	1.12	0.42	1.72	0.65
LRRK2	IPI00175649	Leucine-rich repeat serine/threonine-protein kinase 2	0.00	nd	nd	0.54	0.00	6.18	nd	3.36	1.41
MET	IPI00294528	Hepatocyte growth factor receptor	0.00	nd	nd	nd	nd	3.89	nd	3.89	0.00
NEK2	IPI00021331	Serine/threonine-protein kinase Nek2	0.00	nd	nd	7.73	3.02	7.53	nd	7.63	0.05
NME4	IPI00855980	Nucleoside diphosphate kinase	0.00	8.35	2.84	nd	nd	4.63	13.10	8.69	1.73
TYK2	IPI00022353	Non-receptor tyrosine-protein kinase TYK2	0.00	nd	nd	11.90	0.00	6.93	nd	9.42	1.24
TNK1	IPI00552691	Non-receptor tyrosine-protein kinase TNK1	0.00	nd	nd	17.28	0.00	5.06	nd	11.17	3.06
PKM2	IPI00479186	Pyruvate kinase isozymes M1/M2	0.00	16.65	1.26	nd	nd	11.96	5.68	11.43	2.25
TFG/ALK fusion	IPI00297452	Tyrosine-protein kinase receptor	0.00	nd	nd	16.70	0.00	nd	8.28	12.49	2.11
MYLK3	IPI00304648	Putative myosin light chain kinase 3	0.00	11.56	4.52	13.45	0.00	nd	nd	12.50	0.47
TBK1	IPI00293613	Serine/threonine-protein kinase TBK1	0.00	11.04	4.56	11.00	0.92	5.15	28.36	13.88	4.35
MAP3K7IP1	IPI00019459	Mitogen-activated protein kinase kinase kinase 7-interacting protein 1	0.00	13.20	0.00	nd	nd	15.54	13.40	14.05	0.53
FER	IPI00029263	Proto-oncogene tyrosine-protein kinase FER	0.00	17.93	1.24	17.49	0.07	8.66	14.06	14.54	1.85
NME3	IPI00012315	Nucleoside diphosphate kinase 3	0.00	8.42	1.54	16.98	0.17	20.08	nd	15.16	2.47
MINK1	IPI00166680	Misshapen-like kinase 1	0.00	nd	nd	nd	nd	14.03	16.61	15.32	0.65
IKBKE	IPI00029045	Inhibitor of nuclear factor kappa-B kinase subunit epsilon	0.00	26.43	0.00	17.24	0.57	6.15	12.01	15.46	3.73
AURKA	IPI00298940	Serine/threonine-protein kinase 6	0.00	nd	nd	23.25	4.78	7.84	nd	15.54	3.85
MAP2K5	IPI00158248	Dual specificity mitogen-activated protein kinase kinase 5	0.00	nd	nd	17.59	1.36	10.42	21.15	16.39	2.23
PGK1	IPI00169383	Phosphoglycerate kinase 1	0.00	23.83	5.16	30.15	3.84	8.58	5.37	16.98	5.16
MAPK9	IPI00024673	Mitogen-activated protein kinase 9	0.00	nd	nd	20.52	1.56	13.59	nd	17.06	1.73
EPHA7	IPI00016645	Ephrin type-A receptor 7	0.00	nd	nd	nd	nd	17.67	nd	17.67	0.00
BCKDK	IPI00298612	[3-methyl-2-oxobutanoate dehydrogenase [lipoamide]] kinase	0.00	nd	nd	25.01	0.00	11.33	nd	18.17	3.42
AURKB	IPI00176642	Serine/threonine-protein kinase 12	0.00	nd	nd	18.47	2.10	19.44	nd	18.96	0.24
PFKL	IPI00332371	6-phosphofructokinase, liver type	0.00	22.14	0.00	nd	nd	nd	16.21	19.17	1.48
PFKP	IPI00009790	6-phosphofructokinase type C	0.00	19.61	3.37	31.37	6.76	11.38	15.62	19.49	3.72
MERTK	IPI00029756	Proto-oncogene tyrosine-protein kinase MER	0.00	20.78	0.00	nd	nd	nd	nd	20.78	0.00
DAPK2	IPI00033388	Death-associated protein kinase 2	0.00	nd	nd	29.60	7.17	13.51	nd	21.56	4.02
PDGFRB	IPI00015902	Beta-type platelet-derived growth factor receptor	0.00	21.61	0.00	nd	nd	nd	nd	21.61	0.00
ALDH18A1	IPI00008982	Delta-1-pyrroline-5-carboxylate synthetase	0.00	20.02	4.32	42.69	0.00	nd	3.82	22.18	7.97
PDPK1	IPI00002538	3-phosphoinositide-dependent protein kinase 1	0.00	nd	nd	26.10	5.65	18.44	nd	22.27	1.92
MYLK	IPI00336081	Myosin light chain kinase, smooth muscle	0.00	31.06	0.00	14.93	0.00	nd	nd	23.00	4.03
BMPR2	IPI00783156	Bone morphogenetic protein receptor type-2	0.00	16.15	0.00	39.79	0.00	13.76	nd	23.24	5.87
PHKB	IPI00514327	Phosphorylase b kinase regulatory subunit beta	0.00	22.36	0.00	38.02	11.27	15.23	19.39	23.75	4.31
MAP2K6	IPI00003814	Dual specificity mitogen-activated protein kinase kinase 6	0.00	nd	nd	32.54	7.32	15.08	nd	23.81	4.36
PHKA2	IPI00004237	Phosphorylase b kinase regulatory subunit alpha, liver isoform	0.00	nd	nd	34.19	4.20	23.10	17.59	24.96	3.45
MAPK3	IPI00018195	Mitogen-activated protein kinase 3	0.00	34.24	4.19	25.27	3.18	17.44	23.92	25.22	3.00
AXL	IPI00296992	Tyrosine-protein kinase receptor UFO	0.00	12.15	0.00	60.13	0.00	5.36	nd	25.88	12.19
ADK	IPI00290279	Adenosine kinase	0.00	45.44	0.00	nd	nd	7.70	nd	26.57	9.43
MAP2K2	IPI00003783	Dual specificity mitogen-activated protein kinase kinase 2	0.00	30.15	3.46	30.10	0.48	17.28	29.61	26.79	2.75
MAP2K4	IPI00024674	Dual specificity mitogen-activated protein kinase kinase 4	0.00	nd	nd	24.09	0.00	29.50	nd	26.80	1.35
PHKG2	IPI00012891	Phosphorylase b kinase gamma catalytic chain, testis/liver isoform	0.00	nd	nd	41.41	6.04	20.31	19.26	26.99	5.10
AAK1	IPI00479760	AP2-associated protein kinase 1	0.00	20.58	5.91	38.94	9.70	15.01	35.12	27.41	4.95

Kinase	Protein ID	Protein Name	PEP	Caki1 K_d [µM]	Caki1 SEM	Caki2 K_d [µM]	Caki2 SEM	A498 K_d [µM]	MDA-MB-435S K_d [µM]	average K_d [µM]	average SEM
STK4	IPI00011488	Serine/threonine-protein kinase 4	0.00	26.35	0.00	40.71	0.06	12.54	30.35	27.49	5.05
STK3	IPI00411984	Serine/threonine-protein kinase 3	0.00	nd	nd	46.14	2.34	9.13	27.30	27.52	7.56
IRAK4	IPI00007641	Interleukin-1 receptor-associated kinase 4	0.00	nd	nd	21.86	2.03	33.35	nd	27.60	2.87
YES1	IPI00013981	Proto-oncogene tyrosine-protein kinase Yes	0.00	21.77	10.18	30.23	8.04	32.08	nd	28.03	2.24
PTK2	IPI00413961	Focal adhesion kinase 1	0.00	30.40	9.87	34.51	1.79	5.64	43.43	28.50	7.00
NEK9	IPI00301609	Serine/threonine-protein kinase Nek9	0.00	35.58	0.00	36.47	1.86	14.16	nd	28.74	5.16
PRKCA	IPI00385449	Protein kinase C alpha type	0.00	75.98	6.30	0.54	0.00	10.94	nd	29.15	16.69
MAP3K11	IPI00000977	Mitogen-activated protein kinase kinase kinase 11	0.00	42.57	0.00	21.78	2.05	17.03	36.24	29.40	5.19
LYN	IPI00298625	Tyrosine-protein kinase Lyn	0.00	14.72	1.60	36.05	7.26	44.82	23.40	29.75	5.77
PRKDC	IPI00296337	DNA-dependent protein kinase catalytic subunit	0.00	55.80	26.04	24.50	1.22	8.14	31.73	30.04	8.58
PDXK	IPI00013004	Pyridoxal kinase	0.00	37.86	3.75	41.83	1.61	18.67	22.09	30.11	4.95
PHKA1	IPI00216725	Phosphorylase b kinase regulatory subunit alpha, skeletal muscle isoform	0.00	nd	nd	58.10	15.94	16.71	16.35	30.39	9.80
BMP2K	IPI00337426	BMP-2-inducible protein kinase	0.00	36.48	20.57	39.09	14.21	18.63	32.87	31.77	3.95
MAP4K4	IPI00006752	Mitogen-activated protein kinase kinase kinase kinase 4	0.00	nd	nd	33.02	1.80	10.19	53.08	32.10	8.76
PTK2B	IPI00029702	Protein tyrosine kinase 2 beta	0.00	58.01	0.00	nd	nd	6.64	nd	32.33	12.84
MAPK1	IPI00003479	Mitogen-activated protein kinase 1	0.00	47.76	5.52	28.90	4.93	17.94	35.67	32.57	5.41
ABL2	IPI00329488	Tyrosine-protein kinase ABL2	0.00	nd	nd	59.98	0.00	33.40	4.86	32.74	11.25
PAK4	IPI00014068	Serine/threonine-protein kinase PAK 4	0.00	43.62	0.00	39.49	7.45	19.02	28.94	32.77	4.79
CHEK2	IPI00423156	Serine/threonine-protein kinase Chk2	0.00	30.85	0.00	36.48	1.28	11.73	52.10	32.79	7.22
MAP3K2	IPI00513803	Mitogen-activated protein kinase kinase kinase 2	0.00	39.09	9.49	45.43	9.50	15.05	nd	33.19	6.54
MAP2K1	IPI00219604	Dual specificity mitogen-activated protein kinase kinase 1	0.00	28.32	2.87	37.23	4.27	21.70	48.90	34.04	5.10
GSK3B	IPI00216190	Glycogen synthase kinase-3 beta	0.00	65.16	13.34	31.84	2.43	14.25	24.97	34.06	9.51
LCK	IPI00515097	Proto-oncogene tyrosine-protein kinase LCK	0.00	nd	nd	49.52	0.00	18.79	nd	34.15	7.68
DCK	IPI00020454	Deoxycytidine kinase	0.00	3.39	0.00	45.37	9.98	10.96	80.47	35.05	15.31
TNIK	IPI00514275	TRAF2 and NCK-interacting protein kinase	0.00	46.24	13.79	39.39	3.63	16.82	38.53	35.24	5.52
CSNK2B	IPI00640088	Casein kinase 2 beta	0.00	nd	nd	52.26	2.67	19.13	34.78	35.39	6.77
MAPK8	IPI00220306	Mitogen-activated protein kinase 8	0.00	69.39	0.00	19.02	0.00	18.93	nd	35.78	11.88
CSNK2A2	IPI00020602	Casein kinase II subunit alpha	0.00	nd	nd	42.80	0.86	16.81	48.09	35.90	6.84
FN3KRP	IPI00099986	Ketosamine-3-kinase	0.00	49.03	0.00	32.49	3.38	26.82	nd	36.11	4.71
RPS6KA3	IPI00020898	Ribosomal protein S6 kinase alpha-3	0.00	46.37	7.39	38.83	1.10	13.38	47.56	36.54	6.89
NME1-NME2	IPI00604590	Nucleoside diphosphate kinase	0.00	49.97	7.92	42.05	5.89	29.68	26.52	37.05	4.73
STK17A	IPI00646659	Serine/threonine-protein kinase 17A	0.00	58.93	0.00	33.06	0.47	20.53	nd	37.50	7.99
MAP4K5	IPI00294842	Mitogen-activated protein kinase kinase kinase kinase 5	0.00	33.95	10.22	49.96	10.58	15.29	54.42	38.41	7.68
SRC	IPI00328867	Proto-oncogene tyrosine-protein kinase Src	0.00	nd	nd	45.63	3.09	29.28	41.59	38.83	3.48
MAP4K3	IPI00217024	Mitogen-activated protein kinase kinase kinase kinase 3	0.00	87.49	0.00	22.57	2.32	6.96	nd	39.01	17.44
CDK7	IPI00000685	Cell division protein kinase 7	0.00	63.53	0.00	38.77	4.78	20.25	nd	40.85	8.86
RPS6KA1	IPI00477982	Uncharacterized protein RPS6KA1	0.00	67.80	21.60	33.97	5.37	10.01	52.81	41.15	10.80
GAK	IPI00298949	Cyclin G-associated kinase	0.00	52.64	0.00	44.62	3.05	18.82	49.08	41.29	6.64
CSNK2A1	IPI00016613	CSNK2A1 protein	0.00	58.30	11.77	54.65	1.91	19.89	33.45	41.57	7.86
PRKAG1	IPI00413318	5'-AMP-activated protein kinase subunit gamma-1	0.00	66.45	28.79	49.17	1.25	39.52	22.87	44.50	7.89
EPHB2	IPI00252979	Ephrin type-B receptor 2	0.00	70.92	0.00	45.70	0.86	22.94	nd	46.52	9.80
EPHB4	IPI00289342	Ephrin type-B receptor 4	0.00	82.30	0.00	nd	nd	11.53	nd	46.91	17.69
CSNK1D	IPI00011102	Casein kinase I isoform delta	0.00	89.20	28.17	37.34	8.06	15.02	nd	47.19	15.54
CSNK1A1	IPI00790374	CSNK1A1 protein	0.00	112.15	0.00	32.19	2.56	13.27	nd	52.54	21.43

Table 13 Binding results (K_d-values [µM]) for SU11248 against endogenous non-kinase targets

Symbol	Protein Name	Caki1 K_d [µM]	Caki1 SEM	Caki2 K_d [µM]	Caki2 SEM	A498 (100309) K_d [µM]	435S (111107) K_d [µM]	average K_d [µM]	average SEM
NQO2	Ribosyldihydronicotinamide dehydrogenase [quinone]	3.19	0.60	5.89	0.39	3.11	4.36	4.14	0.56
PYGM	Glycogen phosphorylase, muscle form	1.21	0.00	4.51	0.00	4.47	12.51	5.67	2.08
ACOT7	Acyl-CoA thioesterase 7	7.93	0.00	nd	nd	nd	3.49	5.71	1.11
CBR1	Carbonyl reductase [NADPH] 1	6.73	1.06	21.06	0.68	6.97	5.42	10.04	3.19
GAPDH	Glyceraldehyde-3-phosphate dehydrogenase	15.03	2.00	nd	nd	9.49	13.10	12.54	1.15
ENO1	Alpha-enolase	19.25	3.74	nd	nd	14.07	4.30	12.54	3.10
PRDX2	Peroxiredoxin-2	7.92	0.76	14.48	0.00	17.12	11.42	12.73	1.72
EEF1A2	Elongation factor 1-alpha 2	11.69	1.74	23.55	1.00	9.49	11.45	14.05	2.78
LYPLA1	Acyl-protein thioesterase 1	13.57	0.00	16.42	0.00	12.23	nd	14.07	0.87
PYGB	Glycogen phosphorylase, brain form	8.73	1.76	31.94	6.55	2.77	14.66	14.52	5.45
PHGDH	D-3-phosphoglycerate dehydrogenase	23.37	3.72	16.55	0.00	7.73	11.45	14.77	2.93
LDHA	L-lactate dehydrogenase A chain	20.06	3.30	29.79	1.96	13.21	5.21	17.07	4.52
MARS	Methionyl-tRNA synthetase, cytoplasmic	14.87	0.00	25.13	0.00	nd	11.33	17.11	2.93
ENO3	Beta-enolase	14.58	2.36	36.21	0.00	12.73	6.67	17.55	5.58
CAD	CAD protein	15.24	3.27	27.44	1.61	7.53	20.02	17.56	3.62
PPIA	Peptidyl-prolyl cis-trans isomerase A	18.44	3.64	nd	nd	23.63	11.12	17.73	2.57
ADSL	Adenylosuccinate lyase	21.40	3.34	14.75	0.00	nd	nd	18.07	1.66
GFPT1	Glucosamine--fructose-6-phosphate aminotransferase [isomerizing] 1	8.45	0.00	35.11	3.33	11.66	nd	18.41	5.94
TUBB	Tubulin beta chain	19.93	2.51	30.17	3.49	8.97	15.17	18.56	3.87
AHCY	Adenosylhomocysteinase	22.12	2.79	33.67	1.48	8.74	10.34	18.72	5.03
IMPDH2	Inosine-5'-monophosphate dehydrogenase 2	11.98	0.00	31.83	10.07	nd	13.23	19.01	4.54
MAT2A	S-adenosylmethionine synthetase isoform type-2	13.86	1.80	37.04	6.74	8.04	17.17	19.03	5.45
DDX3X	ATP-dependent RNA helicase DDX3X	18.15	2.37	20.17	0.00	nd	nd	19.16	0.50
PRDX4	Peroxiredoxin-4	13.92	1.67	26.96	0.29	nd	16.63	19.17	2.81
PRDX3	Thioredoxin-dependent peroxide reductase, mitochondrial precursor	17.22	4.25	36.27	0.33	9.13	15.53	19.54	5.06
UBE2I	Ubiquitin carrier protein	5.79	1.79	35.29	0.00	nd	nd	20.54	7.37
LDHB	L-lactate dehydrogenase B chain	17.22	1.41	45.03	13.74	14.81	5.83	20.72	7.33
NQO1	NAD(P)H dehydrogenase [quinone] 1	32.24	1.86	26.92	3.75	11.75	17.70	22.16	3.97
PAICS	Multifunctional protein ADE2	15.19	1.16	44.26	6.29	9.78	20.18	22.35	6.59
GLS	Glutaminase kidney isoform, mitochondrial precursor	24.45	5.18	32.37	4.44	10.47	nd	22.43	4.53
XRCC6	ATP-dependent DNA helicase 2 subunit 1	29.26	5.39	35.73	0.00	15.24	11.91	23.03	4.90
DUSP12	Dual specificity protein phosphatase 12	23.63	0.00	32.36	5.13	13.62	nd	23.20	3.83
ALDH7A1	Alpha-aminoadipic semialdehyde dehydrogenase	24.07	8.92	25.58	0.00	21.14	nd	23.60	0.92
CS	Citrate synthase, mitochondrial precursor	24.08	3.39	nd	nd	nd	nd	24.08	3.39
KIAA0828	Putative adenosylhomocysteinase 3	19.72	0.00	30.58	0.00	nd	nd	25.15	2.72
ARF3	ADP-ribosylation factor 3	21.12	3.62	50.50	13.36	16.40	15.14	25.79	7.22
TUBA1A	Tubulin alpha-1A chain	20.31	2.67	51.47	8.96	17.51	13.90	25.80	7.50
NPEPPS	Puromycin-sensitive aminopeptidase	17.99	3.57	34.36	0.00	nd	nd	26.18	4.09
PRDX6	Peroxiredoxin-6	36.19	16.37	44.60	9.75	13.91	10.74	26.36	7.20
DARS	Aspartyl-tRNA synthetase, cytoplasmic	31.77	9.25	37.01	2.75	14.19	23.72	26.68	4.31
ARF4	ADP-ribosylation factor 4	33.81	6.45	38.35	0.04	12.12	23.60	26.97	5.05
ALDH9A1	4-trimethylaminobutyraldehyde dehydrogenase	35.04	3.41	34.05	9.86	12.74	nd	27.28	5.14
DHX15	Putative pre-mRNA-splicing factor ATP-dependent RNA helicase DHX15	32.85	5.67	36.57	0.97	15.85	24.16	27.36	4.01
VARS	Valyl-tRNA synthetase	45.11	17.49	29.04	1.66	19.57	20.02	28.44	5.17
TUBA1C	Tubulin alpha-1C chain	26.41	3.80	60.62	6.06	15.37	13.78	29.05	9.43
TUBA4A	Tubulin alpha-4A chain	31.25	7.62	53.75	2.73	18.93	13.41	29.34	7.75
ATP1A1	Sodium/potassium-transporting ATPase subunit alpha-1 precursor	31.72	10.59	43.78	0.00	nd	13.20	29.57	6.29
PSMC1	26S protease regulatory subunit 4	13.68	0.00	45.78	0.00	nd	nd	29.73	8.02
HSPA8	Heat shock cognate 71 kDa protein	40.19	11.14	48.72	9.50	17.47	16.63	30.75	7.02
TXN	Thioredoxin	3.05	0.02	85.67	41.67	17.08	18.25	31.01	16.06
EEF1A1	Elongation factor 1-alpha 1	16.49	1.60	78.14	29.26	17.52	13.59	31.44	13.50
GLUD1	Glutamate dehydrogenase 1, mitochondrial precursor	22.52	2.42	40.36	3.32	nd	nd	31.44	4.46
RAN	GTP-binding nuclear protein Ran	17.27	1.83	82.95	22.54	17.17	9.52	31.73	14.87
MDH2	Malate dehydrogenase, mitochondrial precursor	33.96	6.61	84.58	0.00	7.82	6.75	33.28	15.78
GNB2	Guanine nucleotide-binding protein G(I)/G(S)/G(T) subunit beta-2	22.08	5.97	45.62	0.00	nd	nd	33.85	5.89
YWHAZ	14-3-3 protein zeta/delta	27.08	3.52	85.71	28.84	15.11	8.89	34.19	15.23
DDX17	Probable ATP-dependent RNA helicase DDX17	17.25	4.04	41.42	0.00	nd	50.79	36.49	7.07
PTGES3	Prostaglandin E synthase 3	29.21	1.54	57.79	7.30	24.37	nd	37.12	7.37
CCT8	T-complex protein 1 subunit theta	25.50	2.14	50.43	10.33	nd	nd	37.97	6.23

Beside kinase targets very interesting non-kinase targets such as Ribosyldihydronicotinamide dehydrogenase (NQO2), NAD(P)H menadione oxidoreductase 1 (NQO1), Alpha-enolase (ENO1), Beta-Enolase (ENO3), Acyl-CoA thioester hydrolase (ACOT7) as well as dehydrogenases such as ALDH9A1, ALDH1A1 or Glycogen phosphorylases including PYGM and PYGB, all involved in key metabolic pathways like energy utilization, glycolysis and fatty acid metabolism, could be identified as high affinity SU11248 targets.

In summary, quantitative K_d-values show a broad target spectrum similarly inhibited by SU11248. High affinity targets identified with the applied semi-quantitative approach in a broad panel of cancer cell lines and tumor samples could be confirmed by the quantitative method and low molecular K_d-values were calculated for those targets.

The good correlation of semi-quantitative and quantitative target-affinities in a broad spectrum of different cancer cell lines and tumor samples confirms the significance and utility of the semi-quantitative method. The advantage of this semi-quantitative method is that no time-consuming cell labelling is necessary, it can be used in a high throughput manner and is suitable for tumor samples which cannot be metabolically labelled.

Taken together, both methods in combination are good tools to comprehensively reveal drug-target interaction profiles and target affinities of SU11248 directly from cells. This concept cannot only be used for the small-molecule kinase inhibitor SU11248, as described here, but also for other inhibitors in general.

Moreover, to rank and prioritize targets by their drug affinities and the comparison of drug target affinities in cancer cell lines and primary tumor samples helps in the discovery of *in vivo* relevant sites of drug action. It could be shown that out of originally 313 qualitatively detected putative cellular SU11248 kinase targets, a panel of only 35- 40 kinases had similar high binding affinities in cancer cell lines and tumors. These targets are more likely to be important during patient treatment. Their functional annotation showed prominent implications in many different cancer types, all being reactive to SU11248 treatment as shown in the performed cell-based sensitivity screen in this study as well as ongoing clinical trials and already approved applications such as liver, breast, brain, pancreas and mRCC as well as GIST. The target annotation is shown in Table 14.

Table 14 KEGG annotation of high affinity SU11248 targets

cancer types	fold enrichment	p-Value	Benjamini
Glioma	7.52	0.00	0.00
Non-small cell lung cancer	5.79	0.00	0.00
Thyroid cancer	5.57	0.01	0.07
Bladder cancer	5.27	0.00	0.02
Prostate cancer	4.84	0.00	0.00
Melanoma	4.80	0.00	0.00
Acute myeloid leukemia	4.38	0.00	0.02
Chronic myeloid leukemia	4.07	0.00	0.01
Type II diabetes mellitus	4.01	0.02	0.09
Endometrial cancer	3.61	0.02	0.12
Renal cell carcinoma	3.59	0.01	0.04
Pancreatic cancer	3.30	0.01	0.07
Colorectal cancer	3.19	0.01	0.05

Interestingly, high affinity SU11248 targets are not only key proteins in cancer development and progression but are also implicated in other diseases such as Type II Diabetes.

7.5 *In vitro* binding studies and cellular kinase assays

To validate the MS binding data, the interaction of several identified target proteins with SU11248 was confirmed by western blotting. *In vitro*-association experiments were performed. Total cell lysates from Hs578T, MDA-MB-231, MDA-MB-435S, U1242 and A590 cells were subjected to *in vitro*-association with either control or SU11248 matrix beads, immunoblotted and protein detection confirmed specific binding of AURKA, PAK4, PDGFRb, GSK3b, RSK1, RON, AXL and FAK to the SU11248 matrix in a ligand concentration-dependent manner (Figure 50). No binding to control beads was observed.

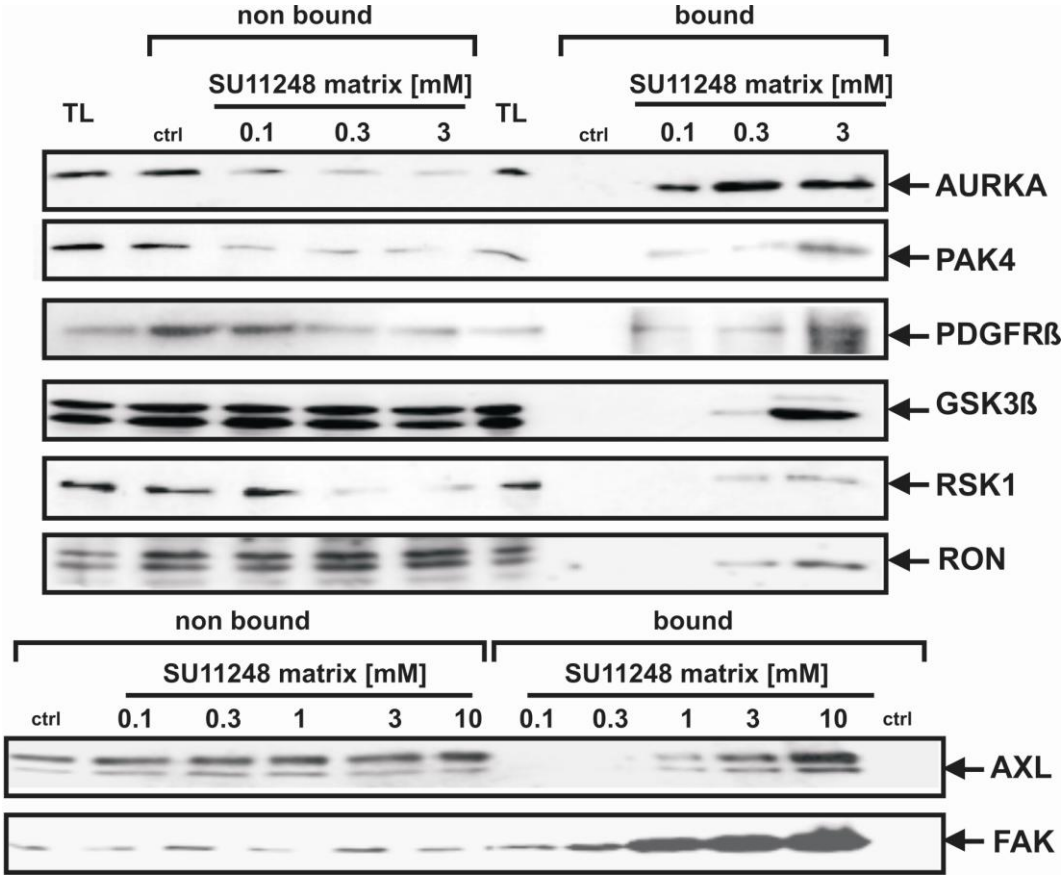

Figure 50 *in vitro*-association experiments confirmed specific SU11248 interaction with newly identified kinase targets.
Total cell lysates from Hs578T, MDA-MB-231, MDA-MB-435S, U1242 and A590 cells were subjected to *in vitr*- association with either control or SU11248 matrix beads of increasing concentrations, immunobloted and protein detection confirmed specific binding of AURKA, PAK4, PDGFRb, GSK3b, RSK1, RON, AXL and FAK to the SU11248 matrix in a ligand concentration-dependent manner. In the non bound fractions target depletion was observed. There was no protein binding to the control-matrix.

Furthermore, cellular kinase assays in the presence of different inhibitor concentrations were performed to determine the SU11248 concentrations required for half maximal kinase inhibition of already known and newly identified receptor tyrosine kinase targets (Figure 51).

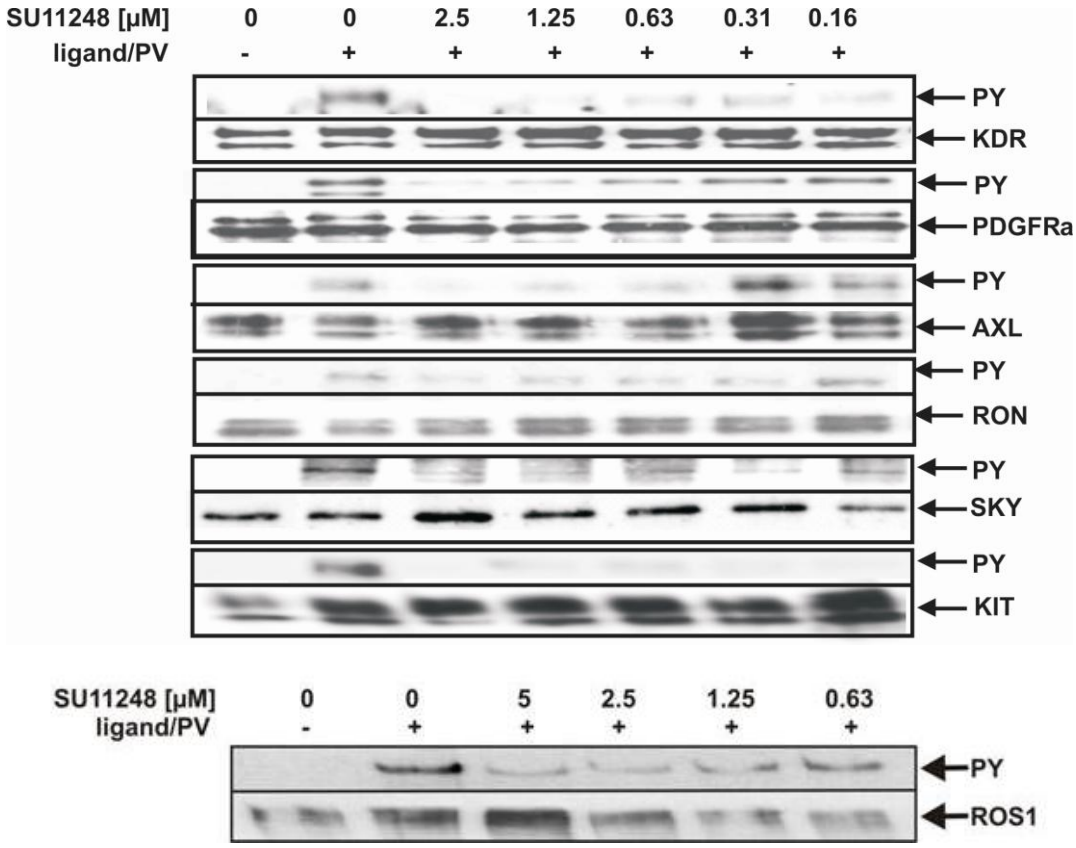

Figure 51 Cellular kinase assays of known and newly identified SU11248 receptor tyrosine kinase targets.

Cancer cells were seeded in 6-well cell culture plates with 80 % confluency, starved for 24h and incubated with increasing SU11248 concentrations for 2h. Control cells received the drug vehicle DMSO. After ligand or pervanadate stimulation for 5min, cells were lysed, subjected to immunoprecipitation with target-antibodies and western blotted. Blots were immunostained with an anti-phosphotyrosine antibody, then stripped and reprobed with specific antibodies for KIT, PDGFRa, AXL, RON, SKY, VEGFR2 and ROS1. Receptor tyrosine autophosphorylation was inhibited in a dose-dependent manner by SU11248.

All tested kinases were potently inhibited by low micromolar SU11248 concentrations. Dose-inhibition curves are shown for two RTKs in Figure 52. IC_{50}-values are shown in Table 15. Half maximal inhibition of newly identified SU11248 targets like ROS1, AXL and RON occurred at SU11248 concentrations similar to those measured for known targets as PDGFRa and PDGFRb. Furthermore, the SU11248 efficacy against the RTK SKY was tested because it belongs to the same kinase family as the receptor tyrosine kinase AXL which is strongly inhibited by SU11248 (IC_{50}= 0.43 µM). The data show that SU11248 also potently inhibits ligand stimulated SKY autophosphorylation on tyrosine residues (IC_{50}= 0.16 µM).

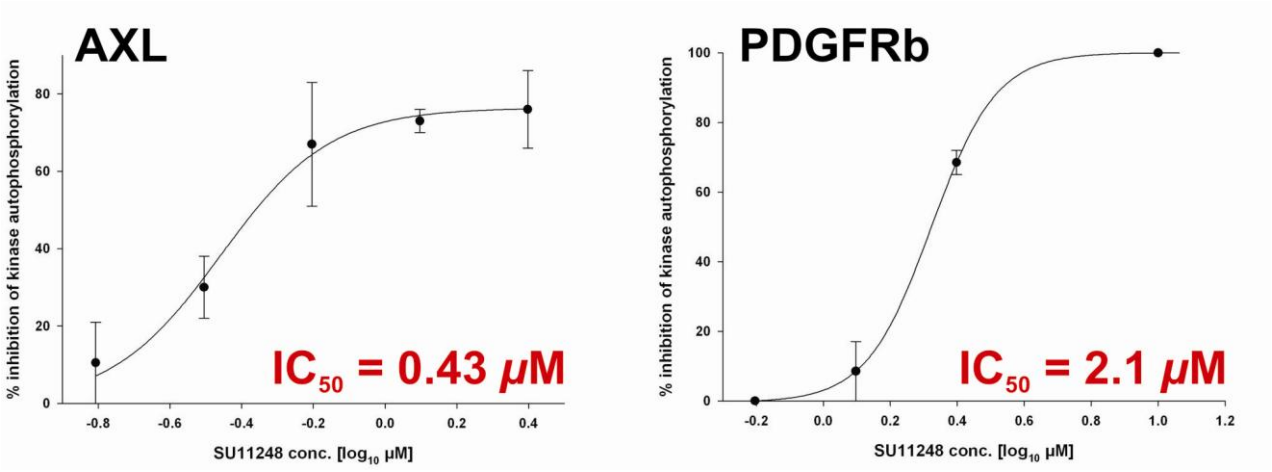

Figure 52 Dose-inhibition curves of the receptor tyrosine kinases AXL and PDGFRb against SU11248.
Cellular kinase assays were quantified with the *AIDAImageAnalyzer* software and IC_{50}-values calculated in *SigmaPlot 10.0* using a simple-ligand binding sigmoidal-dose-response curve fitting algorithm on log-transformed data.

Table 15 IC_{50}-values of receptor tyrosine kinase autophosphorylation inhibition by SU11248

RTK	IC_{50} value [μ M]
PDGFRa	0.11
KDR	0.12
SKY	0.16
KIT	< 0.16
RON	0.31
AXL	0.43
PDGFRb	2.09
ROS1	2.38

In summary, the results obtained from *in vitro* binding studies and cellular kinase assays could confirm the specific binding and inhibition of already known and new SU11248 kinase targets identified by affinity chromatography and mass spectrometry.

7.6 Quantification of relative target amount binding to SU11248 in sensitive and insensitive cancer cell lines

After globally profiling SU11248 targets and their affinities in different cancer cell lines and mRCC tumor samples, the question rose whether there are binding differences of interaction partners, differences in the target expression levels and target affinity patterns between SU11248 sensitive and insensitive cancer cell lines. To find functionally relevant targets responsible for SU11248 action and efficacy *in vitro* the comparison of binding differences between sensitive and less sensitive cell lines is important. Functionally relevant interaction partners should be over-represented in SU11248 responsive cancer cell lines. Therefore, two cell line categories were classified based on their SU11248 sensitivity observed in the cellular toxicity

screen. The subdivision is shown in Figure 53. The median SU11248 responsiveness was taken for normalization and cell line sensitivity is shown in fold-change in respect to the median.

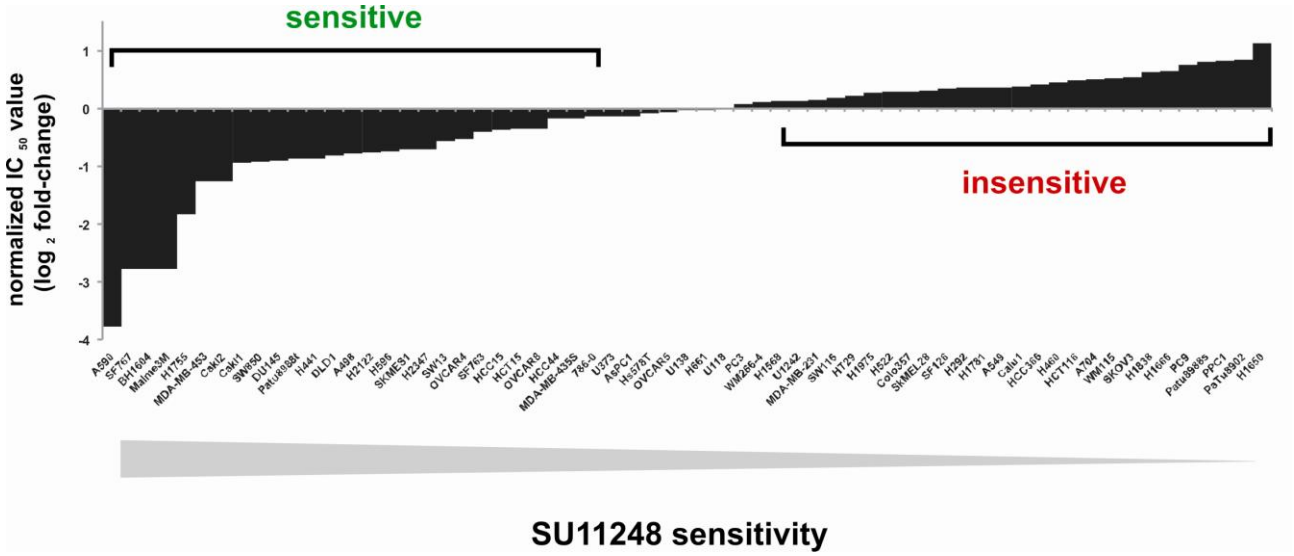

Figure 53 Cancer cell line classification in respect to SU11248 sensitivity.
Two cell line categories, sensitive and insensitive, respectively, were classified based on their SU11248 responsiveness observed in the cellular toxicity screen. The median SU11248 activity (IC_{50}-values of cell viability inhibition) was taken for normalization and cell line sensitivity is shown in fold-change (log2) to the median.

To analyze and quantify target binding differences in cancer cell lines showing different SU11248 responsiveness a quantitative chemical proteomics approach was used. A panel of sensitive and insensitive cancer cell lines was metabolically labelled with either normal arginine and lysine (Arg^0/Lys^0) or combinations of isotopic variants of the two amino acids (Arg^6/Lys^4, Arg^{10}/Lys^8) and subjected to *in vitro* binding experiments with a SU11248 matrix. To quantify the target amounts being retained on the SU11248 matrix in each cell line, a lysate pool of all used cell lines was taken as an internal quantification reference. Cell line specific target binding amounts were quantified in relation to the mean target amount captured on the SU11248 matrix. Identification and quantification of SU11248 binding partners was done by mass-spectrometry and the MaxQuant software. The workflow is shown in Figure 54.

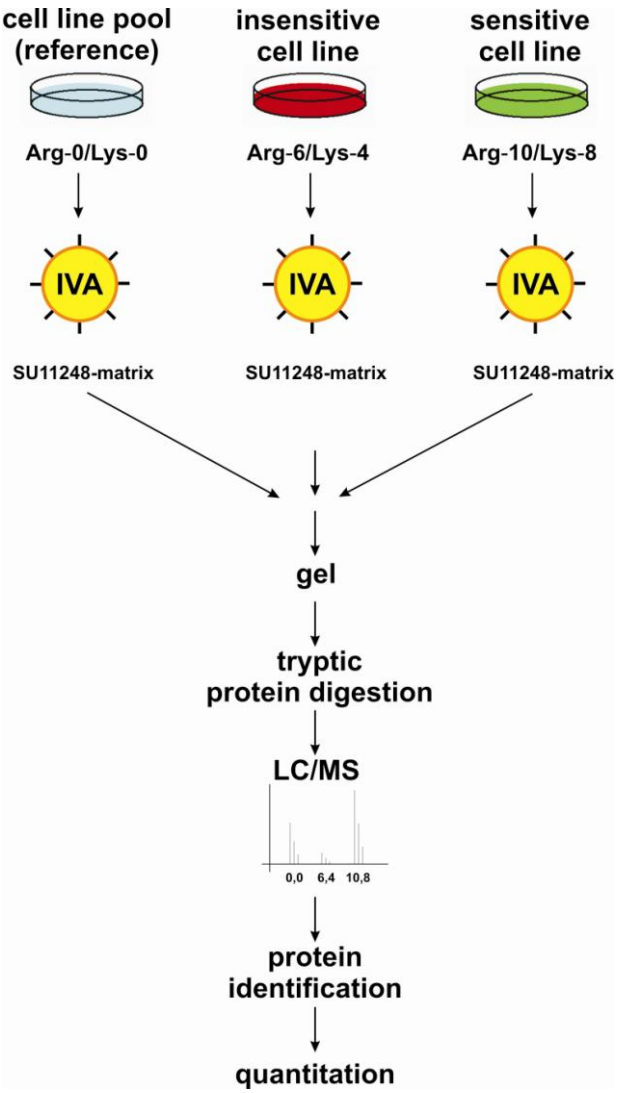

Figure 54 Workflow of target binding quantification in SU11248 sensitive and insensitive cancer cell lines.
To analyze and quantify target binding differences in cancer cell lines showing different SU11248 responsiveness a quantitative chemical proteomics approach was used. A panel of sensitive and insensitive caner cell lines was metabolically labelled with either normal arginine and lysine (Arg^0/Lys^0) or combinations of isotopic variants of the two amino acids (Arg^6/Lys^4, Arg^{10}/Lys^8) and subjected to *in vitro* binding experiments with a SU11248 matrix. Elution fractions were pooled, proteins separated by gel-electrophoresis, trypsin-digested and analyzed by LC/MS. To quantify the target amounts being retained on the SU11248 matrix in each cell line, a lysate pool of all used cell lines was taken as an internal quantification reference. Cell line specific target binding amounts were quantified in relation to the mean target amount captured on the SU11248 matrix (cell line reference pool). Identification and quantification of SU11248 binding partners was done by mass-spectrometry and the MaxQuant software.

Relative target binding differences between these two cell systems might reveal interaction patterns and target clusters being highly relevant for SU11248 efficacy in tumors in general. Targets observed and over-represented in sensitive cancer cell lines are more likely important cellular sites of drug action than interaction partners detected in all cell lines. They may function as prediction clusters.

The relative kinase binding to the SU11248 matrix in sensitive and insensitive cell lines is shown as the mean binding (amount of protein captured on the matrix) in each group normalized to the internal reference-cell line pool.

Figure 55 shows kinases being highly enriched in sensitive cell lines based on a SOTA-analysis of the binding data.

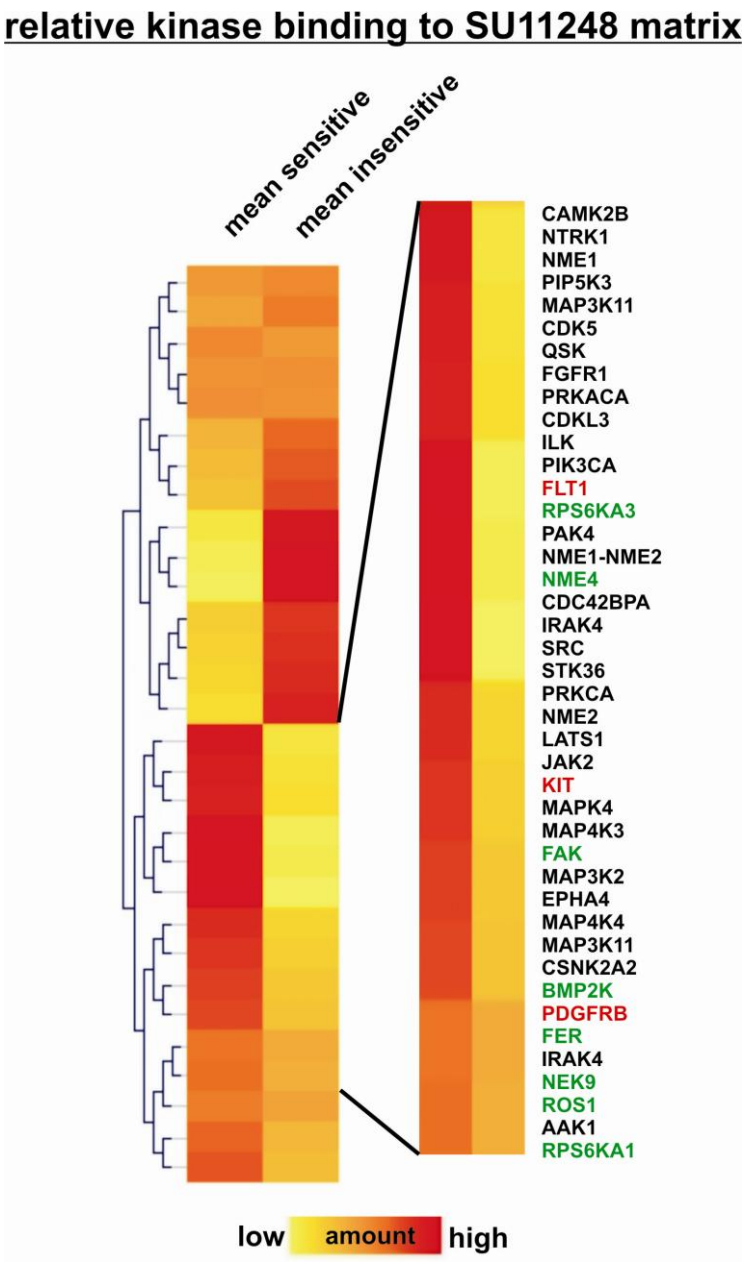

Figure 55 SOTA cluster of relative kinase target protein amounts binding to SU11248 in sensitive and insensitive cancer cell lines.
Based on the relative protein amount retained on the SU11248 matrix in either SU11248 sensitive or insensitive cancer cell lines kinase targets were clustered using a self-organizing tree algorithm (SOTA). The average of binding amounts in responsive compared to less responsive cell lines was used as the basis for analysis. All protein amounts were quantified to an internal reference reflecting the average amount of a particular target being captured on the matrix. Kinases enriched in sensitive cell lines are highlighted and known targets are marked in red. High affinity interaction partners also detected in the target-profiling screen are indicated in green.

Enriched kinases might be responsible for the high SU11248 susceptibility of sensitive cancer cell lines. Interestingly, targets which are enriched in almost all sensitive cell lines like NME1, NME4, ROS1,

PDGFRb, FER, NEK9, BMP2K, FAK, IRAK4, AAK1 and CamKinases (CAMK2B) were mostly high affinity binding partners of SU11248. In summary, known and newly identified high affinity targets of SU11248 are over-represented in sensitive cancer cell lines. They might be considered as targets of a signature of sensitivity.

7.7 Gene expression analysis of SU11248 sensitive and less responsive cancer cell lines of different cancer types

Beside the expression of direct drug targets the genetic background of a cell influences its sensitivity towards a small-molecule inhibitor. To elucidate expression differences between SU11248 sensitive and insensitive cancer cell lines, in-house macro-arrays were performed. The same two cell line categories as classified in section 7.6 were used for the genome analysis. Differences in gene expression levels between these two cell line groups may reveal potential mechanisms of resistance and prediction markers for SU11248 sensitivity.

Moreover, to obtain a comprehensive picture of SU11248 action, gene expression changes upon inhibitor treatment were determined.

The used Macro-Arrays are filter-based and were produced in-house. The hybridization filters contained plasmids covering the human kinome, almost all phosphatases and selected cancer related genes such as growth factors, metalloproteinases, differentiation marker and transcription factors.

cDNA probes were radioactive labelled and hybridized to the filter. Spot analysis and quantification was done using ArrayVision from GE Healthcare. The median expression levels of a particular gene in SU11248 sensitive and insensitive cell lines were compared and divided into two groups, namely highly over-represented in responsive or less responsive cell lines, respectively.

Over-represented genes in SU11248 insensitive cancer cell lines are listed in Table 16.

Table 16 Overexpressed genes in SU11248 insensitive cancer cell lines of different tissue origins.

gene symbol	gene name	NM annotation	median expression sensitive cell lines	median expression insensitive cell lines	fold-enrichment sensitive cell lines
CDK8	Cyclin-dependent kinase 8	NM_001260	0.65	1.01	0.6
CCL7	Chemokine (C-C motif) ligand 7	NM_006273	0.38	0.59	0.6
ROR2	Receptor tyrosine kinase-like orphan receptor 2	NM_004560	0.47	0.73	0.6
CCNC	Cyclin C	NM_001013399	2.63	4.08	0.6
TAK1	Mitogen-activated protein kinase kinase kinase 7	NM_003188	1.65	2.57	0.6
MMP14	Matrix metallopeptidase 14 (membrane-inserted)	NM_004995	0.85	1.33	0.6
MAP2K6	Mitogen-activated protein kinase kinase 6	NM_002758	1.25	1.96	0.6
EPHB1	EPH receptor B1	NM_004441	1.55	2.44	0.6
SGK1	Serum/glucocorticoid regulated kinase	NM_005627	16.99	26.86	0.6
PP1-Calpha	Protein phosphatase 1, catalytic subunit, alpha isoform	NM_002708	19.92	31.58	0.6
MMP7	Matrix metallopeptidase 7 (matrilysin, uterine)	NM_002423	3.66	5.81	0.6
ENPP1	Ectonucleotide pyrophosphatase/phosphodiesterase 1	NM_006208	0.99	1.58	0.6
AMHR2	Anti-Mullerian hormone receptor, type II	NM_020547	0.93	1.49	0.6
CCK-4	PTK7 protein tyrosine kinase 7	NM_152880	9.74	15.63	0.6
MEF2C	Myocyte enhancer factor 2C	NM_002397	2.33	3.76	0.6
DAPK3	Death-associated protein kinase 3	NM_001348	0.40	0.65	0.6
Calla	Membrane metallo-endopeptidase	NM_000902	2.54	4.14	0.6
PRKACA	Protein kinase, cAMP-dependent, catalytic, alpha	NM_002730	1.33	2.19	0.6
VEGF	Neuropilin 1	NM_003873	1.41	2.35	0.6
CCNB2	Cyclin B2	NM_004701	16.07	26.87	0.6
GUCY2C	Guanylate cyclase 2C (heat stable enterotoxin receptor)	NM_004963	1.10	1.85	0.6
PRKCB1	Protein kinase C, beta 1	NM_212535	2.54	4.31	0.6
EPHA8	EPH receptor A8	NM_020526	0.87	1.47	0.6
ACTR2B	Activin A receptor, type IIB	NM_001106	0.98	1.66	0.6
EDG4	Endothelial differentiation, lysophosphatidic acid G-protein-coupled receptor, 4	NM_004720	1.27	2.17	0.6
p91/ISGF-3	Signal transducer and activator of transcription 1, 91kDa	NM_007315	3.37	5.75	0.6
RBL1	Retinoblastoma-like 1 (p107)	NM_002895	2.00	3.41	0.6
E2F6	E2F transcription factor 6	NM_198256	1.06	1.84	0.6
EPHA1	EPH receptor A1	NM_005232	0.96	1.70	0.6
CCNG1	Cyclin G1	NM_004060	2.22	3.90	0.6
EPHA2	EPH receptor A2	NM_004431	20.37	35.82	0.6
EDG7	Endothelial differentiation, lysophosphatidic acid G-protein-coupled receptor, 7	NM_012152	0.48	0.85	0.6
WEE1	WEE1	NM_003390	1.08	1.91	0.6
TRRAP	Transformation/transcription domain-associated protein	NM_003496	8.58	15.23	0.6
STK19	Serine/threonine kinase 19	NM_004197	2.30	4.11	0.6
AAK1	AP2 associated kinase 1	NM_014911	3.44	6.17	0.6
EDG6	Endothelial differentiation, lysophosphatidic acid G-protein-coupled receptor, 6	NM_003775	0.57	1.02	0.6
CCR7	Chemokine (C-C motif) receptor 7	NM_001838	1.31	2.37	0.6
CCND3	Cyclin D3	NM_001760	4.40	7.94	0.6
PDGFB	Platelet-derived growth factor beta polypeptide	NM_033016	0.62	1.12	0.6
ARG1	Arginase, liver	NM_000045	1.81	3.29	0.6
TLK1	Tousled-like kinase 1	NM_012290	0.64	1.17	0.5
BRS3	Bombesin-like receptor 3	NM_001727	0.29	0.53	0.5
ADCK4	AarF domain containing kinase 4	NM_024876	0.77	1.43	0.5
SIRPalpha1	Signal-regulatory protein alpha	NM_001040022	2.00	3.70	0.5
mlkl	Mixed lineage kinase domain-like	NM_152649	0.70	1.29	0.5
p19	Cyclin-dependent kinase inhibitor 2D (p19, inhibits CDK4)	NM_001800	1.63	3.07	0.5
SIRPbeta 1	Signal-regulatory protein beta 1	NM_001083910	1.10	2.07	0.5
MMP15	Matrix metallopeptidase 15 (membrane-inserted)	NM_002428	1.64	3.14	0.5
mFurin	Furin (paired basic amino acid cleaving enzyme)	X54056	0.60	1.16	0.5
CDKN1C	Cyclin-dependent kinase inhibitor 1C (p57, Kip2)	NM_000076	0.45	0.88	0.5
PRKAR2A	Protein kinase, cAMP-dependent, regulatory, type II, alpha	NM_004157	1.37	2.71	0.5
Mnk2	MAP kinase-interacting serine/threonine kinase 2	NM_021462	1.50	2.96	0.5
HDAC6	Histone deacetylase 6	NM_006044	1.15	2.29	0.5
PRKCE	Protein kinase C, epsilon	NM_005400	1.17	2.34	0.5
YES1	V-yes-1 Yamaguchi sarcoma viral oncogene homolog 1	NM_005433	6.25	12.58	0.5
LMR3	Lemur tyrosine kinase 3	NM_001080434	0.82	1.66	0.5
CDH2	Cadherin 2, type 1, N-cadherin (neuronal)	NM_001792	0.84	1.72	0.5
ADAM8	ADAM metallopeptidase domain 8	NM_001109	2.20	4.50	0.5
CCND1	Cyclin D1	NM_053056	5.46	11.29	0.5
INS	Insulin	NM_000207	9.53	20.51	0.5
AREG	Amphiregulin (schwannoma-derived growth factor)	NM_001657	5.24	11.43	0.5
CCRK	Cell cycle related kinase	NM_012119	1.09	2.44	0.4
TSSK6	Testis-specific serine kinase 6	NM_032037	2.02	4.56	0.4
MAST1	Microtubule associated serine/threonine kinase 1	NM_014975	0.60	1.36	0.4
MMP13	Matrix metallopeptidase 13 (collagenase 3)	NM_002427	1.35	3.20	0.4
MMP10	Matrix metallopeptidase 10 (stromelysin 2)	NM_002425	1.43	3.55	0.4
E2F3	E2F transcription factor 3	NM_001949	0.54	1.39	0.4
ERK2	Mitogen activated protein kinase 1	NM_011949	0.66	1.68	0.4
MPSK-1	Serine/threonine kinase 16	NM_003691	0.72	1.84	0.4
PYST1	Dual specificity phosphatase 6	NM_001946	5.25	13.61	0.4
GRPR	Gastrin-releasing peptide receptor	NM_005314	0.43	1.14	0.4
CXCR4	Chemokine (C-X-C motif) receptor 4	NM_001008540	1.47	3.93	0.4
CCND2	Cyclin D2	NM_001759	0.73	1.98	0.4
ADAM20	ADAM metallopeptidase domain 20	NM_003814	0.40	1.14	0.4
TLK2	Tousled-like kinase 2	NM_006852	0.46	1.34	0.3
VCAM	Vascular cell adhesion molecule 1	NM_001078	14.86	44.59	0.3
CCNE2	Cyclin E2	NM_057735	0.22	0.65	0.3
TGFR-2	Transforming growth factor, beta receptor II (70/80kDa)	NM_003242	0.27	0.84	0.3
IL13	Interleukin 13	NM_002188	0.19	0.66	0.3
UHMK1	U2AF homology motif (UHM) kinase 1	NM_175866	0.52	1.91	0.3
MAP3K5	Mitogen-activated protein kinase kinase kinase 5	NM_005923	0.18	0.65	0.3
PRKAR1A	Protein kinase, cAMP-dependent, regulatory, type I, alpha	NM_002734	0.18	0.69	0.3
MAPK13	Mitogen-activated protein kinase 13	NM_002754	1.01	4.13	0.2
MMP8	Matrix metallopeptidase 8 (neutrophil collagenase)	NM_002424	0.35	1.57	0.2
AREG	Amphiregulin (schwannoma-derived growth factor)	NM_001657	10.50	51.74	0.2
HCK	Hemopoietic cell kinase	NM_002110	22.14	206.86	0.1

Insensitive cancer cell lines towards SU11248 expressed higher levels of matrix-metalloproteinases (MMPs) and receptor ligands such as VEGF, PDGF, IL13 and amphiregulin compared to SU11248 sensitive cell lines. In addition, three members of the endothelial differentiation lysophosphatidic acid G-protein-coupled receptor family as well as Ephrin receptors were identified being over-represented in less responsive cells. An overview of over- and under-represented genes is shown in Figure 56.

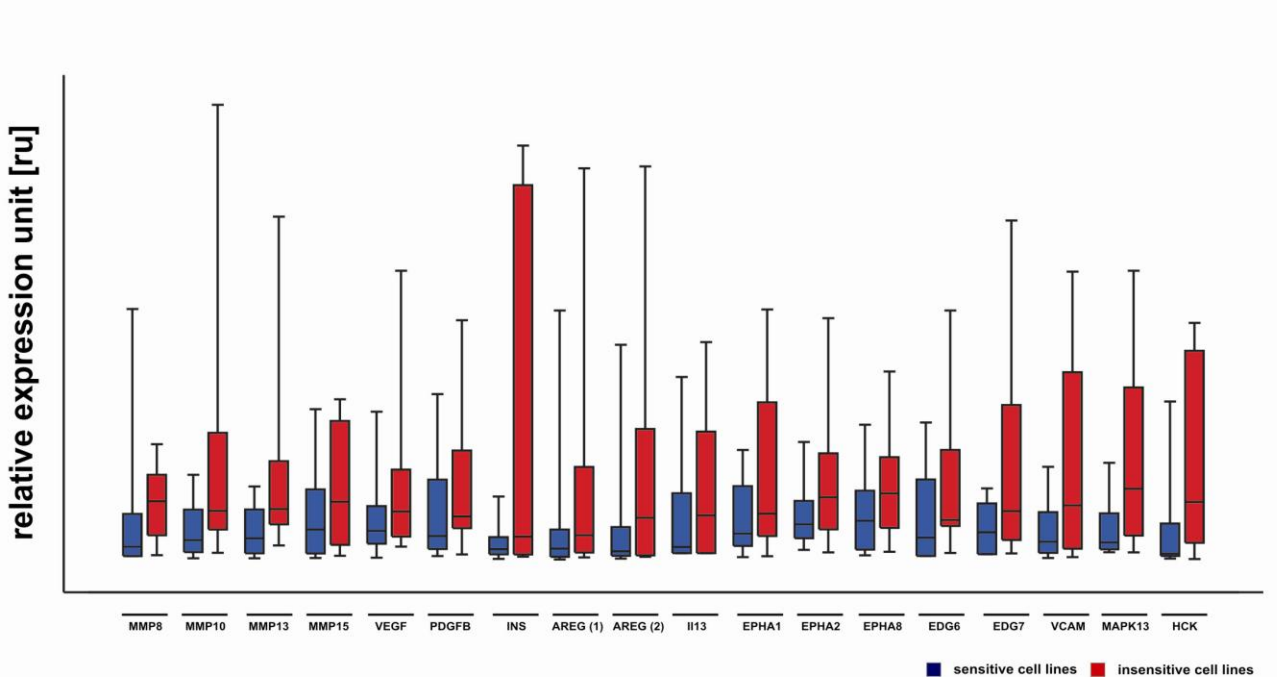

Figure 56 Differential expressed genes in SU11248 sensitive and insensitive cancer cell lines.
Expression-data obtained from in-house macro-arrays are shown for genes being overexpressed in SU11248 insensitive cancer cell lines marked in red. Genes are sorted by their function and protein family belonging. Box Plots show the 5^{th}/95^{th} percentile.

In the past, up-regulation of MMPs and high levels of receptor ligands could be shown to determine a mechanism of drug resistance in cancer cells in the sense of apoptosis-resistance and autocrine growth stimulation (Ansell et al., 2009; Mitsiades et al., 2001; Reckamp et al., 2008).

Based on the finding that SU11248 is able to induce mesenchymal-to epithelial transition (MET) in cancer cells as shown in the functional screening in section 7.1.4, the special focus was on the expression levels of the two cell-markers Vimentin for mesenchymal-like and E-cadherin for epithelial-like cells in SU11248 sensitive and insensitive cell lines. Interestingly, all sensitive cell lines such as A590, Caki1, Caki2, A498, Hs578T, MDA-MB-231 and MDA-MB-435S expressed high levels of Vimentin and no E-cadherin and *vice versa*. There was almost no expression of Vimentin observed in the insensitive cell lines such as HT29, HCT116, AsPc1 and PaTu but high levels of E-cadherin (Figure 57 A). The expression differences could be confirmed by protein expression analysis (Figure 57 B).

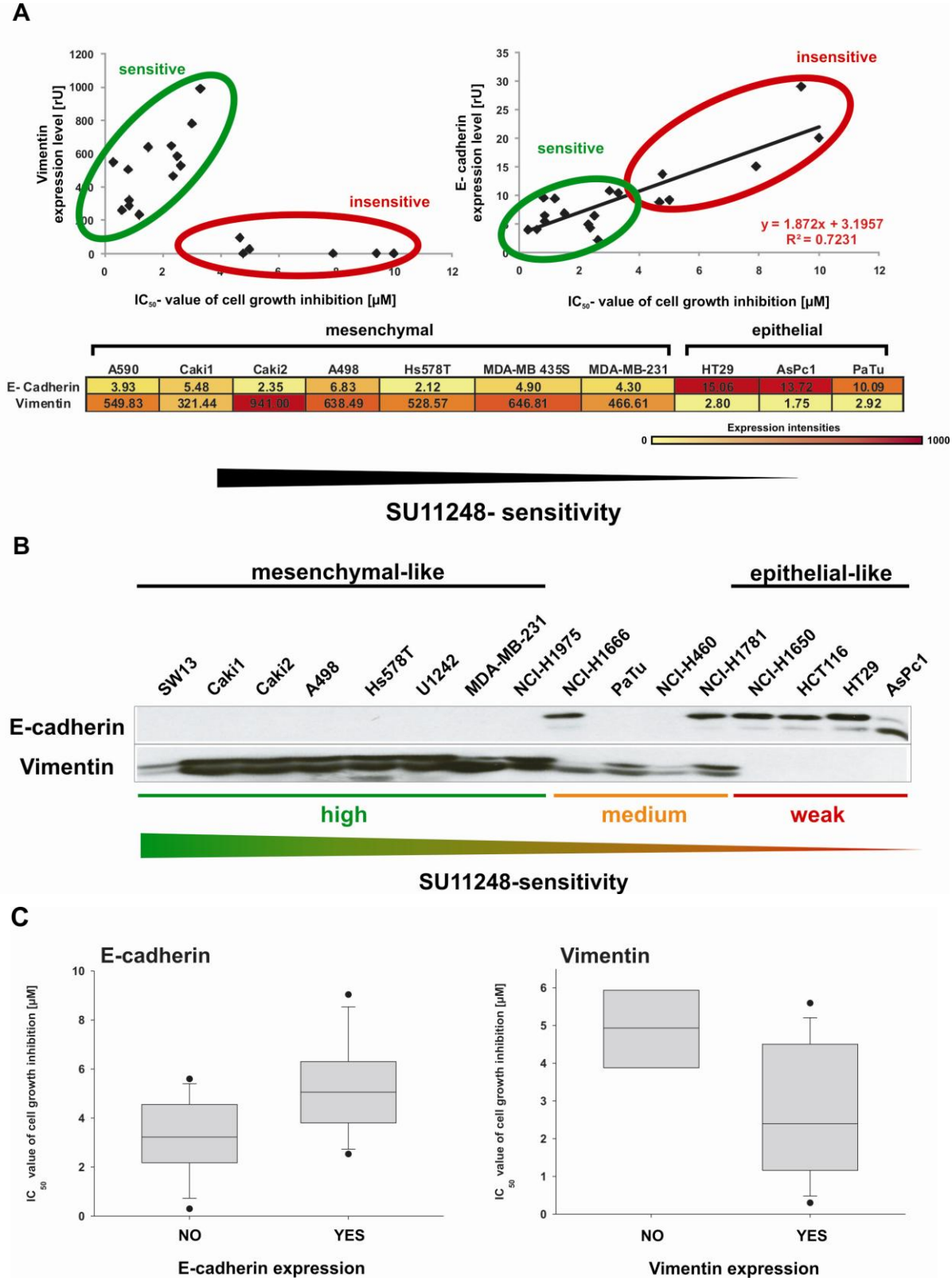

Figure 57 Expression of the mesenchymal-cell-marker Vimentin and the epithelial-cell-marker E-cadherin in SU11248 sensitive and insensitive cancer cell lines of different tissue origins.
The expression level of Vimentin and E-cadherin was correlated to SU11248 sensitivity. In A) gene expression data are compared and correlated to cellular IC_{50}-values of cell growth inhibition induced by SU11248. In B) protein expression was analyzed by western blotting with specific antibodies against E-cadherin and Vimentin. Cancer cell lines are sorted by SU11248 sensitivity. In C) the protein expression of E-cadherin and Vimentin quantified by western blotting was correlated to cellular IC_{50}-values of SU11248 cell growth inhibition and is plotted in a Box-Plot using SigmaPlot 10.0.

These data strongly indicated that the state of a cell, namely mesenchymal- or epithelial-like, is responsible for the SU11248 activity in those cell systems. In summary, mesenchymal-like more aggressive cell lines are highly responsive to SU11248 treatment whereas epithelial-like cell lines seem to be resistant to the drug.

7.8 Phosphoproteomic analysis of cancer cell lines treated with SU11248

Kinases are key components and regulators of cellular signalling pathways implicated in essential processes such as cell survival, cell proliferation, cell differentiation and motility. Controlled cellular signalling is accomplished by consecutive phosphorylation and dephosphorylation events on specific amino acid residues through the interaction of kinases and phosphatases organized in signalling cascades. Phosphorylation on serine, threonine and tyrosine sites regulates the activation state of a particular kinase. Therefore, the inhibition of kinase activity, for example by a small-molecule kinase inhibitor such as SU11248, has a strong impact on cellular signalling networks. The inhibition is passed down as a secondary signalling event resulting in impaired maintenance of cell-homeostasis. To study this cell-wide impact of SU11248 on cancer cells a mass-spectrometry based quantitative phosphoproteomic analysis was used to identify cellular sites of inhibition. For a detailed insight in an inhibitor` s molecular function not only the direct target inhibition profile is important but also the signalling networks being impaired by the drug.

Due to the fact that kinases are the key regulators of signalling events and that their activities are often controlled via phosphorylation events on tyrosine residues the focus of interest was on the tyrosine-phosphoproteome of SU11248 treated cells.

Cancer cell lines of different tissue origins were metabolically labelled and treated with 2.5 or 5 µM SU11248 for 6 or 24h, respectively. Control cells obtained the drug vehicle DMSO. Phospho-peptides were enriched by two consecutive steps. First, phosphorylated proteins were retained from total cell lysates by an anti-phospho-tyrosine immunoprecipitation and trypsin-digested. In a second step, phosphopeptides were enriched by titanium dioxide beads being positively charged and analyzed by LC/MS. The workflow is shown in Figure 58.

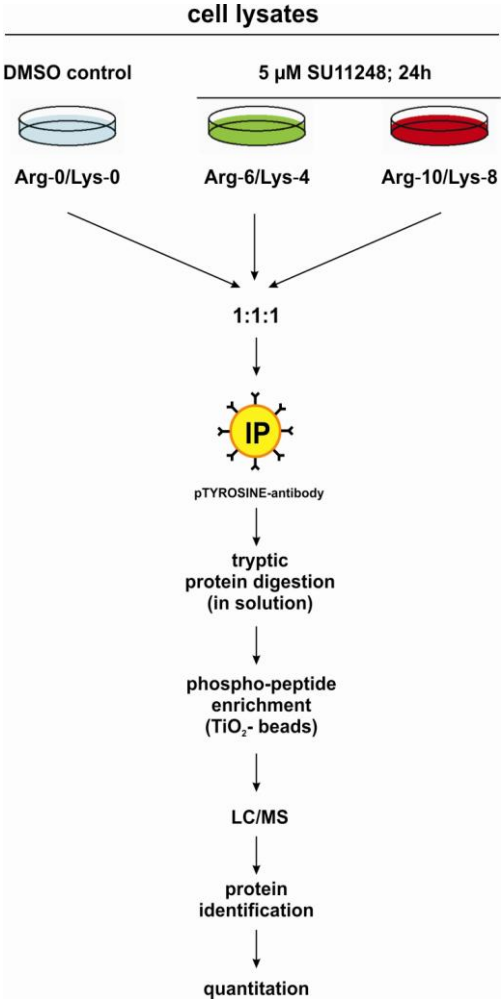

Figure 58 Workflow of phosphoproteomic analysis of SU11248 treated cancer cell lines based on quantitative mass-spectrometry
Cancer cell lines of different tissue origins were metabolically labelled with either normal arginine and lysine (Arg^0/Lys^0) or combinations of isotopic variants of the two amino acids (Arg^6/Lys^4, Arg^{10}/Lys^8). Arg^6/Lys^4 and Arg^{10}/Lys^8 cells were treated with 5 µM SU11248 for 24h. Control cells (Arg^0/Lys^0-encoded cells) obtained the drug vehicle DMSO. Phospho-peptides were enriched by two consecutive steps. First, phosphorylated proteins were retained from total cell lysates by an anti-phospho-tyrosine immunoprecipitation and trypsin-digested. In a second step, phospho-peptides were enriched by titanium-dioxide (TiO_2) beads being positively charged and analyzed by LC/MS. Protein identification, phospho-site alignment and quantification was done with the software MaxQuant (version 1.0.11.1).

The phosphoproteome was analyzed in 22 cancer cell lines of different tissue origins. Based on the cell line classification described in section 7.6, cell lines being responsive and as well as less responsive to SU11248 treatment were chosen.

In total, 3257 distinct phosphorylation sites on 1272 different proteins were detected. Their temporal dynamics and concentration dependency upon SU11248 treatment was analyzed. The distribution of phosphorylation sites by amino acids and their down-regulation is shown in Table 17. For the analysis of dynamic changes as a result of SU11248 treatment, a cut-off value of a 2-fold change down in the SU11248 treated cell fractions was taken. A total of 1536 phosphopeptides were in this category, which are termed here “regulated phosphopeptides.”

All listed phosphorylation sites are class I sites with a localization probability greater than 75%. The definition of class I phospho-sites was adapted from Olsen et al., Cell, 2006 (Olsen et al., 2006). Given the peptide sequence and number of phosphorylation sites for each phosphopeptide, potential phosphorylation sites were grouped into categories depending on their PTM localization score and motifs. In the category with highest confidence in localization (class I), the site in question had a localization probability for the phospho-group of at least 0.75. That is, the added probability of all other potential sites is less than 0.25.

Table 17 Distribution of phosphorylation sites by amino acids

pSTY-sites	proteins	amino acid	class I	percent	pSTY-sites(total)	regulated	percent	amino acid	regulated	percent 1	percent 2
		S	2366	72.60%				S	997	65%	18%
3257	1272	T	394	12.10%	7729	1536	19.9	T	235	15.30%	24.95%
		Y	497	15.30%				Y	304	19.80%	24.17%

The obtained phospho-data set was normally distributed with a slight shift to lower ratios reflecting increased down-regulation of phosphorylation after SU11248 treatment. The statistical analysis is shown in Figure 59.

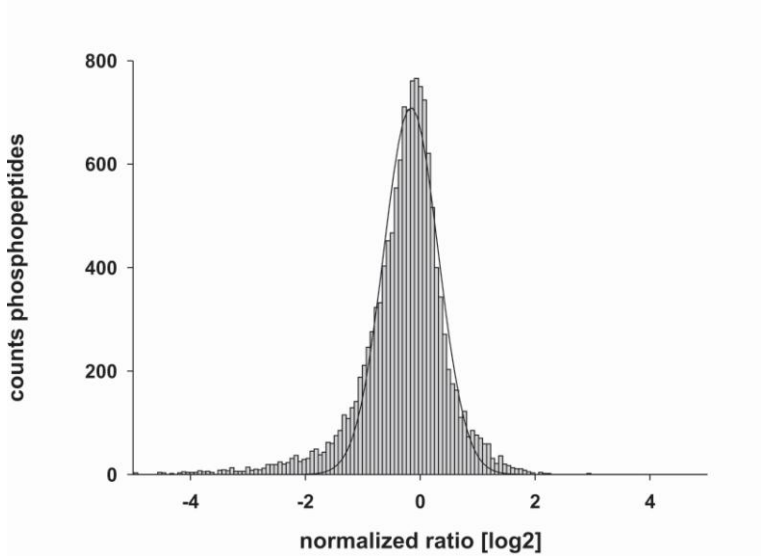

Figure 59 Normal distribution of phosphopeptides.
Phosphopeptides of all experiments with a significance of pep< 0.01 were analyzed for normal distribution using SigmaPlot 10.0 based on a Gaussian, 3 parameter curve fitting algorithm on log2-transformed ratios between SU11248 treated and control- cell fractions. A slight shift to lower ratios was observed reflecting the increased down-regulation of phosphorylation after SU11248 treatment.

In the classic study using phosphoamino acid analysis, Hunter and co-workers found relative abundances of 0.05%, 10%, and 90% for phosphotyrosine (pY), phosphothreonine (pT), and phosphoserine (pS) in normally growing cells (Hunter and Sefton, 1980). Olsen and co-workers identified a distribution of pY, pT, and pS sites of 1.8%, 11.8%, and 86.4% - very close to the original estimate for serine and threonine, but an order of magnitude higher for tyrosine. Here the distribution between individually identified class I sites was determined to be 497 pY, 394 pT, and 2366 pS sites reflecting 15.3%, 12.1% and 72.6%, respectively. With

respect to serine and threonine phosphorylation this data set, based on more than 1200 phosphoproteins, is similar to previous studies but much higher for tyrosine. This apparent discrepancy is due the enrichment of tyrosine-phosphorylated proteins carried out by immunoprecipitation prior to the phosphoproteomic analysis. The proportion of regulated phospho-sites per amino acid after SU11248 treatment was higher in tyrosine and threonine compared to serine residues with tyrosine phosphorylation being the strongest inhibited fraction after SU11248 treatment. This is in accordance with the fact that SU11284 is a small-molecule kinase inhibitor. Kinases activity is predominantly carried out by phospho-tyrosine phosphorylation. Observed inhibition of serine and threonine phosphorylated residues is mostly due to secondary inhibition effects occurring in signalling cascades downstream of the primary site of inhibition.

As an initial step to screen for phosphotyrosine signalling changes upon inhibitor treatment a semi-quantitative approach using the number of phosphopeptide assignments (spectral counts) to approximate the amount of phosphopeptide present in the sample was adopted from a previous study surveying aberrant kinase signalling in lung cancer (Rikova et al., 2007). Roughly speaking, the wider the peak eluting from the LC column the more frequently a phosphopeptide is detected by LC/MS and hence the more phosphopeptide present in the sample. This semi-quantitative approach was used for all analyzed cancer cell lines and combined all sites on a given protein.

To get a global and universal insight in SU11248 cellular action the data of all 22 treated cancer cell lines from different tissue origins were combined and analyzed together. The distribution of cellular abundance of phosphorylated proteins is shown for tyrosine kinases and non-tyrosine kinases in Figure 60 A and B.

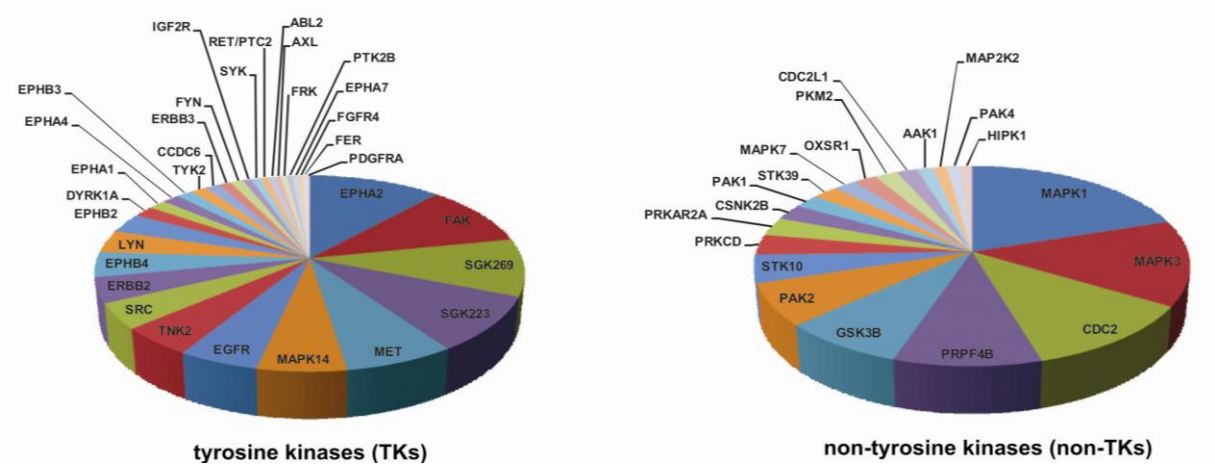

Figure 60 Distribution of the amount of phosphorylation among kinases in cancer cell lines.
The numbers of phosphopeptides assigned to each kinase combining all phospho-sites on a particular protein are represented by the wedges of the pies. A) Spectral counts among tyrosine kinases (TK). The total numbers of observed phosphopeptide spectra assigned to each TK over all cancer cell lines with a significance of pep< 0.01 are represented as fractions of the total TK spectra observed. B) Distribution of phoshopeptides among non-tyrosine kinases (non-TK). The total numbers of observed spectra assigned to each non-TK over all cancer cell lines with a significance of pep< 0.01 are represented as fractions of the total TK spectra observed.

The amount of phosphorylated proteins is expressed in number phosphorylated peptides per protein and represented by the wedges of the pie. The tyrosine kinases EPHA2, FAK, SGK269, SGK223, MET, MAPK14 and EGFR showed the highest levels of tyrosine kinase phosphorylation while MAPK1, MAPK3, CDC2, PRPF4B, GSK3b and PAK were the most frequently phoshorylated non-tyrosine kinases among all cancer cell lines.

To see which kinases are frequently inhibited by SU11248 the same analysis as described above was performed for down-regulated phosphopeptides observed in all cancer cell lines. The number of regulated phosphopeptides assigned to one kinase was summarized over all cell lines combining all phosphorylation sites on a particular protein. Based on the statistical analysis of the normal distribution of the data-set a 2-fold change of the phospho-ratio between SU11248 treated and DMSO vehicle control treated cells in either direction was considered to be significantly regulated by the inhibitor. The data are shown for tyrosine kinases in Figure 61 and non-tyrosine kinases in Figure 62 being down-regulated by SU11248.

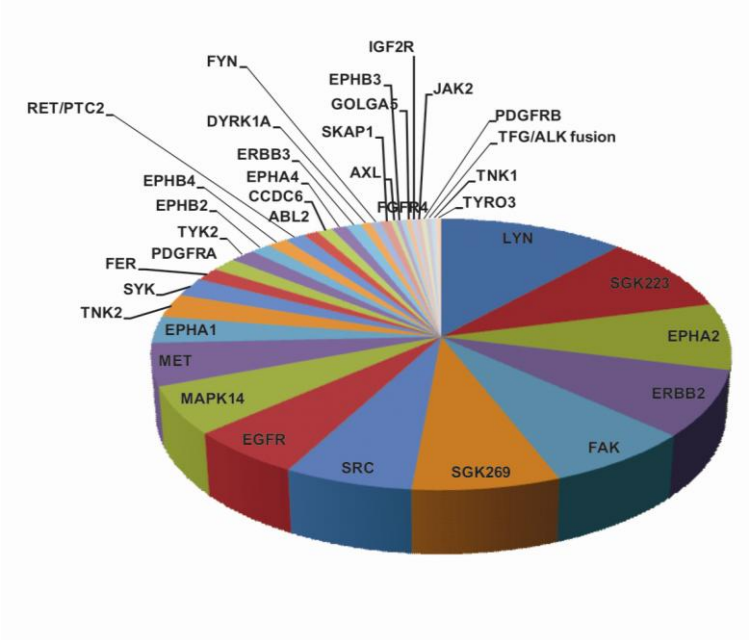

Figure 61 Distribution of the amount of down-regulated phosphopeptides among tyrosine kinases in cancer cell lines after SU11248 treatment.

The number of at least 2-fold down- regulated phosphopeptides assigned to each tyrosine kinase combining all phospho-sites on a particular protein is represented by the wedges of the pies. The total numbers of down-regulated phosphopeptide spectra assigned to each TK over all cancer cell lines with a significance of pep< 0.01 and a cut-off value of a 2-fold-change are represented as fractions of the total regulated TK spectra observed.

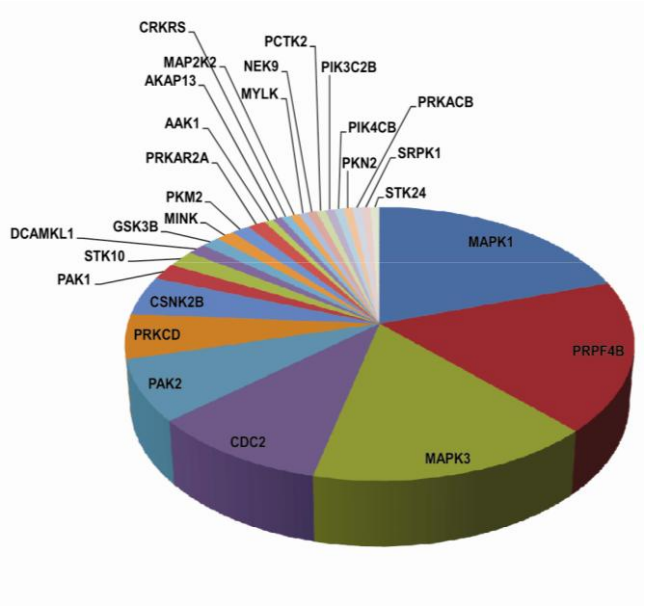

Figure 62 Distribution of the amount of down-regulated phosphopeptides among non-tyrosine kinases in cancer cell lines after SU11248 treatment.
The number of at least 2-fold down- regulated phosphopeptides assigned to each non-tyrosine kinase (non-TK) combining all phospho-sites on a particular protein is represented by the wedges of the pies. The total numbers of down-regulated phosphopeptide spectra assigned to each non-TK over all cancer cell lines with a significance of pep< 0.01 and a cut-off value of a 2-fold-change are represented as fractions of the total regulated non-TK spectra observed.

The amount and frequency of down-regulated kinases among all cancer cell lines is expressed in number down-regulated phosphorylated peptides per protein and represented by the wedges of the pie. Among all identified tyrosine kinases LYN, SGK223, EPHA2, ERBB2, FAK, SGK269, SRC, EGFR, MAPK14 and MET showed the highest number of down-regulated phosphopeptides while MAPK1, PRPF4B, MAPK3, CDC2, PAK2 and CSNK2B were the most frequently down-regulated non-tyrosine kinases in all cancer cell lines. The number of down-regulated phosphopeptides assigned to a particular kinase reflects the frequency of kinase inhibition and the number of sites being impaired by SU11248. In many cases, the quantity of down-regulated phosphopeptides assigned to a kinase correlates with the total number of phosphorylated peptides detected for this particular kinase. Nevertheless, a closer look reveals that the exact distribution between the number of phosphorylated and down-regulated peptides assigned to a particular kinase over all observed kinases, meaning the ranking, is not the same which shows that some kinases are more frequently inhibited by SU11248 than others. This was observed for tyrosine kinases such as FER, PDGFRa, PDGFRb, LYN, SRC, ERBB2 and EPHA1 as well as non tyrosine kinases including PAK2, NEK9 and CSNK2B. Other kinases for example, such as FAK, MET, TNK2, EGFR and MAPK14 as well as CDC2 and GSK3b showed lesser amounts of phosphopeptide regulation compared to their total levels of phosphorylation. The percentage inhibition of a certain kinase by SU11248, expressed as the ratio of down-regulated phosphopeptides assigned to each kinase compared to the total number of detected phosphopeptides, is illustrated in Figure 63 for tyrosine kinases and non-tyrosine kinases. The percentage inhibition helps to rank and prioritize kinase inhibition by the drug for a detailed understanding of underlying molecular mechanisms of the inhibitor` s function.

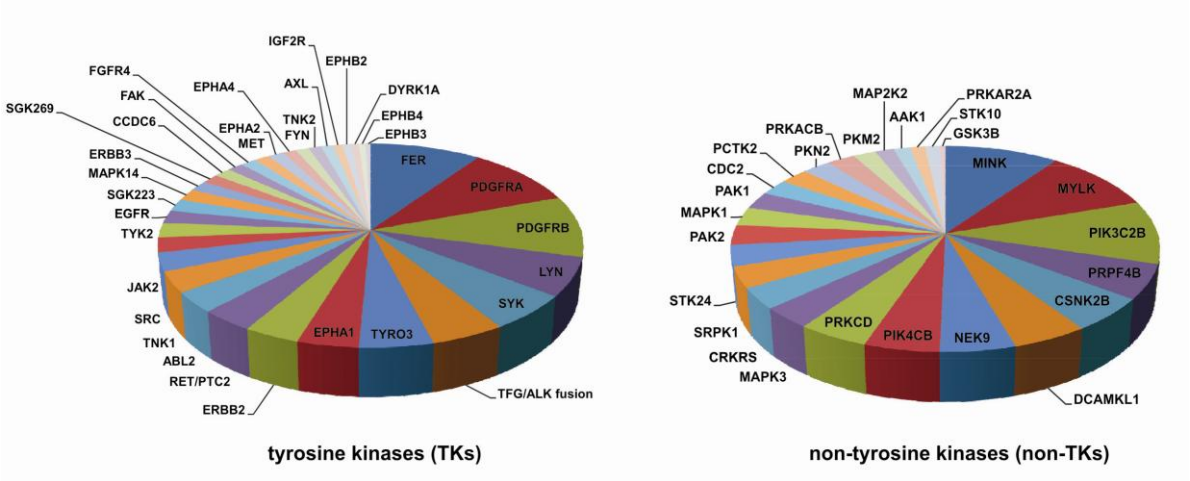

Figure 63 Percentage inhibition of tyrosine and non-tyrosine kinases phosphorylation by SU11248.
The percentage inhibition of kinase phosphorylation by SU11248 is expressed as the ratio of at least 2-fold down-regulated phosphopeptides compared to the total number of phosphopeptides assigned to each kinase and represented by the wedges of the pie. The results are shown for tyrosine kinases in the left and for non-tyrosine kinases in the right panel.

The detected inhibition rates of kinase phosphorylation by SU11248 revealed new kinase targets being potently inhibited by the drug. Beyond known tyrosine kinase targets including PDGFRa, PDGFRb and RET, newly identified tyrosine kinases such as FER, LYN, TYRO3, SRC and JAK2 were characterized to be important sites of cellular action of the small-molecule kinase inhibitor and show its broad impact on cellular signalling. Furthermore, receptor tyrosine kinases such as AXL, FGFR4, MET and Ephrin receptors were shown to be impaired after drug treatment. In addition to tyrosine kinase inhibition non-tyrosine kinase regulation was found after treatment with SU11248. Important protein kinases are MAPK1, MAPK3, MAP2K2, NEK9 and CSNK2B as well as other non protein kinases such as PIK3C2B and PRPF4B all implicated in the regulation of key cellular processes including cell proliferation, survival and motility.

Many kinases showing down-regulated phosphorylation upon SU11248 treatment were detected as high affinity interaction partners in the target profiling screen. The combination of both assays is a direct proof of target binding and inhibition by SU11248 revealing a comprehensive picture of the cellular mode of action of the small-molecule inhibitor.

Beside kinases other signalling molecule were detected to be inhibited or impaired in general by SU11248. Functional annotation of phosphoproteins identified with at least one unique 2-fold down-regulated phosphopeptide was performed with Gene Ontology and impaired signalling pathways upon drug treatment are shown in Figure 64.

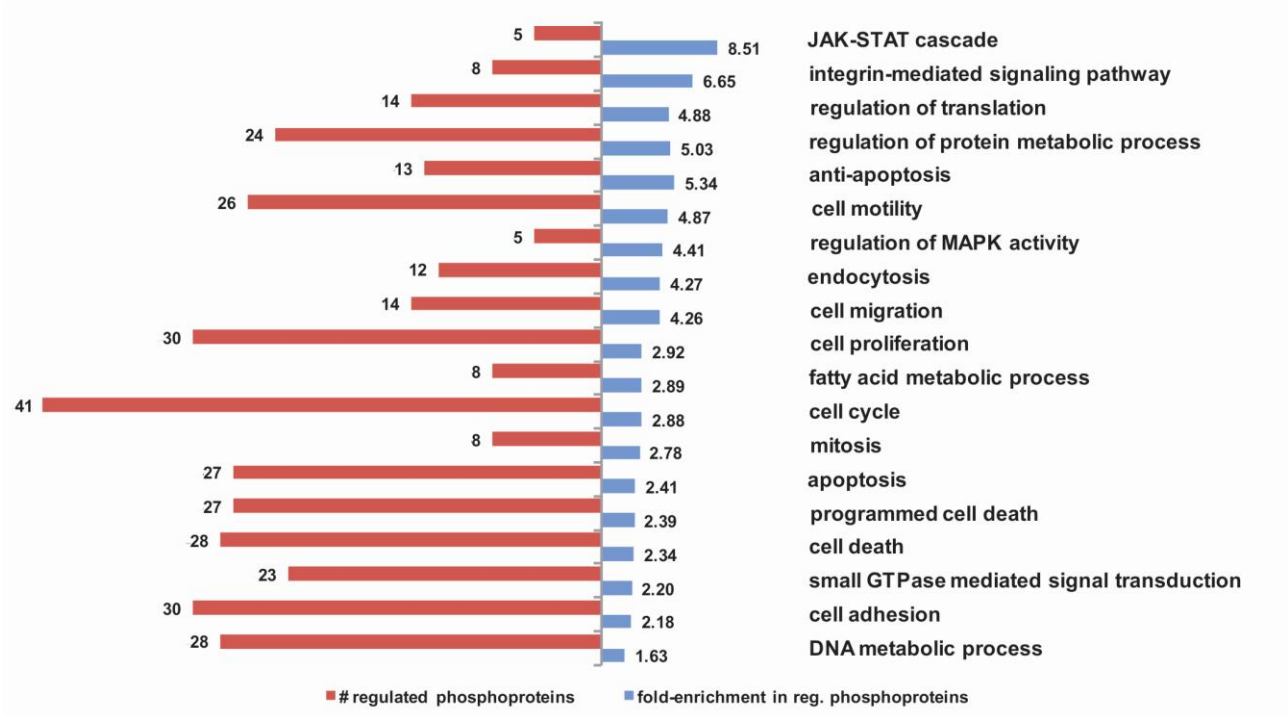

Figure 64 Impaired signalling pathways in cancer cells after SU11248 treatment.
Phosphoproteins with at least one unique 2-fold down-regulated phosphopeptide were functional annotated using Cytoscape 2.5.1 with the BINGO plugin. Shown are in red the number of regulated proteins assigned to each category and in blue the fold-enrichment of regulated biological processes compared to their normal distribution in the human proteome. The significance threshold of enrichment was set to $p < 0.01$.

Key cellular processes such as cell proliferation, cell survival, cell motility and migration as well as metabolic pathways such as fatty acid, translation and DNA metabolism are impaired by SU11248. This is in accordance with observed physiological phenotypes in cancer cells after drug treatment.

In summary, the applied quantitative phosphoproteomic approach revealed direct and indirect sites of inhibition of the small-molecule kinase inhibitor SU11248 within cancer cell lines of different tissue origins thereby giving a deep insight into its molecular function.

Beside these general patterns of SU11248 inhibition in cancer cell lines of different tissue origins the inhibition differences between SU11248 responsive and less responsive cell lines is of great importance to reveal prediction markers for SU11248 sensitivity and biomarkers reflecting SU11248 activity as a sensitivity read-out in treated cancer cells. Therefore, in a next step, the main focus was on kinase inhibition differences and signalling pathways being differentially impaired by the drug in SU11248 sensitive and less sensitive cancer cell lines. Phospho-inhibition profiles in these two cell line groups were compared and differences are listed in Table 18.

Table 18 Differential regulated phosphoproteins in SU11248 sensitive and insensitive cancer cell lines

Phosphoprotein regulation is expressed in % inhibition and compared between the two cell line groups. A cut-off value for sensitivity markers was set to an at least 5 % higher inhibition rate observed in sensitive cancer cell lines.

	cancer cell lines						
Gene Names	sensitive % inhibition	sensitive # pSTYpeptides	sensitive down-regulated # pSTYpeptides	insensitive % inhibition	insensitive # pSTYpeptides	insensitive down-regulated # pSTYpeptides	delta inhibition
KIAA1522	100	1	1	0	1		100
LRRFIP1	100	1	1	0	1		100
MAP2	100	1	1	0	1		100
MSN	100	1	1	0	1		100
PHACTR4	100	1	1	0	1		100
TMEM40	100	3	3	0	1		100
ZC3H15	100	1	1	0	1		100
TCEA1	75	4	3	0	1		75
SYK	70	10	7	0	2		70
BAIAP2L1	67	6	4	0	3		67
CRIP2	67	3	2	0	1		67
PLCG1	67	3	2	0	1		67
HIST1H1E	50	2	1	0	1		50
LMO7	50	10	5	0	2		50
PCTK2	50	2	1	0	2		50
PSEN1	50	2	1	0	1		50
RAVER1	50	4	2	0	1		50
SH3PXD2A	50	2	1	0	1		50
SMARCC2	44	9	4	0	2		44
PAG1	81	31	25	40	5	2	41
SLC38A2	38	13	5	0	7		38
IFI16	38	8	3	0	1		38
RIN1	36	11	4	0	2		36
CDV3	83	6	5	50	4	2	33
TRIM29	100	1	1	67	3	2	33
COPB2	33	3	1	0	2		33
HIST1H1B	33	6	2	0	2		33
PRKACB	33	3	1	0	1		33
PAK1	30	10	3	0	1		30
PSMD2	30	10	3	0	5		30
DSP	29	7	2	0	1		29
LRRFIP2	29	7	2	0	1		29
POP1	29	7	2	0	3		29
IRS2	28	39	11	0	21		28
DHX57	27	11	3	0	2		27
CDH1	25	4	1	0	1		25
DAB2IP	25	4	1	0	1		25
ERCC5	25	8	2	0	1		25
FCHSD2	25	4	1	0	1		25
HSPH1	25	8	2	0	1		25
PDHA1	25	12	3	0	2		25
PDLIM4	25	8	2	0	2		25
PKM2	25	8	2	0	2		25
SORBS3	25	12	3	0	1		25
TLE3	25	8	2	0	1		25
TOM1L1	25	4	1	0	2		25
CCDC43	23	13	3	0	3		23
ABI1	22	9	2	0	1		22
TRAFD1	22	9	2	0	3		22
EPRS	21	14	3	0	5		21
RAB7A	45	11	5	25	8	2	20
ACSS2	20	5	1	0	1		20
BIRC6	20	5	1	0	2		20
CASC3	20	5	1	0	1		20
FAM40A	20	5	1	0	3		20
INADL	20	5	1	0	3		20
SF3A1	20	10	2	0	1		20
VAMP4	20	5	1	0	1		20
KIAA1618	18	11	2	0	3		18
MAP1B	18	159	28	0	6		18
YAP2	29	21	6	11	9	1	17
MAPK1	35	68	24	18	33	6	17
ANKRD15	17	6	1	0	1		17
FAM83F	17	6	1	0	1		17
LARP7	17	6	1	0	1		17
MLPH	17	6	1	0	5		17
SLC9A3R1	17	12	2	0	2		17

	cancer cell lines						
Gene Names	sensitive % inhibition	sensitive # pSTYpeptides	sensitive down-regulated # pSTYpeptides	insensitive % inhibition	insensitive # pSTYpeptides	insensitive down-regulated # pSTYpeptides	delta inhibition
LMNA	24	29	7	8	13	1	16
C14orf32	15	13	2	0	4		15
HDAC1	15	13	2	0	2		15
HSPB1	15	26	4	0	7		15
PURB	15	13	2	0	3		15
EPS15	40	5	2	25	4	1	15
TNKS1BP1	32	19	6	17	6	1	15
DKC1	14	7	1	0	1		14
HDGFRP2	14	7	1	0	2		14
HNRPK	14	7	1	0	2		14
LRRC47	14	7	1	0	1		14
MRE11A	14	7	1	0	2		14
NOL5A	14	14	2	0	1		14
PTPN12	14	7	1	0	1		14
SMC4	14	7	1	0	3		14
TMEM106B	14	7	1	0	2		14
TPI1	14	7	1	0	2		14
ZYX	14	22	3	0	2		14
RPLP0	13	15	2	0	3		13
SPTBN1	13	15	2	0	3		13
IFITM3	33	6	2	20	5	1	13
EIF5B	17	82	14	5	22	1	13
DCBLD1	13	8	1	0	2		13
WDR26	12	25	3	0	8		12
MCM3	12	17	2	0	1		12
CALD1	11	9	1	0	1		11
ERBB2IP	11	18	2	0	4		11
GAB1	33	70	23	22	32	7	11
MCM2	11	28	3	0	8		11
TJP2	28	39	11	18	34	6	11
IGF2R	10	10	1	0	2		10
KRT13	60	5	3	50	2	1	10
SNTB2	10	10	1	0	2		10
ARHGAP12	18	11	2	8	12	1	10
RPLP1	20	15	3	10	29	3	10
DPM1	9	11	1	0	1		9
SGK269	17	124	21	8	25	2	9
KIAA0712	20	5	1	11	9	1	9
HNRNPC	9	23	2	0	5		9
LSR	13	15	2	5	21	1	9
ITGB4	29	7	2	20	5	1	9
PLEC1	16	32	5	7	14	1	8
BYSL	8	12	1	0	3		8
HNRPD	8	12	1	0	3		8
NAP1L4	8	12	1	0	4		8
ARHGAP5	8	13	1	0	5		8
NUP98	8	13	1	0	1		8
ST13	8	13	1	0	4		8
TJP3	8	13	1	0	3		8
ZDHHC8	8	13	1	0	4		8
DNAJC5	21	14	3	14	7	1	7
EPHB4	7	56	4	0	9		7
HUWE1	7	14	1	0	1		7
DCBLD2	7	29	2	0	9		7
DEK	7	15	1	0	1		7
GSK3B	7	30	2	0	11		7
HNRPH1	7	15	1	0	5		7
SAPS3	7	15	1	0	8		7
HN1	6	32	2	0	9		6
RAPTOR	6	16	1	0	4		6
FAK	16	129	20	9	32	3	6
EPHB3	6	17	1	0	5		6
PCBP2	6	17	1	0	2		6
PLEKHA5	56	9	5	50	2	1	6
TNK2	13	52	7	8	25	2	5
SMN1	5	19	1	0	9		5
SQSTM1	5	19	1	0	5		5

Interestingly, proteins such as PLCG1, a substrate of receptor tyrosine kinase signalling, and the MAP Kinase ERK2 were down-regulated to a much higher extend in SU11248 sensitive cancer cell lines. This could also be shown by western blotting. Furthermore, adaptor proteins such as PAG1, IRS2 and the small GTPase RAB7A were stronger inhibited in SU11248 sensitive cell lines upon inhibitor treatment. These

proteins have to be further investigated and may function as biomarkers for SU11248 activity as a sensitivity read-out while patient treatment in the clinic in the future. A summary of down-regulated phosphosites on kinases after SU11248 treatment is shown in Table 19. Kinases are listed alphabetically and only at least 2-fold down-regulated phosphotyrosine residues were considered as significantly inhibited by SU11248. The peptide significance was set to $p < 0.01$. The averaged inhibition rate for each phosphosite over all analyzed cancer cell lines is given in the Table 19. In addition, many phosphoserine and phosphothreonine sites were dephosphorylated upon drug application.

Table 19 Down-regulated phosphotyrosine sites in kinases after SU11248 treatment of cancer cells.

Protein	Gene Names	Modified Sequence	fold- decrease by SU11248	NO Phospho	Amino Acid	Position	FPR	Mascot Score	PTM Score	m/z	Mass Error [ppm]
IPI00552750	ACK1	_VSSTHY(ph)YLLPERPSYLER_	2.7	1	Y	913	0.00	23.47	63.562	764.03498	-0.22329
IPI00296992	AXL	_Y(ph)VLCPSTTPSPAQPADR_	1.9	1	Y	866	0.00	59.84	140.19	970.43462	-0.22863
IPI00179326	BAIAP2L1	_EIEY(ph)VETVTSR_	8.4	1	Y	163	0.00	36.37	88.89	703.31597	0.37313
IPI00026689	CDC2	_IGEGTYGVVY(ph)K_	1.9	1	Y	19	0.00	23.96	88.89	633.29431	0.329
IPI00023530	CDK5	_IGEGTY(ph)GTVFK_	2.1	1	Y	15	0.00	31.1	77.144	626.28649	-0.63192
IPI00014344	DYRK1A	_IYQY(ph)IQSR_	2.0	1	Y	321	0.00	27.97	152.86	575.76826	-0.42696
IPI00304942	DYRK2	_VYTY(ph)IQSR_	2.1	1	Y	382	0.02	23.7	100.48	555.25499	0.43105
IPI00304942	DYRK2	_VYTY(ph)IQSR_	2.6	1	Y	382	0.04	24.02	100.48	555.25499	0.091929
IPI00018274	EGFR	_YSSDPTGALTEDSIDDTFLPVPEY(ph)INQSVPK_	1.9	1	Y	1092	0.00	35.51	126.3	1160.199	1.3088
IPI00018274	EGFR	_RPAGSVQNPVY(ph)HNQPLNPAPSR_	2.7	1	Y	1110	0.00	40.65	103.74	827.07119	0.33921
IPI00018274	EGFR	_GSTAENAEY(ph)LR_	2.3	1	Y	1197	0.00	40.93	88.89	645.77173	-0.24788
IPI00294250	EPHA1	_LWLKPY(ph)VDLQAYEDPAQGALDFTR_	2.0	1	Y	599	0.00	86.37	173.61	963.80015	1.0314
IPI00294250	EPHA1	_PYVDLQAY(ph)EDPAQGALDFTR_	2.7	1	Y	605	0.00	86.37	173.61	1175.0254	0.11389
IPI00294250	EPHA1	_LLDDFDGTY(ph)ETQGGK_	2.3	1	Y	781	0.00	57.6	135.02	869.86401	-0.14607
IPI00021267	EPHA2	_TYVDPHTY(ph)EDPNQAVLK_	1.9	1	Y	594	0.00	40.37	140.19	690.64538	0.039982
IPI00021267	EPHA2	_TYVDPHTY(ph)EDPNQAVLK_	1.8	1	Y	594	0.00	61.05	166.84	1035.4644	-0.27026
IPI00008318	EPHA4	_T(ph)YVDPFTY(ph)EDPNQAVR_	2.3	2	Y	602	0.00	55.69	153.23	1037.9134	-0.051527
IPI00008318	EPHA4	_TYVDPFTY(ph)EDPNQAVR_	2.2	1	Y	602	0.00	28.99	148.23	997.93022	-2.2975
IPI00016645	EPHA7	_VIEDDPEAVY(ph)TTTGGK_	2.1	1	Y	791	0.00	46.59	140.19	887.89277	-0.41268
IPI00289329	EPHB3	_LQQY(ph)IAPGM(ox)K_	1.9	1	Y	600	0.01	17.06	71.667	622.79088	0.7027
IPI00289329	EPHB4	_VY(ph)IDPFTYEDPNEAVR_	1.9	1	Y	608	0.00	75.08	244.94	1004.4404	0.53318
IPI00018195	ERK1	_IADPEHDHTGFLTEY(ph)VATR_	2.4	1	Y	204	0.00	47.67	119.49	751.33884	0.45476
IPI00018195	ERK1	_IADPEHDHTGFLTEY(ph)VATR_	2.4	1	Y	204	0.00	37.48	119.49	751.33884	0.30798
IPI00003479	ERK2	_VADPDHDHTGFLTEY(ph)VATR_	2.5	1	Y	187	0.00	53.34	137.83	556.74812	-0.10925
IPI00003479	ERK2	_PDHDHTGFLTEY(ph)VATR_	2.1	1	Y	187	0.00	43.18	127.99	646.95091	0.44078
IPI00029702	FAK2	_YIEDEDY(ph)YK_	2.8	1	Y	579	0.00	13.22	91.115	659.24977	-0.90777
IPI00029702	FAK2	_YIEDEDYY(ph)K_	2.1	1	Y	580	0.00	13.22	91.115	659.24977	0.65247
IPI00029702	FAK2	_EVGY(ph)LEFTGPPQKPPR_	2.1	1	Y	849	0.02	18.08	56.476	632.30815	-0.090982
IPI00029702	FAK2	_EVGY(ph)LEFTGPPQKPPR_	3.3	1	Y	849	0.03	26.08	72.706	632.30815	-0.29204
IPI00029263	FER	_VQENDGKEPPPVVNY(ph)EEDAR_	2.6	1	Y	402	0.00	38.71	142.6	789.01631	-0.46672
IPI00029263	FER	_VQENDGKEPPPVVNY(ph)EEDAR_	5.7	1	Y	402	0.00	59.27	153.05	789.01631	-0.57923
IPI00029263	FER	_QEDGGVY(ph)SSSGLK_	3.5	1	Y	714	0.00	24.85	77.135	703.7954	-0.21333
IPI00029263	FER	_(py)QEDGGVY(ph)SSSGLK_	3.9	1	Y	714	0.08	26.68	66.85	695.28213	-0.33947
IPI00795611	GIT1	_SQSDLDDQHDY(ph)DSVAS(ph)DEDTDQEPLR_	2.7	2	Y	392	0.00	47.17	126.39	1047.389	-0.24353
IPI00300384	HER2	_LLDIDETEY(ph)HADGGK_	2.3	1	Y	877	0.00	54.1	126.06	585.92062	-0.41902
IPI00300384	HER2	_FVVIQNEDLGPASPLDSTFY(ph)R_	2.2	1	Y	1005	0.00	68.94	153.93	1224.5778	-0.33488
IPI00298285	HER3	_HSLLTPVTPLSPPGLEEEDVNGY(ph)VMPDTHLK_	1.9	1	Y	1159	0.00	31.92	94.226	1155.8931	0.25085
IPI00298285	HER3	_EGTLSSVGLSSVLGTEEEDEDEEY(ph)EYMNR_	12.4	1	Y	1197	0.00	43.86	93.28	1116.4605	0.44396
IPI00298285	HER3	_SLEATDSAFDNPDY(ph)WHSR_	2.1	1	Y	1328	0.00	41.48	144.91	730.96366	-0.13227
IPI00016371	HER4	_NGDLQALDNPEY(ph)HNASNGPPK_	2.1	1	Y	1188	0.00	31.7	93.412	777.67277	-0.20488
IPI00747261	HIPK1	_AVCSTY(ph)LQSR_	2.7	1	Y	352	0.00	39.24	101.9	632.77322	-0.24974
IPI00025803	INSR	_DIY(ph)ETDY(ph)DYYRK_	3.1	2	Y	1205	0.05	13.24	66.159	763.28603	-0.75489
IPI00025803	INSR	_DIY(ph)ETDY(ph)YRK_	1.9	2	Y	1209	0.05	13.24	66.159	763.28603	-0.17144
IPI00025803	INSR	_DIY(ph)ETDYY(ph)RK_	1.9	2	Y	1210	0.07	13.17	66.159	763.28603	0.73007
IPI00031016	JAK2	_EVGDY(ph)GQLHETEVLLK_	3.0	1	Y	570	0.00	7.16	72.706	637.30295	-0.153
IPI00219418	JAK3	_DLNSLISSDY(ph)ELLSDPTPGALAPR_	2.6	1	Y	785	0.00	28.78	97.285	1312.6282	-0.79416
IPI00872474	LYN	_VIEDNEY(ph)TAR_	3.3	1	Y	467	0.00	35.2	124.44	645.27411	0.30026
IPI00872474	LYN	_VIEDNEY(ph)TAR_	3.6	1	Y	467	0.00	45.97	109.86	645.27411	-0.40309
IPI00872474	LYN	_AEERPTFDYLQSVLDDFYTATEGQY(ph)QQQP_	2.1	1	Y	578	0.07	72.24	72.429	1173.847	1.2554
IPI00294528	MET	_CVAPY(ph)PSLLSSEDNADDEVDTRPASFWETS_	5.4	1	Y	1383	0.56	30.12	36.663	1146.8167	0.40016
IPI00166680	MINK1	_NLLHADSNGY(ph)TNLPDVVQPSHSPTENSK_	2.5	1	Y	906	0.00	27.72	85.068	1038.8103	-0.23074
IPI00027721	PDGFRA	_QADTTQY(ph)VPMLER_	11.1	1	Y	742	0.05	35.09	66.85	816.36039	-1.4474
IPI00027721	PDGFRA	_QADTTQY(ph)VPMLER_	12.4	1	Y	742	0.00	58.7	99.64	816.36039	-0.10189
IPI00027721	PDGFRA	_DIMHDSNY(ph)VSK_	3.7	1	Y	849	0.00	26.6	101.42	694.78124	-0.014773
IPI00027721	PDGFRA	_VDSDNAY(ph)IGVTYK_	3.6	1	Y	988	0.00	76	111.87	762.83453	-0.91092
IPI00015902	PDGFRB	_DESVDY(ph)VPMLDMK_	4.5	1	Y	751	0.00	28.56	99.64	811.32991	-0.028446
IPI00292056	PIK3C2B	_LLGSVDY(ph)DGINDAITR_	3.6	1	Y	228	0.00	79.17	115.78	901.42203	-0.28589
IPI00329236	PRKCD	_SDSASSEPVGIY(ph)QGFEK_	4.6	1	Y	313	0.00	40.68	133.02	940.90113	0.85671
IPI00329236	PRKCD	_TGVAGEDMQDNSGTY(ph)GK_	6.7	1	Y	334	0.00	30.33	88.592	905.35349	-0.23192
IPI00329236	PRKCD	_TGVAGEDMQDNSGTY(ph)GK_	2.4	1	Y	334	0.00	37.79	109.81	905.35349	0.44877
IPI00013721	PRPF4B	_LCDFGSASHVADNDITPY(ph)LVSR_	5.9	1	Y	849	0.00	47.06	156.3	839.70871	0.065422
IPI00013721	PRPF4B	_LCDFGSASHVADNDITPY(ph)LVSR_	7.7	1	Y	849	0.00	39.69	156.3	839.70871	-0.21227
IPI00413961	PTK2	_THAVSVSETDDY(ph)AEIIDEEDTYTMPSTR_	2.2	1	Y	419	0.24	30.26	58.342	1628.1816	0.12195
IPI00413961	PTK2	_Y(ph)MEDSTYYK_	2.0	1	Y	592	0.00	13.36	124.79	640.23306	-0.1522
IPI00413961	PTK2	_Y(ph)MEDSTYYK_	2.7	1	Y	592	0.00	26.16	120.16	640.23306	0.62572
IPI00413961	PTK2	_VY(ph)ENVTGLVK_	2.9	1	Y	947	0.00	39.71	140.1	601.29685	0.22246
IPI00413961	PTK2	_VY(ph)ENVTGLVK_	3.4	1	Y	947	0.00	48.98	96.239	601.29685	0.10817
IPI00030273	RON	_DILDREY(ph)YSVQQHR_	1.9	1	Y	1238	0.00	24.5	126.54	634.62291	-0.60985
IPI00288965	ROS1	_EGLNY(ph)MVLATECGQGEEK_	2.6	1	Y	2274	0.00	25.03	49.345	1054.4392	1.311
IPI00739386	SGK223	_LEDEGVNSSPY(ph)SK_	2.3	1	Y	79	0.00	58.87	111.87	752.81379	0.1963
IPI00739386	SGK223	_CPPAY(ph)TMVGLHNLEPR_	4.0	1	Y	159	0.00	25.33	90.648	645.62661	-1.7059
IPI00737545	SGK269	_Y(ph)QEVWTSSTSPR_	3.1	1	Y	531	0.00	53.39	114.75	760.8245	-0.034327
IPI00328867	SRC	_LIEDNEY(ph)TAR_	2.4	1	Y	425	0.00	44.51	140.1	652.28193	0.23138
IPI00018597	SYK	_(py)QESTVSFNPY(ph)EPELAPWAADK_	2.6	1	Y	323	0.00	25.04	100.32	1221.5305	0.37473
IPI00003843	TJP2	_SIDQDY(ph)ER_	2.1	1	Y	249	0.00	33.88	126.04	553.21352	0.59072
IPI00003843	TJP2	_SIDQDY(ph)ER_	2.2	1	Y	249	0.00	38.68	152.63	553.21352	-0.17991
IPI00003843	TJP2	_HPDIY(ph)AVPK_	2.0	1	Y	1118	0.01	31.6	83.524	616.80739	0.38839
IPI00022353	TYK2	_LLAQAEGEPCY(ph)IR_	2.1	1	Y	292	0.00	51.06	152.77	800.36547	-0.39016
IPI00022353	TYK2	_LLAQAEGEPCY(ph)IR_	1.9	1	Y	292	0.00	29.28	111.87	800.36547	-0.23996

In summary, SU11248 showed a strong impact on cellular kinase signalling networks which are involved in a broad spectrum of cellular processes such as the regulation of cancer cell proliferation, migration, invasion and survival. The inhibition of tyrosine kinase phosphorylation was observed on many prominent oncogenes including receptor tyrosine kinases such as AXL, INSR, MET, PDGFRa, PDGFRb, RON and ROS1, as well as important cytosolic kinases such as FAK, SRC and TYK2. The concurrent inhibition of several different

signalling pathways increases the efficacy of a drug and reduces the risk of cancer cells developing drug resistances.

7.9 Functional characterization of SU11248 targets by knock-down experiments

7.9.1 High affinity SU11248 targets – their relevance for functional processes in cancer cell lines

An inhibitor`s target profile reflects molecular sites of action of the drug within a cell and gives insights into its mechanisms of action. Nevertheless, a target interaction map does not elucidate the biological relevance of a particular target for cellular processes such as cancer cell proliferation, survival and migration by which the observed phenotype upon drug treatment is executed.

To test whether the inhibition of identified SU11248 target proteins might be responsible for the biological effect of SU11248 in cancer cells it is of great importance to understand their physiological functions within cancer cells. RNAi experiments were performed for a detailed functional characterization of putative SU11248 targets. With SU11248 showing a strong anti-proliferative and apoptosis-inducing effect in a broad spectrum of tested cancer cell lines the focus of interest was on high affinity targets identified in cancer cell lines and tumor samples which were already described to be involved in cell-cycle progression such as AURKA, AURKB and survival including RPS6KA1, RPS6KA3, FAK as well as new SU11248 targets such as ROS1, BMP2K, NME4, TBK1, RON, NEK9 and other NEK-kinase-family members with so far relatively unknown functions.

According to protein expression level analysis of identified targets the breast cancer cell lines MDA-MB-435S, MDA-MB-231, Hs578T, the mRCC cell lines Caki1, Caki2, A498, SW13, the glioblastoma cell line U1242, the colon cancer cell lines HT29, HCT116 and the pancreatic cancer cell lines AsPc1, PaTu and A590 were employed in RNAi experiments.

7.9.1.1 High affinity SU11248 targets – their relevance for cancer cell viability, cell growth and proliferation

In a first step, identified high affinity SU11248 targets were analyzed in the context of cell viability and cell growth. After target depletion by RNAi cells were checked for impaired cell viability and cell growth by MTT-assays 72h post-transfection. The results are shown in Figure 65.

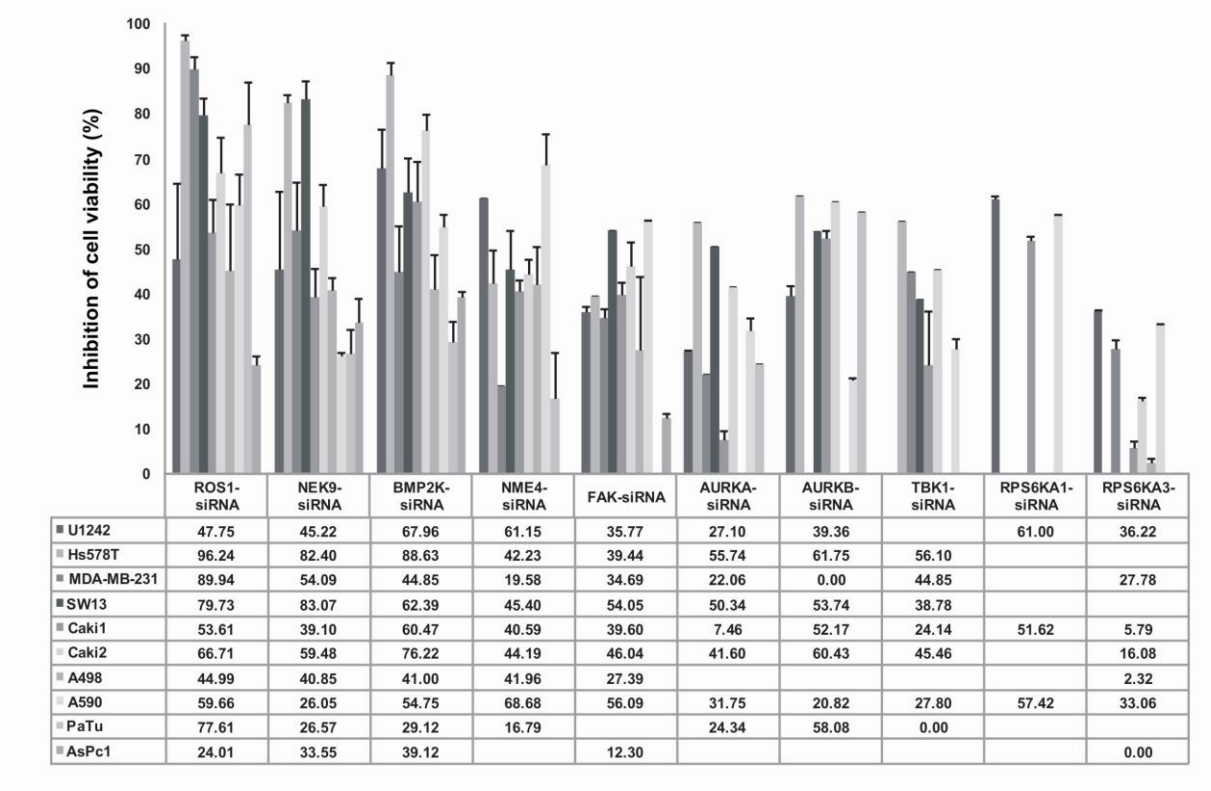

	ROS1-siRNA	NEK9-siRNA	BMP2K-siRNA	NME4-siRNA	FAK-siRNA	AURKA-siRNA	AURKB-siRNA	TBK1-siRNA	RPS6KA1-siRNA	RPS6KA3-siRNA
U1242	47.75	45.22	67.96	61.15	35.77	27.10	39.36		61.00	36.22
Hs578T	96.24	82.40	88.63	42.23	39.44	55.74	61.75	56.10		
MDA-MB-231	89.94	54.09	44.85	19.58	34.69	22.06	0.00	44.85		27.78
SW13	79.73	83.07	62.39	45.40	54.05	50.34	53.74	38.78		
Caki1	53.61	39.10	60.47	40.59	39.60	7.46	52.17	24.14	51.62	5.79
Caki2	66.71	59.48	76.22	44.19	46.04	41.60	60.43	45.46		16.08
A498	44.99	40.85	41.00	41.96	27.39					2.32
A590	59.66	26.05	54.75	68.68	56.09	31.75	20.82	27.80	57.42	33.06
PaTu	77.61	26.57	29.12	16.79		24.34	58.08	0.00		
AsPc1	24.01	33.55	39.12		12.30					0.00

Figure 65 Inhibition of cell viability after knock-down of high affinity SU11248 targets.
Target depletion was achieved by transient RNAi experiments and the effect on cancer cell viability was measured 72h post-transfection by a colorimetric MTT-assay. Cancer cells were either transfected with control or target-specific siRNA and grown for three days under serum conditions. Reduced cell viability after target knock-down is expressed in percentaged inhibition relative to control as the average of three to five independent experiments (error bars: s.e.m.).

Target depletion by RNAi of the high affinity targets ROS1, NEK9, BMP2K, NME4, FAK, AURKB and TBK1 resulted in a strong inhibition of cell viability and reduced cell growth by up to 95 %. The strongest impact was observed for ROS1, NEK9 and BMP2K. To a lesser but still significantly relevant, extensive inhibition of cell growth was seen for NME4, FAK, AURKB and TBK1. Similar results were obtained for AURKA, RPS6KA1 and RPS6KA3, also identified to be potently inhibited by SU11248. The RNAi experiments were performed in cancer cell lines of different tissue origins showing similar results. This broad anti-cancer effect after target depletion characterizes these targets as universally important proteins for cancer cell viability and cell growth, two hallmarks of cancer development and progression.

In a second step, the effect of target depletion on cancer cell proliferation was monitored using a BrdU S-phase incorporation assay as a direct measure of proliferating cells. Cells were transfected with either control or target-specific siRNA and impaired cell proliferation was measured 72h post-transfection as performed for the control of cell viability after target knock-down. The results are shown in Figure 66.

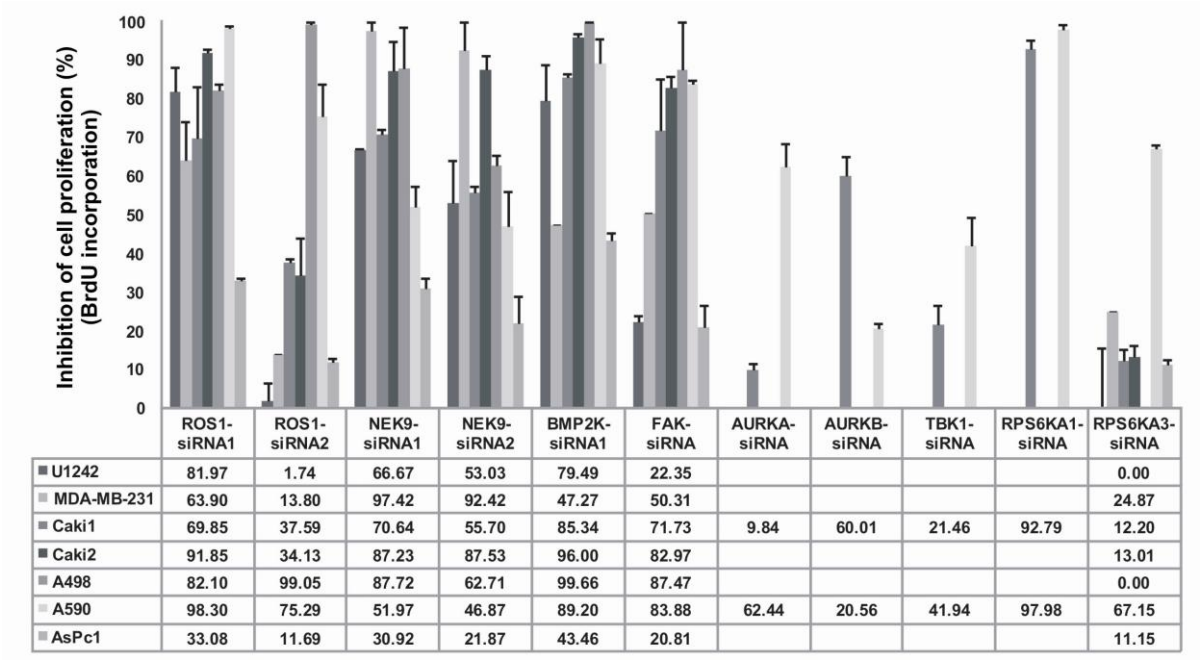

	ROS1-siRNA1	ROS1-siRNA2	NEK9-siRNA1	NEK9-siRNA2	BMP2K-siRNA1	FAK-siRNA	AURKA-siRNA	AURKB-siRNA	TBK1-siRNA	RPS6KA1-siRNA	RPS6KA3-siRNA
U1242	81.97	1.74	66.67	53.03	79.49	22.35					0.00
MDA-MB-231	63.90	13.80	97.42	92.42	47.27	50.31					24.87
Caki1	69.85	37.59	70.64	55.70	85.34	71.73	9.84	60.01	21.46	92.79	12.20
Caki2	91.85	34.13	87.23	87.53	96.00	82.97					13.01
A498	82.10	99.05	87.72	62.71	99.66	87.47					0.00
A590	98.30	75.29	51.97	46.87	89.20	83.88	62.44	20.56	41.94	97.98	67.15
AsPc1	33.08	11.69	30.92	21.87	43.46	20.81					11.15

Figure 66 Inhibition of cell proliferation after knock-down of high affinity SU11248 targets.
Target depletion was achieved by transient RNAi experiments and the effect on cancer cell proliferation was measured 72 h post-transfection by BrdU incorporation. Cancer cells were either transfected with control or target-specific siRNA and grown for three days under serum conditions. Reduced cell proliferation after target knock-down is expressed in percentaged inhibition relative to control.

Target depletion by RNAi of the high affinity targets ROS1, NEK9, BMP2K, NME4, FAK, AURKB and TBK1 resulted in a strong inhibition or even a complete block of cell proliferation. The strongest impact was observed for ROS1, NEK9, BMP2K and FAK. To a lesser but still significantly relevant extent, inhibition of cell proliferation was observed for AURKA, AURKB, TBK1, RPS6KA1 and RPS6KA3. Similar results were seen for ROS1 and NEK9 using a second siRNA sequence. Again, the RNAi experiments were performed in cancer cell lines of different tissue origins showing similar results. In accordance to the universal importance of these proteins for cancer cell viability and cell growth, high affinity SU11248 targets play also a critical role in cell proliferation promoting unlimited cell growth of cancer cells.

Taken together, newly identified high affinity targets of the small-molecule kinase inhibitor SU11248 play crucial roles in cancer cell viability, cancer cell growth and proliferation. Functional characterization by RNAi experiments showed their significant biological relevance for cancer cells thus being potential sites of SU11248 action critical for its activity in tumor cells.

7.9.1.2 High affinity SU11248 targets – their relevance for cancer cell survival

Being involved in the regulation of cancer cell viability and growth the question emerged whether high affinity SU11248 targets are also implicated in cancer cell survival. Therefore the effects of target depletion by RNAi experiments on programmed cell death effects were assessed by measuring caspase-3/7-activity as well as the number of dead cells by flow cytometry upon the functional elimination of respective targets.

Programmed cell death is regulated and executed by caspases interacting in signalling cascades. Depending on the genetic background of the cell two main effector caspases are involved in promoting the apoptotic

signal, Caspase 3 and Caspase 7, respectively (Bratton and Cohen, 2001; Kumar, 2007; Miller, 1997; Takahashi, 1999; Thornberry, 1997). Therefore, measuring intrinsic caspase-3/7-activity is a direct measure for apoptotic cells. The results are shown in Figure 67.

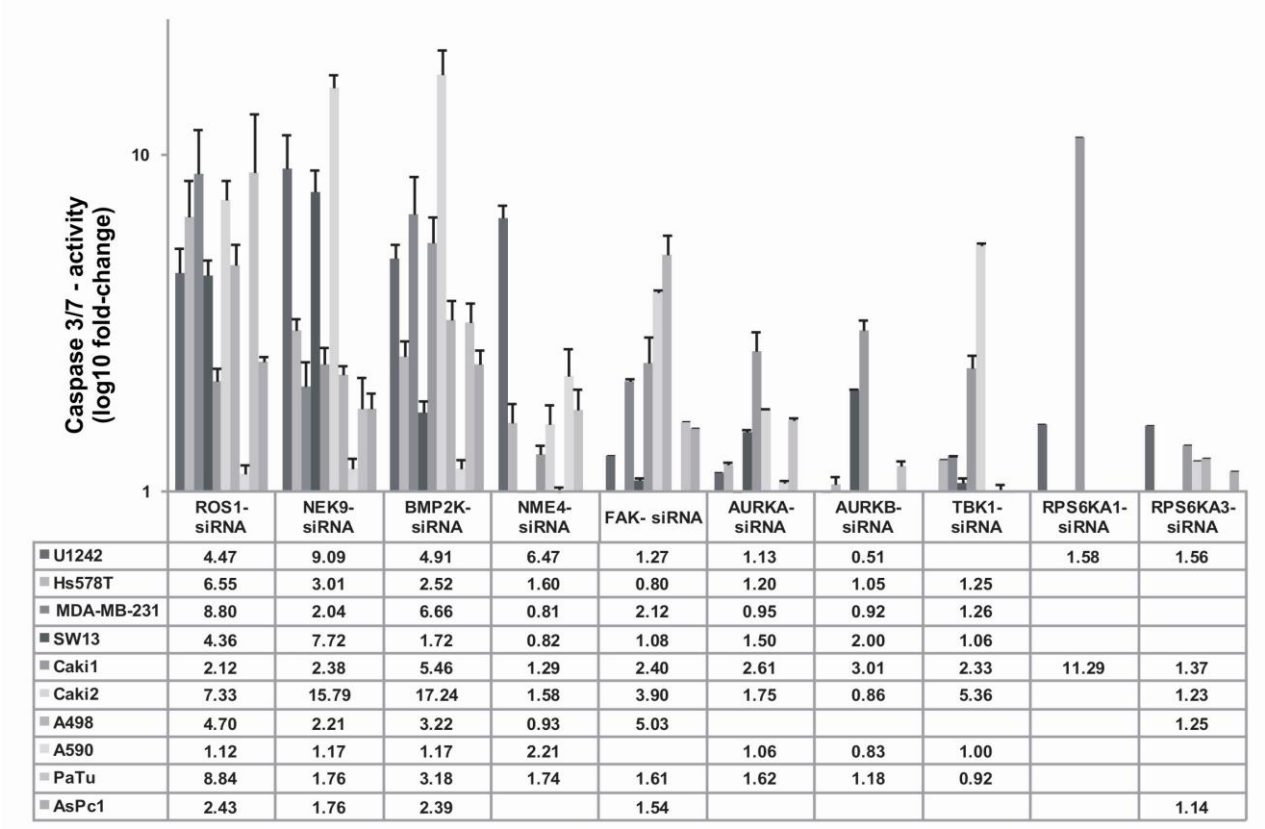

	ROS1-siRNA	NEK9-siRNA	BMP2K-siRNA	NME4-siRNA	FAK- siRNA	AURKA-siRNA	AURKB-siRNA	TBK1-siRNA	RPS6KA1-siRNA	RPS6KA3-siRNA
U1242	4.47	9.09	4.91	6.47	1.27	1.13	0.51		1.58	1.56
Hs578T	6.55	3.01	2.52	1.60	0.80	1.20	1.05	1.25		
MDA-MB-231	8.80	2.04	6.66	0.81	2.12	0.95	0.92	1.26		
SW13	4.36	7.72	1.72	0.82	1.08	1.50	2.00	1.06		
Caki1	2.12	2.38	5.46	1.29	2.40	2.61	3.01	2.33	11.29	1.37
Caki2	7.33	15.79	17.24	1.58	3.90	1.75	0.86	5.36		1.23
A498	4.70	2.21	3.22	0.93	5.03					1.25
A590	1.12	1.17	1.17	2.21		1.06	0.83	1.00		
PaTu	8.84	1.76	3.18	1.74	1.61	1.62	1.18	0.92		
AsPc1	2.43	1.76	2.39		1.54					1.14

Figure 67 Induction of programmed cell death after knock-down of high affinity SU11248 targets. Target depletion was achieved by transient RNAi experiments and the effect on cancer cell survival was measured 72h post-transfection by caspase-3/7-activity. Cancer cells were either transfected with control or target-specific siRNA and grown for three days under serum conditions. Caspase-3/7-activity in siRNA transfected cells is expressed as fold-change in relation to control cells on a log10-scale. Increased programmed cell death after target knock-down is averaged over three to five independent experiments (error bars: s.e.m.).

Caspase activity analysis showed a strong impact for ROS1, NEK9 and BMP2K on cancer cell survival. Their depletion by siRNA resulted in an increased caspase-activity in a variety of cancer cell lines of different tissue origins which indicates a fundamental function of these high affinity SU11248 targets in the survival of cancer cells. Inhibition of these kinases by SU11248 might be one molecular mechanistic explanation for the strong apoptosis inducing effect of SU11248 in a broad spectrum of cancer cell lines. Beside this, also other SU11248 targets where shown to be involved in cancer cell survival but to a lesser extent as observed for the kinases NME4, FAK, AURKA, AURKB, TBK1 and RPS6KA1 (Figure 67). For the high affinity target RPS6KA3 no apoptosis relevance could be seen.

To proof the target relevance of high affinity SU11248 targets in apoptosis a second assay was used to determine dead cells after target depletion. Flow cytometric analysis confirmed the targets` function in cancer cell survival. Cell cycle distribution and apoptotic cells after target knock-down were measured using

a propidiumiodide staining method. Apoptotic cells were quantified from the subG$_1$-peak. Quantification results of apoptosis rates after target knock-down are shown in Figure 68.

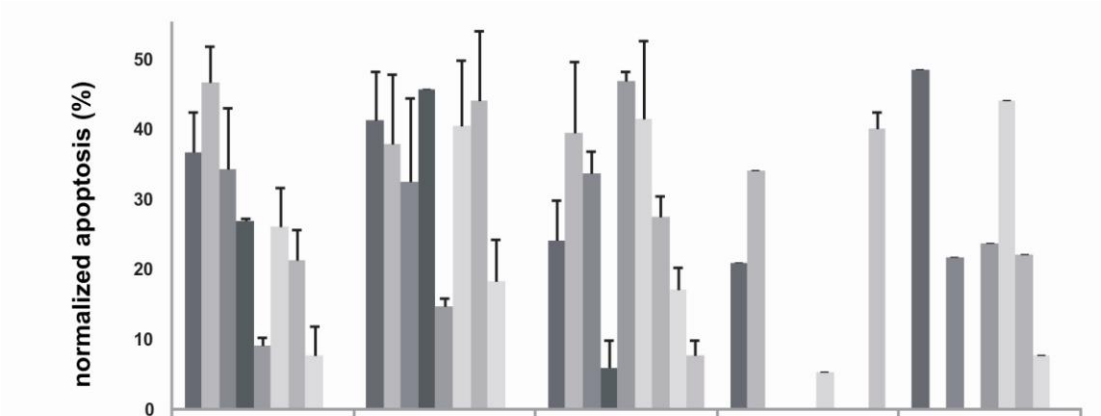

	ROS1- siRNA	NEK9- siRNA	BMP2K- siRNA	NME4- siRNA	FAK- siRNA
U1242	36.60	41.06	23.93	20.87	48.33
Hs578T	46.60	37.80	39.36	34.01	
MDA-MB-231	34.17	32.42	33.60		21.63
SW13	26.83	45.53	5.73	0.00	
Caki1	8.90	14.55	46.81		23.51
Caki2	26.02	40.42	41.42	5.23	43.99
A498	21.23	44.00	27.35		22.04
AsPc1	7.68	18.23	17.07		7.65
PaTu	0.00	0.00	7.61	39.92	

Figure 68 Induction of apoptosis after knock-down of high affinity SU11248 targets.
Target depletion was achieved by transient RNAi experiments and the effect on cancer cell survival was measured 72 h post-transfection by flow cytometry. Cancer cells were either transfected with control or target-specific siRNA and grown for three days under serum conditions. Dead cells were quantified from the subG$_1$-peak seen in the FACS image using the analyzing software CellQuestPro. Apoptosis induction upon target knock-down is expressed in percent relative to mock-treated cells and averaged over two to three independent experiments (error bars: s.e.m.).

Morphological changes of cancer cells transfected with ROS1, NEK9 and BMP2K siRNA are shown in Figure 69. The cell number is dramatically reduces after target depletion and correlates with the high anti-proliferative and apoptosis inducing effects observed in these cells after target knock-down.

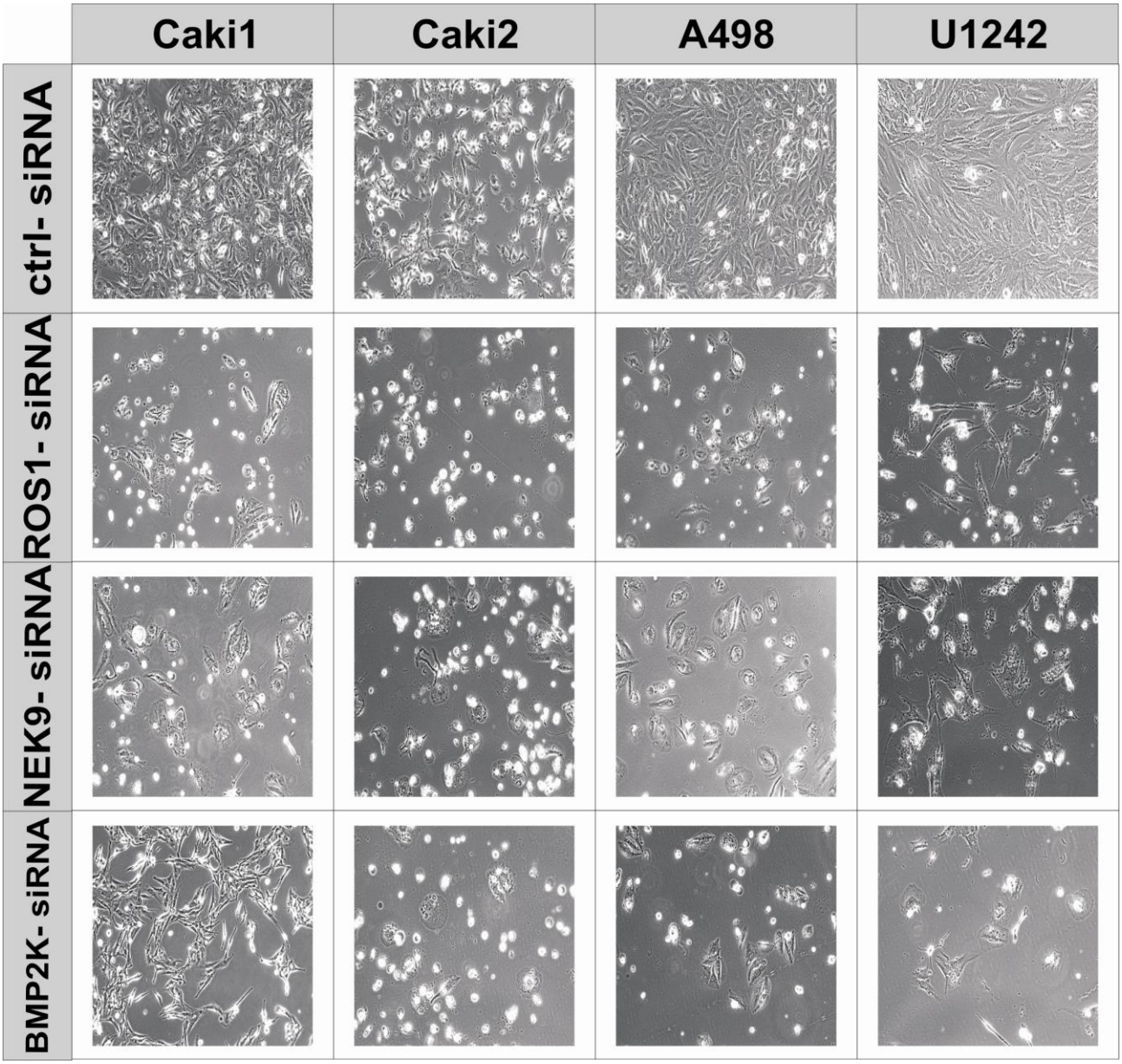

Figure 69 Morphological changes of cancer cells of different tumor indications transfected with siRNA against ROS1, NEK9 and BMP2K for 72h.
The kidney cancer cell lines Caki1, Caki2, A498 and the glioblastoma cell line U1242 were seeded in 6-well flat-bottom cell culture plates 24h prior to transfection, cultured under serum conditions and transfected with either ctrl- or target siRNA against ROS1, NEK9 and BMP2K. Photomicrographs were taken 3 days post-transfection (x4).

7.9.2 Functional correlation of target expression and SU11248 efficacy in cancer cell lines

The functional characterization of identified high affinity SU11248 targets with RNAi experiments showed a strong correlation between the target relevance, target inhibition by SU11248 and observed phenotypes of SU11248 treatment on cancer cell lines. Nevertheless, the knowledge of a target´ s function alone is not sufficient to prove its relevance for the SU11248 activity. To test whether identified high affinity targets are truly relevant sites of molecular action and important for the drug´ s efficacy a combination of RNAi experiments and inhibitor treatment was used. This approach reveals direct links between target function, target expression and SU11248 sensitivity and efficacy.

Cancer cells were transfected with either control or target-specific siRNA and treatment with increasing SU11248 concentrations. SU11248 efficacy on cancer cell viability was measured using MTT. The depletion of high affinity SU11248 targets with RNAi significantly decreased the SU11248 efficacy in the respective cell line showing that the respective target is highly relevant for SU11248 activity *in vitro* (Figure 70).

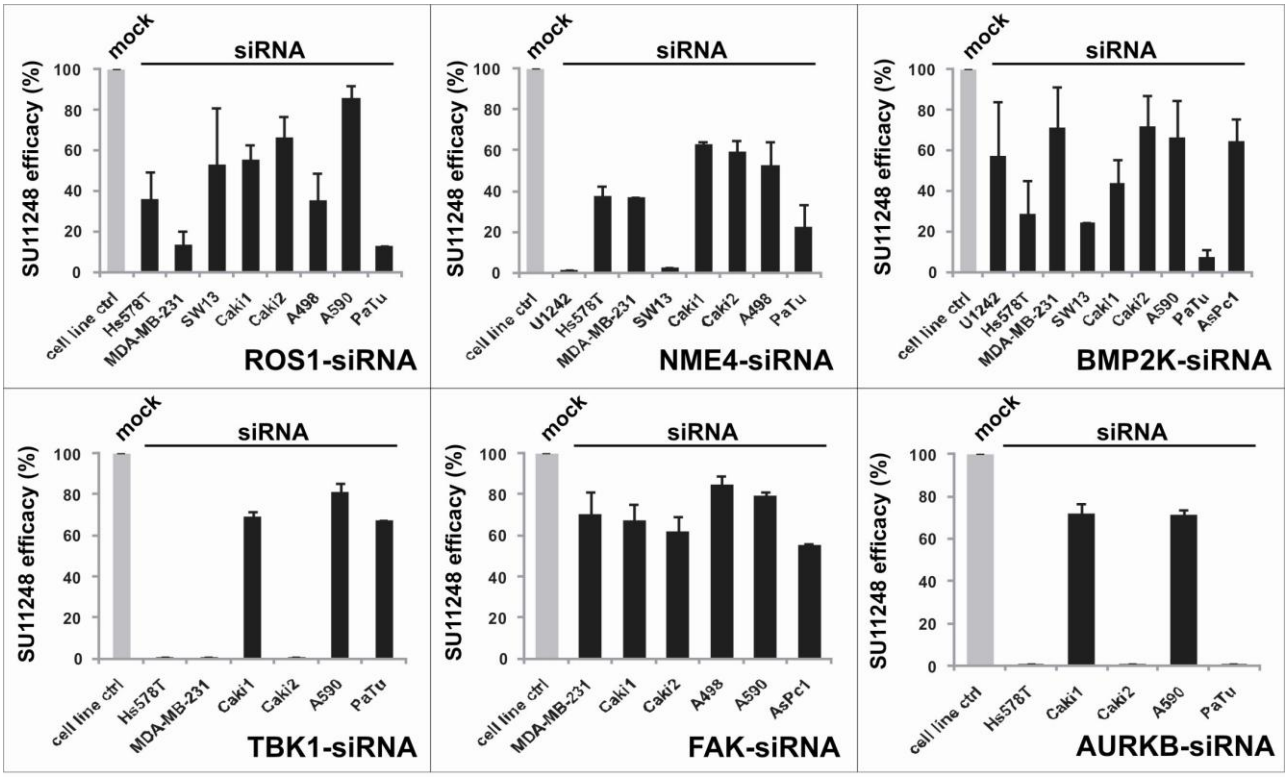

Figure 70 Depletion of high affinity SU11248 targets with RNAi reduces the drug´ s activity in cancer cell lines of different tissue origins.
Target depletion was achieved by transient RNAi experiments and the SU11248 efficacy was measured using a standard MTT colorimetric method. Cancer cells were either transfected with control or target-specific siRNA, grown for two days under serum conditions and treated with increasing SU11248 concentrations for 72h. SU11248 efficacy is shown at 5 µM and expressed in percent relative to mock-transfected, SU11248 treated cells. Results are averaged over three to five independent experiments (error bars: s.e.m.).

SU11248 activity is expressed in percentaged inhibition efficacy on cancer cell viability measured by a colorimetric MTT-assay. The SU11248 efficacy in normal, control-transfected cells is set to one hundred percent (grey bar) and the drug efficiency after target depletion in the respective cell line is shown relative to the wildtype SU11248 effect. For six high affinity SU11248 targets a correlation between target expression and SU11248 efficacy could be shown. Depending on the genetic background of a certain cancer cell line as well as the target relevance in those cells, the reduction of SU11248 activity after target depletion differed from cell line to cell line. Nonetheless, the tendency for each target was similar over a broad spectrum of cancer cell lines from different tumor types thereby revealing a universal target function and importance for the anti-tumor effect of SU11248.

Using Protein Kinase C (PKC) and Protein Kinase A (PKA) inhibitors (Bisindolylmaleimide I and 14-22 Amide, respectively) further targets being relevant and essential for the SU11248 efficacy on tumor cells could be identified. The results are shown in Figure 71.

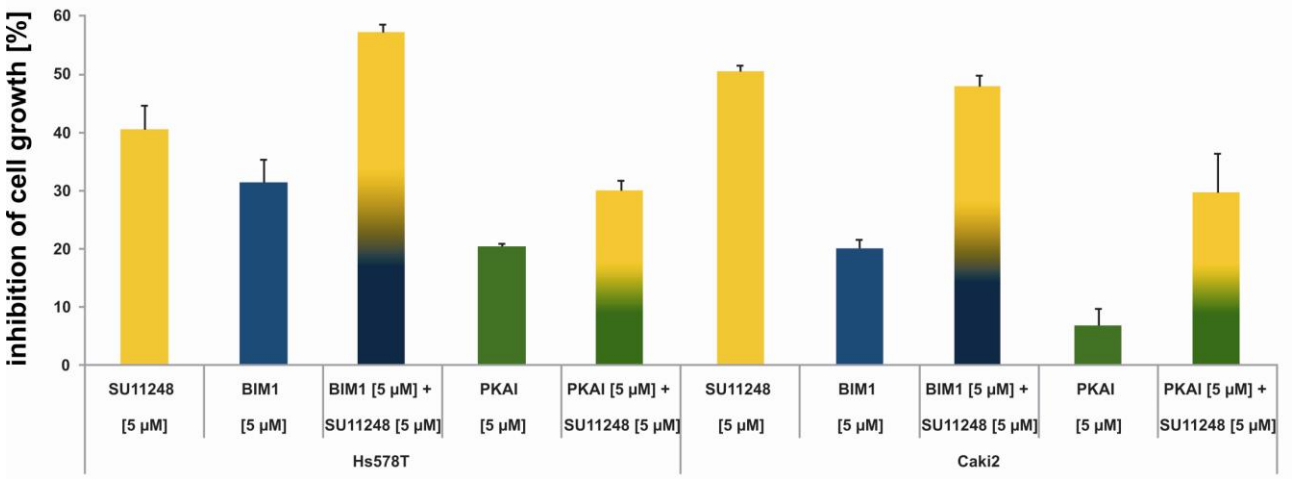

Figure 71 SU11248 exerts its anti-proliferative effects on cancer cells through PKC and PKA involved signalling pathways.
The application of PKC and PKA inhibitors in combination with SU11248 led to competitive effects of these inhibitors on cancer cell growth as shown by a colorimetric MTT-assay after 72h of inhibitor treatment. Would the inhibitors act independently from each other via distinct pathways or targets in general, an additive effect would be observed in the combined application. In contrast, the combination of 5 µM SU11248 and either 5 µM of the PKC (BIM1) or 5 µM of the PKA inhibitor (PKAI) resulted in reduced SU11248 inhibitory effects in the cancer cell lines Hs578T (breast) and Caki2 (kidney).

The combination of SU11248 and the PKC inhibitor BIM1 and the PKA inhibitor PKAI, respectively, reduced the SU11248 efficacy on cancer cell growth in the treated breast cancer cell line Hs578T and kidney cancer cell line Caki2. These results give a hint for PKC and PKA as relevant or even essential target proteins for the SU11248 efficacy within tumor cells.

Taken together, this comprehensive functional target analysis revealed newly identified SU11248 kinase targets as potential general markers of SU11248 responsiveness and very important sites of action of the small-molecule kinase inhibitor within cancer cells. The expression levels of these kinase target proteins in tumors may be taken as biomarkers for drug response prediction in the clinic. They might help in an optimal patient selection and improve SU11248 based targeted cancer therapy.

Taken together, these data suggest that kinases like ROS1, BMP2K, NEK9, NME4, AURKA, AURKB, TBK1, RPS6KA1, RPS6KA3 and FAK might be, amongst others, the essential SU11248 targets relevant for the observed phenotype such as cell cycle block, induction of apoptosis and migration inhibition after SU11248 treatment in a broad variety of cancer cells from different tissue origins. Whenever a functional relevance of a certain target in the cancer cell line was observed it led to a reduced SU11248 sensitivity in this cell line after target depletion by RNAi. SU11248 exerts its anti-proliferative and apoptosis-inducing effect through the essential high affinity targets ROS1, NME4, BMP2K, TBK1, AURKB and FAK.

7.10 Functional characterization of the receptor tyrosine kinase ROS1

7.10.1 ROS1 plays a key role in cancer cell proliferation and survival

Using RNAi for a functional screening and characterization of high affinity SU11248 targets, the receptor tyrosine kinase ROS1 was identified as highly relevant and essential for proliferation and survival of cancer cell lines of different tumor types, including brain, breast, kidney, lung and pancreas. It seems to have a universal function in cancer cell homeostasis and plays a key role in cancer cell viability. Its depletion drives tumor cells into apoptosis. A summary of the biological characterization and functional relevance of ROS1 *in vitro* is provided in Figure 72.

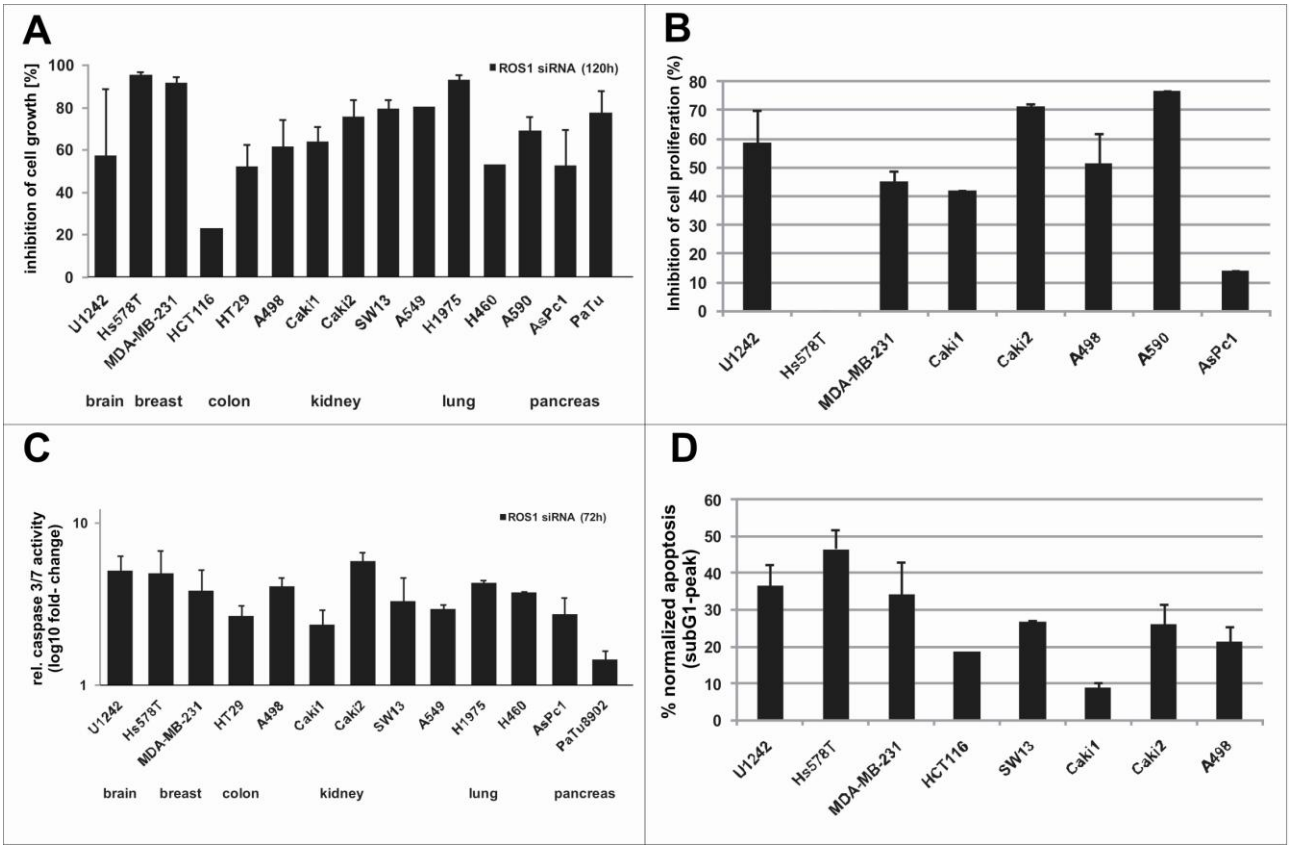

Figure 72 ROS1 function in cancer cell lines of different tumor types.
Loss-of-function screen of the receptor tyrosine kinase ROS1 with siRNA, reveals its broad and essential role in cancer cell proliferation and survival in a wide spectrum of cancer cell lines from different tumor types, including brain (U1242), breast (Hs578T, MDA-MB-231), colon (HCT116), kidney (SW13, Caki1, Caki2, A498) and pancreas (A590, AsPc1, PaTu). Cells were either transfected with target-specific or control-siRNA, grown under serum conditions for three days and cellular effects of target depletion monitored by a colorimetric MTT method for the inhibition of cell viability (A), a BrdU incorporation assay for cell proliferation (B) and FACS (C) and caspase-3/7-activtiy assay (D) for the induction of apoptosis, respectively. Results are the average of two to five independent experiments (error bars: s.e.m.).

The knock-down of ROS1 in cancer cell lines from brain, breast, colon, kidney and pancreas resulted in a strong inhibition of cell proliferation as well as a significant induction of programmed cell death as observed by an augmented caspase -3/7-activtiy after target depletion. Similar results were obtained in non-small cell lung cancer cell lines.

Figure 73 shows the morphological changes of cancer cells transfected with ROS1 siRNA after 72h. The cell number is dramatically decreased in comparison to control transfected cells and the cell shape is bigger, including less cytoplasm and an expanded nucleus.

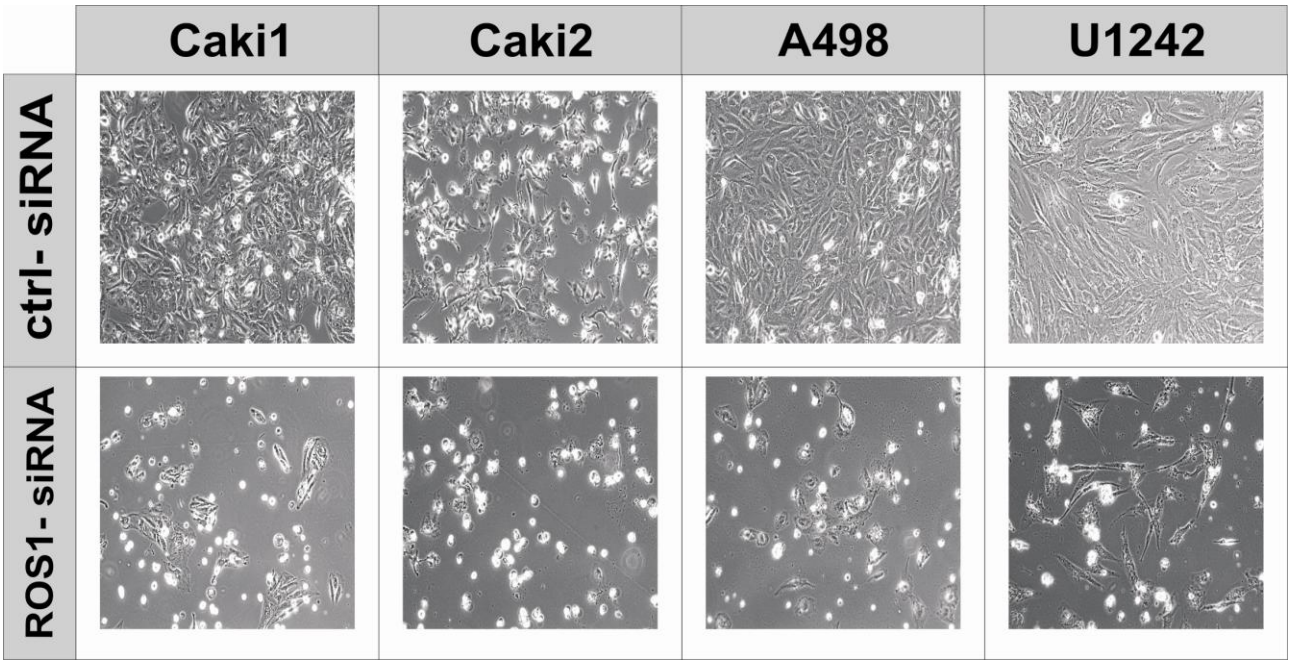

Figure 73 Morphological changes of cancer cells after RNAi of the receptor tyrosine kinase ROS1.
The depletion of the receptor tyrosine kinase ROS1 by RNAi leads to inhibition of cell proliferation and programmed cell death in cancer cells of different tumor types. The kidney cancer cell lines Caki1, Caki2, A498 and the glioblastoma cell line U1242 were transfected with either ROS1 or control siRNA and photomicrographs (x4) were taken 72h post-transfection. Cell numbers are significantly decreased after target knock-down. The cell shape of knock-down cells is bigger and the cytoplasmic-to-nuclear volume ratio much smaller than in control transfected cells.

In the literature, ROS1 is described to be a potent oncogene in glioblastoma and was already observed in 1987 to be overexpressed in glioblastoma-derived cell lines.

Glioblastoma multiforme is the most advanced astrocytic neoplasm, and is one of the most aggressive human cancers with a median survival of less than one year. Despite decades of therapeutic research, effective chemotherapeutic treatment for high grade astrocytomas is not yet available, and patient care ultimately focuses on palliative management (Hess et al., 2005; Holland, 2000; Ohgaki and Kleihues, 2007)

In a survey of 45 different human tumor cell lines, the tyrosine kinase ROS1 was found to be expressed in glioblastoma-derived cell lines at high levels, while not expressed at all or expressed minimally in the remaining cell lines (Birchmeier et al., 1987; Rabin et al., 1987). ROS1 kinase is a receptor tyrosine kinase that is homologous to the Drosophila Sevenless tyrosine kinase receptor (Charest et al., 2003a; Charest et al., 2003b; Nagarajan et al., 1986; Tessarollo et al., 1992). It is encoded by ROS1-gene which is located at the chromosome 6 region 6q16 → 6q22. This region is involved in non-random chromosomal arrangements in specific neoplasias. A microdeletion at 6q21 results in the fusion of FIG, a gene coding for a Golgi apparatus-associated protein, to the kinase domain of the proto-oncogene ROS1. The fused protein product

FIG-ROS is a potent oncogene, and its transforming potential resides in its ability to interact with and become localized at Golgi apparatus. The ectopic expression of ROS1 receptor protein has been reported mainly in meningiomas and astrocytomas (25% of low grade and 30% of malignant glioma tumors) suggesting a key role for ROS1 kinase in these CNS malignancies (Charest et al., 2003a; Jun et al., 2009). Hence the targeting of the tyrosine kinase ROS1 could be a useful strategy for treatment of astrocytic neoplasms. Moreover, ROS1 was shown to be rate-limiting for promoting cell proliferation and survival of breast, lung and kidney cancer cells in a shRNA loss-of-function screen (Grueneberg et al., 2008).

To get a comprehensive understanding of the cancerous function of ROS1, it is important to know its implication in different tumor types. As such, an expression profile of the kinase in cancer cell lines derived from a variety of different cancer indications serves as a first indication of tumor relevance. Cancer driving genes are often overexpressed in malignant cells compared to normal surrounding cells of the tumor. Overexpression is often associated with an oncogenic function of the respective protein. Therefore an expression screening of ROS1 by macro-gene arrays as well as on the protein level was performed. The receptor tyrosine kinase ROS1 is widely expressed among cancer cell lines of a broad spectrum of different tumor indications. Its expression was observed in cancer cell lines derived from brain, breast, colon, kidney, lung, ovary, pancreas, prostate and skin (Figure 74).

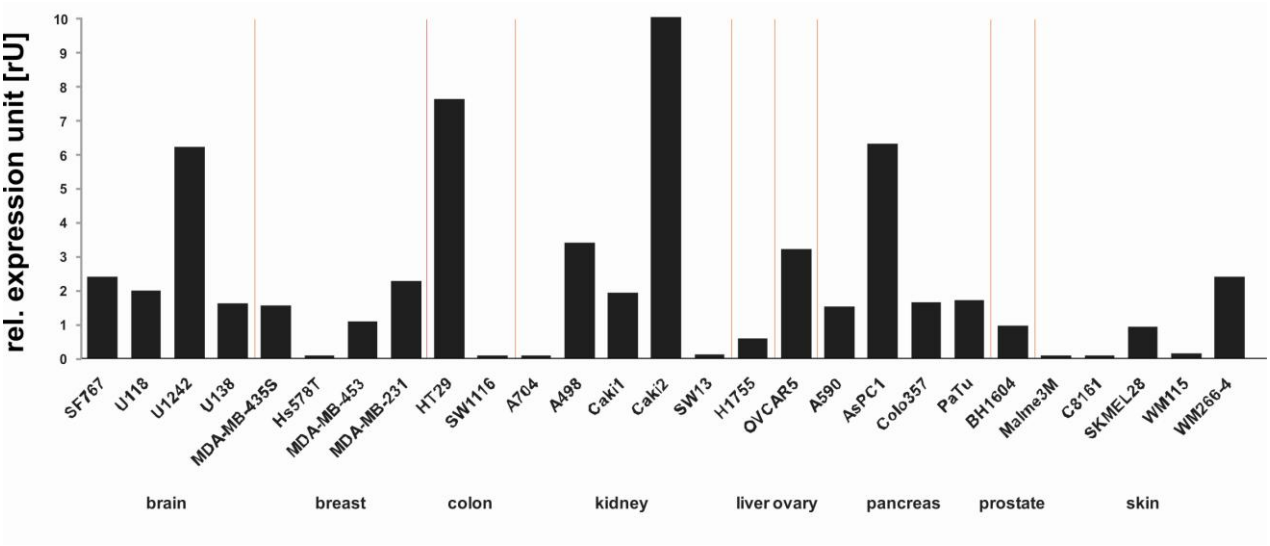

Figure 74 ROS1 gene expression in cancer cell lines of different tumor indications.
ROS1 gene expression in cancer cell lines of different tumor types was screened using in house macro-gene-arrays. Expression levels are expressed in relative expression units [rU] normalized to total expression on the gene-arrays.

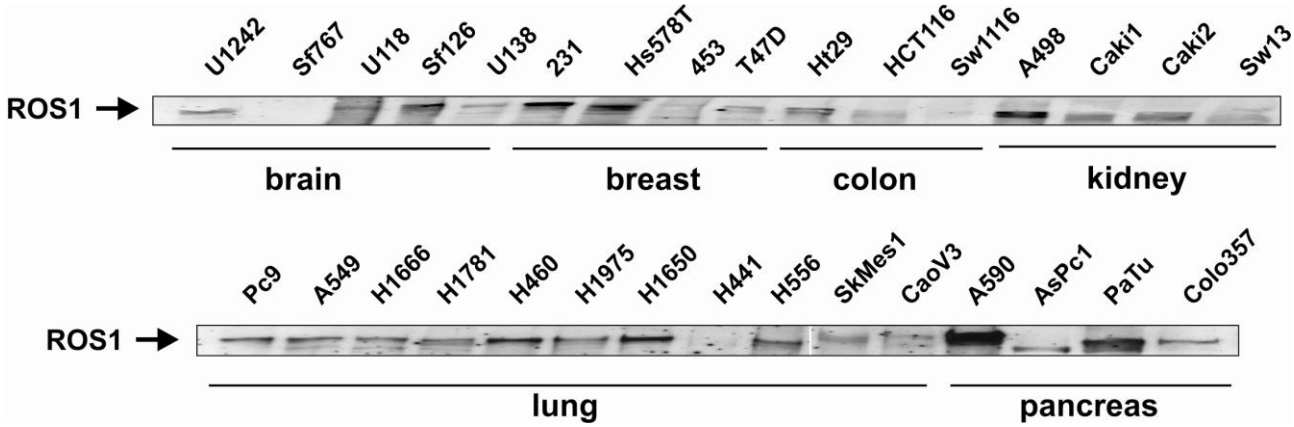

Figure 75 ROS1 protein expression in cancer cell lines of different tumor indications.

The RNA expression was proved on the protein level using Western Blot Analysis. Protein expression of the receptor tyrosine kinase ROS1 is shown in Figure 75.

In summary, the receptor tyrosine kinase ROS1 could be shown to be widely expressed in cancer cell lines derived from different human tumors, indicating a potential universal role of the kinase in cancer cell proliferation and survival. Shown to be implicated in tumors of the brain, such as glioblastoma multiforme, the tumor relevance of ROS1 in other indications has to be proven in human primary tumors. This can be achieved by performing tissue arrays staining for the expression of ROS1 in tumor samples of diverse origin.

A first hint for a function in kidney cancer is given by the fact that the receptor tyrosine kinase ROS1 is highly expressed in primary renal cell carcinoma tumor samples but very weak or not at all in the normal tissue from the same organ (Figure 76).

Cancer specific expression is important for an oncogenic potential of a certain kinase and a prerequisite for potential target-specific cancer therapy with small-molecule kinase inhibitors in future.

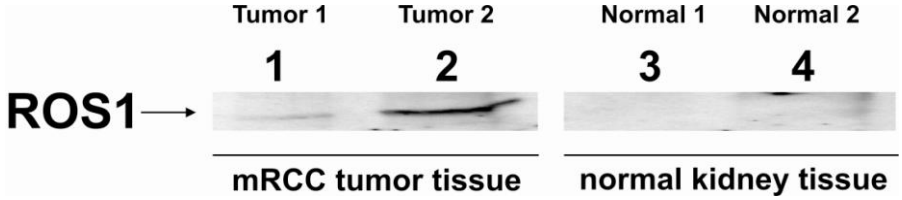

Figure 76 ROS1 protein expression in metastatic renal cell carcinoma (mRCC) tumors and normal kidney tissues from the same patients.

The expression of the receptor tyrosine kinase ROS1 in normal and cancerous tissues of the kidney was analyzed by immunoblotting. Equal amounts of protein samples were separated by 1D-SDS-gel electrophoresis and probed for ROS1 with a goat-anti-ROS1 antibody.

7.10.2 ROS1 expression seems to correlate with chemoresistance to Taxol treatment of cancer cell lines from different tumor types

Since the receptor tyrosine kinase ROS1 is highly implicated in cancer cell proliferation and survival the question rose whether ROS1 might play a role in drug sensitivity of cancer cells towards standard-of-care medicine. Do high protein expression levels of ROS1 promote resistance to chemotherapeutic agents such as Taxol, Cisplatin, Doxorubicin and Dacarbazine? To test this hypothesis, chemotherapeutics of different functional groups were used. In several studies, it has been shown that overexpression of certain cancer related proteins such as receptor tyrosine kinases including HER3, is associated with drug resistance. Down-regulation of HER3 synergistically enhances dacarbazine-induced apoptosis in melanoma cell lines (Reschke et al., 2008). Overexpression of receptor tyrosine kinases and oncogenes in general is connected to augmented signal events leading to aberrant activation of signaling cascades driving tumor chemoresistance.
The glioblastoma cancer cell lines U138, U1242, the kidney cancer cell lines Caki1, Caki2, A498, the breast cancer cell lines Hs578T, MDA-MB-231 and the pancreas cancer cell lines A590 and AsPc1 were treated with the chemotherapeutic agents Dacarbazine, Taxol, Cisplatin and Doxorubicin and their apoptotic phenotype after treatment surveyed by FACS analysis measuring dead cells based on a propidiumiodide staining. Drug sensitivity was correlated to ROS1 expression levels and only for Taxol a significant accordance was seen between response rate and protein levels. Results are shown in Figure 77. Response rates to drug treatment are expressed in percentaged apoptosis and cellular ROS1 protein expression was divided into three distinct classes of low (+), medium (++) and high expression (+++). An overview is given in Table 20. No clear correlations were observed for the chemotherapeutics Cisplatin, Dacarbazine and Doxorubicin.

Table 20 ROS1 protein expression in cancer cell lines of different tumor types
Protein expression was analyzed by Western Blot Analysis and divided into three distinct classes of low (+), medium (++) and high expression (+++).

cancer cell line	tissue	ROS1 expression
U138	brain	+
Hs578T	breast	+
HT29	colon	+
Caki1	kidney	+
SW13	kidney	+
U1242	brain	++
MDA-MB-231	breast	++
Caki2	kidney	++
A498	kidney	+++
A590	pancreas	+++
AsPc1	pancreas	+++

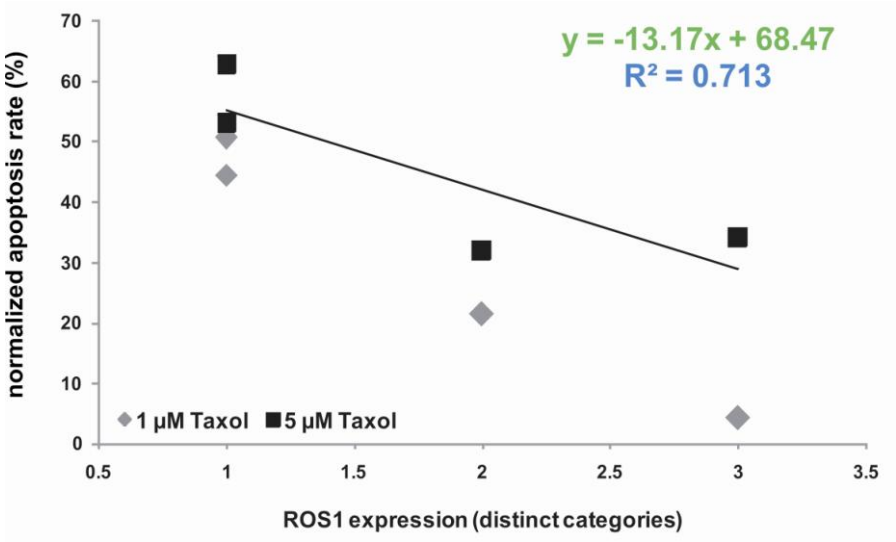

Figure 77 Increasing ROS1 protein expression levels reduce the sensitivity of cancer cells towards the chemotherapeutic agent Taxol.
The glioblastoma cancer cell lines U138, U1242, the kidney cancer cell lines Caki1, Caki2, A498, the breast cancer cell lines Hs578T, MDA-MB-231 and the pancreas cancer cell lines A590 and AsPc1 were treated under serum conditions with two different concentrations (1 and 5 μM) of the chemotherapeutic agent Taxol and their apoptotic phenotype after treatment was surveyed by FACS analysis measuring dead cells based on a propidiumiodide staining. Drug sensitivity of tested cancer cell lines was plotted against their respective ROS1 expression levels. Response rates to drug treatment are expressed in percentaged normalized apoptosis and cellular ROS1 protein expression was divided into three distinct classes of low (1), medium (2) and high expression (3) on the x-axis. For both Taxol concentrations a negative correlation of response rate and the amount of cellular ROS1 was observed. The correlation coefficient was r^2= 0.713.

Protein expression levels negatively correlate with drug sensitivity and elevated ROS1 expression leads to chemoresistance of cancer cells of different tumor types to the chemotherapeutic agent Taxol.

Taxol (Paclitaxel) is a mitotic inhibitor used in cancer chemotherapy. It was discovered in a National Cancer Institute program at the Research Triangle Institute in 1967 when Monroe E. Wall and Mansukh C. Wani isolated it from the bark of the Pacific Yew tree, *Taxus brevifolia* and named it 'taxol'. Taxol is now used to treat patients with lung, ovarian, breast cancer, head and neck cancer, and advanced forms of Kaposi's sarcoma. Taxol stabilizes microtubules and as a result, interferes with the normal breakdown of microtubules during cell division. Together with docetaxel, it forms the drug category of the taxanes.

Further research has indicated that Taxol induces programmed cell death (apoptosis) in cancer cells by binding to an apoptosis stopping protein called Bcl-2 (B-cell leukemia 2) and thus arresting its function.

In addition to stabilizing microtubules Taxol may act as a molecular mop by sequestering free tubulin effectively depleting the cells supply of tubulin monomers and/or dimers. This activity may trigger the aforementioned apoptosis.

One common characteristic of most cancer cells is their rapid rate of cell division. In order to accommodate this, the cytoskeleton of a cell undergoes extensive restructuring. Taxol is an effective treatment for aggressive cancers because it adversely affects the process of cell division by preventing this restructuring. Cancer cells are also destroyed by the aforementioned anti-Bcl-2 mechanism. Other cells are also affected

adversely, but since cancer cells divide much faster than non-cancerous cells, they are far more susceptible to Taxol treatment.

Comparing the molecular function of Taxol and the fact that ROS1 is triggering cancer cell survival one explanation for the negative correlation of ROS1 expression and Taxol sensitivity of cancer cells could be the assumption that ROS1 exerts its anti-apoptotic function via Bcl-2 and that an aberrant expression and activation of the receptor tyrosine kinase leads to increased Bcl-2 expression levels within the cell, counteracting the programmed cell death inducing effect of Taxol, that binds to and inactivates the pro-survival factor Bcl-2. Caused by elevated ROS1 signalling the balance between the amount of drug and Bcl-2 levels in the cell is pushed in the direction of free and active Bcl-2 thereby decreasing the drug´ s efficacy.

The exact mechanism of action of ROS1 has still to be elucidated with further experiments. One possibility is the identification of ROS1 interaction partners acting downstream of the receptor tyrosine kinase.

7.10.3 Identification of ROS1 interaction partners with mass spectrometry

The receptor tyrosine kinase ROS1 plays a key role in cancer cell proliferation and survival as shown by RNAi experiments. Based on these cancer relevant functions it is of great interest to reveal underlying molecular mechanisms by which ROS1 exerts its cellular function. Since receptor tyrosine kinase signalling is organized in signalling cascades which mediate extracellular signals, such as ligand stimulation, to the nucleus, interaction partners of the receptor are important. To identify potential interaction partners involved in the signalling network connected to ROS1, a quantitative mass-spectrometry based immunoprecipitation strategy was used. This method allows for the identification and affinity estimation of potential binding partners. It combines SILAC-based quantitative mass spectrometry for binding partner identification with a two-step affinity purification protocol for ROS1 with an anti-ROS1 antibody directly from cell lysates. The workflow is shown in Figure 78. Based on the expression analysis of ROS1, the kidney cancer cell line A498 was employed for the detection of interaction partners. A498 cells were metabolically labeled with either normal arginine and lysine (Arg^0/Lys^0) or combinations of isotopic variants of the two amino acids (Arg^6/Lys^4, Arg^{10}/Lys^8). The Arg^0/Lys^0-encoded cell lysates was incubated with proteinA beads displaying immobilized ROS1 antibody, whereas Arg^6/Lys^4-labelled extract was added to control beads devoid of antibody. In case of the Arg^{10}/Lys^8-encoded lysate, supernatant from the first binding to ROS1 antibody-beads was subjected to a second incubation with the same amount of antibody. The elution fractions were pooled, proteins separated by 1D-SDS-PAGE, trypsin-digested and analyzed by LC/MS. Protein identification and quantification was done with the MaxQuant software (Cox and Mann, 2008). Binding patterns for three distinct target-affinities of interaction partners are indicated in the lower three panels. High affinity interaction partners are enriched in the first elution fraction, low affinity interaction partners also bind in the second incubation with ROS1 antibody and unspecific background binders are equally retained in both fractions as well as the control-beads devoid of antibody. Cell lysis was performed under native conditions to maintain protein complexes formed within the intact cell. The workflow is illustrated in Figure 78.

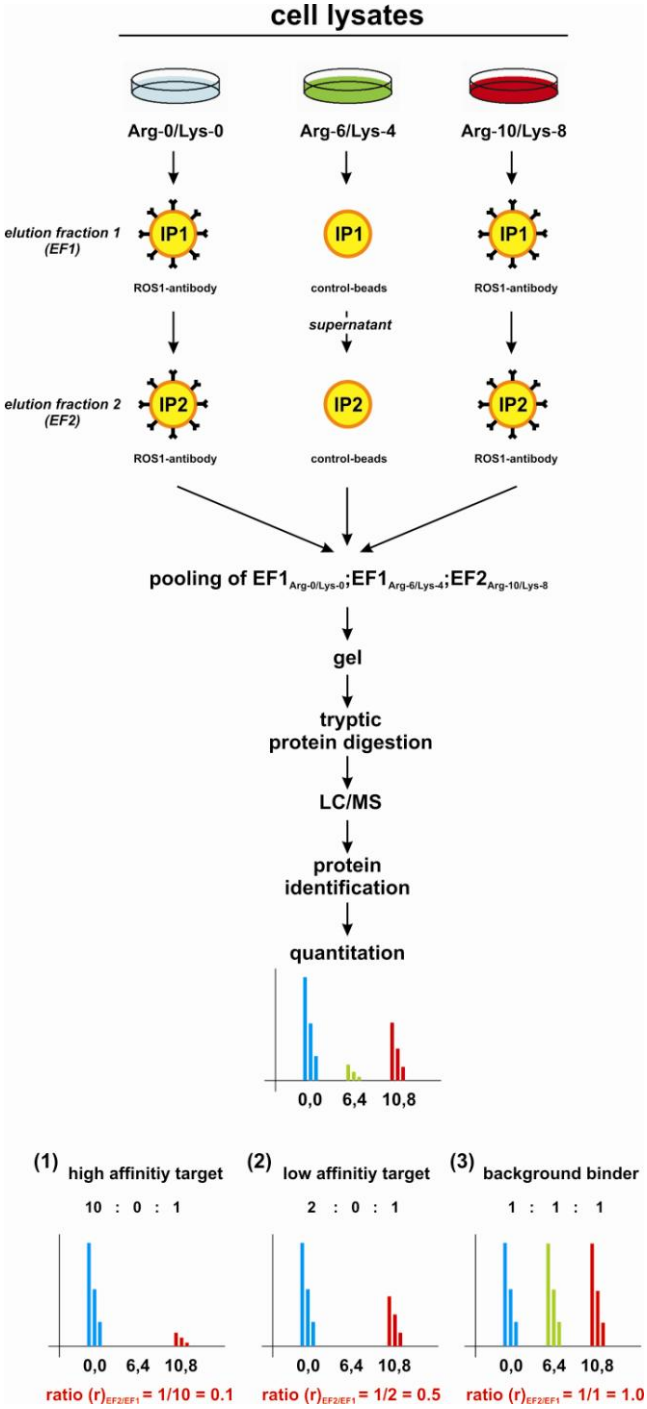

Figure 78 Workflow of ROS1 interaction partner identification based on quantitative mass spectrometry combined with a two-step immunoprecipitation ROS1 purification strategy.
The kidney cancer cell line A498 was metabolically labelled with either normal arginine and lysine (Arg^0/Lys^0) or combinations of isotopic variants of the two amino acids (Arg^6/Lys^4, Arg^{10}/Lys^8). The Arg^0/Lys^0-encoded cell lysates was incubated with the proteinA beads displaying immobilized ROS1 antibody, whereas Arg^6/Lys^4-labelled extract was added to control beads devoid of antibody. In case of the Arg^{10}/Lys^8-encoded lysate, supernatant from the first binding to ROS1 antibody was subjected to a second incubation with the same amount of antibody. The elution fractions were pooled, proteins separated by 1D-SDS-PAGE, trypsin-digested and analyzed by LC/MS. Protein identification and quantification was done with the MaxQuant software (Cox and Mann, 2008). Binding patterns for three distinct target-affinities of interaction partners are indicated in the lower three panels. High affinity interaction partners are enriched in the first elution fraction, low affinity interaction partners also bind in the second incubation with ROS1 antibody and unspecific background binders are equally retained in both fractions as well as the control-beads devoid of antibody.

Potential ROS1 interaction partners, detected with at least one unique peptide in the mass-spectrometry analysis and a significance of $p<0.01$, are listed in Table 21.

A background-cut off for the ratio between the control- and antibody-fraction was set to $r \leq 0.5$. Proteins binding to control-beads with a greater ratio than 0.5 were considered to be unspecific background binders captured on the beads.

Table 21 ROS1 interaction partners detected by quantitative mass-spectrometry.
Background- and affinity-cut-offs for specific binding partners were set to $r \leq 0.5$ (ratio M/L and ratio H/L, respectively).

Protein Names	Gene Names	GOBP Names	PEP	Ratio M/L	Ratio H/L
Acyl-CoA dehydrogenase	ACADVL	organic acid metabolic process	0.00	0.3	0.25
Aldo-keto reductase family 1 member B10	AKR1B10	aldehyde metabolic process	0.00	0.4	0.10
Delta-1-pyrroline-5-carboxylate synthetase	ALDH18A1	organic acid metabolic process	0.00	0.1	0.11
Retinal dehydrogenase 1	ALDH1A1	aldehyde metabolic process	0.00	0.4	0.09
Fructose-bisphosphate aldolase A	ALDOA	system process	0.00	0.5	0.09
Annexin A5	ANXA5	anti-apoptosis	0.00	0.4	0.11
AP-2 complex subunit alpha-2	AP2A2	transport	0.00	0.5	0.01
B-cell receptor-associated protein 31	BCAP31	immune system process	0.01	0.3	0.21
Caldesmon	CALD1	cell motility	0.00	0.4	0.06
Calnexin precursor	CANX	angiogenesis	0.00	0.4	0.08
Cell cycle associated protein 1	CAPRIN1		0.00	0.5	0.08
CDNA FLJ44063 fis, clone TESTI4035637	DKFZp686E07118		0.01	0.1	0.06
Putative uncharacterized protein DKFZp686H20196	DKFZp686H20196	proteolysis	0.00	0.0	0.01
Putative uncharacterized protein DKFZp779B0247	DKFZp779B0247	regulation of transcription, DNA-dependent	0.01	0.5	0.08
Dihydropyrimidinase-related protein 2	DPYSL2	nucleobase, nucleoside, nucleotide and nucleic acid metabolic process	0.00	0.4	0.11
DYNC1H1 protein	DYNC1H1	transport	0.00	0.1	0.26
Epidermal growth factor receptor precursor	EGFR		0		0.15
Alpha-enolase	ENO1	negative regulation of transcription from RNA polymerase II promoter	0.00	0.4	0.14
highly similar to RNA-BINDING PROTEIN EWS	EWSR1		0.00	0.4	0.11
Coagulation factor V	F5	cell adhesion	0.00	0.1	0.04
Fragile X mental retardation 1 protein	FMR1		0.00	0.5	0.07
Uncharacterized protein FSCN1	FSCN1	organelle organization and biogenesis	0.00	0.3	0.10
Fragile X mental retardation syndrome-related protein 1	FXR1	apoptosis	0.00	0.4	0.07
Ras GTPase-activating protein-binding protein 2	G3BP2	cell communication	0.00	0.5	0.07
Glycyl-tRNA synthetase	GARS	organic acid metabolic process	0.00	0.5	0.03
1,4-alpha-glucan-branching enzyme	GBE1	carbohydrate metabolic process	0.00	0.4	0.08
Glucose-6-phosphate isomerase	GPI	immune system process	0.00	0.5	0.10
HNRPR protein	HNRPR	nucleobase, nucleoside, nucleotide and nucleic acid metabolic process	0.00	0.5	0.07
Nucleoporin-like protein RIP	HRB	RNA export from nucleus	0.00	0.3	0.17
60 kDa heat shock protein, mitochondrial precursor	HSPD1	protein folding	0.00	0.5	0.10
Keratin, type I cytoskeletal 19	KRT19	organelle organization and biogenesis	0.00	0.1	0.05
Laminin subunit alpha-5 precursor	LAMA5	angiogenesis	0.00	0.2	0.14
La-related protein 1	LARP1		0.00	0.5	0.11
L-lactate dehydrogenase B chain	LDHB	carbohydrate metabolic process	0.00	0.5	0.11
Leucine-rich repeat flightless-interacting protein 1	LRRFIP1	regulation of transcription, DNA-dependent	0.00	0.5	0.23
Microtubule-associated protein 4 isoform 1 variant	MAP4	negative regulation of microtubule depolymerization	0.00	0.5	0.11
Myristoylated alanine-rich C-kinase substrate	MARCKS		0.00	0.5	0.03
Non-POU domain-containing octamer-binding protein	NONO	nucleobase, nucleoside, nucleotide and nucleic acid metabolic process	0.00	0.3	0.10
Nuclear fragile X mental retardation-interacting protein 2	NUFIP2		0.00	0.4	0.08
Protein disulfide-isomerase precursor	P4HB	protein modification process	0.00	0.4	0.12
Protein disulfide-isomerase A3 precursor	PDIA3	protein targeting	0.00	0.5	0.11
Protein disulfide-isomerase A4 precursor	PDIA4	protein secretion	0.00	0.5	0.09
Profilin-1	PFN1	organelle organization and biogenesis	0.00	0.4	0.09
Phosphoglycerate kinase 1	PGK1	phosphorus metabolic process	0.00	0.4	0.10
Phosphatidylinositol 4-kinase alpha	PI4KA	lipid metabolic process	0.00	0.3	0.07
Peptidyl-prolyl cis-trans isomerase A	PPIA	protein folding	0.00	0.4	0.08
Peptidyl-prolyl cis-trans isomerase B precursor	PPIB	protein folding	0.00	0.0	0.00
Serine/threonine-protein phosphatase 2A	PPP2R1A	inactivation of MAPK activity	0.00	0.5	0.16
Protein kinase C alpha type	PRKCA	induction of apoptosis	0.00	0.5	0.08
Trypsin-3 precursor	PRSS3	protein modification process	0.00	0.1	0.03
RNA-binding protein 14	RBM14	nucleobase, nucleoside, nucleotide and nucleic acid metabolic process	0.00	0.4	0.08
Aminopeptidase B	RNPEP	proteolysis	0.01	0.4	0.11
Proto-oncogene tyrosine-protein kinase ROS precursor	ROS1		0.31		<0.001
Reticulon-4	RTN4	negative regulation of anti-apoptosis	0.00	0.4	0.13
Splicing factor, proline- and glutamine-rich	SFPQ	nucleobase, nucleoside, nucleotide and nucleic acid metabolic process	0.00	0.2	0.10
Spectrin beta chain, erythrocyte	SPTB		0.00	0.1	0.09
STIP1 protein	STIP1	response to stress	0.00	0.5	0.14
Tyrosine-protein kinase receptor	TFG/ALK fusion	protein modification process	0.00	0.5	0.09
Ubiquitin-like modifier-activating enzyme 1	UBA1	protein modification process	0.00	0.4	0.09
Ubiquitin-associated protein 2-like	UBAP2L		0.00	0.4	0.05
Vinculin	VCL	cell morphogenesis	0.00	0.4	0.06
Voltage-dependent anion-selective channel protein 2	VDAC2	transport	0.00	0.5	0.01
Voltage-dependent anion-selective channel protein 3	VDAC3	transport	0.00	0.5	0.06
YTH domain family protein 3	YTHDF3		0.01	0.5	0.09
Zyxin	ZYX	cell communication	0.00	0.4	0.09

Many proteins were identified to specifically bind to the receptor tyrosine kinase ROS1 showing a broad spectrum of biological functions. One interesting finding was the interaction of ROS1 with the epidermal growth factor receptor (EGFR), which could be confirmed by co-immunoprecipitation experiments (Figure 79). EGFR is a receptor tyrosine kinase involved in cancer cell proliferation and survival and one of the most prominent oncogenes widely expressed in human cancers. EGFR is implicated in non-small cell lung cancer (NSCLC), as well as breast, ovary, glioblastoma multiforme and other tumor indications. Interaction and cross-activation of ROS1 and EGFR may be an interesting new aspect of oncogenic kinase signalling

involved in tumor driving cancer cell proliferation and survival. One may speculate that a combined targeted therapy of EGFR and ROS1 will have synergistic effects and improve the treatment of aggressive cancers such as NSCLC, where already approved inhibitors such as gefitinib and erlotinib show promising but not completely satisfying effects (2009; Emery et al., 2009; Zhou et al., 2009). It was shown that ROS1 is implicated in murine lung cancer progression and overexpressed in tumor compared to normal lung tissue (Bonner et al., 2004).

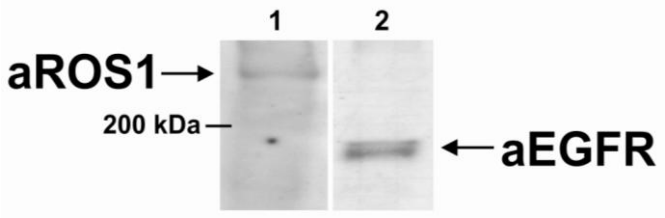

Figure 79 Co-immunoprecipitation of ROS1 and EGFR to confirm the interaction of these two proteins as determined by mass spectrometry.
Total cell lysates of the kidney cancer cell line A498 were subjected to anti-ROS1 immunoprecipitation, equal amounts of eluted proteins separated by 1D-SDS-gel electrophoresis and probed for ROS1 (lane 1) and EGFR (lane 2), respectively.

Other very interesting binding partners that were identified as specific interaction proteins with high affinity to ROS1 are Annexin V and PKCalpha. Both showed similar affinities to ROS1, 0.11 for Annexin V and 0.08 for PKCalpha, respectively, which indicates a 1:1 stoichiometry of binding. Both interaction partners might be involved in the anti-apoptotic effect of ROS1. A possible mechanism of action is drawn in Figure 80.

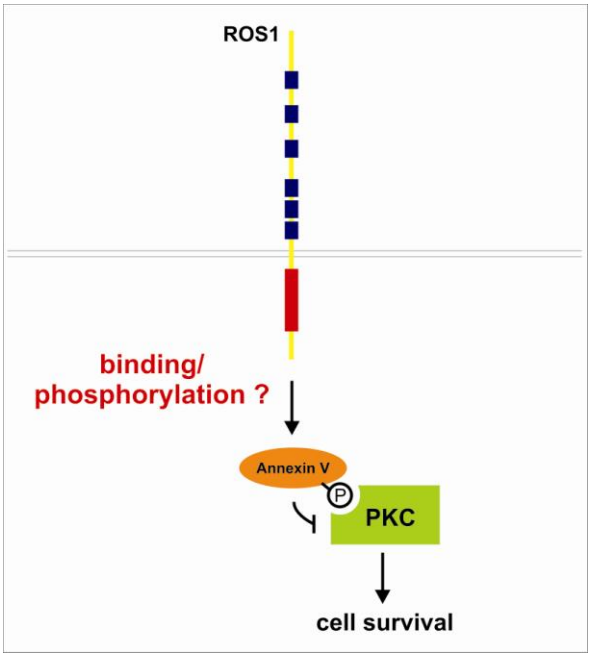

Figure 80 Potential ROS1 mechanism of action to trigger cancer cell survival.
Upon activation ROS1 binds to Annexin V and phosphorylates it. Phosphorylated Annexin V can then bind to PKC alpha thereby inactivating it which leads to survival of cancer cells. In the absence of ROS1, after for example down-regulation by siRNA, Annexin V is not phosphorylated and does not bind to PKC alpha. Hence, PKC alpha is active and triggers apoptosis of cancer cells.

Upon activation ROS1 binds to Annexin V and phosphorylates it. Phosphorylated Annexin V can then bind to PKC alpha thereby inactivating the kinase which leads to survival of cancer cells. In the absence of ROS1, after for example down-regulation by siRNA, Annexin V is not phosphorylated and does not bind to PKC alpha. Hence, PKC alpha is active and triggers apoptosis of cancer cells. This very preliminary hypothesis has to be proven by further experiments and only gives a first hint of the molecular mechanism of ROS1 receptor tyrosine kinase signalling regulating cancer cell survival.

In summary, based on this study and additional findings in the past, ROS1 is widely expressed in a broad range of cancer cell lines of different tumor indications and seems to play an essential, not cancer-type specific, role in cancer cell proliferation and survival. This universal function in the regulation of cancer cell apoptosis was shown by RNAi experiments *in vitro*. Therefore, the receptor tyrosine kinase ROS1 might be a prominent target for target-specific cancer therapy in the future. Targeted cancer therapy with small-molecule kinase inhibitors has the main goal of killing cancer but not interfering with normal cells in the body. A cancer specific function was observed for glioblastoma multiforme as well as kidney cancer where an expression of the kinase was only seen in tumor cells but not or to a much lesser extent in normal tissue from the same organ.
Due to its important function in cancer cell proliferation and survival and its potential as an universal cancer-specific target for targeted kinase therapy by small-molecule inhibitors, a specific small-molecule kinase inhibitor for the possible use in the treatment of ROS1 driven cancer types was developed.

7.10.4 Screening of compound libraries against the receptor tyrosine kinase ROS1-identification and characterization of a small-molecule kinase inhibitor of ROS1 kinase activity *in vitro*

Drug discovery, the process of identification of small-molecule inhibitors towards a specific target such as kinases, is usually divided into several consecutive steps of compound library screening against a certain kinase target, compound testing in vitro, rescreening of a subset of inhibiting hits and their final specificity and activity proof in cellular model systems. The drug screening workflow used in this study is shown in Figure 81.
Two libraries, consisting of 875 and 1192 compounds, respectively, were screened for ROS1 autophosphorylation inhibition *in vitro* by using the IMAP® Fluorescence Polarization technology (Sportsman et al., 2004).

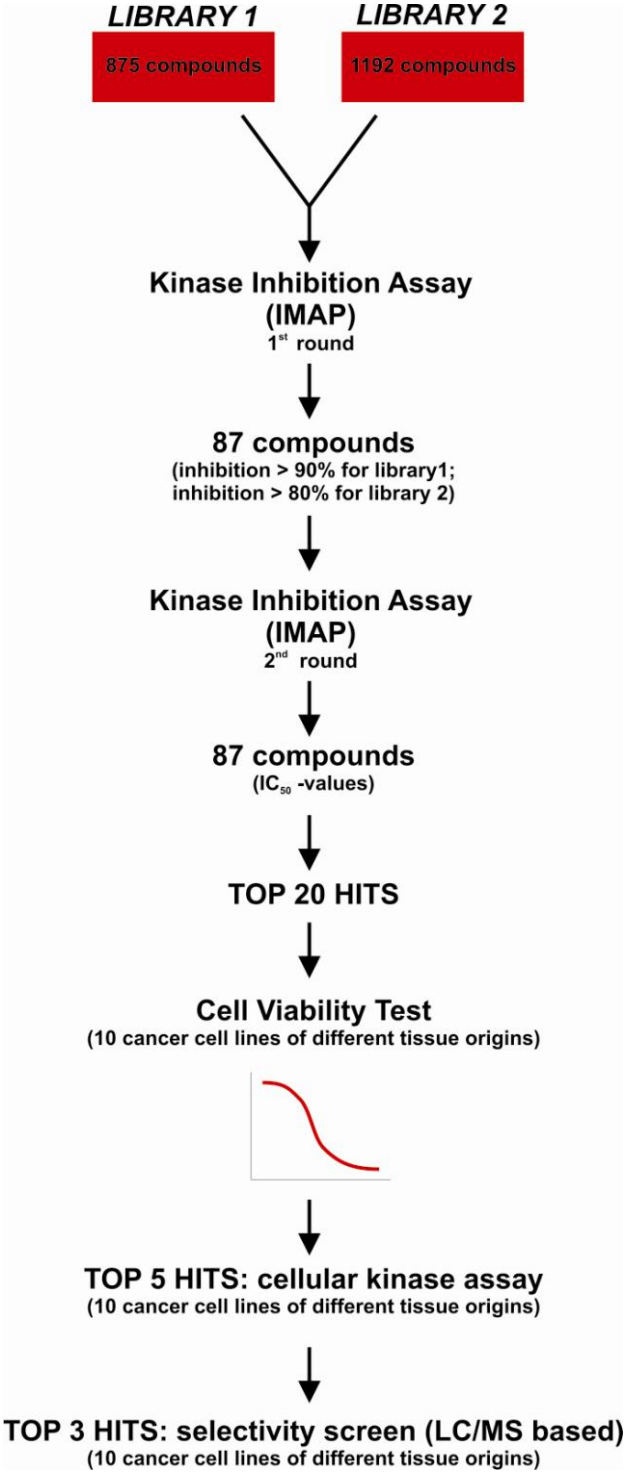

Figure 81 Workflow of inhibitor screening against the receptor tyrosine kinase ROS1.
Two compound libraries, consisting of 875 and 1192 compounds respectively, were screened against the receptor tyrosine kinase ROS1 using the IMAP technology. In the first round each compound was tested at a concentration of 10 µM for ROS1 kinase activity inhibition. A cut-off inhibition rate of > 90 % for the first and 80 % for the second library was taken as an exclusion criteria for compounds for the second round of screening. For 87 compounds IC_{50}-values were determined. Since the IMAP technology is a cell-free kinase assay with recombinant ROS1, the top20 hits were subsequently tested in a cell based viability screen using a colorimetric MTT-assay. The inhibitory effect on cancer cell viability was tested in 10 cancer cell lines of different tissue origins. For the top5 hits cellular kinase assays were performed and the compound` s selectivity profile determined via mass spectrometry using a chemical proteomic approach.

The IMAP® Fluorescence Polarization technology is a homogeneous antibody-free method for analysis of kinases, phosphatases, and phosphodiesterases. The analysis of phosphorylation is a key component in the discovery and development of new therapeutic agents. Protein kinases and phosphatases comprise a considerable fraction of primary and secondary targets for determining efficacy and selectivity of hits and leads in drug discovery. Over the last years, several screening labs have adopted the IMAP® technology for a significant portion of their kinase screening effort. The growth of IMAP is due to several factors: the inherent robustness of fluorescence polarization (FP) detection, IMAP' s high selectivity of recognition of phosphorylation, the generality of the technology, and the additional robustness that IMAP adds to the FP method. IMAP is based on the high-affinity binding of phosphate by immobilized trivalent metals on nanoparticles. This IMAP "Binding Reagent" complexes with phosphate groups on phosphopeptides generated in a kinase reaction. Such binding causes a change in the rate of the molecular motion of the peptide and results in an increase in the FP value observed for the fluorescent label attached at the end of the peptide (Figure 82).

As the IMAP `Binding Reagent` interacts directly with phosphate through metal–ligand coordinate covalent bonds, detection of kinases that phosphorylate Ser, Thr, or Tyr residues is equally enabled, and there is no sensitivity to the sequence of flanking amino acids. This generality of phosphate recognition overcomes a major limitation of kinase assays that use phosphorylation-selective antibodies.

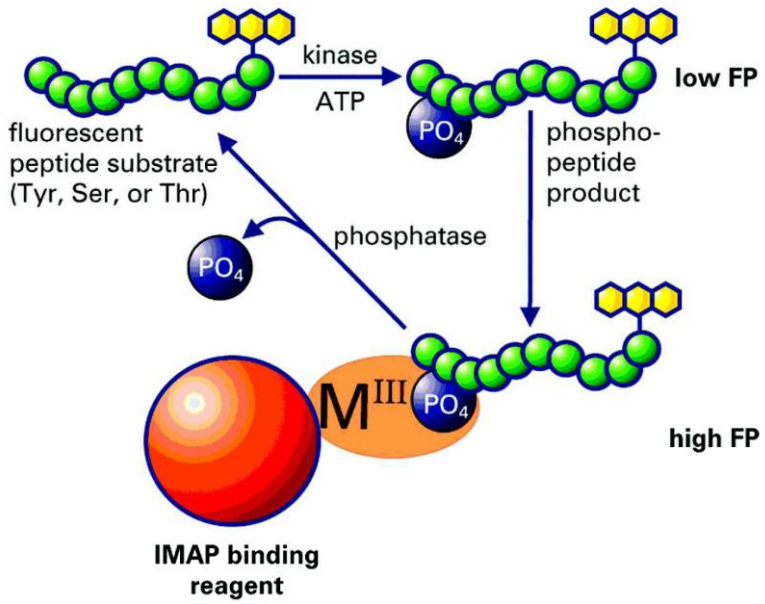

Figure 82 Principle of the IMAP assay.
Phosphorylation of a fluorescent peptide substrate is detected by addition of the IMAP `Binding Reagent` that stops the reaction and binds to product, but not substrate. Hence, FP is proportional to degree of phosphorylation. Phosphatase assays are done by running the enzymatic reaction step "in reverse" (Sportsman et al., 2004).

After the first round of drug screening only hits with an inhibition rate greater than 90 % for the first and 80 % for the second library against the receptor tyrosine kinase ROS1 were considered to be positive. In total, 87 compounds out of 2067 remained for a second round of screening. In the second round of screening, IC_{50}-values for each positive hit from the first round were calculated. In contrast to the first round, where a fixed concentration of 10 µM for each compound was used, a concentration range from 0.0001 to 10 µM was taken in the second screening. The top20 hits are listed in Table 22. These hits potently inhibited ROS1 kinase autophosporylation with IC_{50} values $\leq$ 1 µM. The library screening was performed in collaboration with the company Proteros, Martinsried, Germany. Since the IMAP technology is a cell-free protein kinase screening method, a crucial next step in the process of inhibitor development is the test of compound inhibitor potency *in vivo*. Therefore, cellular cytotoxicity assays were performed in a panel of cancer cell lines from different tumor indications. The top20 hits were screened in a colorimetric MTT-assay for their inhibitory effect on cancer cell viability. Cellular IC_{50}-values are summarized in Table 23 and results from the MTT-assay are shown in Figure 83.

Table 22 Top20 hits of small-molecule inhibitors against the receptor tyrosine kinase ROS1. Compound hits are sorted by increasing IC_{50}-values.

cpd ID	max compound CONCENTRATION (µM)	IC_{50} [µM]
229_0146_0005	10	0.09
294_4003_0087	10	0.09
1173	10	0.15
16719	10	0.17
229_0146_0333	10	0.18
VI 16366	10	0.38
229_0144_0087	10	0.39
229_0236_0347	10	0.44
VI 18367	10	0.44
229_0223_4141	10	0.50
229_0146_0087	10	0.50
229_0223_0333	10	0.55
229_0153_0199	10	0.56
VI 17504	10	0.68
VI 18380	10	0.69
VI 16641	10	0.72
VI 18387	10	0.74
229_0223_0087	10	0.85
VI 18366	10	0.90
VI 18395	10	1.02

Figure 83 Effects of top20 screening compound hits on cancer cell viability.
The 20 most effective inhibitory compounds against the receptor tyrosine kinase ROS1 were tested for their effects on cell viability of cancer cell lines from different tissue origins. The pancreas cancer cell lines PaTu, the kidney cancer cell lines Caki1, Caki2, the breast cancer cell line Hs578T, the colon cancer cell line HT29 and the ovary cancer cell lines Ovcar5 and SkOv3 were treated with three different inhibitor concentrations (2.5, 5 and 10 µM, respectively) for 72h under serum conditions (10 % FCS). Cell viability was measured using a colorimetric MTT-assay. As a control, cell lines were treated with SU11248. Inhibitory effects of the compounds are shown as percentaged inhibition of cell viability relative to DMSO vehicle control treated cells where no inhibition was observed.

Table 23 Cellular IC_{50}-values of cell growth inhibition of inhibitory compounds directed against the receptor tyrosine kinase ROS1.

Compounds are sorted by their activity (IC_{50}-value in µM) against ROS1 based on the *in vitro* IMAP kinase assay. Cellular IC_{50}-values of cell growth inhibition are listed by cancer cell lines and summarized by the median over all determined IC_{50}-values for each compound.

compound	IMAP assay IC_{50} [µM]	cancer cell line	tissue	cell-based assay IC_{50} [µM]	cell-based assay median IC_{50} [µM]
229_0146_0005	0.09	PaTu	pancreas	> 10	> 10
		Caki2	kidney	> 10	
		Caki1	kidney	> 10	
		Hs578T	breast	> 10	
		HT29	colon	> 10	
		Ovcar5	skin	> 10	
		SkOv3	skin	> 10	
294_4003_0087	0.09	PaTu	pancreas	> 10	6.77
		Caki2	kidney	5.68	
		Caki1	kidney	7.86	
		Hs578T	breast	> 10	
		HT29	colon	9.06	
		Ovcar5	skin	> 10	
		SkOv3	skin	4.96	
1173	0.15	PaTu	pancreas	> 10	> 10
		Caki2	kidney	> 10	
		Caki1	kidney	> 10	
		Hs578T	breast	> 10	
		HT29	colon	> 10	
		Ovcar5	skin	> 10	
		SkOv3	skin	> 10	
16719	0.17	PaTu	pancreas	< 2.5	< 2.5
		Caki2	kidney	< 2.5	
		Caki1	kidney	< 2.5	
		Hs578T	breast	< 2.5	
		HT29	colon	< 2.5	
		Ovcar5	skin	< 2.5	
		SkOv3	skin	< 2.5	
229_0146_0333	0.18	PaTu	pancreas	> 10	> 10
		Caki2	kidney	> 10	
		Caki1	kidney	> 10	
		Hs578T	breast	> 10	
		HT29	colon	> 10	
		Ovcar5	skin	> 10	
		SkOv3	skin	> 10	
16366	0.38	PaTu	pancreas	3.21	2.73
		Caki2	kidney	< 2.5	
		Caki1	kidney	< 2.5	
		Hs578T	breast	6.13	
		HT29	colon	2.69	
		Ovcar5	skin	2.67	
		SkOv3	skin	2.73	
229_0144_0087	0.39	PaTu	pancreas	6.42	7.78
		Caki2	kidney	> 10	
		Caki1	kidney	7.46	
		Hs578T	breast	> 10	
		HT29	colon	8.3	
		Ovcar5	skin	9.87	
		SkOv3	skin	7.78	
229_0236_0347	0.44	PaTu	pancreas	> 10	> 10
		Caki2	kidney	> 10	
		Caki1	kidney	> 10	
		Hs578T	breast	> 10	
		HT29	colon	> 10	
		Ovcar5	skin	> 10	
		SkOv3	skin	> 10	

compound	IMAP assay IC_{50} [µM]	cancer cell line	tissue	cell-based assay IC_{50} [µM]	cell-based assay median IC_{50} [µM]
229_0223_4141	0.5	PaTu	pancreas	9.6	> 10
		Caki2	kidney	> 10	
		Caki1	kidney	> 10	
		Hs578T	breast	> 10	
		HT29	colon	> 10	
		Ovcar5	skin	> 10	
		SkOv3	skin	> 10	
229_0146_0087	0.5	PaTu	pancreas	5.88	4.355
		Caki2	kidney	4.28	
		Caki1	kidney	3.77	
		Hs578T	breast	9.32	
		HT29	colon	3.34	
		Ovcar5	skin	> 10	
		SkOv3	skin	4.43	
229_0223_0333	0.55	PaTu	pancreas	8.9	> 10
		Caki2	kidney	> 10	
		Caki1	kidney	> 10	
		Hs578T	breast	> 10	
		HT29	colon	> 10	
		Ovcar5	skin	> 10	
		SkOv3	skin	> 10	
229_0153_0199	0.56	PaTu	pancreas	> 10	> 10
		Caki2	kidney	> 10	
		Caki1	kidney	> 10	
		Hs578T	breast	> 10	
		HT29	colon	> 10	
		Ovcar5	skin	> 10	
		SkOv3	skin	> 10	
229_0223_0087	0.85	PaTu	pancreas	> 10	> 10
		Caki2	kidney	8.7	
		Caki1	kidney	> 10	
		Hs578T	breast	> 10	
		HT29	colon	> 10	
		Ovcar5	skin	> 10	
		SkOv3	skin	> 10	
229_0236_0001	1.17	PaTu	pancreas	> 10	> 10
		Caki2	kidney	> 10	
		Caki1	kidney	> 10	
		Hs578T	breast	> 10	
		HT29	colon	> 10	
		Ovcar5	skin	> 10	
		SkOv3	skin	> 10	
SU11248		PaTu	pancreas	> 10	5.21
		Caki2	kidney	< 2.5	
		Caki1	kidney	3.57	
		Hs578T	breast	7.79	
		HT29	colon	2.72	
		Ovcar5	skin	5.21	
		SkOv3	skin	6.54	

5 out of 20 compounds showed significant effects on cancer cell viability with IC_{50}-values between < 1 and 7.78 µM, averaged over all tested cancer cell lines. They had similar efficacies as or were even more effective than the control drug SU11248 with an IC_{50}-value of 5.21 µM. All other tested compounds had low inhibitory potential on cancer cell viability and were not selected for further experiments.

The cell-based assays revealed differences between the IC_{50}-values of direct ROS1 inhibition observed in the *in vitro* IMAP kinase assays and the physiological efficacy of respective compounds. For example, one of the two most active hits in the cell-free setting, compound 229_0146_0005, had no significant inhibitory effect on cancer cell viability at concentrations equal to 10 µM and lower. Similar results were seen for several other high affinity ROS1 inhibitors detected in the IMAP screen with IC_{50}-values smaller than 1 µM. For these compounds there was no direct correlation between kinase inhibition activity and biological impact on cancer cell proliferation and survival. These discrepancies might be due to several reasons: for example, inadequate solubility of the compound in aqueous solution such as cell culture media, reduced or

very weak cell permeability and/or no binding capability to the native conformation of ROS1 within the cell. Hence, a cell-free kinase assay only gives hints for potential screening hits which have to be analyzed further in cellular model systems followed by *in vivo* experiments to obtain potential lead drugs for clinical investigations.

In order to get a comprehensive picture of compound efficacies and tumor specificities the most effective top6 compounds (16366 (cmpd 1), 16719 (cmpd 3), 229_0223_0087 (cmpd 4), 294_4003_0087 (cmpd 5), 229_0144_0087 (cmpd 6), 229_0146_0087 (cmpd 7)) and one negative (1173 (cmpd 2)) as well as positive control (SU11248) from the first round of the cell-based cytotoxicity screen were used for a more detailed analysis of drug activity in 32 cancer cell lines of different tissue origins. The following cancer cell lines were used: *U118, U1242, SF126 (brain); A590, AsPc1, 786-0, Patu8902, Patu8988t, Patu8988s (pancreas); Caki1, Caki2, SW13, A498, A704 (kidney); MDA-MB-435S, MDA-MB-231, Hs578T (breast); HT29 (colon); H2122, HCC44, H1838, HCC366, H1781, H460, H2347, HCC15, H1650, H522, H1568, H1975, H661, A549 (lung).*

To measure the compound effects on cancer cell growth a colorimetric MTT-assay was used. The results are shown in Figure 84, 85, 86 and 87. The cellular IC_{50}-values of each compound in the respective cancer cell line are listed in Table 24.

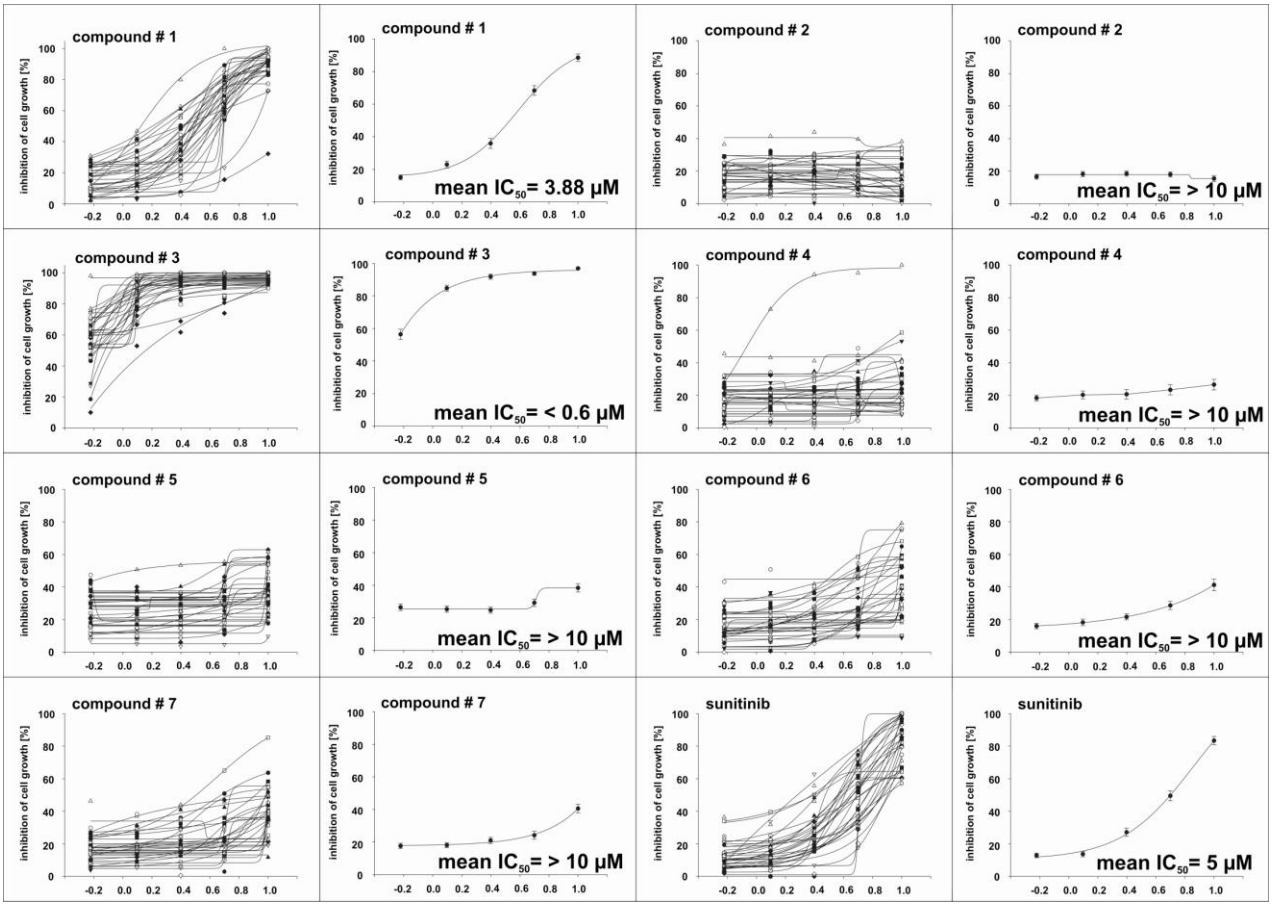

Figure 84 Dose-dependent inhibition curves of cancer cell growth shown for each ROS1 inhibitory compound in every cell line (left panel) and the averaged inhibition curve for a single compound over all tested cancer cell lines (right panel) after 72h of drug treatment.

Mean IC_{50}-values are listed in the Figure. Growth-inhibition curves were calculated using the simple-ligand binding sigmoidal-dose-response curve fitting algorithm in SigmaPlot 10.0 on log-transformed data points.

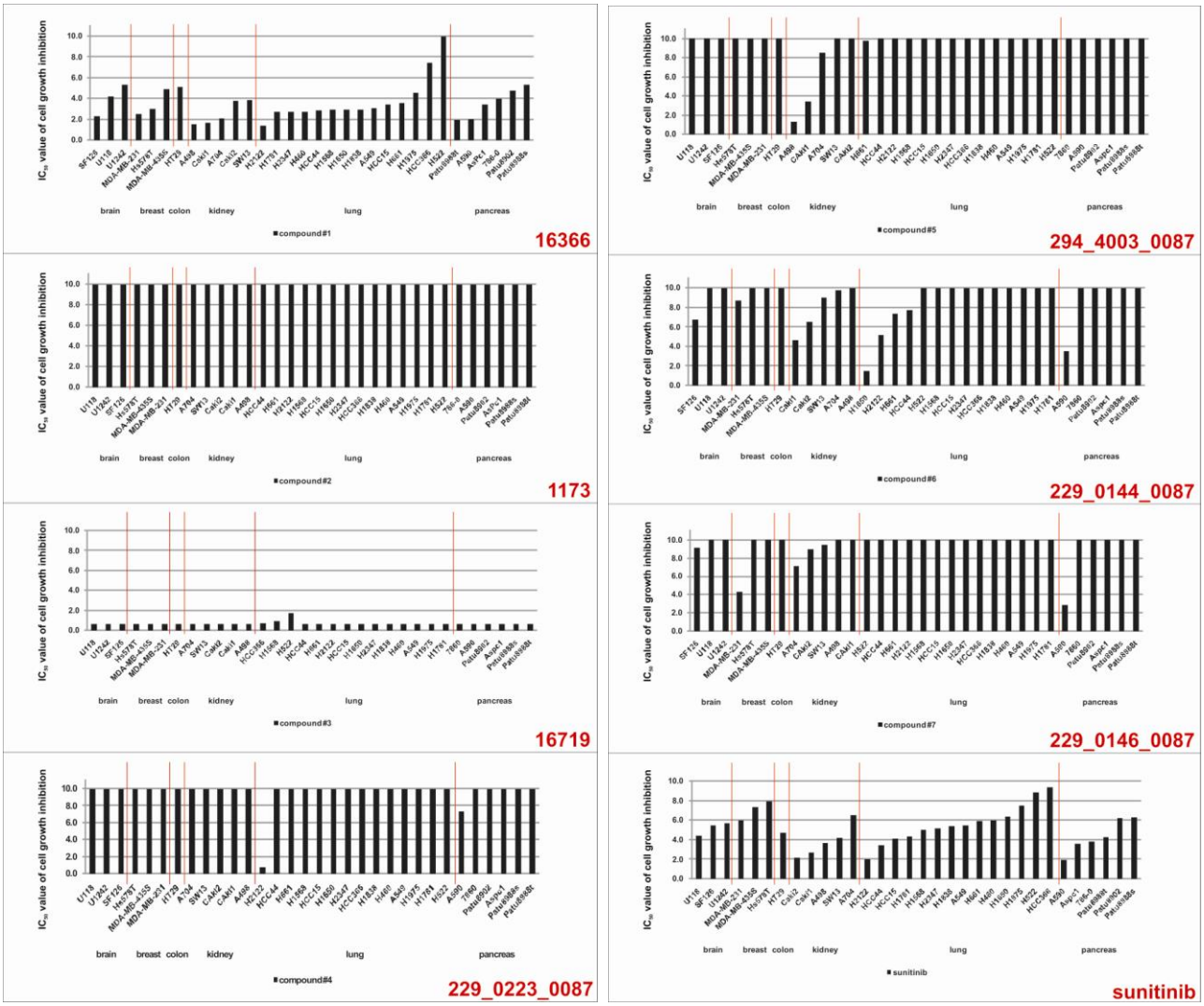

Figure 85 IC_{50}-values of cell growth inhibition of cancer cells by ROS1 inhibitors after 72h of drug treatment.

The IC_{50}-values are sorted by cell line origin and decreasing sensitivity. IC_{50}-values represent the average of three independent experiments and were calculated with Sigma Plot 10.0 using a sigmoidal-dose-response curve fitting algorithm on log-transformed data.

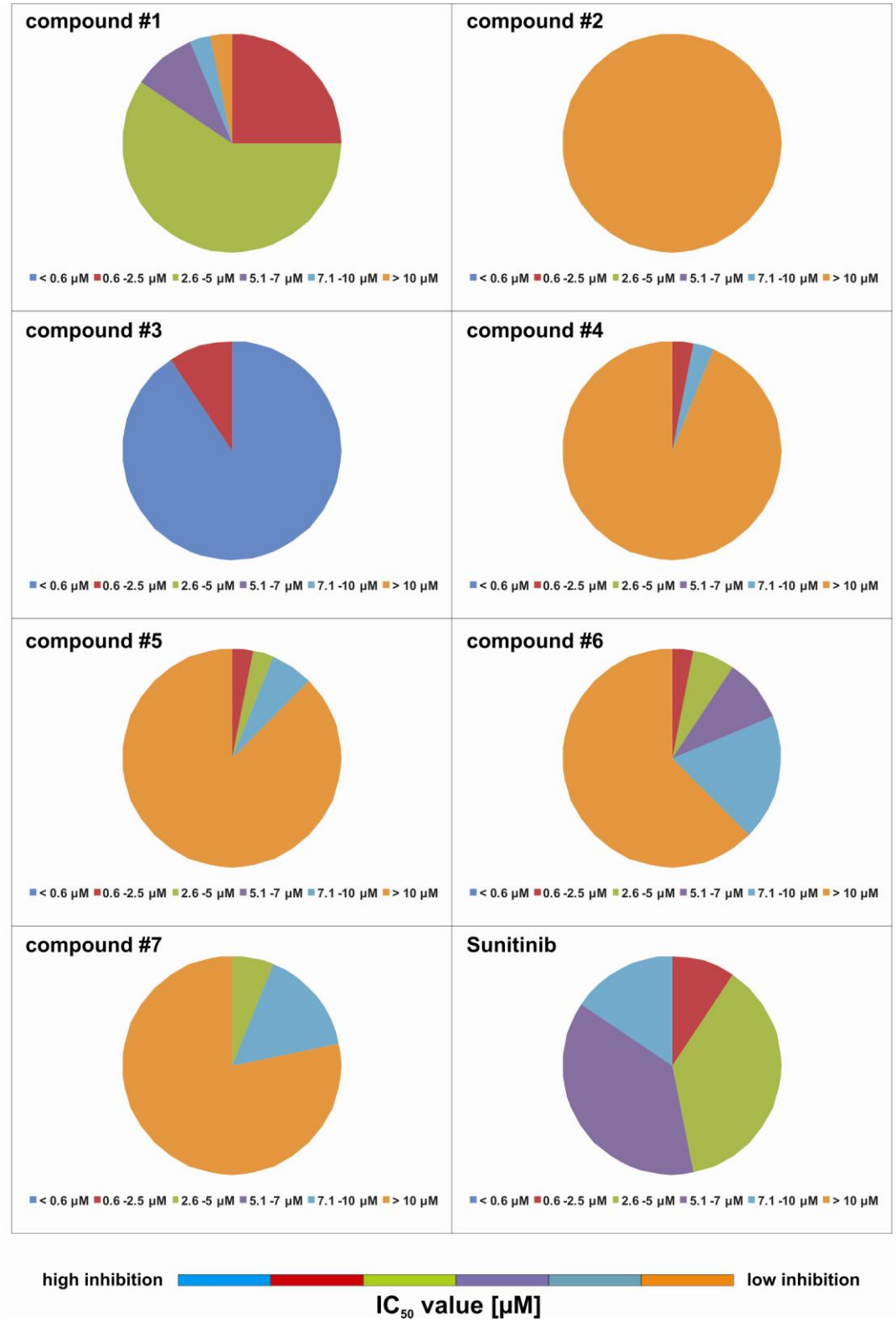

Figure 86 Compound IC_{50}-values of cell growth inhibition grouped by sensitivity.
IC_{50}-values are grouped into six distinct categories ranging from very low IC_{50}-values smaller than 0.6 µM to very high IC_{50}-values greater than 10 µM. Each category is represented by the wedges of the pie chart. ROS1 inhibitory compounds are sorted numerically and sunitinib was taken as a control.

Table 24 IC_{50}-values of cell growth inhibition of different ROS1 inhibitors after 72h of drug treatment.

Inhibition data are obtained by a colorimetric MTT cell growth assay. Cell lines are tissue-sorted.

		IC_{50} [µM]							
tissue	cell line	compound 1	compound 2	compound 3	compound 4	compound 5	compound 6	compound 7	sunitinib
brain	SF126	2.3	> 10	< 0.6	> 10	> 10	6.7	9.1	5.5
brain	U118	4.2	> 10	< 0.6	> 10	> 10	> 10	> 10	4.4
brain	U1242	5.3	> 10	< 0.6	> 10	> 10	> 10	> 10	5.7
breast	Hs578T	3.0	> 10	< 0.6	> 10	> 10	> 10	> 10	8.0
breast	MDA-MB-231	2.5	> 10	< 0.6	> 10	> 10	8.8	4.3	6.0
breast	MDA-MB-435S	4.9	> 10	< 0.6	> 10	> 10	> 10	> 10	7.3
colon	HT29	5.2	> 10	< 0.6	> 10	> 10	> 10	> 10	4.7
kidney	A498	1.5	> 10	< 0.6	> 10	1.3	> 10	> 10	3.6
kidney	A704	2.1	> 10	< 0.6	> 10	8.6	9.8	7.1	6.5
kidney	Caki1	1.7	> 10	< 0.6	> 10	3.5	4.6	> 10	2.7
kidney	Caki2	3.8	> 10	< 0.6	> 10	> 10	6.5	9.0	2.2
kidney	SW13	3.9	> 10	< 0.6	> 10	> 10	9.0	9.4	4.2
lung	A549	3.1	> 10	< 0.6	> 10	> 10	> 10	> 10	5.5
lung	H1568	3.0	> 10	0.9	> 10	> 10	> 10	> 10	5.0
lung	H1650	3.0	> 10	< 0.6	> 10	> 10	1.4	> 10	6.4
lung	H1781	2.7	> 10	< 0.6	> 10	> 10	> 10	> 10	4.4
lung	H1838	3.0	> 10	< 0.6	> 10	> 10	> 10	> 10	5.4
lung	H1975	4.5	> 10	< 0.6	> 10	> 10	> 10	> 10	7.5
lung	H2122	1.4	> 10	< 0.6	0.7	> 10	5.2	> 10	2.0
lung	H2347	2.7	> 10	< 0.6	> 10	> 10	> 10	> 10	5.2
lung	H460	2.7	> 10	< 0.6	> 10	> 10	> 10	> 10	6.0
lung	H522	10.0	> 10	1.8	> 10	> 10	> 10	> 10	8.9
lung	H661	3.6	> 10	< 0.6	> 10	9.8	7.4	> 10	5.9
lung	HCC15	3.4	> 10	< 0.6	> 10	> 10	> 10	> 10	4.1
lung	HCC366	7.4	> 10	0.7	> 10	> 10	> 10	> 10	9.3
lung	HCC44	2.9	> 10	< 0.6	> 10	> 10	7.7	> 10	3.4
pancreas	786-0	4.0	> 10	< 0.6	> 10	> 10	> 10	> 10	3.8
pancreas	A590	2.0	> 10	< 0.6	7.4	> 10	3.5	2.8	1.9
pancreas	AsPc1	3.5	> 10	< 0.6	> 10	> 10	> 10	> 10	3.6
pancreas	Patu8902	4.7	> 10	< 0.6	> 10	> 10	> 10	> 10	6.2
pancreas	Patu8988s	5.3	> 10	< 0.6	> 10	> 10	> 10	> 10	6.3
pancreas	Patu8988t	2.0	> 10	< 0.6	> 10	> 10	> 10	> 10	4.2

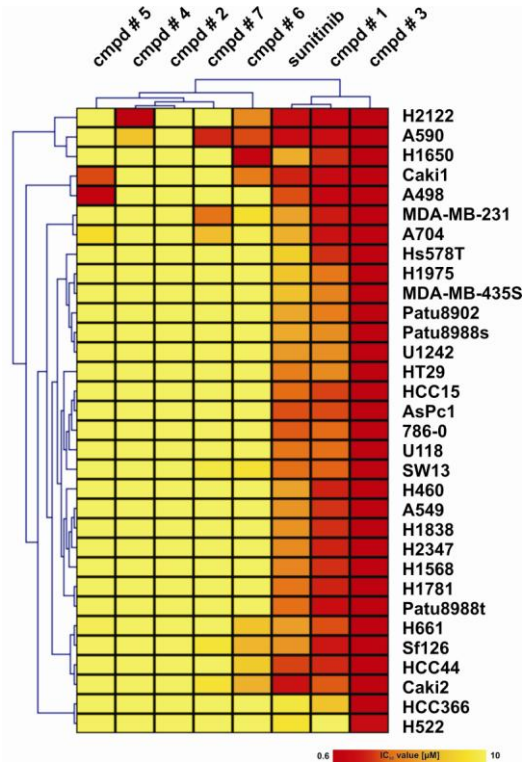

Figure 87 Two-dimensional hierarchical cluster analysis of compound specific IC_{50}-values and cell line sensitivity.

Compounds and cancer cell lines were clustered based on the specific IC_{50}-values measured for each compound in each cell line. A two-dimensional average linkage hierarchical cluster algorithm was used with Euclidean Distance as the distance metric selection using the open source program MultiExperimentViewer (MeV 4.0).

Compound 2, 4 and 5 did not show strong inhibitory potencies and were not considered for further analysis. Compound 1 and 3 had the strongest effects on cancer cell growth, followed by compound 6 and 7.

Since the compounds were designed and screened to inhibit the activity of the receptor tyrosine kinase ROS1 it came into focus whether these drugs can also induce apoptosis in cancer cells and not only inhibit cancer cell growth alone. The drug effects of inducing programmed cell death would be in accordance to the results seen after ROS1 knock-down. ROS1 depletion drives tumor cells into apoptosis. To test weather the top3 ROS1 inhibitors have anti-survival effects in tumor cells, a caspase-3/7-activity assay was performed. Sunitinib was taken as a control and the results are shown in Figure 88.

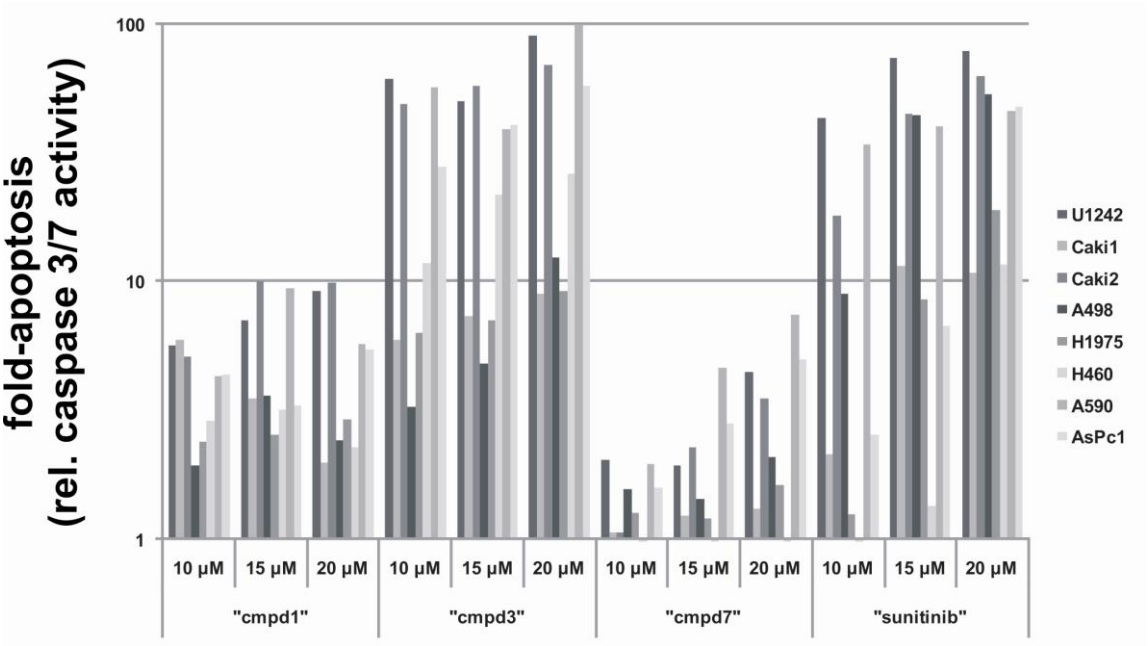

Figure 88 Dose-dependent apoptosis inducing effects of the top3 ROS1 inhibitors on cancer cell lines of different tissue origins after 36h.
The cancer cell lines U1242 (brain), Caki1, Caki2, A498 (kidney), H460, H1975 (lung) and A590, AsPc1 (pancreas) were grown under high serum conditions (10 % FCS (w/v)) and treated with increasing inhibitor concentrations (10, 15, 20 µM) or DMSO vehicle control for 36h. The caspase-3/7-activity was measured using a luminescence based assay from Promega (*Caspase-3/7-Glo-Assay*). Caspase-3/7-activity as a direct measure for cells undergoing programmed cell death is shown as fold-change to DMSO vehicle control on a log10-scale for each dose and cell line.

The data illustrate a strong apoptosis inducing effect of the tested compounds on cancer cells after 36h in a dose-dependent manner.

Taken together it could be demonstrated that out of 20 potential ROS1 inhibitors identified in an *in vitro* kinase assay, 4 turned out to be very potent in cell-based biological assays. They had strong anti-proliferative and apoptosis inducing effects on a broad spectrum of cancer cell lines of different tumor origins. Furthermore, it could be shown that these leading compounds inhibit the autophosphorylation of the receptor tyrosine kinase ROS1 in a cellular kinase assay (data not shown). These cellular efficacies of potential inhibitors in tumor cells are the first prerequisite for lead structures in the process of drug development. Such lead structures have then to be chemically modified, retested in cell-based physiological assays and checked for their anti-tumor efficacy in tumor mouse models.

But before testing lead structures *in vivo*, it is of great importance to know the precise target-panel of a respective drug to get an idea of potential off-targets effects.

Therefore, a target selectivity profile of the top2 compounds 16366 and 16719 was evaluated using a chemical proteomics approach based on affinity-chromatography and subsequent mass-spectrometry analysis. The workflow is shown in Figure 89.

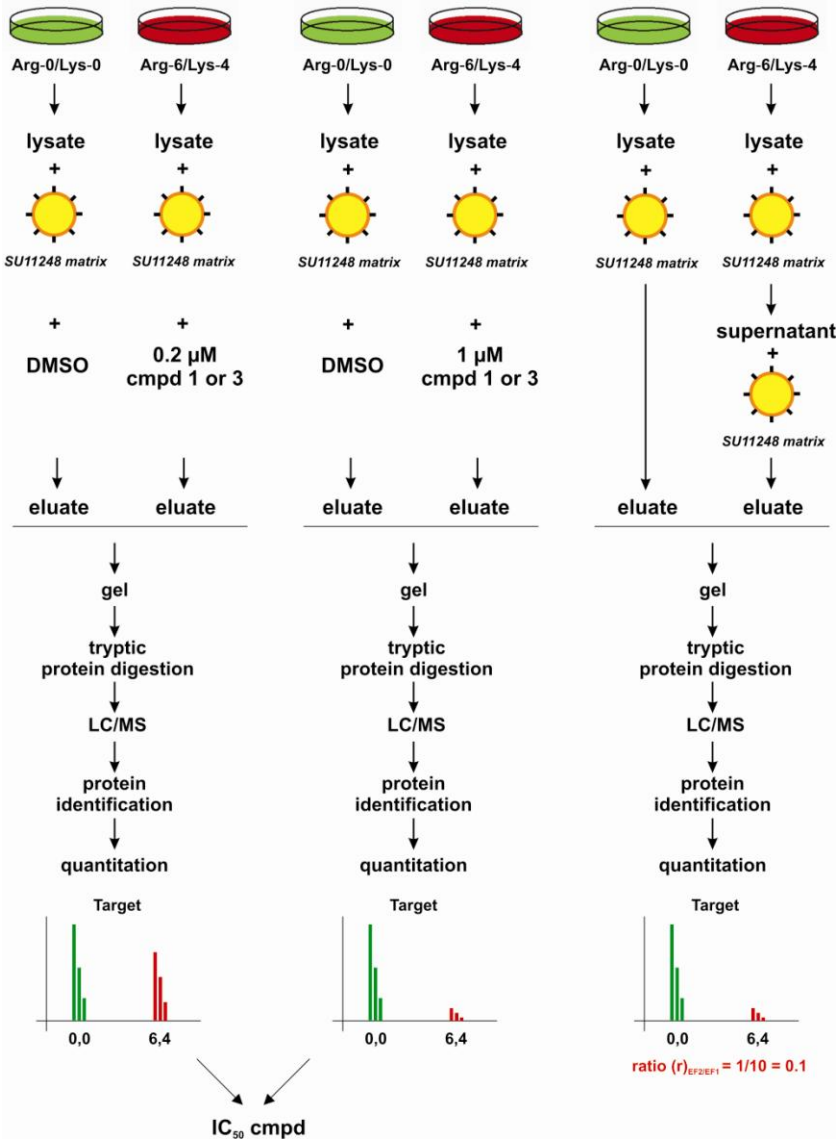

Figure 89 Workflow of compound target selectivity screening using a combinatorial strategy of affinity chromatography and mass spectrometry.

A498 cells were SILAC-encoded with normal or stable isotope-labeled arginine and lysine. Cell lysates were prepared and subjected to either one or two *in vitro* associations with SU11248 containing beads (SU11248 matrix) (very right setting). The two elution fractions were pooled and analyzed by quantitative liquid chromatography–mass spectrometry (LC/MS) to identify specific binders. Based on peptide ratios determined for target proteins in the second (EF2) versus the first incubation (EF1) an enrichment ratio *r* was determined. This ratio *r* permitted the calculation of target-specific dissociation constants $K_d(\text{inhibitor})_{im}$ for immobilized SU11248 as indicated, as binding equilibria were reached in the presence of a molar excess of immobilized SU11248 and in the absence of competing Mg^{2+}-ATP complexes. In the left and middle setting lysates from SILAC-encoded cells were incubated with SU112486 beads in the presence of different compound concentrations of either compound 1 or 3. Bound protein fractions were combined as indicated and quantitatively assessed in parallel LC/MS experiments. IC_{50}(compound) values for compound-dependent displacement from the SU11248 resin were determined and then used to calculate target-specific dissociation constants K_d(compound) for the free compound according to the Cheng-Prusoff equation.

The target selectivity spectra (target panels) of the two ROS1 inhibitors compound 1 and 3 are summarized in Figure 90. Shown are the competition curves for the compound-dependent displacement of kinase targets from the SU11248 resin. Target-specific dissociation constants K_d(compound) for free compound were calculated according to the Cheng-Prusoff equation (Figure 90 B). The identified targets for each compound are sorted by increasing K_d-values and listed in Figure 90 C.

A

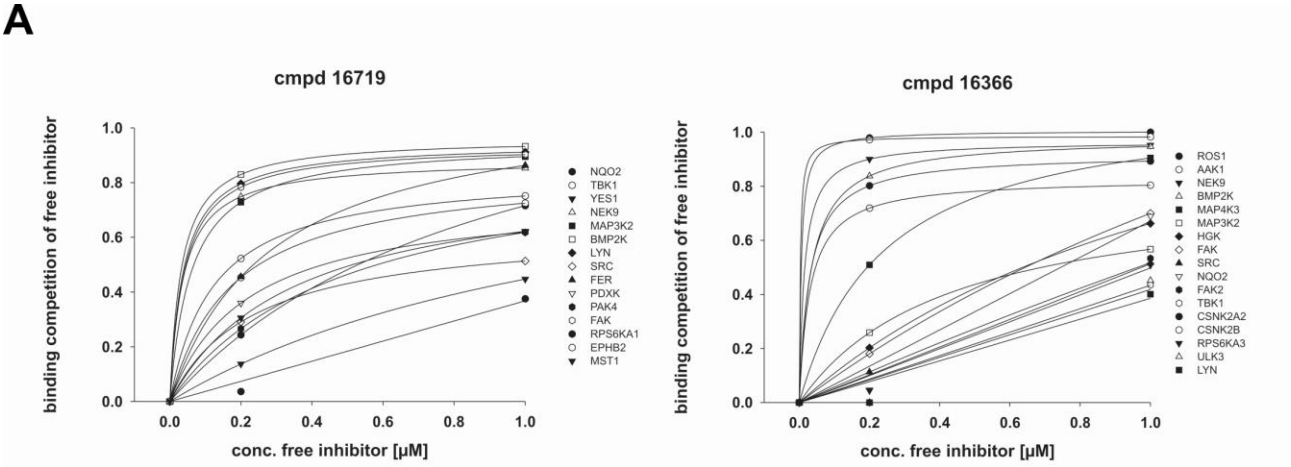

B

$$\text{A: } K_d(\text{inhibitor})_{im} = [I]_{effective} * r/(1-r)$$

$$\text{B: Cheng-Prusoff: } K_d(\text{inhibitor})_{free} = K_d(\text{inhibitor})_{im}/([I]_{effective} + K_d(\text{inhibitor})_{im}) * IC_{50}(\text{inhibitor})_{free}$$

C

cmpd 16366

gene name	IC_{50} [µM] (inhibitor)$_{free}$	K_d [µM] (inhibitor)$_{im}$	K_d [µM] (inhibitor)$_{free}$
AAK1	0.006	10.61	0.002
NEK9	0.016	22.78	0.009
CSNK2A2	0.035	10.23	0.014
CSNK2B	0.045	11.00	0.018
BMP2K	0.034	27.31	0.022
NQO2	0.746	2.75	0.112
MAP4K3	0.192	58.86	0.152
HGK	0.633	30.84	0.420
MAP3K2	0.691	27.15	0.439
FAK	0.641	90.95	0.547
SRC	0.961	40.47	0.694
FAK2	0.977	48.48	0.739
RPS6KA3	1.000	49.48	0.760
ROS1	0.003	nd	nd
TBK1	> 1	14.04	nd
LYN	> 1	36.43	nd
ULK3	> 1	4.07	nd

cmpd 16719

gene name	IC_{50} [µM] (inhibitor)$_{free}$	K_d [µM] (inhibitor)$_{im}$	K_d [µM] (inhibitor)$_{free}$
BMP2K	0.035	27.31	0.022
NEK9	0.047	22.78	0.028
LYN	0.043	36.43	0.030
FAK	0.047	90.95	0.040
MAP3K2	0.066	27.15	0.042
EPHB2	0.180	12.21	0.079
NQO2	0.527	2.75	0.079
TBK1	0.250	14.04	0.118
FER	0.234	41.38	0.170
MST1	0.516	7.84	0.173
PDXK	0.434	57.36	0.341
PAK4	0.586	62.54	0.469
SRC	0.879	40.47	0.634
YES1	> 1	16.69	nd
RPS6KA1	> 1	211.85	nd

Figure 90 Target selectivity patterns of two ROS1 inhibitors 16719 and 16366.
(A) Binding curves for compound 16719 und 16366 against endogenous expressed kinase targets. (B) Equations for calculating the target-specific dissociation constants K_d (inhibitor)$_{free}$ for the free compounds 16719 und 16366. Based on the target affinities of the respective kinases towards the SU11248 matrix (K_d (inhibitor)$_{im}$) the binding affinities of the free ROS1 inhibitors towards these targets were calculated. A compound-dependent competition ratio of equal or smaller 0.6 in the highest inhibitor concentration [1 µM] was taken as a cut for specific binding to the free inhibitor to calculated target-specific IC_{50}-values. This was performed using the simple ligand binding one site saturation curve fitting algorithm in Sigma Plot 10.0. (C) Target spectrum and corresponding dissociation constants of ROS1 inhibitor targets sorted by decreasing compound affinity.

The target spectrum analysis of two ROS1 inhibitors identified tight binding of the compounds to the receptor tyrosine kinase ROS1 (IC_{50}-values of 0.003 µM for compound 16366). Beside ROS1, other high affinity targets such as AAK1, NEK9, CSNK2A2, CSNK2B, BMP2K, NQO2, MAP4K3, HGK, MAP3K2, FAK and RPS6KA3 for 16366 and BMP2K, NEK9, LYN, FAK, MAP3K2, EPHB2, NQO2, TBK1, FER, MST1, PDXK, PAK4 and SRC for 16719 were detected. Interestingly many targets such as NEK9, BMP2K, SRC, NQO2, MAP3K2, FAK and TBK1 are inhibited by both compounds. Beside NQO2 all identified targets of both inhibitors are kinases belonging to different kinase families such as tyrosine or serine/threonine kinases. Having a closer look at the detected high affinity kinase targets it is interesting to see that many of these proteins including NEK9, BMP2K, FAK and TBK1 or RPS6KA1and RPS6KA3 are involved in cancer cell proliferation and survival as shown by RNAi experiments in this study. These biological functions of the targets are in accordance with the phenotype of the respective compounds on tumor cells seen after drug treatment for 72h as shown in the cell viability and caspase-3/7 assay in a large panel of different cancer cell lines. These findings show a direct correlation between target function, biological relevance of the respective target, target inhibition by the small-molecule inhibitor and drug phenotypes on cancer cells.

The universal cancer related role of identified high affinity targets, beside ROS1, such as NEK9, BMP2K and FAK might be the explanation for the broad anti-tumor activity of the two ROS1 inhibitors observed in a diverse spectrum of cancer cell lines from different tumor indications such as brain, breast, colon, kidney, lung, ovary and pancreas.

Nevertheless, the mass-spectrometry based off-target screen revealed that the identified ROS1 inhibitors are not quiet specific for ROS1 and might therefore be rather classified as multi-targeted than single-targeted small-molecule kinase inhibitors. In comparison to SU11248, the target panel of the two newly identified ROS1 inhibitors 16366 and 16719 is much smaller. To develop a specific ROS1 inhibitor, further chemical modifications would be necessary. Nonetheless, the identified new inhibitors have great potencies for *in vivo* studies based on their very potent inhibitory efficacies in cellular assays with IC_{50}- values smaller than 0.6 µM and strong cell-death inducing effects at concentrations of 10 µM and even lower.

Structural analysis of the top5 screening hits revealed that three out of five potential kinase inhibitors belong to the class of imidazo[1,2a]pyridazin-6-amines with almost structural identity. The structure of all five potent ROS1 inhibiting compounds is shown in Figure 91. Compound 16719 had the strongest effect on cancer cell viability with a median IC_{50}-value of smaller than 0.6 µM, followed by compound 16366 (3.88 µM) and compound 6, 7 and 5.

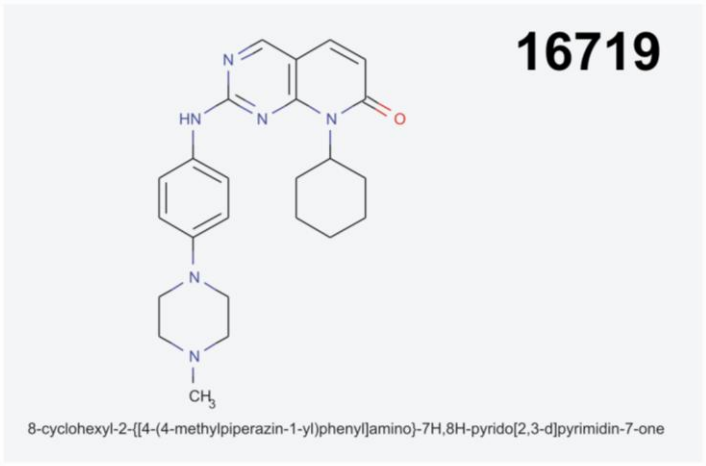

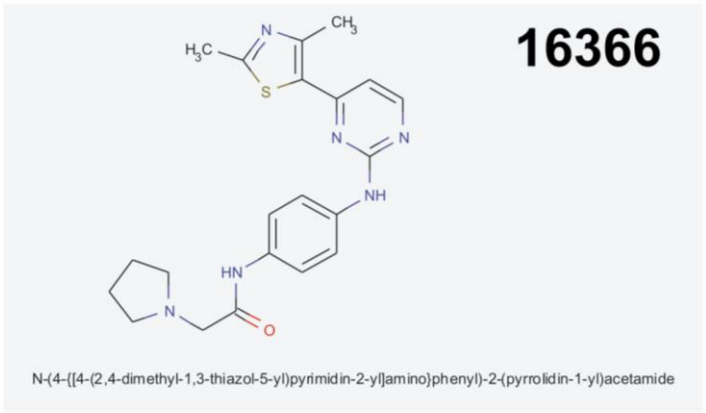

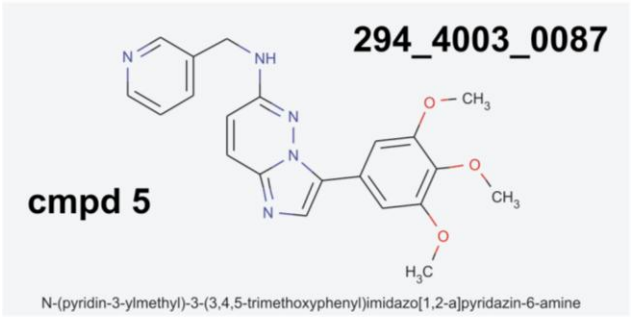

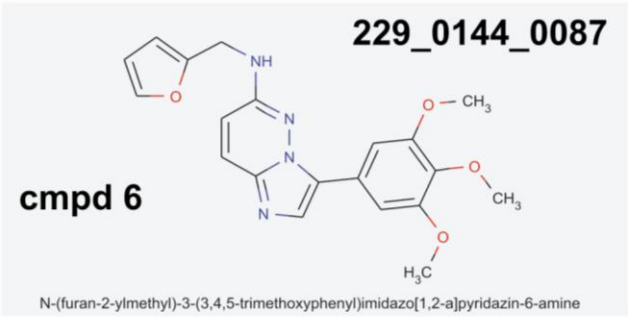

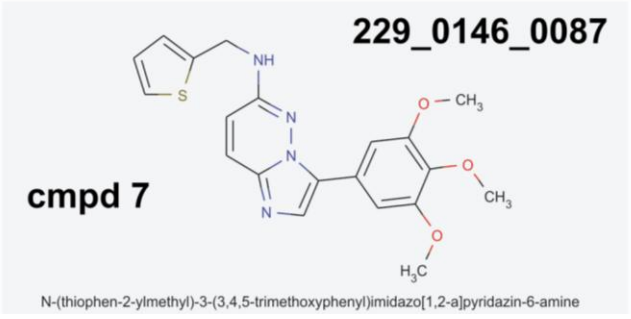

Figure 91 Chemical structure of five potent ROS1 kinase inhibitors with anti-proliferative and programmed cell death inducing effects on cancer cell lines from different tissue origins.

Taken together, the drug screening for ROS1 tyrosine kinase inhibitors revealed the chemical class of imidazo[1,2a]pyridazin-6-amines as a potent lead structure for the development of a selective kinase inhibitor against the receptor tyrosine kinase ROS1. The top5 screening hits were highly effective in cell-based toxicity assays and showed a strong impact on cancer cell proliferation and survival. High inhibition rates of cell viability, with up to 100 % dead cells at concentrations lower than 2.5 μM, were observed in a spectrum of cancer cells from different tissue origins including brain, breast, colon, kidney, lung, ovary and pancreas.

In summary, the identified compounds are the first step in the development of selective kinase inhibitors against the receptor tyrosine kinase ROS1 and have to be analyzed in detail and improved further to increase their cellular efficacy on cancer cells. One possible next step in the drug development process would be the synthesis and screening of chemical derivates with even stronger inhibition activities and better selectivity against the receptor tyrosine kinase ROS1. Moreover, compound activity *in vivo* is a major issue in drug discovery and the effect of lead structures in mouse xenograft models a crucial step from `bench- to bedside`.

8 Discussion

8.1 Global characterization of the small molecule kinase inhibitor SU11248

Protein kinases play critical roles in cellular signal transduction cascades and are directly involved in many diseases, including cancer where they are regulating cancer cell proliferation, survival and metastasis. Aberrant activation of protein kinases is a hallmark of, and critical mechanism for, oncogenic cell transformation. Targeting protein kinases with more than 500 potential intervention sites within a single cell (Manning et al., 2002) has become a potent tool in cancer therapy over the last decade (Cohen, 2002). Based on the functional knowledge of certain receptor tyrosine kinases like VEGFR2 playing an important role in vascularization (Millauer et al., 1993) and PDGF receptors being involved in cell proliferation and survival, the first selective small molecule kinase inhibitors like imatinib (Gleevec) for chronic myeloid leukaemia (CML) (Capdeville et al., 2002), gefitinib (Iressa) and erlotinib (Tarceva) for non-small cell lung cancer (Muhsin et al., 2003),(Blackhall et al., 2005), or SU5402 and SU6668 as the first oxindole-based compounds (Hoekman, 2001), have been developed.

These first generations of small molecule kinase inhibitors (SMKI) were initially thought to be quite specific, mainly targeting only one or two protein kinases (Knight and Shokat, 2005; Morin, 2000; Salmon et al., 1994). However, in recent years it became evident that SMKIs are not specific for one target and simultaneous inhibition of more than one kinase family could actually result in greatly augmented single-agent anti-tumor activity in preclinical and clinical studies compared to specifically agents like monoclonal anti-bodies targeting one kinase alone (Daub et al., 2004b). Therefore multi-targeted inhibitors came into the focus of interest.

SU11248, based on the specific indolinone precursor compounds SU5402 and SU6668, was developed as the first multi-targeted small molecule inhibitor (Atkins et al., 2006) addressing class III and class V RTKs, including PDGF receptors, VEGF receptors, KIT, and FLT3 (Abrams et al., 2003a; Faivre et al., 2006a; Mendel et al., 2003; Motzer et al., 2006b; Murray et al., 2003; O'Farrell et al., 2003a). *In vitro*, it inhibits these RTKs in biochemical, ligand-dependent phosphorylation with IC_{50}-values in the low micromolar range. *In vivo*, SU11248 is highly efficacious (frequently cytoreductive) in all tumour xenograft models investigated (Zhang et al., 2009b) and its full anti-tumour efficacy against solid tumours was so far associated with inhibition of receptor tyrosine kinases like PDGFR and VEGFR (Mendel et al., 2003; Schueneman et al., 2003).

Clinical studies with SU11248 showed a strong efficacy in advanced renal cell carcinoma (RCC) (Motzer et al., 2006b; Polyzos, 2008; Reddy, 2006) and in gastrointestinal stromal tumours (GIST) that are refractory or intolerant to imatinib (Demetri et al., 2006; Norden-Zfoni et al., 2007; Prenen et al., 2006). Furthermore, ongoing therapeutic investigations in several other tumour indications as acute myeloid leukemia (AML) or metastatic breast cancer as well as hepatocellular carcinoma provide hints of a broad antitumor activity spectrum of SU11248 (Abrams et al., 2003a; Abrams et al., 2003b; Fiedler et al., 2005; Kim et al., 2006; Motzer et al., 2006a; Murray et al., 2003; O'Farrell et al., 2003b).

Due to the therapeutic potential of SU11248 as a multi-targeted small-molecule receptor tyrosine kinase inhibitor showing strong anti-tumor and anti-angiogenic activity *in vitro* and *in vivo* in a variety of different tumor indications, it is of great general interest to globally understand the underlying molecular mechanisms of action responsible for its therapeutic efficacy. In this context, the drug target profile of SU11248 is of major importance by providing insights into putative sites of cellular activities. The knowledge about an inhibitor´ s true selectivity is a prerequisite for the correct interpretation of its biological effects thus allowing a better predictability of its efficacy in a certain tumour type which is of great importance for clinical application. In addition to target patterns, sensitivity profiles of a compound in a broad spectrum of cancer cell lines may lead to a better understanding of the anti-tumor activity and aid in the optimal selection of clinical indications for the drug in future.

This study was performed to understand the underlying molecular mechanisms of SU11248 action on cancer cells in order to obtain a molecular signature of tumor sensitivity as a basis for response prediction and further applications in new tumor indications. The molecular definition of a drug leads the prediction of its pharmacodynamic function and therapeutic impact *in vivo*. Moreover, a comprehensive analysis of SU11248, as done in this work, helps to avoid possible severe treatment side-effects such as cardiovascular toxicity and liver failure as observed in the past (Di Lorenzo et al., 2009; Joensuu, 2007; Machiels et al., 2008; Schmidinger et al., 2009; Schmidinger et al., 2008; Weise et al., 2009).

The anticancer drug SU11248 was originally designed to inhibit predominantly split kinases like PDGFRa, PDGFRb, KIT and VEGFR2 involved in tumor angiogenesis and proliferation (Abrams et al., 2003a; Kim et al., 2006; Mendel et al., 2003; O'Farrell et al., 2003a). Due to its broad activity in many different cancer types, as shown in the performed cell line screen and also revealed in several running clinical studies, ranging from advanced hepatocellular carcinoma to breast cancer (Fiedler et al., 2005; Murray et al., 2003; O'Farrell et al., 2003b; Polyzos, 2008; Zhu et al., 2009b), the question rose whether there are more than the known SU11248 targets being relevant for its clinical efficacy. To get a better and more global understanding of the mechanisms of action of the small molecule inhibitor in cancer cells which might lead to a more predictable drug efficiency in a certain cancer type we used a chemical proteomics approach in 30 different sensitive cancer cell lines of different tissue origin and primary mRCC tumor samples to reveal the global target pattern of SU11248. The advantage of this method in comparison to *in vitro* kinase assays or overexpressing systems as described before (Fabian et al., 2005; Karaman et al., 2008) for drug target screens is that the combination of an affinity purification strategy with immobilized SU11248 and subsequent MS-based protein identification enables the identification of potential proteome wide and not only kinase drug targets directly from cells profiling the interaction of the small molecule inhibitor with endogenously expressed protein kinases and other ATP- or purine-binding proteins such as helicases, ATPases, motor proteins and metabolic enzymes. It takes also into consideration the activation status of certain targets which is not taken into account if used recombinant proteins for a selectivity screen as well as native conformations, post-translational modifications, isoform expression and interaction with regulatory and functional relevant binding partners under physiological conditions.

Moreover, the performed target evaluation directly from primary tumor samples increases the significance and clinical relevance of identified SU11248 interaction partners as potential molecular site of action. The comparison of cell-based and tumor-based target profiles and the identification of shared hits solidify their therapeutic importance and can be translated into biomarkers for SU11248 efficacy in the context of individualized targeted cancer therapy. In addition, the identification of high affinity targets in various cancer cell lines from different tumor indications strengthens their essential functions for the anti-tumor activity of SU11248 *in vivo*.

Furthermore, this work reveals cancer tissue specific interaction maps showing that an inhibitor` s target spectrum differs from indication to indication which is in accordance to the genetic diversity of the cancer genome (Stratton et al., 2009). As such, the identification of cancer type specific SU11248 targets may be of great benefit for choosing the right sub-indication of a certain tumor type suitable for SU11248 treatment of patients in the future. Moreover, tissue-unique target profiles provide a more detailed insight into indication specific drug action which is not revealed by *in vitro* kinase target screens testing the drug` s affinity towards a fixed panel of recombinant proteins (Fabian et al., 2005; Karaman et al., 2008).

In this study, 313 endogenously expressed kinases were identified as potential SU11248 targets among all tested cancer cell lines and mRCC tumors. The number of identified kinase binding partners in each cell line varied between 25 and 146 specific kinases. Beside known targets such as PDGFRα, PDGFRβ, KIT, VEGFR2, RET and CSF1R, new receptor tyrosine kinase targets including AXL, SKY, MERTK, FGFR1, RON, MET and ROS1 were detected to be specifically targeted by the small molecule kinase inhibitor SU11248. Interestingly, so far only shown to inhibit receptor tyrosine kinases, the cellular target-profiling of SU11248 revealed its strong interaction also with cytosolic tyrosine kinases such as FAK, FER, LYN, FYN, JAK1, YES1 and SRC as well as non-tyrosine kinases including NEK9, BMP2K, TBK1, AAK1, RPS6KA1 and other proteins such as non-protein kinases like NME4, metabolic enzymes or small-GTPases all carrying purine-binding sites. These data strongly support the multi-targeted character of the small-molecule kinase inhibitor SU11248. The broad target spectrum is in accordance with its efficient anti-tumor effects as seen for metastatic renal cell carcinoma (Le Tourneau et al., 2007), GIST (Janeway et al., 2009) but also in ongoing clinical studies in brain, breast, liver, melanoma and many more tumor indications (Bajetta et al., 2009; Battistella et al., 2009; Burstein et al., 2008; Kelleher and McDermott, 2008).

Originally designed to interact with and inhibit tyrosine kinases, SU11248 also targets kinases of other families such as TKL, CMGC and STE. The broad kinase panel is reflected in the activity spectrum and biological function of respective kinases. Gene Ontology annotation of SU11248 kinase targets revealed the overrepresentation of kinases being involved in cancer cell proliferation, migration, invasion and survival as well as other functions such as regulating cell differentiation. Identified non-kinase SU11248 interaction partners are implicated in key metabolic pathways such as glycolysis, fatty acid metabolism and purine- and pyrimidine-biosynthesis as well as translation. Surprisingly, based on the very diverse target spectrum and the interference of the small molecule inhibitor with key components of the cellular energy homeostasis, one would expect severe side-effects in the clinic. Nonetheless, the observed toxicities are in a normal range compared to other small molecule inhibitors targeting only single proteins such as imatinib for BCR-ABL or

gefitinib for EGFR. Observed side-effects are fatigue, nausea, and other less awkward disorders. In some rare cases, cardiovascular toxicity or liver failure was reported. In one case, SU11248 treatment caused myxedema coma (Chen et al., 2009). The reason for this low *in vivo* toxicity might be the cancer specific target profile of the drug. Directed only against oncogenic kinase signalling makes a drug selective for fast dividing tumor cells whereas normal quiescent cells are not susceptible to the drug. Normal cells do not rely on single pathways but on several redundant ones. This phenomenon helps them to escape drug-toxicities.

With 313 potential kinase and even more non-kinase targets in hands, the question rose, which of those identified binding partners are essential for the anti-tumor effect of SU11248 on diverse cancer cell lines and tumors *in vivo*. One important and critical step is to rank and prioritize molecular interaction by binding affinities. This helps to identify the strongest molecular associations that are likely the most relevant in physiological conditions. Targets are blocked at different concentrations that may or may not be reached *in vivo* upon inhibitor treatment.

Two different, a semi-quantitative and quantitative affinity-chromatography and mass-spectrometry based methods were used to estimate the binding affinities of endogenously expresses proteins towards the small molecule kinase inhibitor SU11248 directly form cancer cell lines and tumor samples. The combination of semi-quantitative and quantitative strategies enables the estimation of target affinities over a broad range of different cancer cell lines and tumor tissues. Target affinities for a particular protein may differ from cell line to cell line due to conformation and activation differences caused by target mutations, differentially expressed cofactors and activation status within the respective cancer cell type. Therefore it is of great importance to screen for molecular interaction patterns and binding affinities in a diverse spectrum of cellular cancer models to obtain a global and profound understanding of the drug. The advantage of cell-based over *in vitro* screening methods as performed earlier for SU11248 in two recombinant kinase assay studies (Fabian et al., 2005; Karaman et al., 2008) is the comprehension of native target conformations, cellular ATP concentration, post-translational modifications and physiological conditions in general, which all influences target affinities towards the small molecule kinase inhibitor and is not taken into account using *in vitro* kinase assays. In particular, the use of the semi-quantitative approach allows the affinity profiling in primary tumor samples where metabolic cell labelling for a quantitative K_d-value calculation is not possible. This study was the first one reporting target-affinities of a small-molecule inhibitor directly from tumor samples thereby increasing the validity and reliability of obtained target data for the interpretation of drug efficacies and tumor responsiveness *in vivo*. The biochemical basis for the calculation of target affinities was their ability of being retained by a SU11248 matrix used for affinity-chromatography. In the case of the semi-quantitative approach, the amount of bound protein to the matrix was expressed in sequence-to-spectrum matches reflecting the peak height and width in the LC/MS analysis. The more protein is eluted the wider the peak, the bigger the number of identified spectra for this particular protein. In the case of the quantitative method the protein amount retained on the affinity matrix was directly measured by relative peptide intensities integrated over the elution profile and all peptides belonging to one protein. The consecutive double enrichment strategy of proteins directly from cell lysates and tumor probes enables the calculation of binding affinities based on enrichment factors. The stronger the molecular interaction between

a respective target and the small molecule kinase inhibitor is the more protein is retained in the first round of incubation. High affinity targets should almost be depleted from the cell extract in the first binding step whereas moderate binding partners bind equally in both rounds of affinity chromatography and low affinity interaction proteins are only captured in the second incubation step. This approach led to the identification of tissue specific high affinity SU11248 targets.

A positive correlation was observed between the target detection frequency in the qualitative binding screen and strong binding capacities of a certain target in the second approach. Beside the known targets such as CSF1R, FLT3, VEGFR2, KIT, PDGFRα, PDGFRβ and RET, which were considered as internal positive controls, other very interesting kinase targets were identified to be strongly inhibited by SU11248. For example the receptor tyrosine kinase AXL was strongly inhibited in breast cancer and renal cell carcinoma cells lines which could be validated in cellular kinase assays with an IC_{50}-value of 0.43 µM. Axl is described to be involved in cancer cell migration and invasion (Zhang et al., 2008). Its inhibition by SU11248 might describe the anti-migratory and anti-invasive phenotype of SU11248 seen in aggressive cancer cell lines. The cellular IC_{50}-value of AXL auto-phosphorylation inhibition by SU11248 was in the same range of earlier described potential inhibitors such as SKI-606. Therefore, AXL could be a promising new SU11248 target in aggressive cancers such as breast or metastatic renal cell carcinoma in the clinic in future and might be taken as a biomarker of responsiveness. The exact functional correlation between target expression and SU11248 sensitivity of respective tumors has to be proven further by RNAi *in vitro* or tissue arrays of SU11248 responsive cancers in the clinic. Also other receptor tyrosine kinases including MET, MER, FGFR family members, RON and ROS1 are promising new targets and might be responsible for the broad activity of SU11248 on cancer cell lines of diverse tumor types. Aberrant receptor tyrosine kinase signalling has been implicated in several diseases such as cancer, inflammatory diseases and autoimmune defects, e.g. diabetes. As such, this strongly suggests a therapeutic potential for SU11248 beyond cancer. First hints were observed in cancer patients having diabetes. A remission of diabetes in these patients was reported while on SU11248 treatment for renal cell carcinoma (Templeton et al., 2008).

The comparison of high affinity targets identified in cancer cell lines of a variety of different tumor types and tight interaction partners detected in tumor samples of primary metastatic renal cell carcinoma lead to a robust, comprehensive identification of 24 direct SU11248 targets as potential important sites of molecular action of the drug. Their *in vitro* and *in vivo* relevance is increased by their independent identification in a broad spectrum of different tumor indications as well as patient material. Beside interesting new kinase targets such as ROS1, NEK9, BMP2K, NME4, FAK, FER and TBK1, the applied proteome wide cell-based approach of SU11248 target identification revealed non-kinase targets for which a strong binding to the small molecule inhibitor could be shown by quantitative K_d determination directly from cell extracts. Most prominent non-kinase interaction partners are the Ribosyldihydronicotinamide dehydrogenase (NQO2), glycogen phosphorylases, the Acyl-CoA thioesterase 7 (ACOT7), NAD(P)H dehydrogenase 1 (NQO1), Alpha-Enolase (ENO1), Beta-Enolase (ENO3) and other purine-binding enzymes involved in key metabolic pathways and protein biosynthesis.

Altogether, in comparison to previous studies this proteome wide target screen of SU11248 in a variety of different cellular cancer systems and primary tumors gives rise to a more complete and comprehensive target picture and allows to define more precisely potential mechanisms of action responsible for the drug` s efficacy.

The identification of new non- kinase targets including NQO2, ACOT7, NQO1, ENO1, ENO3 and other metabolic enzymes suggests for the first time an impact of SU11248, and perhaps small-molecule kinase inhibitors in general, on key metabolic processes like fatty acid metabolism, citrate cycle, glycolysis and amino acid metabolism which are implicated or associated with several cancer types (Begleiter et al., 2005; Chao et al., 2006; Cresteil and Jaiswal, 1991; Lewis et al., 2005; Racz et al., 2000; Trojanowicz et al., 2009). Furthermore, the identification of the oxidoreductase NQO2 as a new SU11248 target could already be shown to be also targeted by the small-molecule kinase inhibitor imatinib (Gleevec) (Bantscheff et al., 2007). This supports the hypothesis of small-molecule inhibitors not only interfering with oncogenic kinase signalling but also with cancer relevant metabolic events. Moreover, this work is the first one identifying non-kinase SU11248 targets in a global manner.

The good correlation between interaction maps and target affinities from cell lines and tumors shows the good performance and reliability of the used method and underlies the quality of cell line models for *in vitro* cancer studies not only for characterization of small molecule inhibitors but for cancer relevant aspects in general. The advantage of the applied semi-quantitative method for affinity calculation of small molecule inhibitor interaction partners is that there is no need of time-consuming cell labelling processes and it can be used in a high-throughput manner also in tumor samples where labelling is restricted. A good correlation between quantitative and semi-quantitative K_d-values could be shown. In comparison to earlier kinase affinity studies for SU11248 like the two AMBIT-Biosciences studies (Fabian et al., 2005; Karaman et al., 2008), the endogenous K_d-values in this study are slightly higher but with a large overlapping target panel. The difference between affinities determined in biochemical recombinant *in vitro*-kinase assays and cellular systems occur due to higher cellular ATP-levels. As SU11248 is a competitive inhibitor of ATP-binding towards the kinase domain, increasing ATP-levels under physiological conditions cause a shift of target affinities towards putative worse half-maximum inhibition concentrations than in biochemical assays. Nevertheless, this cell-based approach leads to more realistic binding affinities transformative for *in vivo* situations while patient treatment in the clinic.

The broad target spectrum might be a reason for the strong SU11248 sensitivity in many different cancer cell lines of a lot of different tumour types as seen in the biological screen of 63 cancer cell lines in this work or ongoing clinical studies and previously shown data. Usually, inhibitors targeting only few proteins are more likely to be restricted with their efficacy to a small number of tumour indications, depending on the expression status and tumour dependency of the inhibitor targets. Targeting many different proteins increases the efficacy of a drug even in completely different genetic backgrounds of cancer cells and reduces the probability of a cell developing resistance mechanisms against the drug (Daub et al., 2004b).

Due to the identification of cellular drug interaction partners directly from cells, this study reveals a target pattern of SU11248 in a physiological background which can be directly correlated to its biological

functions. Furthermore, the broad sensitivity screen of 63 cancer cells lines of different tumor origins against SU11248 underlines its strong efficacy in cancer therapy, as shown in ongoing clinical studies and gives evidence for potential new therapeutic intervention in tumour indications like the highly aggressive tumours glioblastoma or pancreas cancer.

Taken together, the target interaction study revealed prominent 24 high affinity targets of SU11248 as potential site of molecular drug action within cancer cells.

In general, the advantage of the used approach to investigate drug target profiles, target affinities and biological functions of an inhibitor is that in comparison to *in vitro* kinase assays or over-expressing systems with recombinant proteins as previously described (Fabian et al., 2005; Karaman et al., 2008), the combination of an affinity purification strategy with immobilized SU11248 and subsequent MS-based binding partner identification enables the detection of potential proteome wide and not only kinase drug targets directly from cell lysates or tumor samples under native conditions. Proteins are endogenously expressed and present under physiological ATP concentrations in their active state while binding to the drug. In addition, native conformations, post- translational modifications, isoform expression and interaction with regulatory and functionally relevant binding partners of putative targets are taken into consideration all influencing the drug` s target affinity. Furthermore, the competition of an interaction partner with other targets in the cell is not taken into consideration in biochemical assays. In addition, screens using purified protein substrates do not accurately represent biological levels of target proteins, potentially leading to generations of incorrect hypotheses for on- or off-target drug effects. Higher attrition rates in later stages of drug development, optimization and response prediction of efficacies and possible side-effects arising from unanticipated or undetected off-target effects, or lack of relevance of the target protein to the underlying disease process is a major problem of *in vitro* kinase assays lacking the biological context.

Moreover, the applied strategy is an unbiased target identification tool also applicable in tumor samples where metabolic labeling is restricted. The method is scalable and general, requiring little optimization across different tumor indications and could be used for small-molecule inhibitors of different classes.

Furthermore, from the standpoint of drug safety and efficacy, unbiased identification of proteins and associated molecular complexes that bind to a drug allows direct evaluation of its polypharmacology and provides valuable insight into mode of action and avenues for compound optimization in a robust, comprehensive manner.

A crucial step in the comprehensive characterization of a small molecule inhibitor and particular in the identification of important drug targets which are relevant for the drug` s efficacy *in vivo*, is the biological relevance of respective high affinity targets in the context of tumor development and progression. Functional target importance of high affinity SU11248 targets in cancer cells was assessed using an RNAi approach.

The knock- down of high affinity kinase targets such as ROS1, NEK9, BMP2K, TBK1, AURKB, FAK and NME4 led to anti-proliferative and programmed cell death inducing effects. These biological functions are consistent with SU11248 effects on cancer cell lines of different tissue origins. A direct proof of target importance could be revealed by the combination of RNAi and SU11248 treatment. Importantly, the

depletion of ROS1, BMP2K, TBK1, AURKB, FAK and NME4 significantly reduced the SU11248 efficacy. These observations directly link target expression and target function to inhibitor efficacy.

With ROS1, NEK9, BMP2K and NME4, not previously described as being involved in cancer cell proliferation and survival, the functional RNAi target screen identified new apoptosis and cell proliferation relevant genes in cancer. This not only elucidated important molecular mechanisms of SU11248 action but also provides a basis for future intervention therapy in cancer by focussed inhibition of these kinases.

These new targets, ROS1, BMP2K, TBK1 and NME4 may be considered as biomarkers for SU11248 sensitivity in future.

Inhibition of ROS1 and other protein kinase targets involved in apoptosis, like NEK9, BMP2K, NME4, AURKA, AURKB, RPS6KA1, RPS6KA3, TBK1 and FAK by SU11248, might be the reason for the strong apoptosis-inducing effect of SU11248 on cancer cells. Inhibition of FAK might also be responsible for the anti-migratory effect of SU11248 (Jones et al., 2001; Sieg et al., 1999). In addition, other targets such as FER, FYN, LYN, SRC and YES1 were described earlier to play key roles in cancer cell migration and invasion (Nelson and Nusse, 2004). Other identified targets including CDKs, NEK kinase family members and PCTAIREs might be involved in the cell cycle block seen after SU11248 treatment.

To underline the importance of high affinity interaction partners for the drug` s efficacy *in vivo*, the question rose whether there are differences in target binding patterns and expression levels between SU11248 responsive and less sensitive cancer cell lines. Based on the cell-based phenotypic screen of SU11248 responsiveness, cancer cell lines of the different tumor indications were grouped into two classes in accordance to their SU11248 sensitivity. To elucidate genetic differences of sensitive and less-sensitive cell lines in-house makro-arrays were performed to compare the cellular expression profiles. Moreover, binding patterns and the amount of retained specific SU11248 targets between theses two cell line groups were compared using a quantitative mass-spectrometry based affinity chromatography approach. The comparison of kinase binding revealed that high affinity targets including the new interaction partners ROS1, BMP2K, NEK9, NME4, TBK1, FAK, FER, RPS6KA1 and RPS6KA3, as well as known targets such as KIT and PDGFRβ, are highly enriched in SU11248 sensitive cell lines. This indicates a potential essential function and relevance of these targets for the SU11248 activity *in vitro* and *in vivo*.

Gene expression analysis revealed the overexpression of interesting genes involved in drug resistance mechanisms and autocrine receptor activation in SU11248 insensitive or less-responsive cancer cell lines. Higher levels of matrixmetalloproteinases (MMPs), elevated levels of G-protein coupled receptors such as EDG7 and EDG3, as well as increased expression of receptor ligands were observed over a panel of different tumor types indicating an universal drug resistance mechanism of cancer cells towards the small-molecule kinase inhibitor SU11248. The most prominent finding of expression differences between sensitive and insensitive cells was in the context of cell transition from an epithelial-to-mesenchymal state. Gene and protein expression profiling showed that SU11248 sensitive cell lines are mesenchymal- like with high levels of Vimentin, compared to insensitive cell lines which are more epithelial-like, expressing high levels of E-cadherin. The expression of these two proteins in tumors could therefore be used to screen for sensitivity to SU11248. One reason for this sensitivity difference might be the fact that mesenchymal-like cells are more

aggressive with higher proliferation rates in comparison to more quiescent epithelial-like cancer cells and thereby being more susceptible to the drug treatment. This effect could already be shown in the past for tumor versus normal cells where the higher rate of proliferation as occurring in tumor cells was an important factor in the sense of drug responsiveness. A positive correlation between fast-proliferating active tumor cells and drug susceptibility was observed and one reason for the development of chemotherapeutics and later target specific cancer therapies.

Target interaction patterns alone do not reveal the complete function of an inhibitor. To truly and fully understand its molecular action and activity the cell-wide impact on signalling events regulating cellular homeostasis is important. Not only direct target and protein interactions are essential for a drug` s efficacy, but also second, third and higher level inhibition events. The observation of target inhibition alone does not comprehensively uncover the complete picture of the cellular drug action. As signalling pathways are arranged in cascades, it is very crucial that direct inhibition events by the inhibitor taking place at the cell surface or innercell membrane, are transferred to the nucleus influencing gene expression und subsequent cellular processes. To elucidate these complex networks of inhibitory processes taking place upon inhibitor treatment, a phosphoproteomic study of cancer cells being incubated with SU11248 was performed.

The phospho-SILAC-study showed a strong impact of SU11248 on a broad range of different signalling pathways within the cell. The impaired networks are involved in the regulation of cancer cell proliferation, migration, invasion, survival and exo-/enodcytosis. These findings are in accordance to the observed phenotypes of cancer cell lines reacting to SU11248.

In conclusion, the applied phosphoanalysis of drug treated cancer cells revealed for the very first time a comprehensive picture of small-molecule inhibitory sites within a cell not only for SU11248 but inhibitors in general which haven` t yet been analyzed on a proteome wide phospholevel giving a very detailed insight into the drug` s mechanism of action not only on direct targets but affected signalling networks in general. Understanding an inhibitor` s true function by knowing its target profile and global interference map on key pathways of cellular signalling is a prerequisite for drug efficacy prediction, estimating potential side effects in patients and drug development and improvement of small-molecule inhibitors in general in the future.

Taken together, this study comprehensively reveals the multi-targeted mechanism of action of SU11248. This is in accordance with previous reports showing the broad target spectrum of SU11248 *in vitro* (Fabian et al., 2005; Karaman et al., 2008). This report shows that beyond already described targets such as PDGF receptors, VEGF receptors, CSF1R, RET and FLT3, there are important other high affinity targets being highly relevant for the SU11248 efficacy and its strong anti-tumor action.

Together with target clusters enriched in sensitive cancer cell lines, the phenomenon of mesenchymal-like cell lines being more responsive to SU11248 than epithelial-like and potential resistance mechanisms, deduced from insensitive and less sensitive cell systems, such as higher levels of MMPs, elevated levels of G- protein coupled receptors and increased expression of receptor ligands, this study initiates a new era of SU11248 therapy application and drug response predictability which may lead to improved clinical benefit due to a better selection of candidate patients by taking the individual genetic background of the tumor into account.

Furthermore, we could show for the first time the biological relevance, potency and impact of high affinity SU11248 targets in cellular systems resembling a tight correlation between target inhibition and SU11248 efficacy in different cell lines ranging from mRCC, breast cancer, glioblastoma and pancreatic cancer thereby revealing the mechanism of molecular action of SU11248. A direct proof of target importance could be revealed by showing decreased SU11248 efficacy after target depletion with RNAi. Furthermore, with our functional RNAi target-screen we could identify completely new cell survival and cell proliferation relevant genes in cancer, namely ROS1, NEK9 and BMP2K, so far not described being involved in such processes, thereby not only elucidating important molecular mechanisms of SU11248 efficacy but also giving a basis for further target intervention in cancer therapy in general by inhibiting kinases like ROS1, NEK9 and BMP2K with new selective small molecule inhibitors in future. Taken together, targets like ROS1, NEK9, BMP2K and NME4 amongst others like RPS6KA3, FAK and AURORA Kinases can be considered as biomarkers for SU11248 sensitivity in the future.

The understanding of an inhibitor` s true mechanism of action by knowing its target profile and comprehensive interference map in key pathways of cellular signalling is a prerequisite for drug efficacy prediction, estimating potential side effects in patients and improvement of small molecule kinase inhibitor development in general.

In summary, this study provides detailed insights into SU11248 action which have to be proven further in patients. Correlation of target expression, the consideration of markers of responsiveness and tumor sensitivity has to be performed in a broad spectrum of tumor indications to confirm the target relevance in humans.

8.2 Characterization of the receptor tyrosine kinase ROS1 and the development of a small molecule kinase inhibitor specifically inhibiting the proto-oncogene kinase

Cancer is a genetic disease permanently undergoing molecular changes while progressing. With the identification of cancer driving genes such as kinases, an era of new therapeutic intervention started. The development of specific small molecule inhibitors against oncogenic kinases such as EGFR and KIT or BCR-ABL revealed that targeted cancer therapy is possible. Since then, many inhibitors have been developed and reached the clinic. Nonetheless, cancer is still a devastating disease escaping targeted therapy. Genetic instability of cancer cells is one reason for fast developing drug resistances while cancer therapy. As such, there is an urgent need of more target-specific kinase inhibitors in the context of curing cancer or making it at last a chronic disease. The application of inhibitor cocktails based on the individual genetic background of tumors and patients might be one possibility for a successful cancer therapy in the future.

ROS1 seems to have a universal function in cancer cell proliferation and survival which could be shown by RNAi experiments. The knock-down of the receptor tyrosine kinase significantly induced programmed cell death and a proliferation stop in a diverse spectrum of different cancer cell lines including brain, breast, colon, kidney, lung and pancreas. This key role brought ROS1 in the focus of drug discovery and development. Killing cancer is a major goal of targeted therapy. Moreover, ROS1 was shown to be implicated in glioblastoma multiforme (Birchmeier et al., 1990; Birchmeier et al., 1987) and tumor

rearrangements in general (Rabin et al., 1987). Another advantage of ROS1 as a target in cancer therapy is the fact that it could be already shown to be druggable either in this work by the small-molecule kinase inhibitor SU11248 or in a previous drug development screen (Park et al., 2009).

For a better understanding of underlying molecular mechanisms of ROS1 signalling, a crucial step was to analyze potential interaction partners binding to ROS1. To elucidate signalling platforms and networks, a mass-spectrometry based quantitative method was used. Interaction profiling revealed interesting binding partners such as the epidermal-growth factor receptor tyrosine kinase (EGFR) or Annexin V and PKCα. The screen was performed only once, but provides first hints for a molecular mechanism of ROS1 signalling controlling cancer cell proliferation and survival. The interaction of ROS1 and EGFR could be confirmed by western blot analysis and might be a potential very interesting new aspect of oncogenic kinase signalling. The observation that ROS1 is highly expressed in NSCLC, its anti-apoptotic function in lung cancer as shown by knock-down experiments and the finding that EGFR is a driving factor of lung cancer development and progression (Metro et al., 2006; Mukohara et al., 2003) leads to the hypothesis that the concurrent inhibition of ROS1 and EGFR by small-molecule kinase inhibitors might have synergistically effects thereby increasing drug response rates in lung cancer and improving the treatment for this aggressive type of cancer. This has to be proven *in vitro* and *in vivo* in further experiments.

The drug screening of compound libraries against the receptor tyrosine kinase ROS1 performed in this study resulted in five potent ROS1 inhibitors, inhibiting ROS1 auto-phosphorylation in a biochemical assay in a low-molecular range. IC_{50}-values were determined for concentrations equal to and below 1 µM. Since ATP concentrations are relatively high in *in vitro* kinase assays, it is important to validate the receptor tyrosine kinase auto-phosphorylation inhibition in cellular systems. A next step in the development of a specific ROS1 inhibitor would be therefore the performance of cellular kinase assays. These experiments are in process. For three potent ROS1 inhibitors a cellular kinase activity inhibition was observed.

In the process of developing potential new drugs it is important to screen for cell-based phenotypes of the respective small-molecule inhibitor. Compounds inhibiting tyrosine kinase signalling *in vitro* are not necessary useful for the treatment of patients at later stages. They might not show anti-tumor effects *in vivo.* One possible reason could be the fact that the compound cannot penetrate into the cells or does not bind to the active conformation of the respective target. Therefore, the top20 screening hits out of the biochemical assay were applied to a phenotypic screen. Their effect on cancer cell proliferation and survival was assessed using a colorimetric cytotoxicity assay. The inhibitory effect on cancer cell growth was monitored after 72h of drug application. 5 compounds out of 20 showed strong anti-tumor effects in a broad spectrum of cancer cell lines of different tumor indications such as brain, breast, ovary, kidney, lung, pancreas and colon. They are promising candidates for further detailed characterization and may lead to in the clinic applicable drugs. Beside a strong anti-proliferative effect, the top3 compounds also heavily induced programmed cell death detected by caspase-3/7-activity in diverse cancer cell lines. Both cellular drug phenotypes, namely the inhibition of cancer cell proliferation and survival, are important drug actions for effective anti-tumor effects *in vivo*. The real compound efficacy *in vivo* has to be tested in mouse-xenograft and tumor models.

The structural analysis of these small molecules revealed a structural relationship for three of them. They belong to the class of imidazo[1,2a]pyridazin 6- amines and might be a new class of ROS1 inhibitors. The class of imidazo-pyridazin 6-amines is not yet described as tyrosine kinase inhibitors used in the treatment of cancer. They might be a potential new class of anti-cancer drugs.

The other two lead compounds belong to the class of pyrido-pyrimidins and pyrimidins, respectively. Pyrido-pyrimidins are already reported to inhibit kinases such as CDK4, Src and Abl (Antczak et al., 2009; VanderWel et al., 2005; Vu et al., 2003).

In the development process of new potential anti-cancer drugs, their target selectivity is of great importance. Drug target spectra are responsible for the compound anti-tumor effectivities and possible side-effects during patient treatment. Their specificity was proven by using a chemical proteomics approach as performed for the small-molecule kinase inhibitor SU11248 in this study. The target selectivity screen revealed ROS1 as the top-kinase to be inhibited by the lead compounds. Moreover, other kinases such as AAK1, TBK1, NEK9, BMP2K, SRC, FER and FAK were shown to be potently inactivated by the drugs. These multi-targeted efficacies might be very promising for good *in vivo* anti-tumor results. The panel of inhibited kinases plays a key role in cancer cell proliferation and survival as demonstrated by RNAi experiments in this study and might be an explanation for the potent drug activities observed in a broad spectrum of cancer cell lines of different tumor types.

In summary, the functional characterization of high affinity SU11248 targets by RNAi revealed the receptor tyrosine kinase ROS1 as a potential new target for specific cancer therapy. Its universal function in cancer cell proliferation and survival and implication in tumors of the brain makes it of special interest for new targeted drug discovery. Moreover, its wide expression in cancer cell lines of different tumor indications and the possible oncogenic potential as shown by a very weak expression in normal tissue of the kidney, might lead to a broad band inhibitor useful for different cancer types. The shown interaction with the receptor tyrosine kinase EGFR is another very interesting aspect of the kinase and may be of clinical benefit, for example in the treatment of NSCLC. The drug screening method performed in this study provides first lead compounds in the development of a specific ROS1 inhibitor which have to be analyzed further and tested *in vivo*, as for example xenografts, on the way to a clinical application.

9 Abbreviations

Within this thesis the abbreviations showed in the following list were used.

ABL	c-abl oncogene 1, receptor tyrosine kinase
AGC	Containing PKA, PKG, PKC families
AML	acute myeloid leukemia
ATP	adenosine triphosphate
BCR	breakpoint cluster region
BMP2K	BMP2 inducible kinase
BMI1	Bisindolylmaleimide I
CAMK	Calcium/calmodulin-dependent protein kinase
cDNA	complementary DNA
CK1	Casein kinase 1
CMGC	Containing CDK, MAPK, GSK3, CLK families
CML	chronic myeloid leukemia
CMPD	compound
CRC	colorectal cancer
CSF1R	colony stimulating factor 1 receptor
DMSO	Dimethylsulfoxide
ECM	extracellular matrix
EGFR	epidermal growth factor receptor
ELISA	Enzyme-linked immunosorbent assay
EMT	epithelial-to-mesenchymal-transition
FACS	Fluorescence-activated cell sorting
FAK	focal adhesion kinase
FCS	fetal calf serum
FDA	US Food and Drug administration
FGFR1	fibroblast growth factor receptor 1
FISH	fluorescence *in situ* hybridization
FLT3	fms-related tyrosine kinase 3
FPLC	Fast protein liquid chromatography
GIST	gastro intestinal stromal tumor
HER2	v-erb-b2 erythroblastic leukemia viral oncogene homolog 2, neuro/glioblastoma derived oncogene homolog (avian)
HPLC	high-pressure liquid chromatography
IC	inhibitor concentration
IVA	*in vitro* association
KIT	v-kit Hardy-Zuckerman 4 feline sarcoma viral oncogene homolog
LC	liquid chromatography
LD	lethal dose
LTQ-Orbitrap™	linear ion trap orbitrap
MeOH	methanol
MET	mesenchymal-to-epithelial transition
MIN	microsatellite instability
MMP	matrix-metalloproteinase
MMR	mismatch-repair
mRCC	metastatic renal cell carcinoma
MS	mass-spectrometry
MTT	3-(4,5-Dimethylthiazol-2-yl)-2,5-diphenyltetrazolium bromide
NEK9	NIMA (never in mitosis gene a)- related kinase 9
NER	nucleotide-excision repair
NET	neuroendocrine tumor
NSCLC	non-small-cell lung cancer
NME4	non-metastatic cells 4, protein expressed in

PDGF	platelet-derived growth factor
PDGFR	platelet-derived growth factor receptor
PI	propidium iodide
PKA	Protein Kinase A
PKAI	Protein Kinase A inhibitor
PKC	Protein Kinase C
pS	phosphoserine
pT	phosphothreonine
PTK	protein tyrosine kinase
pY	phosphotyrosine
RET	ret proto-oncogene
RNA	ribonucleic acid
RNAi	ribonucleic acid interference
ROS1	c-ros oncogene 1, receptor tyrosine kinase
RTK	receptor tyrosine kinase
SCF	KIT ligand
SCLC	small cell lung cancer
SEM	standard error of the mean
SILAC	stable isotope labelling with amino acids in cell culture
SMKI	small molecule kinase inhibitor
SOTA	self-organizing tree algorithm
SRB	Sulforhodamine B
Src	v-src sarcoma (Schmidt-Ruppin A-2) viral oncogene homolog (avian)
STE	Homologs of yeast Sterile 7, Sterile 11, Sterile 20 kinases
STK	serine/threonine kinase
TBK1	TANK-binding kinase 1
TGF β RII	transforming growth factor- β receptor II
TK	tyrosine kinase
TKL	tyrosine kinase-like
VEGF	vascular endothelial growth factor

10 References

(2009). Gefitinib: a second look. Non-small cell lung cancer: still very disappointing. Prescrire Int *18*, 145-147.
Abraham, R., Schafer, J., Rothe, M., Bange, J., Knyazev, P., and Ullrich, A. (2005). Identification of MMP-15 as an anti-apoptotic factor in cancer cells. J Biol Chem *280*, 34123-34132.
Abrams, T. J., Lee, L. B., Murray, L. J., Pryer, N. K., and Cherrington, J. M. (2003a). SU11248 inhibits KIT and platelet-derived growth factor receptor beta in preclinical models of human small cell lung cancer. Mol Cancer Ther *2*, 471-478.
Abrams, T. J., Murray, L. J., Pesenti, E., Holway, V. W., Colombo, T., Lee, L. B., Cherrington, J. M., and Pryer, N. K. (2003b). Preclinical evaluation of the tyrosine kinase inhibitor SU11248 as a single agent and in combination with "standard of care" therapeutic agents for the treatment of breast cancer. Mol Cancer Ther *2*, 1011-1021.
al-Obeidi, F. A., Wu, J. J., and Lam, K. S. (1998). Protein tyrosine kinases: structure, substrate specificity, and drug discovery. Biopolymers *47*, 197-223.
Ansell, A., Jerhammar, F., Ceder, R., Grafstrom, R., Grenman, R., and Roberg, K. (2009). Matrix metalloproteinase-7 and -13 expression associate to cisplatin resistance in head and neck cancer cell lines. Oral Oncol *45*, 866-871.
Antczak, C., Veach, D. R., Ramirez, C. N., Minchenko, M. A., Shum, D., Calder, P. A., Frattini, M. G., Clarkson, B., and Djaballah, H. (2009). Structure-activity relationships of 6-(2,6-dichlorophenyl)-8-methyl-2-(phenylamino)pyrido[2,3-d]pyrimidin-7-on es: toward selective Abl inhibitors. Bioorg Med Chem Lett *19*, 6872-6876.
Arora, A., and Scholar, E. M. (2005). Role of tyrosine kinase inhibitors in cancer therapy. J Pharmacol Exp Ther *315*, 971-979.
Atkins, M., Jones, C. A., and Kirkpatrick, P. (2006). Sunitinib maleate. Nat Rev Drug Discov *5*, 279-280.
Bain, J., McLauchlan, H., Elliott, M., and Cohen, P. (2003). The specificities of protein kinase inhibitors: an update. Biochem J *371*, 199-204.
Bajetta, E., Guadalupi, V., and Procopio, G. (2009). Activity of sunitinib in patients with advanced neuroendocrine tumors. J Clin Oncol *27*, 319-320; author reply 320.
Bantscheff, M., Eberhard, D., Abraham, Y., Bastuck, S., Boesche, M., Hobson, S., Mathieson, T., Perrin, J., Raida, M., Rau, C., *et al.* (2007). Quantitative chemical proteomics reveals mechanisms of action of clinical ABL kinase inhibitors. Nat Biotechnol *25*, 1035-1044.
Bao, S., Wu, Q., McLendon, R. E., Hao, Y., Shi, Q., Hjelmeland, A. B., Dewhirst, M. W., Bigner, D. D., and Rich, J. N. (2006). Glioma stem cells promote radioresistance by preferential activation of the DNA damage response. Nature *444*, 756-760.
Baratte, S., Sarati, S., Frigerio, E., James, C. A., Ye, C., and Zhang, Q. (2004). Quantitation of SU1 1248, an oral multi-target tyrosine kinase inhibitor, and its metabolite in monkey tissues by liquid chromatograph with tandem mass spectrometry following semi-automated liquid-liquid extraction. J Chromatogr A *1024*, 87-94.
Barker, A. J., Gibson, K. H., Grundy, W., Godfrey, A. A., Barlow, J. J., Healy, M. P., Woodburn, J. R., Ashton, S. E., Curry, B. J., Scarlett, L., *et al.* (2001). Studies leading to the identification of ZD1839 (IRESSA): an orally active, selective epidermal growth factor receptor tyrosine kinase inhibitor targeted to the treatment of cancer. Bioorg Med Chem Lett *11*, 1911-1914.
Baselga, J. (2006). Targeting tyrosine kinases in cancer: the second wave. Science *312*, 1175-1178.
Bates, R. C., and Mercurio, A. M. (2005). The epithelial-mesenchymal transition (EMT) and colorectal cancer progression. Cancer Biol Ther *4*, 365-370.
Battistella, M., Mateus, C., Lassau, N., Chami, L., Boukoucha, M., Duvillard, P., Cribier, B., and Robert, C. (2009). Sunitinib efficacy in the treatment of metastatic skin adnexal carcinomas: report of two patients with hidradenocarcinoma and trichoblastic carcinoma. J Eur Acad Dermatol Venereol.
Begleiter, A., Norman, A., Leitao, D., Cabral, T., Hewitt, D., Pan, S., Grandis, J. R., Siegfried, J. M., El-Sayed, S., Sutherland, D., *et al.* (2005). Role of NQO1 polymorphisms as risk factors for squamous cell carcinoma of the head and neck. Oral Oncol *41*, 927-933.
Benhar, M., Engelberg, D., and Levitzki, A. (2002). ROS, stress-activated kinases and stress signaling in cancer. EMBO Rep *3*, 420-425.
Birchmeier, C., O'Neill, K., Riggs, M., and Wigler, M. (1990). Characterization of ROS1 cDNA from a human glioblastoma cell line. Proc Natl Acad Sci U S A *87*, 4799-4803.
Birchmeier, C., Sharma, S., and Wigler, M. (1987). Expression and rearrangement of the ROS1 gene in human glioblastoma cells. Proc Natl Acad Sci U S A *84*, 9270-9274.
Blackhall, F. H., Rehman, S., and Thatcher, N. (2005). Erlotinib in non-small cell lung cancer: a review. Expert Opin Pharmacother *6*, 995-1002.
Blume-Jensen, P., and Hunter, T. (2001). Oncogenic kinase signalling. Nature *411*, 355-365.
Bonner, A. E., Lemon, W. J., Devereux, T. R., Lubet, R. A., and You, M. (2004). Molecular profiling of mouse lung tumors: association with tumor progression, lung development, and human lung adenocarcinomas. Oncogene *23*, 1166-1176.
Bosman, F. T., and Stamenkovic, I. (2003). Functional structure and composition of the extracellular matrix. J Pathol *200*, 423-428.

Bratton, S. B., and Cohen, G. M. (2001). Caspase cascades in chemically-induced apoptosis. Adv Exp Med Biol *500*, 407-420.

Bulgaru, A. M., Mani, S., Goel, S., and Perez-Soler, R. (2003). Erlotinib (Tarceva): a promising drug targeting epidermal growth factor receptor tyrosine kinase. Expert Rev Anticancer Ther *3*, 269-279.

Burstein, H. J., Elias, A. D., Rugo, H. S., Cobleigh, M. A., Wolff, A. C., Eisenberg, P. D., Lehman, M., Adams, B. J., Bello, C. L., DePrimo, S. E., *et al.* (2008). Phase II study of sunitinib malate, an oral multitargeted tyrosine kinase inhibitor, in patients with metastatic breast cancer previously treated with an anthracycline and a taxane. J Clin Oncol *26*, 1810-1816.

Cahill, D. P., Kinzler, K. W., Vogelstein, B., and Lengauer, C. (1999). Genetic instability and darwinian selection in tumours. Trends Cell Biol *9*, M57-60.

Capdeville, R., Buchdunger, E., Zimmermann, J., and Matter, A. (2002). Glivec (STI571, imatinib), a rationally developed, targeted anticancer drug. Nat Rev Drug Discov *1*, 493-502.

Carter, T. A., Wodicka, L. M., Shah, N. P., Velasco, A. M., Fabian, M. A., Treiber, D. K., Milanov, Z. V., Atteridge, C. E., Biggs, W. H., 3rd, Edeen, P. T., *et al.* (2005). Inhibition of drug-resistant mutants of ABL, KIT, and EGF receptor kinases. Proc Natl Acad Sci U S A *102*, 11011-11016.

Chao, C., Zhang, Z. F., Berthiller, J., Boffetta, P., and Hashibe, M. (2006). NAD(P)H:quinone oxidoreductase 1 (NQO1) Pro187Ser polymorphism and the risk of lung, bladder, and colorectal cancers: a meta-analysis. Cancer Epidemiol Biomarkers Prev *15*, 979-987.

Charest, A., Kheifets, V., Park, J., Lane, K., McMahon, K., Nutt, C. L., and Housman, D. (2003a). Oncogenic targeting of an activated tyrosine kinase to the Golgi apparatus in a glioblastoma. Proc Natl Acad Sci U S A *100*, 916-921.

Charest, A., Lane, K., McMahon, K., Park, J., Preisinger, E., Conroy, H., and Housman, D. (2003b). Fusion of FIG to the receptor tyrosine kinase ROS in a glioblastoma with an interstitial del(6)(q21q21). Genes Chromosomes Cancer *37*, 58-71.

Chazin, V. R., Kaleko, M., Miller, A. D., and Slamon, D. J. (1992). Transformation mediated by the human HER-2 gene independent of the epidermal growth factor receptor. Oncogene *7*, 1859-1866.

Chen, S. Y., Kao, P. C., Lin, Z. Z., Chiang, W. C., and Fang, C. C. (2009). Sunitinib-induced myxedema coma. Am J Emerg Med *27*, 370 e371-370 e373.

Chiang, A. C., and Massague, J. (2008). Molecular basis of metastasis. N Engl J Med *359*, 2814-2823.

Choong, N. W., Kozloff, M., Taber, D., Hu, H. S., Wade, J., 3rd, Ivy, P., Karrison, T. G., Dekker, A., Vokes, E. E., and Cohen, E. E. (2009). Phase II study of sunitinib malate in head and neck squamous cell carcinoma. Invest New Drugs.

Cohen, M. H., Johnson, J. R., Chen, Y. F., Sridhara, R., and Pazdur, R. (2005). FDA drug approval summary: erlotinib (Tarceva) tablets. Oncologist *10*, 461-466.

Cohen, P. (2001). The role of protein phosphorylation in human health and disease. The Sir Hans Krebs Medal Lecture. Eur J Biochem *268*, 5001-5010.

Cohen, P. (2002). Protein kinases--the major drug targets of the twenty-first century? Nat Rev Drug Discov *1*, 309-315.

Collett, M. S., and Erikson, R. L. (1978). Protein kinase activity associated with the avian sarcoma virus src gene product. Proc Natl Acad Sci U S A *75*, 2021-2024.

Collins, I., and Workman, P. (2006). New approaches to molecular cancer therapeutics. Nat Chem Biol *2*, 689-700.

Comis, R. L. (2005). The current situation: erlotinib (Tarceva) and gefitinib (Iressa) in non-small cell lung cancer. Oncologist *10*, 467-470.

Cools, J., Mentens, N., Furet, P., Fabbro, D., Clark, J. J., Griffin, J. D., Marynen, P., and Gilliland, D. G. (2004). Prediction of resistance to small molecule FLT3 inhibitors: implications for molecularly targeted therapy of acute leukemia. Cancer Res *64*, 6385-6389.

Copland, M., Hamilton, A., Elrick, L. J., Baird, J. W., Allan, E. K., Jordanides, N., Barow, M., Mountford, J. C., and Holyoake, T. L. (2006). Dasatinib (BMS-354825) targets an earlier progenitor population than imatinib in primary CML but does not eliminate the quiescent fraction. Blood *107*, 4532-4539.

Cox, J., and Mann, M. (2007). Is proteomics the new genomics? Cell *130*, 395-398.

Cox, J., and Mann, M. (2008). MaxQuant enables high peptide identification rates, individualized p.p.b.-range mass accuracies and proteome-wide protein quantification. Nat Biotechnol *26*, 1367-1372.

Cresteil, T., and Jaiswal, A. K. (1991). High levels of expression of the NAD(P)H:quinone oxidoreductase (NQO1) gene in tumor cells compared to normal cells of the same origin. Biochem Pharmacol *42*, 1021-1027.

Dalerba, P., Cho, R. W., and Clarke, M. F. (2007). Cancer stem cells: models and concepts. Annu Rev Med *58*, 267-284.

Daub, H. (2005). Characterisation of kinase-selective inhibitors by chemical proteomics. Biochim Biophys Acta *1754*, 183-190.

Daub, H., Godl, K., Brehmer, D., Klebl, B., and Muller, G. (2004a). Evaluation of kinase inhibitor selectivity by chemical proteomics. Assay Drug Dev Technol *2*, 215-224.

Daub, H., Specht, K., and Ullrich, A. (2004b). Strategies to overcome resistance to targeted protein kinase inhibitors. Nat Rev Drug Discov *3*, 1001-1010.

Davies, S. P., Reddy, H., Caivano, M., and Cohen, P. (2000). Specificity and mechanism of action of some commonly used protein kinase inhibitors. Biochem J *351*, 95-105.

Demetri, G. D., van Oosterom, A. T., Garrett, C. R., Blackstein, M. E., Shah, M. H., Verweij, J., McArthur, G., Judson, I. R., Heinrich, M. C., Morgan, J. A., *et al.* (2006). Efficacy and safety of sunitinib in patients with advanced gastrointestinal stromal tumour after failure of imatinib: a randomised controlled trial. Lancet *368*, 1329-1338.

Di Lorenzo, G., Autorino, R., Bruni, G., Carteni, G., Ricevuto, E., Tudini, M., Ficorella, C., Romano, C., Aieta, M., Giordano, A., *et al.* (2009). Cardiovascular toxicity following sunitinib therapy in metastatic renal cell carcinoma: a multicenter analysis. Ann Oncol *20*, 1535-1542.

Diehn, M., and Clarke, M. F. (2006). Cancer stem cells and radiotherapy: new insights into tumor radioresistance. J Natl Cancer Inst *98*, 1755-1757.

DiGiovanna, M. P., Stern, D. F., Edgerton, S. M., Whalen, S. G., Moore, D., 2nd, and Thor, A. D. (2005). Relationship of epidermal growth factor receptor expression to ErbB-2 signaling activity and prognosis in breast cancer patients. J Clin Oncol *23*, 1152-1160.

Downward, J., Yarden, Y., Mayes, E., Scrace, G., Totty, N., Stockwell, P., Ullrich, A., Schlessinger, J., and Waterfield, M. D. (1984). Close similarity of epidermal growth factor receptor and v-erb-B oncogene protein sequences. Nature *307*, 521-527.

Druker, B. J. (2002). STI571 (Gleevec) as a paradigm for cancer therapy. Trends Mol Med *8*, S14-18.

Druker, B. J. (2003). Overcoming resistance to imatinib by combining targeted agents. Mol Cancer Ther *2*, 225-226.

Druker, B. J., Talpaz, M., Resta, D. J., Peng, B., Buchdunger, E., Ford, J. M., Lydon, N. B., Kantarjian, H., Capdeville, R., Ohno-Jones, S., and Sawyers, C. L. (2001). Efficacy and safety of a specific inhibitor of the BCR-ABL tyrosine kinase in chronic myeloid leukemia. N Engl J Med *344*, 1031-1037.

Druker, B. J., Tamura, S., Buchdunger, E., Ohno, S., Segal, G. M., Fanning, S., Zimmermann, J., and Lydon, N. B. (1996). Effects of a selective inhibitor of the Abl tyrosine kinase on the growth of Bcr-Abl positive cells. Nat Med *2*, 561-566.

Duensing, A., Heinrich, M. C., Fletcher, C. D., and Fletcher, J. A. (2004). Biology of gastrointestinal stromal tumors: KIT mutations and beyond. Cancer Invest *22*, 106-116.

Edelman, A. M., Blumenthal, D. K., and Krebs, E. G. (1987). Protein serine/threonine kinases. Annu Rev Biochem *56*, 567-613.

Emery, I. F., Battelli, C., Auclair, P. L., Carrier, K., and Hayes, D. M. (2009). Response to gefitinib and erlotinib in Non-small cell lung cancer: a retrospective study. BMC Cancer *9*, 333.

Engelman, J. A., Zejnullahu, K., Mitsudomi, T., Song, Y., Hyland, C., Park, J. O., Lindeman, N., Gale, C. M., Zhao, X., Christensen, J., *et al.* (2007). MET amplification leads to gefitinib resistance in lung cancer by activating ERBB3 signaling. Science *316*, 1039-1043.

Fabian, M. A., Biggs, W. H., 3rd, Treiber, D. K., Atteridge, C. E., Azimioara, M. D., Benedetti, M. G., Carter, T. A., Ciceri, P., Edeen, P. T., Floyd, M., *et al.* (2005). A small molecule-kinase interaction map for clinical kinase inhibitors. Nat Biotechnol *23*, 329-336.

Faivre, S., Delbaldo, C., Vera, K., Robert, C., Lozahic, S., Lassau, N., Bello, C., Deprimo, S., Brega, N., Massimini, G., *et al.* (2006a). Safety, pharmacokinetic, and antitumor activity of SU11248, a novel oral multitarget tyrosine kinase inhibitor, in patients with cancer. J Clin Oncol *24*, 25-35.

Faivre, S., Demetri, G., Sargent, W., and Raymond, E. (2007). Molecular basis for sunitinib efficacy and future clinical development. Nat Rev Drug Discov *6*, 734-745.

Faivre, S., Djelloul, S., and Raymond, E. (2006b). New paradigms in anticancer therapy: targeting multiple signaling pathways with kinase inhibitors. Semin Oncol *33*, 407-420.

Fantl, W. J., Johnson, D. E., and Williams, L. T. (1993). Signalling by receptor tyrosine kinases. Annu Rev Biochem *62*, 453-481.

Fendly, B. M., Winget, M., Hudziak, R. M., Lipari, M. T., Napier, M. A., and Ullrich, A. (1990). Characterization of murine monoclonal antibodies reactive to either the human epidermal growth factor receptor or HER2/neu gene product. Cancer Res *50*, 1550-1558.

Fiedler, W., Serve, H., Dohner, H., Schwittay, M., Ottmann, O. G., O'Farrell, A. M., Bello, C. L., Allred, R., Manning, W. C., Cherrington, J. M., *et al.* (2005). A phase 1 study of SU11248 in the treatment of patients with refractory or resistant acute myeloid leukemia (AML) or not amenable to conventional therapy for the disease. Blood *105*, 986-993.

Flaherty, K. T. (2007). Sorafenib in renal cell carcinoma. Clin Cancer Res *13*, 747s-752s.

Fletcher, J. A., and Rubin, B. P. (2007). KIT mutations in GIST. Curr Opin Genet Dev *17*, 3-7.

Folkman, J. (1971). Tumor angiogenesis: therapeutic implications. N Engl J Med *285*, 1182-1186.

Folkman, J. (1990). What is the evidence that tumors are angiogenesis dependent? J Natl Cancer Inst *82*, 4-6.

Fong, T. A., Shawver, L. K., Sun, L., Tang, C., App, H., Powell, T. J., Kim, Y. H., Schreck, R., Wang, X., Risau, W., *et al.* (1999). SU5416 is a potent and selective inhibitor of the vascular endothelial growth factor receptor (Flk-1/KDR) that inhibits tyrosine kinase catalysis, tumor vascularization, and growth of multiple tumor types. Cancer Res *59*, 99-106.

Foulds, L. (1951). Experimental study of the course and regulation of tumour growth. Ann R Coll Surg Engl *9*, 93-101.

Foulds, L. (1954). The experimental study of tumor progression: a review. Cancer Res *14*, 327-339.

Gavert, N., and Ben-Ze'ev, A. (2008). Epithelial-mesenchymal transition and the invasive potential of tumors. Trends Mol Med *14*, 199-209.

Godl, K., and Daub, H. (2004). Proteomic analysis of kinase inhibitor selectivity and function. Cell Cycle *3*, 393-395.

Godl, K., Wissing, J., Kurtenbach, A., Habenberger, P., Blencke, S., Gutbrod, H., Salassidis, K., Stein-Gerlach, M., Missio, A., Cotten, M., and Daub, H. (2003). An efficient proteomics method to identify the cellular targets of protein kinase inhibitors. Proc Natl Acad Sci U S A *100*, 15434-15439.

Goldstein, D. M., Gray, N. S., and Zarrinkar, P. P. (2008). High-throughput kinase profiling as a platform for drug discovery. Nat Rev Drug Discov *7*, 391-397.

Graham, S. M., Jorgensen, H. G., Allan, E., Pearson, C., Alcorn, M. J., Richmond, L., and Holyoake, T. L. (2002). Primitive, quiescent, Philadelphia-positive stem cells from patients with chronic myeloid leukemia are insensitive to STI571 in vitro. Blood *99*, 319-325.

Greenman, C., Stephens, P., Smith, R., Dalgliesh, G. L., Hunter, C., Bignell, G., Davies, H., Teague, J., Butler, A., Stevens, C., *et al.* (2007). Patterns of somatic mutation in human cancer genomes. Nature *446*, 153-158.

Grueneberg, D. A., Degot, S., Pearlberg, J., Li, W., Davies, J. E., Baldwin, A., Endege, W., Doench, J., Sawyer, J., Hu, Y., *et al.* (2008). Kinase requirements in human cells: I. Comparing kinase requirements across various cell types. Proc Natl Acad Sci U S A *105*, 16472-16477.

Guarino, M., Rubino, B., and Ballabio, G. (2007). The role of epithelial-mesenchymal transition in cancer pathology. Pathology *39*, 305-318.

Hampton, T. (2004). "Promiscuous" anticancer drugs that hit multiple targets may thwart resistance. JAMA *292*, 419-422.

Hanahan, D., and Weinberg, R. A. (2000). The hallmarks of cancer. Cell *100*, 57-70.

Hess, S. M., Anderson, J. G., and Bierbach, U. (2005). A non-crosslinking platinum-acridine hybrid agent shows enhanced cytotoxicity compared to clinical BCNU and cisplatin in glioblastoma cells. Bioorg Med Chem Lett *15*, 443-446.

Hoekman, K. (2001). SU6668, a multitargeted angiogenesis inhibitor. Cancer J *7 Suppl 3*, S134-138.

Holland, E. C. (2000). Glioblastoma multiforme: the terminator. Proc Natl Acad Sci U S A *97*, 6242-6244.

Hubbard, S. R. (2002). Protein tyrosine kinases: autoregulation and small-molecule inhibition. Curr Opin Struct Biol *12*, 735-741.

Hudziak, R. M., Lewis, G. D., Winget, M., Fendly, B. M., Shepard, H. M., and Ullrich, A. (1989). p185HER2 monoclonal antibody has antiproliferative effects in vitro and sensitizes human breast tumor cells to tumor necrosis factor. Mol Cell Biol *9*, 1165-1172.

Huff, C. A., Matsui, W., Smith, B. D., and Jones, R. J. (2006). The paradox of response and survival in cancer therapeutics. Blood *107*, 431-434.

Hunter, T. (1980). Protein phosphorylated by the RSV transforming function. Cell *22*, 647-648.

Hunter, T. (1987). A thousand and one protein kinases. Cell *50*, 823-829.

Hunter, T. (1998). The Croonian Lecture 1997. The phosphorylation of proteins on tyrosine: its role in cell growth and disease. Philos Trans R Soc Lond B Biol Sci *353*, 583-605.

Hunter, T. (2000). Signaling--2000 and beyond. Cell *100*, 113-127.

Hunter, T., and Sefton, B. M. (1980). Transforming gene product of Rous sarcoma virus phosphorylates tyrosine. Proc Natl Acad Sci U S A *77*, 1311-1315.

Huynh, H., Ngo, V. C., Choo, S. P., Poon, D., Koong, H. N., Thng, C. H., Toh, H. C., Zheng, L., Ong, L. C., Jin, Y., *et al.* (2009). Sunitinib (SUTENT, SU11248) suppresses tumor growth and induces apoptosis in xenograft models of human hepatocellular carcinoma. Curr Cancer Drug Targets *9*, 738-747.

Ichihara, M., Murakumo, Y., and Takahashi, M. (2004). RET and neuroendocrine tumors. Cancer Lett *204*, 197-211.

Janeway, K. A., Albritton, K. H., Van Den Abbeele, A. D., D'Amato, G. Z., Pedrazzoli, P., Siena, S., Picus, J., Butrynski, J. E., Schlemmer, M., Heinrich, M. C., and Demetri, G. D. (2009). Sunitinib treatment in pediatric patients with advanced GIST following failure of imatinib. Pediatr Blood Cancer *52*, 767-771.

Joensuu, H. (2007). Cardiac toxicity of sunitinib. Lancet *370*, 1978-1980.

Joensuu, H., Roberts, P. J., Sarlomo-Rikala, M., Andersson, L. C., Tervahartiala, P., Tuveson, D., Silberman, S., Capdeville, R., Dimitrijevic, S., Druker, B., and Demetri, G. D. (2001). Effect of the tyrosine kinase inhibitor STI571 in a patient with a metastatic gastrointestinal stromal tumor. N Engl J Med *344*, 1052-1056.

Jones, G., Machado, J., Jr., and Merlo, A. (2001). Loss of focal adhesion kinase (FAK) inhibits epidermal growth factor receptor-dependent migration and induces aggregation of nh(2)-terminal FAK in the nuclei of apoptotic glioblastoma cells. Cancer Res *61*, 4978-4981.

Jun, H. J., Woolfenden, S., Coven, S., Lane, K., Bronson, R., Housman, D., and Charest, A. (2009). Epigenetic regulation of c-ROS receptor tyrosine kinase expression in malignant gliomas. Cancer Res *69*, 2180-2184.

Karaman, M. W., Herrgard, S., Treiber, D. K., Gallant, P., Atteridge, C. E., Campbell, B. T., Chan, K. W., Ciceri, P., Davis, M. I., Edeen, P. T., *et al.* (2008). A quantitative analysis of kinase inhibitor selectivity. Nat Biotechnol *26*, 127-132.

Kelleher, F. C., and McDermott, R. (2008). Response to sunitinib in medullary thyroid cancer. Ann Intern Med *148*, 567.

Kim, D. W., Jo, Y. S., Jung, H. S., Chung, H. K., Song, J. H., Park, K. C., Park, S. H., Hwang, J. H., Rha, S. Y., Kweon, G. R., *et al.* (2006). An orally administered multitarget tyrosine kinase inhibitor, SU11248, is a novel potent inhibitor of thyroid oncogenic RET/papillary thyroid cancer kinases. J Clin Endocrinol Metab *91*, 4070-4076.

Kinzler, K. W., and Vogelstein, B. (1996). Lessons from hereditary colorectal cancer. Cell *87*, 159-170.

Klein, S., McCormick, F., and Levitzki, A. (2005). Killing time for cancer cells. Nat Rev Cancer *5*, 573-580.
Knight, Z. A., and Shokat, K. M. (2005). Features of selective kinase inhibitors. Chem Biol *12*, 621-637.
Knuutila, S., Bjorkqvist, A. M., Autio, K., Tarkkanen, M., Wolf, M., Monni, O., Szymanska, J., Larramendy, M. L., Tapper, J., Pere, H., *et al.* (1998). DNA copy number amplifications in human neoplasms: review of comparative genomic hybridization studies. Am J Pathol *152*, 1107-1123.
Kobayashi, S., Ji, H., Yuza, Y., Meyerson, M., Wong, K. K., Tenen, D. G., and Halmos, B. (2005). An alternative inhibitor overcomes resistance caused by a mutation of the epidermal growth factor receptor. Cancer Res *65*, 7096-7101.
Kokkinos, M. I., Wafai, R., Wong, M. K., Newgreen, D. F., Thompson, E. W., and Waltham, M. (2007). Vimentin and epithelial-mesenchymal transition in human breast cancer--observations in vitro and in vivo. Cells Tissues Organs *185*, 191-203.
Kulke, M. H., Lenz, H. J., Meropol, N. J., Posey, J., Ryan, D. P., Picus, J., Bergsland, E., Stuart, K., Tye, L., Huang, X., *et al.* (2008). Activity of sunitinib in patients with advanced neuroendocrine tumors. J Clin Oncol *26*, 3403-3410.
Kumar, S. (2007). Caspase function in programmed cell death. Cell Death Differ *14*, 32-43.
La Rosee, P., Johnson, K., Corbin, A. S., Stoffregen, E. P., Moseson, E. M., Willis, S., Mauro, M. M., Melo, J. V., Deininger, M. W., and Druker, B. J. (2004). In vitro efficacy of combined treatment depends on the underlying mechanism of resistance in imatinib-resistant Bcr-Abl-positive cell lines. Blood *103*, 208-215.
Laird, A. D., Vajkoczy, P., Shawver, L. K., Thurnher, A., Liang, C., Mohammadi, M., Schlessinger, J., Ullrich, A., Hubbard, S. R., Blake, R. A., *et al.* (2000). SU6668 is a potent antiangiogenic and antitumor agent that induces regression of established tumors. Cancer Res *60*, 4152-4160.
Lander, E. S., Linton, L. M., Birren, B., Nusbaum, C., Zody, M. C., Baldwin, J., Devon, K., Dewar, K., Doyle, M., FitzHugh, W., *et al.* (2001). Initial sequencing and analysis of the human genome. Nature *409*, 860-921.
le Coutre, P., Tassi, E., Varella-Garcia, M., Barni, R., Mologni, L., Cabrita, G., Marchesi, E., Supino, R., and Gambacorti-Passerini, C. (2000). Induction of resistance to the Abelson inhibitor STI571 in human leukemic cells through gene amplification. Blood *95*, 1758-1766.
Le Tourneau, C., Raymond, E., and Faivre, S. (2007). Sunitinib: a novel tyrosine kinase inhibitor. A brief review of its therapeutic potential in the treatment of renal carcinoma and gastrointestinal stromal tumors (GIST). Ther Clin Risk Manag *3*, 341-348.
Lengauer, C., Kinzler, K. W., and Vogelstein, B. (1997). Genetic instability in colorectal cancers. Nature *386*, 623-627.
Lengauer, C., Kinzler, K. W., and Vogelstein, B. (1998). Genetic instabilities in human cancers. Nature *396*, 643-649.
Levitzki, A., and Gazit, A. (1995). Tyrosine kinase inhibition: an approach to drug development. Science *267*, 1782-1788.
Levitzki, A., and Mishani, E. (2006). Tyrphostins and other tyrosine kinase inhibitors. Annu Rev Biochem *75*, 93-109.
Lewis, A. M., Ough, M., Hinkhouse, M. M., Tsao, M. S., Oberley, L. W., and Cullen, J. J. (2005). Targeting NAD(P)H:quinone oxidoreductase (NQO1) in pancreatic cancer. Mol Carcinog *43*, 215-224.
Machiels, J. P., Bletard, N., Pirenne, P., Jacquet, L., Bonbled, F., and Duck, L. (2008). Acute cardiac failure after sunitinib. Ann Oncol *19*, 597-599.
Manning, G., Whyte, D. B., Martinez, R., Hunter, T., and Sudarsanam, S. (2002). The protein kinase complement of the human genome. Science *298*, 1912-1934.
Markowitz, S., Wang, J., Myeroff, L., Parsons, R., Sun, L., Lutterbaugh, J., Fan, R. S., Zborowska, E., Kinzler, K. W., Vogelstein, B., and et al. (1995). Inactivation of the type II TGF-beta receptor in colon cancer cells with microsatellite instability. Science *268*, 1336-1338.
Mendel, D. B., Laird, A. D., Xin, X., Louie, S. G., Christensen, J. G., Li, G., Schreck, R. E., Abrams, T. J., Ngai, T. J., Lee, L. B., *et al.* (2003). In vivo antitumor activity of SU11248, a novel tyrosine kinase inhibitor targeting vascular endothelial growth factor and platelet-derived growth factor receptors: determination of a pharmacokinetic/pharmacodynamic relationship. Clin Cancer Res *9*, 327-337.
Mertins, P., Eberl, H. C., Renkawitz, J., Olsen, J. V., Tremblay, M. L., Mann, M., Ullrich, A., and Daub, H. (2008). Investigation of protein-tyrosine phosphatase 1B function by quantitative proteomics. Mol Cell Proteomics *7*, 1763-1777.
Metro, G., Finocchiaro, G., Toschi, L., Bartolini, S., Magrini, E., Cancellieri, A., Trisolini, R., Castaldini, L., Tallini, G., Crino, L., and Cappuzzo, F. (2006). Epidermal growth factor receptor (EGFR) targeted therapies in non-small cell lung cancer (NSCLC). Rev Recent Clin Trials *1*, 1-13.
Millauer, B., Wizigmann-Voos, S., Schnurch, H., Martinez, R., Moller, N. P., Risau, W., and Ullrich, A. (1993). High affinity VEGF binding and developmental expression suggest Flk-1 as a major regulator of vasculogenesis and angiogenesis. Cell *72*, 835-846.
Miller, D. K. (1997). The role of the Caspase family of cysteine proteases in apoptosis. Semin Immunol *9*, 35-49.
Mitsiades, N., Poulaki, V., Mitsiades, C. S., and Anderson, K. C. (2001). Induction of tumour cell apoptosis by matrix metalloproteinase inhibitors: new tricks from a (not so) old drug. Expert Opin Investig Drugs *10*, 1075-1084.
Morimoto, A. M., Tan, N., West, K., McArthur, G., Toner, G. C., Manning, W. C., Smolich, B. D., and Cherrington, J. M. (2004). Gene expression profiling of human colon xenograft tumors following treatment with SU11248, a multitargeted tyrosine kinase inhibitor. Oncogene *23*, 1618-1626.

Morin, M. J. (2000). From oncogene to drug: development of small molecule tyrosine kinase inhibitors as anti-tumor and anti-angiogenic agents. Oncogene *19*, 6574-6583.
Morphy, R., Kay, C., and Rankovic, Z. (2004). From magic bullets to designed multiple ligands. Drug Discov Today *9*, 641-651.
Morwick, T., Berry, A., Brickwood, J., Cardozo, M., Catron, K., DeTuri, M., Emeigh, J., Homon, C., Hrapchak, M., Jacober, S., *et al.* (2006). Evolution of the thienopyridine class of inhibitors of IkappaB kinase-beta: part I: hit-to-lead strategies. J Med Chem *49*, 2898-2908.
Motzer, R. J., Hoosen, S., Bello, C. L., and Christensen, J. G. (2006a). Sunitinib malate for the treatment of solid tumours: a review of current clinical data. Expert Opin Investig Drugs *15*, 553-561.
Motzer, R. J., Hutson, T. E., Tomczak, P., Michaelson, M. D., Bukowski, R. M., Rixe, O., Oudard, S., Negrier, S., Szczylik, C., Kim, S. T., *et al.* (2007a). Sunitinib versus interferon alfa in metastatic renal-cell carcinoma. N Engl J Med *356*, 115-124.
Motzer, R. J., Michaelson, M. D., Redman, B. G., Hudes, G. R., Wilding, G., Figlin, R. A., Ginsberg, M. S., Kim, S. T., Baum, C. M., DePrimo, S. E., *et al.* (2006b). Activity of SU11248, a multitargeted inhibitor of vascular endothelial growth factor receptor and platelet-derived growth factor receptor, in patients with metastatic renal cell carcinoma. J Clin Oncol *24*, 16-24.
Motzer, R. J., Michaelson, M. D., Rosenberg, J., Bukowski, R. M., Curti, B. D., George, D. J., Hudes, G. R., Redman, B. G., Margolin, K. A., and Wilding, G. (2007b). Sunitinib efficacy against advanced renal cell carcinoma. J Urol *178*, 1883-1887.
Motzer, R. J., Rini, B. I., Bukowski, R. M., Curti, B. D., George, D. J., Hudes, G. R., Redman, B. G., Margolin, K. A., Merchan, J. R., Wilding, G., *et al.* (2006c). Sunitinib in patients with metastatic renal cell carcinoma. JAMA *295*, 2516-2524.
Muhsin, M., Graham, J., and Kirkpatrick, P. (2003). Gefitinib. Nat Rev Drug Discov *2*, 515-516.
Mukohara, T., Kudoh, S., Yamauchi, S., Kimura, T., Yoshimura, N., Kanazawa, H., Hirata, K., Wanibuchi, H., Fukushima, S., Inoue, K., and Yoshikawa, J. (2003). Expression of epidermal growth factor receptor (EGFR) and downstream-activated peptides in surgically excised non-small-cell lung cancer (NSCLC). Lung Cancer *41*, 123-130.
Murray, L. J., Abrams, T. J., Long, K. R., Ngai, T. J., Olson, L. M., Hong, W., Keast, P. K., Brassard, J. A., O'Farrell, A. M., Cherrington, J. M., and Pryer, N. K. (2003). SU11248 inhibits tumor growth and CSF-1R-dependent osteolysis in an experimental breast cancer bone metastasis model. Clin Exp Metastasis *20*, 757-766.
Nagarajan, L., Louie, E., Tsujimoto, Y., Balduzzi, P. C., Huebner, K., and Croce, C. M. (1986). The human c-ros gene (ROS) is located at chromosome region 6q16----6q22. Proc Natl Acad Sci U S A *83*, 6568-6572.
Naoe, T., and Kiyoi, H. (2004). Normal and oncogenic FLT3. Cell Mol Life Sci *61*, 2932-2938.
Nelson, W. J., and Nusse, R. (2004). Convergence of Wnt, beta-catenin, and cadherin pathways. Science *303*, 1483-1487.
Noble, M. E., Endicott, J. A., and Johnson, L. N. (2004). Protein kinase inhibitors: insights into drug design from structure. Science *303*, 1800-1805.
Norden-Zfoni, A., Desai, J., Manola, J., Beaudry, P., Force, J., Maki, R., Folkman, J., Bello, C., Baum, C., DePrimo, S. E., *et al.* (2007). Blood-based biomarkers of SU11248 activity and clinical outcome in patients with metastatic imatinib-resistant gastrointestinal stromal tumor. Clin Cancer Res *13*, 2643-2650.
O'Farrell, A. M., Abrams, T. J., Yuen, H. A., Ngai, T. J., Louie, S. G., Yee, K. W., Wong, L. M., Hong, W., Lee, L. B., Town, A., *et al.* (2003a). SU11248 is a novel FLT3 tyrosine kinase inhibitor with potent activity in vitro and in vivo. Blood *101*, 3597-3605.
O'Farrell, A. M., Foran, J. M., Fiedler, W., Serve, H., Paquette, R. L., Cooper, M. A., Yuen, H. A., Louie, S. G., Kim, H., Nicholas, S., *et al.* (2003b). An innovative phase I clinical study demonstrates inhibition of FLT3 phosphorylation by SU11248 in acute myeloid leukemia patients. Clin Cancer Res *9*, 5465-5476.
Ohgaki, H., and Kleihues, P. (2007). Genetic pathways to primary and secondary glioblastoma. Am J Pathol *170*, 1445-1453.
Olsen, J. V., Blagoev, B., Gnad, F., Macek, B., Kumar, C., Mortensen, P., and Mann, M. (2006). Global, in vivo, and site-specific phosphorylation dynamics in signaling networks. Cell *127*, 635-648.
Olsen, J. V., de Godoy, L. M., Li, G., Macek, B., Mortensen, P., Pesch, R., Makarov, A., Lange, O., Horning, S., and Mann, M. (2005). Parts per million mass accuracy on an Orbitrap mass spectrometer via lock mass injection into a C-trap. Mol Cell Proteomics *4*, 2010-2021.
Olson, M. F. (2007). Mechanisms of tumour cell invasion and metastasis. J Mol Med *85*, 543-544.
Osusky, K. L., Hallahan, D. E., Fu, A., Ye, F., Shyr, Y., and Geng, L. (2004). The receptor tyrosine kinase inhibitor SU11248 impedes endothelial cell migration, tubule formation, and blood vessel formation in vivo, but has little effect on existing tumor vessels. Angiogenesis *7*, 225-233.
Park, B. S., El-Deeb, I. M., Yoo, K. H., Oh, C. H., Cho, S. J., Han, D. K., Lee, H. S., Lee, J. Y., and Lee, S. H. (2009). Design, synthesis and biological evaluation of new potent and highly selective ROS1-tyrosine kinase inhibitor. Bioorg Med Chem Lett *19*, 4720-4723.
Perez-Soler, R. (2004). The role of erlotinib (Tarceva, OSI 774) in the treatment of non-small cell lung cancer. Clin Cancer Res *10*, 4238s-4240s.

Pevarello, P., Brasca, M. G., Amici, R., Orsini, P., Traquandi, G., Corti, L., Piutti, C., Sansonna, P., Villa, M., Pierce, B. S., *et al.* (2004). 3-Aminopyrazole inhibitors of CDK2/cyclin A as antitumor agents. 1. Lead finding. J Med Chem *47*, 3367-3380.

Polyzos, A. (2008). Activity of SU11248, a multitargeted inhibitor of vascular endothelial growth factor receptor and platelet-derived growth factor receptor, in patients with metastatic renal cell carcinoma and various other solid tumors. J Steroid Biochem Mol Biol *108*, 261-266.

Prenen, H., Cools, J., Mentens, N., Folens, C., Sciot, R., Schoffski, P., Van Oosterom, A., Marynen, P., and Debiec-Rychter, M. (2006). Efficacy of the kinase inhibitor SU11248 against gastrointestinal stromal tumor mutants refractory to imatinib mesylate. Clin Cancer Res *12*, 2622-2627.

Prudkin, L., Liu, D. D., Ozburn, N. C., Sun, M., Behrens, C., Tang, X., Brown, K. C., Bekele, B. N., Moran, C., and Wistuba, II (2009). Epithelial-to-mesenchymal transition in the development and progression of adenocarcinoma and squamous cell carcinoma of the lung. Mod Pathol *22*, 668-678.

Rabin, M., Birnbaum, D., Young, D., Birchmeier, C., Wigler, M., and Ruddle, F. H. (1987). Human ros1 and mas1 oncogenes located in regions of chromosome 6 associated with tumor-specific rearrangements. Oncogene Res *1*, 169-178.

Racz, A., Brass, N., Hofer, M., Sybrecht, G. W., Remberger, K., and Meese, E. U. (2000). Gene amplification at chromosome 1pter-p33 including the genes PAX7 and ENO1 in squamous cell lung carcinoma. Int J Oncol *17*, 67-73.

Rappsilber, J., Ryder, U., Lamond, A. I., and Mann, M. (2002). Large-scale proteomic analysis of the human spliceosome. Genome Res *12*, 1231-1245.

Reckamp, K. L., Gardner, B. K., Figlin, R. A., Elashoff, D., Krysan, K., Dohadwala, M., Mao, J., Sharma, S., Inge, L., Rajasekaran, A., and Dubinett, S. M. (2008). Tumor response to combination celecoxib and erlotinib therapy in non-small cell lung cancer is associated with a low baseline matrix metalloproteinase-9 and a decline in serum-soluble E-cadherin. J Thorac Oncol *3*, 117-124.

Reddy, K. (2006). Phase III study of sunitinib malate (SU11248) versus interferon-alpha as first-line treatment in patients with metastatic renal cell carcinoma. Clin Genitourin Cancer *5*, 23-25.

Renan, M. J. (1993). How many mutations are required for tumorigenesis? Implications from human cancer data. Mol Carcinog *7*, 139-146.

Reschke, M., Mihic-Probst, D., van der Horst, E. H., Knyazev, P., Wild, P. J., Hutterer, M., Meyer, S., Dummer, R., Moch, H., and Ullrich, A. (2008). HER3 is a determinant for poor prognosis in melanoma. Clin Cancer Res *14*, 5188-5197.

Riccardi, C., and Nicoletti, I. (2006). Analysis of apoptosis by propidium iodide staining and flow cytometry. Nat Protoc *1*, 1458-1461.

Rikova, K., Guo, A., Zeng, Q., Possemato, A., Yu, J., Haack, H., Nardone, J., Lee, K., Reeves, C., Li, Y., *et al.* (2007). Global survey of phosphotyrosine signaling identifies oncogenic kinases in lung cancer. Cell *131*, 1190-1203.

Robinson, D. R., Wu, Y. M., and Lin, S. F. (2000). The protein tyrosine kinase family of the human genome. Oncogene *19*, 5548-5557.

Roumiantsev, S., Shah, N. P., Gorre, M. E., Nicoll, J., Brasher, B. B., Sawyers, C. L., and Van Etten, R. A. (2002). Clinical resistance to the kinase inhibitor STI-571 in chronic myeloid leukemia by mutation of Tyr-253 in the Abl kinase domain P-loop. Proc Natl Acad Sci U S A *99*, 10700-10705.

Salmon, S. E., Lam, K. S., Felder, S., Yeoman, H., Schlessinger, J., Ullrich, A., Krchnak, V., and Lebl, M. (1994). One bead, one chemical compound: use of the selectide process for anticancer drug discovery. Acta Oncol *33*, 127-131.

Sapi, E. (2004). The role of CSF-1 in normal physiology of mammary gland and breast cancer: an update. Exp Biol Med (Maywood) *229*, 1-11.

Schmidinger, M., Bojic, A., Vogl, U. M., Lamm, W., and Zielinski, C. C. (2009). Management of cardiac adverse events occurring with sunitinib treatment. Anticancer Res *29*, 1627-1629.

Schmidinger, M., Zielinski, C. C., Vogl, U. M., Bojic, A., Bojic, M., Schukro, C., Ruhsam, M., Hejna, M., and Schmidinger, H. (2008). Cardiac toxicity of sunitinib and sorafenib in patients with metastatic renal cell carcinoma. J Clin Oncol *26*, 5204-5212.

Schroeder, M. J., Shabanowitz, J., Schwartz, J. C., Hunt, D. F., and Coon, J. J. (2004). A neutral loss activation method for improved phosphopeptide sequence analysis by quadrupole ion trap mass spectrometry. Anal Chem *76*, 3590-3598.

Schueneman, A. J., Himmelfarb, E., Geng, L., Tan, J., Donnelly, E., Mendel, D., McMahon, G., and Hallahan, D. E. (2003). SU11248 maintenance therapy prevents tumor regrowth after fractionated irradiation of murine tumor models. Cancer Res *63*, 4009-4016.

Sebolt-Leopold, J. S., and English, J. M. (2006). Mechanisms of drug inhibition of signalling molecules. Nature *441*, 457-462.

Shah, N. P., Tran, C., Lee, F. Y., Chen, P., Norris, D., and Sawyers, C. L. (2004). Overriding imatinib resistance with a novel ABL kinase inhibitor. Science *305*, 399-401.

Sharma, K., Weber, C., Bairlein, M., Greff, Z., Keri, G., Cox, J., Olsen, J. V., and Daub, H. (2009). Proteomics strategy for quantitative protein interaction profiling in cell extracts. Nat Methods *6*, 741-744.

Sieg, D. J., Hauck, C. R., and Schlaepfer, D. D. (1999). Required role of focal adhesion kinase (FAK) for integrin-stimulated cell migration. J Cell Sci *112 (Pt 16)*, 2677-2691.

Slamon, D. J., Clark, G. M., Wong, S. G., Levin, W. J., Ullrich, A., and McGuire, W. L. (1987). Human breast cancer: correlation of relapse and survival with amplification of the HER-2/neu oncogene. Science *235*, 177-182.
Sportsman, J. R., Gaudet, E. A., and Boge, A. (2004). Immobilized metal ion affinity-based fluorescence polarization (IMAP): advances in kinase screening. Assay Drug Dev Technol *2*, 205-214.
Stehelin, D. (1976). The transforming gene of avian tumor viruses. Pathol Biol (Paris) *24*, 513-515.
Stratton, M. R., Campbell, P. J., and Futreal, P. A. (2009). The cancer genome. Nature *458*, 719-724.
Sun, L., Liang, C., Shirazian, S., Zhou, Y., Miller, T., Cui, J., Fukuda, J. Y., Chu, J. Y., Nematalla, A., Wang, X., *et al.* (2003). Discovery of 5-[5-fluoro-2-oxo-1,2- dihydroindol-(3Z)-ylidenemethyl]-2,4- dimethyl-1H-pyrrole-3-carboxylic acid (2-diethylaminoethyl)amide, a novel tyrosine kinase inhibitor targeting vascular endothelial and platelet-derived growth factor receptor tyrosine kinase. J Med Chem *46*, 1116-1119.
Superti-Furga, G., and Courtneidge, S. A. (1995). Structure-function relationships in Src family and related protein tyrosine kinases. Bioessays *17*, 321-330.
Takahashi, A. (1999). Caspase: executioner and undertaker of apoptosis. Int J Hematol *70*, 226-232.
Templeton, A., Brandle, M., Cerny, T., and Gillessen, S. (2008). Remission of diabetes while on sunitinib treatment for renal cell carcinoma. Ann Oncol *19*, 824-825.
Tessarollo, L., Nagarajan, L., and Parada, L. F. (1992). c-ros: the vertebrate homolog of the sevenless tyrosine kinase receptor is tightly regulated during organogenesis in mouse embryonic development. Development *115*, 11-20.
Thompson, E. W., Newgreen, D. F., and Tarin, D. (2005). Carcinoma invasion and metastasis: a role for epithelial-mesenchymal transition? Cancer Res *65*, 5991-5995; discussion 5995.
Thornberry, N. A. (1997). The caspase family of cysteine proteases. Br Med Bull *53*, 478-490.
Thornberry, N. A. (1998). Caspases: key mediators of apoptosis. Chem Biol *5*, R97-103.
Thornberry, N. A., and Lazebnik, Y. (1998). Caspases: enemies within. Science *281*, 1312-1316.
Trojanowicz, B., Winkler, A., Hammje, K., Chen, Z., Sekulla, C., Glanz, D., Schmutzler, C., Mentrup, B., Hombach-Klonisch, S., Klonisch, T., *et al.* (2009). Retinoic acid-mediated down-regulation of ENO1/MBP-1 gene products caused decreased invasiveness of the follicular thyroid carcinoma cell lines. J Mol Endocrinol *42*, 249-260.
Ullrich, A., Coussens, L., Hayflick, J. S., Dull, T. J., Gray, A., Tam, A. W., Lee, J., Yarden, Y., Libermann, T. A., Schlessinger, J., and et al. (1984). Human epidermal growth factor receptor cDNA sequence and aberrant expression of the amplified gene in A431 epidermoid carcinoma cells. Nature *309*, 418-425.
Ullrich, A., and Schlessinger, J. (1990). Signal transduction by receptors with tyrosine kinase activity. Cell *61*, 203-212.
Umezawa, H., Imoto, M., Sawa, T., Isshiki, K., Matsuda, N., Uchida, T., Iinuma, H., Hamada, M., and Takeuchi, T. (1986). Studies on a new epidermal growth factor-receptor kinase inhibitor, erbstatin, produced by MH435-hF3. J Antibiot (Tokyo) *39*, 170-173.
Van Etten, R. A. (2004). Mechanisms of transformation by the BCR-ABL oncogene: new perspectives in the post-imatinib era. Leuk Res *28 Suppl 1*, S21-28.
VanderWel, S. N., Harvey, P. J., McNamara, D. J., Repine, J. T., Keller, P. R., Quin, J., 3rd, Booth, R. J., Elliott, W. L., Dobrusin, E. M., Fry, D. W., and Toogood, P. L. (2005). Pyrido[2,3-d]pyrimidin-7-ones as specific inhibitors of cyclin-dependent kinase 4. J Med Chem *48*, 2371-2387.
Varmus, H., and Bishop, J. M. (1986). Biochemical mechanisms of oncogene activity: proteins encoded by oncogenes. Introduction. Cancer Surv *5*, 153-158.
Verweij, J., and de Jonge, M. (2007). Multitarget tyrosine kinase inhibition: [and the winner is...]. J Clin Oncol *25*, 2340-2342.
Vichai, V., and Kirtikara, K. (2006). Sulforhodamine B colorimetric assay for cytotoxicity screening. Nat Protoc *1*, 1112-1116.
Voulgari, A., and Pintzas, A. (2009). Epithelial-mesenchymal transition in cancer metastasis: Mechanisms, markers and strategies to overcome drug resistance in the clinic. Biochim Biophys Acta.
Vu, C. B., Luke, G. P., Kawahata, N., Shakespeare, W. C., Wang, Y., Sundaramoorthi, R., Metcalf, C. A., 3rd, Keenan, T. P., Pradeepan, S., Corpuz, E., *et al.* (2003). Bone-targeted pyrido[2,3-d]pyrimidin-7-ones: potent inhibitors of Src tyrosine kinase as novel antiresorptive agents. Bioorg Med Chem Lett *13*, 3071-3074.
Weise, A. M., Liu, C. Y., and Shields, A. F. (2009). Fatal liver failure in a patient on acetaminophen treated with sunitinib malate and levothyroxine. Ann Pharmacother *43*, 761-766.
Wessel, D., and Flugge, U. I. (1984). A method for the quantitative recovery of protein in dilute solution in the presence of detergents and lipids. Anal Biochem *138*, 141-143.
Wicha, M. S., Liu, S., and Dontu, G. (2006). Cancer stem cells: an old idea--a paradigm shift. Cancer Res *66*, 1883-1890; discussion 1895-1886.
Williams, C., Ponten, F., Ahmadian, A., Ren, Z. P., Ling, G., Rollman, O., Ljung, A., Jaspers, N. G., Uhlen, M., Lundeberg, J., and Ponten, J. (1998). Clones of normal keratinocytes and a variety of simultaneously present epidermal neoplastic lesions contain a multitude of p53 gene mutations in a xeroderma pigmentosum patient. Cancer Res *58*, 2449-2455.
Wu, Y., and Zhou, B. P. (2008). New insights of epithelial-mesenchymal transition in cancer metastasis. Acta Biochim Biophys Sin (Shanghai) *40*, 643-650.
Yang, J., and Weinberg, R. A. (2008). Epithelial-mesenchymal transition: at the crossroads of development and tumor metastasis. Dev Cell *14*, 818-829.

Yarden, Y., and Ullrich, A. (1988). Growth factor receptor tyrosine kinases. Annu Rev Biochem *57*, 443-478.
Yee, K. W., Schittenhelm, M., O'Farrell, A. M., Town, A. R., McGreevey, L., Bainbridge, T., Cherrington, J. M., and Heinrich, M. C. (2004). Synergistic effect of SU11248 with cytarabine or daunorubicin on FLT3 ITD-positive leukemic cells. Blood *104*, 4202-4209.
Zhang, J., Yang, P. L., and Gray, N. S. (2009a). Targeting cancer with small molecule kinase inhibitors. Nat Rev Cancer *9*, 28-39.
Zhang, L., Smith, K. M., Chong, A. L., Stempak, D., Yeger, H., Marrano, P., Thorner, P. S., Irwin, M. S., Kaplan, D. R., and Baruchel, S. (2009b). In vivo antitumor and antimetastatic activity of sunitinib in preclinical neuroblastoma mouse model. Neoplasia *11*, 426-435.
Zhang, Y. X., Knyazev, P. G., Cheburkin, Y. V., Sharma, K., Knyazev, Y. P., Orfi, L., Szabadkai, I., Daub, H., Keri, G., and Ullrich, A. (2008). AXL is a potential target for therapeutic intervention in breast cancer progression. Cancer Res *68*, 1905-1915.
Zhou, Z. T., Xu, X. H., Wei, Q., Lu, M. Q., Wang, J., and Wen, C. H. (2009). Erlotinib in advanced non-small-cell lung cancer after gefitinib failure. Cancer Chemother Pharmacol *64*, 1123-1127.
Zhu, A. X., Sahani, D. V., Duda, D. G., di Tomaso, E., Ancukiewicz, M., Catalano, O. A., Sindhwani, V., Blaszkowsky, L. S., Yoon, S. S., Lahdenranta, J., *et al.* (2009a). Efficacy, safety, and potential biomarkers of sunitinib monotherapy in advanced hepatocellular carcinoma: a phase II study. J Clin Oncol *27*, 3027-3035.
Zhu, A. X., Sahani, D. V., Duda, D. G., di Tomaso, E., Ancukiewicz, M., Catalano, O. A., Sindhwani, V., Blaszkowsky, L. S., Yoon, S. S., Lahdenranta, J., *et al.* (2009b). Efficacy, Safety, and Potential Biomarkers of Sunitinib Monotherapy in Advanced Hepatocellular Carcinoma: A Phase II Study. J Clin Oncol.

11 Acknowledgements

This study was carried out in the Department of Molecular Biology (Director: Prof. Dr. Axel Ullrich) at the Max Planck Institute of Biochemistry (Martinsried by Munich, Germany). Many people have contributed to this work and have made my PhD time fun and exciting. Thank you all!!!

In particular I would like to express my gratitude and many thanks to,
my supervisor, Prof. Dr. Axel Ullrich, for his great support and the chance to work in the outstanding scientific environment of his laboratory and for giving me the chance to work on this exciting project and for supporting my ideas.

I am very grateful to,
Prof. Dr. Alfons Gierl for supervising and promoting my thesis at the Technical University of Munich,

my current and former lab members, particularly Nina Seitzer, Markus Reschke, Philipp Mertins, Stephan Busche, Laura Leitner, Torsten Winkler, Robert Torka, Yixiang Zhang for all their help, discussions, the relaxed lab atmosphere, the distraction in stressful times…,
and the whole Department of Molecular Biology for their help and the great time in and beyond the lab.

Many thanks to my flat-mates Nina and Markus for a wonderful and relaxing time at home during my entire PhD time here in Munich.

Abschließend möchte ich ganz besonders meiner Familie und Mike für die andauernde Unterstützung während der Zeit dieser Doktorarbeit danken.